

THE UNIVERSITY OF HULL

Sporopollenin: Applications in Water Purification

being a Thesis submitted for the Degree of

Doctor of Philosophy in the University of Hull

by

Aimilia Meichanetzoglou, MSc

October 2021

THE UNIVERSITY OF HULL
Department of Chemistry and Biochemistry
Faculty of Science and Engineering

Sporopollenin: Applications in Water Purification

being a Thesis submitted for the Degree of

Doctor of Philosophy in the University of Hull

by

Aimilia Meichanetzoglou, MSc

October 2021

Sporopollenin: Applications in Water Purification

by

Aimilia Meichanetzoglou, MSc



To Ioanna, Achilles, Guy and the cats.

*«..για να γεννηθείς εσύ
κι εγώ για να σε συναντήσω
γι' αυτό έγινε ο κόσμος..»*

ABSTRACT

Water pollution from emerging contaminants is increasingly in the spotlight, as research on the impacts on the environment is revealing more about the dangers to both animals in the aquatic environment and human health. Pharmaceuticals, personal care products, surfactants and pesticides have been proven to have endocrine-disrupting properties, affecting not only the aquatic life but human life as well. Conventional wastewater treatment plants need to be updated in order to deal with this family of chemicals, since they are currently incapable of removing them using traditional methods. New methods need to be developed since the current ones leave behind around 60 - 90% of the initial contaminant concentration and re-introduce it to the water cycle. Adsorption procedures have been proven to be very effective on water treatment, targeting emerging contaminants, with research focusing on developing new materials, that apart from being effective should also be environmentally friendly.

Sporopollenin is the name of a bio-polymer found in nature, constructing the outer shell (exine) of the capsule of a pollen grain or spore. The capsule itself - sporopollenin exine capsule (SpEC) - evolved to protect the genetic material contained in each grain/spore, hence sporopollenin has been proven to be chemically stable and very resistant to harsh environmental conditions. SpECs can be extracted from pollen grains or spores producing empty capsules (devoid of their genetic material), presenting a variety of differently sized microcapsules and shapes depending on the plant species. These capsules are monodispersed, presenting great mechanical strength as well as permeability. The material has a high surface area due to the porous nature with many multi-directional channels leading to the core of the capsule, giving them features and properties that are ideal for contaminant adsorption.

The focus of this thesis was the investigation of SpECs deriving from *Lycopodium clavatum* by multiple extraction methodologies for applications on emerging contaminant adsorption.

Different extraction procedures were developed, as well as surface modification protocols, in order to optimise the material for the different pollutants. The resulting SpECs were tested against four different contaminants; diclofenac, triclosan, oestradiol and phosphates, under different experimental settings, either lab based or closer to real world conditions. The results revealed that SpECs offer a very promising natural material, presenting high efficiency against the tested contaminants, with low-cost production, offering an environmentally friendly approach to the problem of water purification.

For diclofenac, the most efficient SpECs type was SpECs(3)AM, with a maximum adsorption capacity value of 27.4 mg/g under a packed-bed setup. For triclosan, SpECs(3) was the most efficient type, presenting a maximum adsorption capacity of 37 mg/g under packed-bed setup or a K_F value of $35.14 \text{ mg}^{(1-1/n)}/\text{gL}^{-1/n}$ for adsorption from a solution. For oestradiol adsorption, SpECs(1) worked the best, presenting a maximum adsorption capacity of 42.5 mg/g. For phosphates, all tested SpECs presented similar adsorption capacities, with the water/Fe loaded SpECs(3) presenting the highest, 2.1 mg/g.

SpECs presented adsorption capacity values far beyond what would be required for treating hospital effluent or surface waters and very good adsorption rates, especially for diclofenac and triclosan. Although the oestradiol experiments resulted in excellent maximum adsorption capacity, the rate of adsorption was below what would be required for treating large bodies of flowing water. However all other materials exhibited very promising rates of adsorption, particularly SpECs(3)AM for diclofenac and SpECs(3) for triclosan, warranting scale-up experiments for the treatment of such volumes as hospital effluents (55 - 530 L/min).

SpECs(3) and their aminated form, SpECs(3)AM were proven to be the best candidates for contaminant adsorption, with SpECs(3) ticking all the boxes for a successful adsorbent; apart from their excellent adsorption behaviour, their production is fast and low-cost, they are

environmentally friendly since they derive from plant spores, the chemicals used are not harsh to the environment nor were high temperature treatments or long reaction times required and they also presented good reusability.

ACKNOWLEDGEMENTS

I would like to thank my supervisors, Dr Andrew Boa and Prof. Jeanette Rotchell for their guidance and mentoring, and the Sullied Sediments project, funded by the Interreg North Sea Region European Regional Development Fund.

I would like to express my love to all the wonderful people that I met during this journey: Alberto and Louise, Ana-Maria, Isabelle and Alonso, Nikos, Julia and Romie, Barbara, Owen, Samantha, Nikos and Helena, it was a great pleasure meeting you and having created memorable moments with you.

A big thank you to all the technicians and staff at Hull University for the wonderful working environment and the amazing teamwork: Maggy Harley, Dr Emma Chapman, Bob Knight, Dr Kevin Welham, Dean Moore, Sean Moore and Carol Kennedy, thank you very, very much.

I'm extremely grateful to my parents and brothers for inspiring me every day and supporting me on each new step that I take. You made this journey possible and easier.

Most of all, my deepest and hugest thank you goes to my husband, best friend and soul mate, Guy, for all the support, the help, the love and the patience, especially during the writing period.

This work (and I) would be incomplete without you.

ABBREVIATIONS

1,2,3,8-TCDD	1,2,3,8-tetrachlorodibenzo- <i>p</i> -dioxin
1,2,8-TriCDD	1,2,8-trichlorodibenzo- <i>p</i> -dioxin
12-MPA	12-molybdophosphoric or phosphomolybdic acid
2,3,7-TriCDD	2,3,7-trichlorodibenzo- <i>p</i> -dioxin
2,4-DCP	2,4-dichlorophenol
2,8-DCDD	2,8-dichlorodibenzo- <i>p</i> -dioxin
AO/RPs	advanced oxidation/reduction processes
APS	ammonium persulfate
ARB	antibiotic resistant bacteria
ARGs	antibiotic resistant genes
BPA	bisphenol A
COX	cyclooxygenase
DCF	diclofenac
DNA	deoxyribonucleic acid
E1	estrone
E2	17- β -oestradiol
E3	estriol
EC	European Commission
EDCs	endocrine disrupting chemicals
EE2	17- α -ethinyloestradiol
FT-IR	Fourier transformation infrared spectroscopy
GC-MS	gas chromatography - mass spectrometry
H-NMR	hydrogen - nuclear magnetic resonance
HPLC	high performance liquid chromatography
HPLC-ESI-MS/MS	high performance liquid chromatography coupled with electrospray ionisation analysed by tandem mass spectrometry
ICP-OES	inductively coupled plasma - optical emission spectroscopy
LC-MS	liquid chromatography coupled with mass spectrometry
LOD	limit of detection
LOQ	limit of quantification

MALDI-TOF-MS	matrix assisted laser desorption ionisation - time of flight - mass spectrometry
MDR	multi drug resistant microorganisms
MOFs	metal organic frameworks
NSAID	non-steroidal anti-inflammatory drug
PCBs	polychlorinated biphenyls
PPCPs	pharmaceuticals and personal care products
RNA	ribonucleic acid
SEM	scanning electron microscopy
SpECs	sporopollenin exine capsules
TBHP	<i>tert</i> -butyl hydroperoxide
TCS	triclosan
UV	ultraviolet
UV-Vis	ultraviolet - visible
WFD	water framework directive
WWT	wastewater treatment
WWTP	wastewater treatment plants/procedures

COSHH statement

All of the experiments carried out had a full COSHH and risk assessment signed by the student, supervisor and safety officer and were in accordance with the University of Hull's Health and Safety guidelines.

Funding statement

This work was part of the Sullied Sediments project, funded by the Interreg North Sea Region European Regional Development Fund.

Contents

1. Introduction.....	1
1.1. Water contamination.....	1
1.1.1. EC Priority List and Watch List.....	4
1.2. Water Purification.....	5
1.2.1. Conventional wastewater treatment procedures.....	5
1.2.2. New techniques on wastewater treatment.....	6
1.2.3. Adsorption.....	8
1.2.3.1. Definition.....	8
1.2.3.2. Adsorption isotherms.....	9
1.2.3.2.1. Classification of adsorption isotherms.....	10
1.2.3.2.2. Langmuir model.....	12
1.2.3.2.3. Freundlich model.....	14
1.2.3.3. Adsorption kinetics.....	15
1.2.3.3.1. Pseudo-first order model.....	17
1.2.3.3.2. Pseudo-second order model.....	17
1.2.3.3.3. Intraparticle diffusion.....	18
1.2.3.3.4. Continuous packed-bed adsorption.....	18
1.2.3.4. Factors affecting adsorption.....	20
1.2.3.4.1. Contaminant properties.....	20
1.2.3.4.2. Adsorbent properties.....	21
1.2.3.5. Materials for contaminant adsorption.....	21
1.3 Aims and Objectives.....	24
2. Sporopollenin Exine Capsules.....	25
2.1. Pollens and spores.....	25
2.2. Sporopollenin.....	26
2.3. Sporopollenin exine capsules.....	30
2.3.1. <i>Lycopodium clavatum</i> SpECs.....	31
2.3.2. SpECs applications.....	35
2.4. Aims and Objectives.....	36
2.5. Raw <i>Lycopodium clavatum</i> spores.....	36
2.6. SpECs extraction.....	39
2.6.1. KOH hydrolysis - H ₃ PO ₄ treatment [SpECs(1)].....	40
2.6.2. NaOH hydrolysis [SpECs(2)].....	43
2.6.2.1. HCl treatment of SpECs(2).....	46
2.6.3. HCl hydrolysis [SpECs(3)].....	47

2.6.4. FT-IR comparison of the three extractions and the raw spores.....	51
2.7. Surface modification of SpECs.....	54
2.7.1. NaOCl treatment	55
2.7.2. APS treatment	59
2.7.3. Amination of SpECs(3).....	62
2.7.4. Iron loading onto SpECs	65
2.7.4.1. Iron loading on SpECs(1)	68
2.7.4.2. Iron loading on SpECs(2)	69
2.7.4.3. Iron loading on SpECs(3)	70
2.8. SpECs surface analysis - Boehm titration.....	72
2.9. Conclusions.....	76
3. Diclofenac.....	80
3.1. Introduction.....	80
3.2. Aims and objectives	85
3.3. Diclofenac detection and quantification	86
3.4. Diclofenac adsorption experiments.....	87
3.4.1. Cotton interference in diclofenac adsorption experiments.....	88
3.4.2. Diclofenac adsorption onto SpECs derived from different plants	89
3.4.3. Diclofenac adsorption onto <i>L. clavatum</i> SpECs	90
3.4.3.1. Effect of drying conditions on the adsorption efficiency of SpECs(3).....	96
3.4.3.2. Effect of wettability of SpECs on the adsorption of DCF.....	99
3.4.4. Diclofenac adsorption onto modified SpECs	101
3.4.4.1. Diclofenac adsorption onto ammonium persulfate treated SpECs(2).....	101
3.4.4.2. Diclofenac adsorption onto HCl treated SpECs(2)	106
3.4.4.3. Diclofenac adsorption onto TBHP treated SpECs(2).....	108
3.4.4.4. Diclofenac adsorption onto NaOCl treated SpECs(2).....	109
3.4.4.5. Diclofenac adsorption onto oxidised SpECs(3)	110
3.4.4.6. Comparison on SpECs(2)APSH, SpECs(2)Bl, SpECs(3) and SpECs(3)Bl.....	113
3.4.4.7. Diclofenac adsorption onto aminated SpECs(3)	114
3.4.5. Diclofenac adsorption kinetics.....	118
3.4.5.1. Pseudo-first order model	119
3.4.5.2. Pseudo-second order model	121
3.4.5.3. Intraparticle diffusion model.....	124
3.4.6. Diclofenac adsorption isotherms.....	127
3.4.7. Diclofenac packed-bed studies.....	132
3.4.7.1. Breakthrough curves for SpECs(3)	135
3.4.7.2. Breakthrough curves for SpECs(2)APSH.....	138

3.4.7.2.1. Regeneration and reusability of SpECs(2)APSH.....	140
3.4.7.3. Breakthrough curves for SpECs(3)AM.....	144
3.4.7.3.1. Regeneration and reusability of SpECs(3)AM	146
3.4.7.3.2. Effect of the age of SpECs(3)AM on their DCF adsorption efficiency	150
3.5. Conclusions.....	153
4. Triclosan	157
4.1. Introduction.....	157
4.2. Aims and objectives	161
4.3. Triclosan detection and quantification	161
4.4. Triclosan adsorption experiments	164
4.4.1. Effect of vessel material in triclosan adsorption experiments.....	165
4.4.2. Triclosan adsorption kinetics at high concentrations	167
4.4.3. Triclosan adsorption kinetics at low concentrations	169
4.4.4. Triclosan adsorption isotherms	172
4.4.5. Triclosan packed-bed studies	175
4.4.5.1. Regeneration and reusability of SpECs.....	181
4.4.6. Adsorption of mixture of contaminants: diclofenac and triclosan	185
4.5. Conclusions.....	192
5. Oestradiol.....	195
5.1. Introduction.....	195
5.2. Aims and Objectives	200
5.3. Oestradiol detection and quantification	200
5.4. Oestradiol adsorption experiments.....	202
5.4.1. Cotton interference in oestradiol adsorption experiments.....	203
5.4.2. Oestradiol adsorption kinetics.....	204
5.4.2.1. Pseudo-first order model	205
5.4.2.2. Pseudo-second order model	207
5.4.2.3. Intraparticle diffusion model.....	211
5.4.3. Oestradiol adsorption isotherms.....	213
5.4.4. Oestradiol packed-bed studies	217
5.4.4.1. Regeneration and reusability of SpECs.....	222
5.5. Conclusions.....	226
6. Phosphates	229
6.1. Introduction.....	229
6.2. Aims and Objectives	231
6.3. Phosphates detection and quantification	232
6.3.1. Phosphates colorimetric detection	232

6.3.1.1. The molybdenum blue reaction.....	232
6.3.1.2. Phosphates colorimetric quantification	234
6.4. Phosphates adsorption experiments	235
6.4.1. Cotton interference in phosphates adsorption experiments	237
6.4.2. Phosphates adsorption onto unmodified SpECs	238
6.4.3. Phosphates adsorption onto Fe loaded SpECs	238
6.4.3.1. Phosphates adsorption onto Fe/water loaded SpECs	239
6.4.3.1.1. Effect of contact time on phosphates adsorption onto Fe/water loaded SpECs ..	240
6.4.3.2. Phosphates adsorption onto Fe/acetone loaded SpECs	244
6.4.3.2.1. Effect of contact time on phosphates adsorption onto Fe/acetone loaded SpECs ..	245
6.4.4. Comparisons between the adsorption performances	247
6.5. Conclusions.....	248
7. Conclusions.....	250
8. Experimental	254
8.1. SpECs extraction.....	254
8.1.1. SpECs(1) KOH hydrolysis - H ₃ PO ₄ treatment.....	254
8.1.2. SpECs(2) NaOH hydrolysis	255
8.1.3. SpECs(3)HCl hydrolysis.....	255
8.1.3.1. Drying conditions of SpECs(3).....	255
8.2. SpECs surface modification.....	255
8.2.1. SpECsBL - Bleach (NaOCl) treatment	255
8.2.2. SpECs(2)HCl - HCl treatment	256
8.2.3. SpECsAPS - Ammonium Persulfate treatment.....	256
8.2.3.1. APS 1 M treatment at room temperature - SpECsAPSR1	256
8.2.3.2. APS treatment at 90 °C - SpECsAPSH.....	256
8.2.4. <i>Tert</i> -butyl-hydroperoxide treatment - SpECsTBHP	257
8.2.5. Iron loading onto SpECs	257
8.2.5.1. Iron loading onto SpECs in water	257
8.2.5.2. Iron loading onto SpECs in water under vacuum	257
8.2.5.3. Iron loading in acetone.....	258
8.2.5.4. Magnetic SpECs.....	258
8.2.6. Aminated SpECs	259
8.3. SpECs analysis.....	259
8.3.1. Boehm titration	259
8.3.2. IR analysis.....	259
8.4. Diclofenac experiments	260
8.4.1. Diclofenac reference curve	260

8.4.2. Diclofenac adsorption kinetics.....	261
8.4.3. Diclofenac adsorption isotherms.....	262
8.4.4. SpECs wettability and diclofenac adsorption	262
8.5. Triclosan experiments.....	262
8.5.1. Triclosan reference curve.....	264
8.5.2. Triclosan adsorption kinetics	264
8.5.3. Triclosan adsorption isotherms	265
8.6. Oestradiol experiments	265
8.6.1. Oestradiol solution stability	265
8.6.2. Oestradiol reference curve	266
8.6.3. Oestradiol adsorption kinetics.....	266
8.6.4. Oestradiol Adsorption Isotherms	267
8.7. Mixed contaminants experiment.....	267
8.7.1. Mixed contaminant reference curve.....	268
8.7.2. Mixed contaminants adsorption experiments.....	268
8.8. Phosphates experiments	268
8.8.1. Phosphates detection method.....	269
8.8.2. Phosphates reference curve.....	269
8.8.3. Phosphates adsorption kinetics	270
8.9. Packed-bed studies.....	270
8.9.1. Column preparation.....	270
8.9.2. Packed-bed experiments	270
9. References.....	272

TABLE OF FIGURES

Figure 1: Different pathways of PPCPs reaching the environment.	2
Figure 2: Mode of action of EDCs inside an organism.....	3
Figure 3: Primary and secondary treatment steps for water purification.	6
Figure 4: The four different types of adsorption isotherms according to Limousin et al. and Giles <i>et al.</i> ⁶¹⁻⁶⁵	11
Figure 5: The adsorbent's surface and the adsorbate molecules. (a): Forces of attraction (lines) between the adsorbate molecules and the surface are equal. The molecules are adsorbed more strongly in the left position than in the right, where the only forces towards the molecule are these of the surface. This phenomenon of cooperative adsorption is described by S-type isotherms (b): Strong forces of attraction (thicker lines) between the surface and the adsorbate molecules, very weak forces (dots) between the molecules. The adsorption strength is equal between the right and the left position. This type of adsorption is described by L or H isotherms. ⁶⁵	12
Figure 6: Schematic representation of the cross section of a <i>Lycopodium clavatum</i> spore capsule. ...	25
Figure 7: Size range of pollen grains and spores, a. <i>Myosotis palustris</i> , <i>boraginaceae</i> <10 µm, b. <i>Alkanna orientalis</i> , <i>boraginaceae</i> 10 - 25 µm, c. <i>Syringa vulgaris</i> , <i>oleaceae</i> 25 - 50 µm, d. <i>Plumbago auriculata</i> , <i>plumbaginaceae</i> 50 - 100 µm, e. <i>Cucurbita pepo</i> , <i>cucurbitaceae</i> >100 µm. ¹³³	27
Figure 8: Chemical structures of <i>p</i> -coumaric acid (left) and ferulic acid (right).	29
Figure 9: Chemical structure of pine sporopollenin as suggested by Li <i>et al.</i> ¹⁴⁵ Thioacidolysis of pine sporopollenin gave three major (I, IIa, IIb) and several minor (III-VI) groups that were detected by HPLC-UV-MS.	29
Figure 10: Spore hydrolysis procedures where the genetic material is removed and empty SpECs are produced.....	31
Figure 11: <i>Lycopodium clavatum</i> plant [www.aphotoflora.com].	32
Figure 12: SEM image of <i>L. clavatum</i> SpECs where a) the trilete scar on the bottom of the capsule is visible and b) the particles appear sucked in due to the vacuum employed during SEM.	33
Figure 13: Morphological characteristics of a <i>L. clavatum</i> spore.	34
Figure 14: SEM image of a fragmented SpEC revealing the inside of the spore and providing useful information on the wall thickness and tectal elements.....	34
Figure 15: FT-IR spectrum of raw <i>L. clavatum</i> spores.	37
Figure 16: FT-IR spectra of raw spores and defatted spores derived from <i>L. clavatum</i>	38
Figure 17: Extracted SpECs - the darkest colour corresponds to the HCl extraction SpECs(3), the yellow SpECs(2) are extracted via the NaOH hydrolysis and the brown SpECs(1) are extracted with the two step KOH/H ₃ PO ₄ hydrolysis.	40
Figure 18: SEM image of KOH extracted SpECs [SpECs(1)] followed by H ₃ PO ₄ treatment. Some fragments of the initial spores are present in the final product indicating that the hydrolysis procedure might have been harsh.	41
Figure 19: SEM image of KOH extracted SpECs [SpECs(1)] followed by H ₃ PO ₄ treatment, zoomed in the area of a fragmented spore.	41
Figure 20: FT-IR spectra of SpECs(1) and raw <i>L. clavatum</i> spores. Highlighted is the removal of aromatic ring modes at ~1510 cm ⁻¹	42
Figure 21: SEM image of NaOH extracted SpECs [SpECs(2)] showing the upper and bottom parts of two different spore particles.....	43
Figure 22: SEM image of NaOH extracted SpECs [SpECs(2)] showing imploded particles.....	44
Figure 23: Microscopic image of SpECs(2) dispersed in water, showing the true size of the particles without implosion (scalebar distance between lines 10 µm).....	45
Figure 24: SEM image of SpECs(2) magnified to exhibit the mura of a shell, showing no damage on the tectal elements.....	45

Figure 25: FT-IR spectra of SpECs(2) and raw <i>L. clavatum</i> spores.	46
Figure 26: FT-IR analysis of SpECs(2) before and after HCl treatment [SpECs(2)HCl].	47
Figure 27: SEM image of SpECs(3) focused on the region of the damaged ectexine of a shell.	48
Figure 28: SEM image of HCl extracted SpECs [SpECs(3)].	49
Figure 29: SEM image of SpECs(3). The trilete scar appears to be particularly vulnerable to these extraction conditions. Only this side of the exines exhibits damage to the ectexine.	50
Figure 30: FT-IR spectra of SpECs(3) and raw <i>L. clavatum</i> spores. Highlighted is the significant increase in aromatic ring modes $\sim 1510\text{ cm}^{-1}$	51
Figure 31: FT-IR spectra of the 3 SpECs types and raw <i>L. clavatum</i> spores. Highlighted are the stretching frequencies for carboxylic acids $\sim 1710\text{ cm}^{-1}$ and aromatic ring modes $\sim 1510\text{ cm}^{-1}$ as these groups represent possible adsorption sites for the contaminants.	53
Figure 32: Modified SpECs. The bleaching procedure on SpECs(2) changes the SpECs colour from yellow to white (6 th vial counting from left to right). For SpECs(3) it changes the colour from dark brown to lighter brown (7 th vial).	55
Figure 33: SEM image of SpECs(2)Bl.	56
Figure 34: SEM image of SpECs(2)Bl magnified to exhibit the damage on the surface.	57
Figure 35: FT-IR spectra of NaOCl treated and HCl treated SpECs(2) [SpECs(2)Bl and SpECs(2)HCl respectively].	58
Figure 36: SEM image of SpECs(2)APSH showing the trilete scar and the damage in the decorative section of the shell.	60
Figure 37: SEM image of SpECs(2)APSH focused on the decorative part of the shell, presenting some damage.	61
Figure 38: SEM image of SpECs(2)APSH showing collapsed spores under the vacuum.	61
Figure 39: FT-IR spectra of SpECs(2)APSH and SpECs(2)HCl compared to SpECs(2).	62
Figure 40: FT-IR spectra of SpECs(3) before and after amination (aminated form is SpECs(3)AM).	63
Figure 41: Carboxylic acid amination leading to the formation of a secondary amide.	64
Figure 42: Microscope image of raw spores surrounded by newly formed particles after the magnetic procedure (lens 20 x 0.40).	66
Figure 43: Microscope image of SpECs(3) surrounded by newly formed particles after the magnetic procedure (lens 20 x 0.40).	67
Figure 44: Comparison between inner fragments of iron loaded (left) and unloaded SpECs(1) (right).	68
Figure 45: SEM images of iron loaded SpECs(1) in acetone under vacuum.	69
Figure 46: SEM images of iron loaded (left) and unloaded SpECs(2) (right).	70
Figure 47: SEM images of iron loaded SpECs(3)M19 (left) and unloaded ones (right).	71
Figure 48: SEM image of iron loaded SpECs(3) focused on the surface of the capsule.	71
Figure 49: SEM image of iron loaded SpECs(3) showing the loading of the iron molecules on the surface of the capsule.	72
Figure 50: Reactions between the different bases and the different functional groups present on the surface of SpECs.	73
Figure 51: IR analysis of the extracted SpECs and the ammonium persulfate treated SpECs(2), focused in the 1710 cm^{-1} vibration for a carbonyl peak associated with carboxylic acids.	75
Figure 52: Structure of diclofenac in the monosodium salt form.	80
Figure 53: The principal metabolites of DCF following oral consumption by humans.	81
Figure 54: By-products after photolysis or chlorination of DCF. ^{71,194,195}	83
Figure 55: DCF reference curve at the concentration region of 0 - 25 $\mu\text{g/mL}$ at 275 nm detection wavelength (n=3).	86
Figure 56: Experimental setup for the adsorption experiments describing the three-step procedure: 1) SpECs are added to the contaminant solution, 2) the suspension is shaken in the orbital shaking for a period of time, 3) the suspension is filtered through a pipette equipped with cotton wool.	87

Figure 57: Effect of contact time on DCF adsorption for SpECs derived from rye (<i>Secale cereale</i>), sunflower pollen (<i>Helianthus annuus</i>) and <i>L. clavatum</i> spores by HCl extraction protocol [SpECs(3)] (DCF concentration: 6 mg/L, n=3).	89
Figure 58: Possible interactions between DCF molecules and SpECs surface; A represents π - π interactions, B shows DCF acting as a hydrogen acceptor and C shows DCF acting as a H bonding donor.	90
Figure 59: Effect of contact time on DCF adsorption for different <i>L. clavatum</i> SpECs types and raw spores, (DCF concentration: 6 mg/L, n=3).	91
Figure 60: FT-IR analysis of SpECs(2) before and after HCl treatment [SpECs(2)HCl].....	93
Figure 61: Extract from the IR spectra of the three different extracted SpECs, zoomed in the region around the 1710 cm^{-1} peak.	94
Figure 62: Schematic representation of possible adsorption interactions between DCF and the functional groups on the surface of SpECs.....	96
Figure 63: Effect of drying procedures for SpECs(3) on DCF adsorption. Air dried at the pump (air dried), dried under vacuum in a desiccator (desiccator dried) and dried into an oven at 100 °C (oven dried), (DCF dose: 6 mg/L, n=3).	97
Figure 64: IR spectra of SpECs(3) dried in a desiccator and SpECs(3) oven dried.	98
Figure 65: Comparison of DCF adsorption behaviours of dried and wet SpECs. SpECs(2)APSH accounts for SpECs(2) treated with ammonium persulfate, treatment that will be further analysed in the following sections (DCF dose: 6 mg/L, n=3).....	100
Figure 66: Effect of time for DCF adsorption on modified SpECs(2) treated with different concentrations of ammonium persulfate (APSR1: 1 M ammonium persulfate at room temperature, APSH1: 1 M ammonium persulfate at 90 °C, APSH1.5: 1.5 M ammonium persulfate at 90 °C, APSH0.5: 0.5 M ammonium persulfate at 90 °C, APSH2: 2 M ammonium persulfate at 90 °C) (DCF dose: 6 mg/L, n=3).....	102
Figure 67: FT-IR spectra of SpECs(2), SpECs(2) HCl treated and SpECs(2)APSH. Comparisons between SpECs(2)HCl and SpECs(2)APSH is more accurate for the region around 1600 cm^{-1} because of the absence of the carboxylates peak.....	104
Figure 68: FT-IR spectra of DCF on its own and SpECs(2)APSH.	105
Figure 69: IR spectra of SpECs(2)APSH1 and SpECs(2)APSH1 loaded with DCF.....	105
Figure 70: Effect of time on DCF adsorption for unmodified and modified SpECs(2) compared to SpECs(1). SpECs(2)HCl: treatment with HCl 1 M, (DCF dose: 6 mg/L, n=3).....	107
Figure 71: FT-IR spectra of SpECs(2) and SpECs(2)HCl.....	107
Figure 72: Effect of time on DCF adsorption for unmodified and modified SpECs(2). Different treatments at room temperature: SpECs(2)BL: NaOCl 14%, SpECs(2)TBHP: 70% tert-butyl hydroperoxide (DCF dose: 6 mg/L, n=3).....	108
Figure 73: FT-IR spectra of SpECs(2)HCl and SpECs(2)Bl.	109
Figure 74: Effect of time on DCF adsorption for modified SpECs(3). Different treatments: SpECs(3)BL: 14% NaOCl at room temperature, SpECs(3)APSH1: 1 M ammonium persulfate at 90 °C (DCF dose: 6 mg/L, n=3).....	111
Figure 75: FT-IR spectra of APS treated SpECs(3) [SpECs(3)APSH] compared to NaOCl treated SpECs(3) [SpECs(3)Bl].....	112
Figure 76: FT-IR of NaOCl treated SpECs(3) [SpECs(3)Bl] compared with SpECs(3). Highlighted areas of interest are the complete depletion of the aromatic ring modes (1510 cm^{-1}) and the increase in carboxylic acids \sim 1710 cm^{-1}	112
Figure 77: DCF adsorption performances of SpECs(3), NaOCl treated SpECs(3) [SpECs(3)Bl], NaOCl treated SpECs(2) [SpECs(2)Bl], and ammonium persulfate 1 M treated SpECs(2) [SpECs(2)APSH1] zoomed in the region of 60 - 100% adsorption (n = 3, DCF 6 $\mu\text{g}/\text{mL}$).	114
Figure 78: Possible electrostatic and hydrogen bonding interactions between DCF and the aminated SpECs (R = the SpECs polymer).	115

Figure 79: DCF adsorption; comparison between SpECs(3) and SpECs(3)AM (DCF dose: 6 mg/L, n=3).....	116
Figure 80: Schematic representation of possible adsorption forces between DCF and the surface of aminated SpECs(3).	117
Figure 81: Effect of contact time on DCF adsorption, graph zoomed in the region of 0 - 1 hour of contact time (DCF dose: 6 mg/L). Comparison between the adsorption efficiencies of the different SpECs types and the most efficient modified SpECs (DCF dose: 6 mg/L, n=3).....	118
Figure 82: Kinetic investigation on the adsorption of DCF by different types of SpECs described by the pseudo-first order model.	120
Figure 83: Kinetic investigation on the adsorption of DCF by different types of SpECs described by the pseudo-second order model.....	122
Figure 84: Kinetic investigation on the adsorption of DCF by SpECs(2) described by the pseudo-second order model.	122
Figure 85: Intraparticle diffusion model for the adsorption of DCF onto different types of SpECs where (a) represents the first diffusion step and (b) represents the second diffusion step.....	125
Figure 86: Langmuir linear adsorption isotherms for DCF uptake by different types of SpECs.	129
Figure 87: Langmuir linear adsorption isotherm for DCF uptake by SpECs(2).....	129
Figure 88: Freundlich linear adsorption isotherms for DCF uptake by different types of SpECs.	129
Figure 89: DCF breakthrough curves for 1 g packed SpECs(3) at 10 mg/L DCF initial concentration (C_0) and 2 mL/min flow rate (SpECs(3)[10]) and 1 g packed SpECs(3) with 60 mg/L DCF initial concentration and 1.8 mL/min flow rate (SpECs(3)[60]).	135
Figure 90: Breakthrough curves for 3 g packed SpECs(3) and DCF at 10 mg/L initial concentration (C_0) and two different flow rates: 0.8 mL/min and 0.5 mL/min.	137
Figure 91: DCF breakthrough curves for 0.5 g packed SpECs(2)APSH at 10 mg/L DCF initial concentration (C_0) and two different flow rates: 1.5 mL/min and 3.0 mL/min.	138
Figure 92: Breakthrough curve for SpECs(2)APSH and DCF adsorption, followed by washing of the packed-bed with milliQ water after reaching the saturation point.	141
Figure 93: Breakthrough curves for DCF adsorption at a flow rate of 1.5 mL/min for three cycles of SpECs(2)APSH reuse.	142
Figure 94: Breakthrough curves for DCF adsorption over three cycles of SpECs(2)APSH use and regeneration (flow rate = 3 mL/min).....	142
Figure 95: Comparison of the DCF adsorption capacity (q_0, exp) of SpECs(2)APSH, at two flow rates, over three cycles of use and regeneration.....	143
Figure 96: Breakthrough curves of 0.2 g packed SpECs(3)AM and DCF at 10 mg/L initial concentration at two different flow rates: 2.0 and 3.0 mL/min.....	144
Figure 97: Packed SpECs(3)AM washed with milliQ water after the completion of the DCF breakthrough curve.	147
Figure 98: Breakthrough curves for DCF adsorption at a flow rate of 2 mL/min for two cycles of SpECs(3)AM use.	148
Figure 99: Breakthrough curves for DCF adsorption at a flow rate of 3 mL/min for two cycles of SpECs(3)AM use.	149
Figure 100: Comparison of the DCF adsorption capacity of SpECs(3)AM between each cycle of use.	149
Figure 101: Breakthrough curves of SpECs(3)AM (0.2 g) for DCF adsorption (10 mg/L) at two different flow rates, conducted 20 days after the amination reaction.	151
Figure 102: Comparison of breakthrough curves obtained for DCF (10 mg/L) elution, after different periods of time since the production of SpECs(3)AM. Sample was stored in a tightly closed amber vial, placed in a drawer away from sunlight exposure.....	152
Figure 103: Chemical structure of triclosan.....	157
Figure 104: TCS by-products after ozonation, methylation, chlorination and photolysis.	159

Figure 105: TCS reference curve at the concentration region of 0 - 15 $\mu\text{g/mL}$ at 220 nm detection wavelength (n=3).	162
Figure 106: TCS reference curve at the concentration region of 0 - 15 $\mu\text{g/mL}$ at 280 nm detection wavelength (n=3).	163
Figure 107: TCS reference curve at the concentration range of 0 - 60 ng/mL (n=3).	164
Figure 108: Experimental setup for the adsorption experiments describing the three-step procedure: 1) SpECs are added to the contaminant solution, 2) the suspension is shaken in the orbital shaking for a period of time, 3) the suspension is filtered through a pipette equipped with cotton wool.	165
Figure 109: TCS concentration after different periods of time shaking inside glass vials with either metal lid (n=3) or plastic lids (n=3).	166
Figure 110: Effect of contact time on TCS adsorption by 5 g of raw spores or different SpECs; graph zoomed in the region of 20 - 100% of TCS removal (TCS dose: 6 mg/L , n=3).	168
Figure 111: Effect of contact time on TCS adsorption by different SpECs, graph zoomed in the region of 85 - 100% of TCS adsorption (TCS dose: 2.3 $\mu\text{g/L}$, n=3).	169
Figure 112: Effect of contact time and initial contaminant dose on TCS adsorption by SpECs, graph zoomed in the region of 85 - 100% TCS adsorption (TCS dose H: 6 mg/L , L: 2 $\mu\text{g/L}$, n=3).	170
Figure 113: Schematic representation of possible adsorption forces between TCS and the functional groups on the surface of the different SpECs.	171
Figure 114: Langmuir linear adsorption isotherms for TCS uptake by different types of SpECs.	173
Figure 115: Freundlich linear adsorption isotherms for TCS uptake by different types of SpECs.	174
Figure 116: Breakthrough curves of 0.2 g SpECs(3) for TCS (10 mg/L) adsorption at two flow rates (2 and 3 mL/min).	179
Figure 117: Packed SpECs(3) washed with milliQ water after the completion of the breakthrough curve against TCS.	182
Figure 118: Breakthrough curves for TCS adsorption at a flow rate of 2 mL/min for three cycles of SpECs(3) reuse.	183
Figure 119: Breakthrough curves for TCS adsorption at a flow rate of 3 mL/min for three cycles of SpECs(3) reuse.	183
Figure 120: Comparison of the adsorption capacity of SpECs(3) between each cycle of reuse against TCS.	185
Figure 121: Effect of time on the adsorption of a mixture of DCF (6 mg/L) and TCS (6 mg/L) in water by SpECs(1) (n=3, total contaminant concentration 12 mg/L).	186
Figure 122: Comparison of the adsorption kinetics between single contaminant solution (either DCF or TCS alone, 6 $\mu\text{g/mL}$) and mixed contaminant solution (DCF and TCS together, 6 $\mu\text{g/mL}$ each, indicated by mix in the graph) by SpECs(1) (n=3).	187
Figure 123: Effect of time on the adsorption of a mixture of DCF (6 mg/L) and TCS (6 mg/L) in water by SpECs(2) (n=3, total contaminant concentration 12 mg/L).	188
Figure 124: Comparison of the adsorption kinetics between single contaminant solution (either DCF or TCS alone, 6 $\mu\text{g/mL}$) and mixed contaminant solution (DCF and TCS together, 6 $\mu\text{g/mL}$ each, indicated by mix in the graph) by SpECs(2) (n=3).	188
Figure 125: Effect of time on the adsorption of a mixture of DCF (6 mg/L) and TCS (6 mg/L) in water by SpECs(3) (n=3, total contaminant concentration 12 mg/L).	189
Figure 126: Comparison of the adsorption kinetics between single contaminant solution (either DCF or TCS alone, 6 $\mu\text{g/mL}$) and mixed contaminant solution (DCF and TCS together, 6 $\mu\text{g/mL}$ each, indicated by mix in the graph) by SpECs(3) (n=3).	190
Figure 127: Effect of time on the adsorption of a mixture of DCF (6 mg/L) and TCS (6 mg/L) in water by SpECs(2)APSH (n=3, total contaminant concentration 12 mg/L).	190
Figure 128: Comparison of the adsorption kinetics between single contaminant solution (either DCF or TCS alone, 6 $\mu\text{g/mL}$) and mixed contaminant solution (DCF and TCS together, 6 $\mu\text{g/mL}$ each, indicated by mix in the graph) by SpECs(2)APSH (n=3).	191
Figure 129: Steroidal chemical structure.	195

Figure 130: Chemical structures of the four oestrogens most found in the aquatic environment.....	196
Figure 131: Chemical structures for E2 conjugates a) oestradiol glucuronide b) oestradiol sulfate..	197
Figure 132: E2 reference curve in milliQ water, at 200 nm detection wavelength and at room temperature.	201
Figure 133: Absorbance of E2 standard solutions at different concentrations (0.5 - 10 µg/mL) and their stability after different time periods.	202
Figure 134: Absorbance of E2 solutions of 6 µg/mL over 24 hours (n=4).....	202
Figure 135: Experimental setup for the adsorption experiments describing the three-step procedure: 1) SpECs are added to the contaminant solution, 2) the suspension is shaken in the orbital shaking for a period of time, 3) the suspension is filtered through a pipette equipped with cotton wool.....	203
Figure 136: Effect of contact time on E2 adsorption, (E2 dose: 6 mg/L, n=3).....	205
Figure 137: Kinetic investigation on the adsorption of E2 by different types of SpECs described by the pseudo-first order model.	206
Figure 138: Kinetic investigations on the adsorption of E2 by different types of SpECs described by the pseudo-second order model.....	208
Figure 139: Schematic representation of the possible adsorption mechanisms happening between the SpECs surface and E2 molecules.....	210
Figure 140: Intraparticle diffusion model for the adsorption of E2 onto different types of SpECs...	212
Figure 141: Langmuir linear adsorption isotherms for E2 uptake by different types of SpECs.	215
Figure 142: Freundlich linear adsorption isotherms for E2 uptake by different types of SpECs.	215
Figure 143: Breakthrough curves for 0.2 g packed SpECs(1) and E2 at 6 mg/L initial concentration (C_0) and at two different flow rates: 2 mL/min and 3 mL/min (n=1).	221
Figure 144: Packed SpECs(1) washed with milliQ water after the completion of the breakthrough curve for E2 adsorption.....	222
Figure 145: Breakthrough curves for 0.2 g packed SpECs(1) and E2 at 6 mg/L initial concentration (C_0) at a flow rate of 2 mL/min for three cycles of material reuse.	223
Figure 146: Breakthrough curves for 0.2 g packed SpECs(1) and E2 at 6 mg/L initial concentration (C_0) at a flow rate of 3 mL/min for three cycles of material reuse.	224
Figure 147: Comparison of the E2 adsorption capacity (q_0) of SpECs(1) between each cycle of reuse.	225
Figure 148: Structure of the Keggin ion $[XM_{12}O_{40}]^{n-}$. ^{410,411}	233
Figure 149: Samples containing different concentrations of phosphates (L to R: 0.5, 1, 2, 4, 6 and 8 mg/L) and the blue colour developed after 21 minutes of addition of the mixed reagent.	234
Figure 150: $[PO_4]^{3-}$ reference curve at the concentration region of 0 - 10 µg/mL at 890 nm detection wavelength (LOD = LOQ = 0.004 µg/mL, n=3).....	235
Figure 151: Effect of contact time on phosphates adsorption by different SpECs types, graph zoomed in the region of 0 - 30% of phosphates removal (PO_4^{3-} dose: 6 mg/L, n=3).	238
Figure 152: Schematic representation of the possible adsorption mechanisms happening between the iron loaded SpECs surface and phosphates.....	239
Figure 153: Effect of contact time on phosphates adsorption by Fe loaded SpECs in water without vacuum (PO_4^{3-} dose: 6 mg/L, n=3).....	240
Figure 154: Effect of contact time on phosphates adsorption by Fe loaded SpECs in water under vacuum, graph zoomed in the region of 50 - 100% of phosphates removal (PO_4^{3-} dose: 6 mg/L, n=3).	242
Figure 155: Effect of contact time on phosphates adsorption by Fe loaded SpECs in acetone under vacuum, graph zoomed in the region of 80 - 100% of phosphates removal (PO_4^{3-} dose: 6 mg/L, n=3).	246
Figure 156: Comparison of the phosphates adsorption performance of iron loaded SpECs in water and acetone, graph zoomed-in the region of 60 - 100% phosphates adsorption. M17-M19 SpECs are loaded in acetone. M20-M22 SpECs are loaded in water, both procedures were performed under vacuum (n=3).....	248

TABLE OF TABLES

Table 1: Substances / group of substances suggested for the First Watch List. ⁴⁰	5
Table 2: Elemental analysis results of raw spores.	37
Table 3: Elemental analysis results for SpECs and raw spores.....	39
Table 4: Elemental analysis results for SpECs(2) and HCl treated SpECs(2)HCl.	47
Table 5: IR analysis of the three different SpECs types and raw spores.....	52
Table 6: Elemental analysis results for modified SpECs.	54
Table 7: Elemental analysis results for NaOCl treated and HCl treated SpECs(2).	58
Table 8: Elemental analysis results for 1 M APS treated SpECs(2) at room temperature and at 90 °C.	59
Table 9: Elemental analysis results for SpECs(3) before and after amination.....	65
Table 10: Elemental analysis results for C, H, N content and ICP-OES analysis for Fe of SpECs(1) before and after Fe loading.	69
Table 11: Elemental analysis results for C, H, N content and ICP-OES analysis for Fe of SpECs(2) before and after Fe loading.	70
Table 12: Elemental analysis results for C, H, N content and ICP-OES analysis for Fe of SpECs(3) before and after Fe loading.	71
Table 13: Sodium loading for different types of SpECs. Each analysis was performed in triplicate. .	74
Table 14: Content of acidic functional groups for each SpECs type.	75
Table 15: Results for cotton wool interference in DCF adsorption experiments.....	88
Table 16: Elemental analysis results for SpECs(2) and HCl treated SpECs(2)HCl.	92
Table 17: DCF adsorption performance of SpECs and raw spores after one hour of contact time and their possible adsorption mechanisms.....	95
Table 18: DCF adsorption performance of SpECs(3) and SpECs(3) oven dried, after one hour of contact time and their possible adsorption mechanisms.	99
Table 19: DCF adsorption performance of SpECs(2) and SpECs(2)HCl, after one hour of contact time and the possible adsorption mechanisms.	108
Table 20: Elemental analysis results for SpECs(2) and HCl treated SpECs(2)HCl.	110
Table 21: Elemental analysis results for SpECs(3) and modified SpECs(3).	113
Table 22: Elemental analysis results for SpECs(3) before and after amination.....	115
Table 23: Kinetic parameters for DCF adsorption by different SpECs described by different models.	124
Table 24: Intraparticle diffusion parameters for DCF adsorption by different SpECs involving steps a and b.....	127
Table 25: Isotherm parameters for the adsorption of DCF by different SpECs types.	128
Table 26: DCF adsorption efficiency of 5 g of low iron sand (10 mg/L).	134
Table 27: Yoon-Nelson model parameters for DCF adsorption by SpECs(3) (1 g) at 10 mg/L and 60 mg/L DCF dosage.	136
Table 28: Yoon-Nelson model parameters for DCF adsorption (C_0 at 10 mg/L) by SpECs(3) (3 g) at two different flow rates.....	138
Table 29: Yoon-Nelson model parameters for DCF adsorption (C_0 at 10 mg/L) by SpECs(2)APSH (0.5 g) at two different flow rates.	139
Table 30: DCF recovery rates after washing the packed SpECs(2)APSH with ethanol.	141
Table 31: Yoon-Nelson parameters and sorption capacities for the adsorption of DCF (10 mg/L) by 0.5 g SpECs(2)APSH at two different flow rates.	143
Table 32: Yoon-Nelson model parameters for SpECs(3)AM (0.2 g) and DCF adsorption (10 mg/L initial concentration) at two different flow rates.....	145
Table 33: DCF recovery after washing the packed-bed of SpECs(3)AM with ethanol.....	147

Table 34: Comparison of the Yoon-Nelson model parameters for SpECs(3)AM (0.2 g) and DCF adsorption (10 mg/L initial concentration) at two different flow rates and for two cycles of use.	150
Table 35: Comparison of maximum adsorption capacities of SpECs(3)AM depending on the date of use after production.....	153
Table 36: Comparison of TCS concentrations ($\mu\text{g/mL}$) before and after filtration.	166
Table 37: Adsorption isotherm parameters for the adsorption of TCS by different types of SpECs analysed with the Langmuir and Freundlich models.	175
Table 38: TCS adsorption efficiency of 5 g of low iron sand (10 mg/L).....	176
Table 39: Yoon-Nelson parameters and sorption capacities for the adsorption of TCS (10 mg/L) by 0.2 g SpECs(3) at two different flow rates.....	180
Table 40: Yoon-Nelson parameters and sorption capacities for the adsorption of TCS (10 mg/L) by 0.2 g SpECs(3) at two different flow rates.....	184
Table 41: Comparison of E2 absorbance signals before and after filtration.	204
Table 42: Kinetic parameters for E2 adsorption by different SpECs described by different models.	208
Table 43: Intraparticle diffusion parameters for E2 adsorption by different SpECs.....	213
Table 44: Isotherm parameters for the adsorption of E2 by different types of SpECs.	216
Table 45: E2 adsorption efficiency of 5 g of low iron sand.....	220
Table 46: Yoon-Nelson parameters and sorption capacities for the adsorption of E2 by SpECs(1).	222
Table 47: Yoon-Nelson parameters and sorption capacities for the adsorption of E2 (6 mg/L) by 0.2 g SpECs(1) at two different flow rates.....	225
Table 48: The different sources and concentrations of phosphates in the aquatic environment. ³⁸⁶ ...	230
Table 49: Comparison of phosphates absorbance signals before and after filtration.....	238
Table 50: Results obtained from elemental analysis for CHN and ICP-OES for Fe for SpECs and Fe loaded SpECs in water.	240
Table 51: Results obtained from elemental analysis for CHN and ICP-OES for Fe for SpECs and Fe loaded SpECs in water under vacuum.	241
Table 52: Kinetic parameters for phosphates adsorption by Fe/water loaded SpECs (under vacuum) described by different models.	244
Table 53: Results obtained from elemental analysis for CHN and ICP-OES for Fe for SpECs and Fe loaded SpECs in acetone under vacuum.	245
Table 54: Kinetic parameters for phosphates adsorption by Fe/acetone loaded SpECs (under vacuum) described by different models.	247
Table 55: Adsorption capacities of the different Fe loaded SpECs against phosphates.	247

TABLE OF EQUATIONS

Equation 1	13
Equation 2	13
Equation 3	14
Equation 4	14
Equation 5	14
Equation 6	17
Equation 7	17
Equation 8	18
Equation 9	19
Equation 10	19
Equation 11	19
Equation 12	20
Equation 13	86
Equation 14	88
Equation 15	119
Equation 16	119
Equation 17	121
Equation 18	123
Equation 19	124
Equation 20	127
Equation 21	127
Equation 22	128
Equation 23	132
Equation 24	132
Equation 25	133
Equation 26	133
Equation 27	133
Equation 28	133
Equation 29	133
Equation 30	163
Equation 31	164
Equation 32	164
Equation 33	172
Equation 34	172
Equation 35	176
Equation 36	177
Equation 37	177
Equation 38	177
Equation 39	177
Equation 40	178
Equation 41	178
Equation 42	201
Equation 43	203
Equation 44	206
Equation 45	206
Equation 46	207
Equation 47	209

Equation 48	211
Equation 49	214
Equation 50	214
Equation 51	216
Equation 52	218
Equation 53	218
Equation 54	218
Equation 55	218
Equation 56	219
Equation 57	219
Equation 58	219
Equation 59	235
Equation 60	235
Equation 61	236
Equation 62	236
Equation 63	237

1. Introduction

1.1. Water contamination

The number of water contaminants in Europe is increasing year after year and their impact on the aquatic environment is increasingly raising concern.¹ Chemical compounds present in pharmaceuticals and personal care products (PPCPs), pesticides and detergents, are drawing more and more attention since they are indispensable components of modern life, but are also increasingly abundant in most aquatic environments.² The majority of these chemicals is not completely metabolised, resulting in a difficult removal by conventional waste water treatment plants and procedures (WWTP), posing an escalating cause of concern to human health.¹⁻⁹ Compounds contained in PPCPs are ubiquitous and persistent in water bodies and soil, posing a further threat since they can lead to multi drug resistant (MDR) microbes, antibiotic resistant bacteria (ARB) and antibiotic resistant genes (ARGs). According to a report published in 2014,¹⁰ it is estimated that antimicrobial resistance could be the cause of 10 million deaths per year by 2050.

Pharmaceuticals is a term which covers a large group of organic molecules with several subcategories, such as antibiotics, hormones, anti-inflammatory and analgesic drugs, anti-cancer drugs, antidepressants and many more. In Europe alone, the number of different compounds referred to as pharmaceuticals has been reported to be around 3000.¹ There are several pathways of water contamination with pharmaceutical compounds (**Figure 1**), with healthcare facilities, households and pharmaceutical industries being the main sources. Human waste is a significant source of water contamination since urine and faeces contain a significant load of pharmaceutical compounds.¹¹ Almost 70% of the consumed compounds leave the human body either unmetabolized as active ingredients, or as metabolites *via* urine.⁴ Of

particular concern is that many of these chemicals are suspected to be endocrine disrupting chemicals (EDCs) for organisms, including humans.^{1,3}

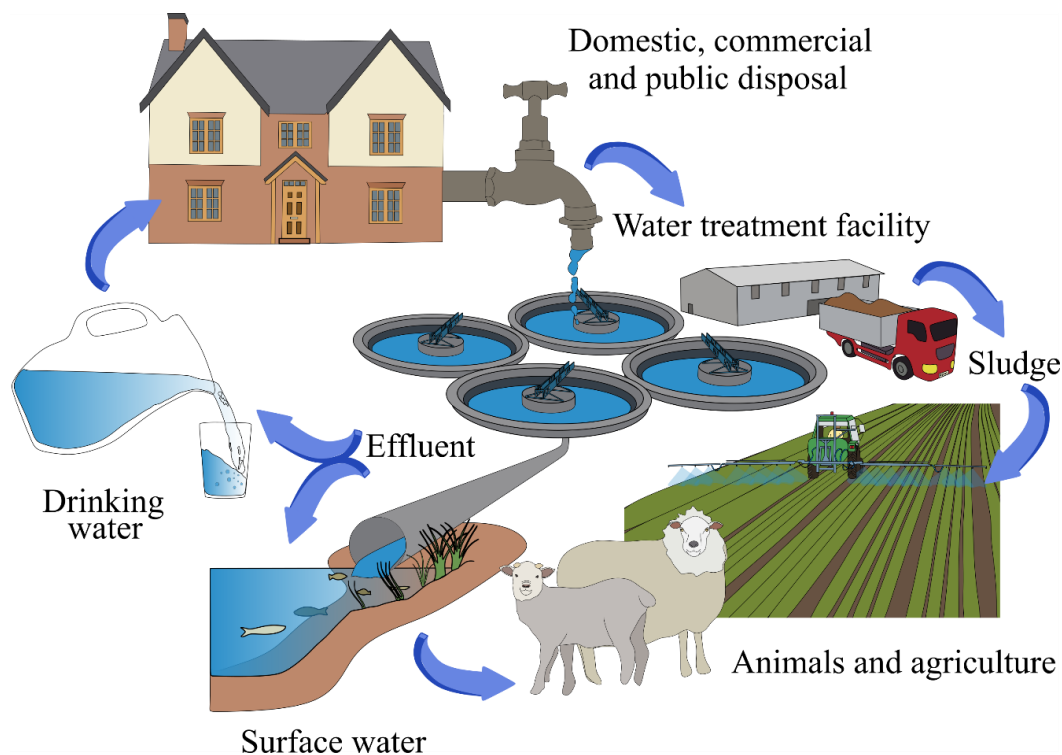


Figure 1: Different pathways of PPCPs reaching the environment.

EDCs are chemical compounds that are able to mimic, block or disrupt the synthesis and metabolism of natural hormones in humans and wildlife, therefore affecting their reproductive systems, **Figure 2**.^{12,13} Even at concentrations as low as ng/L they can cause reproductive and other anomalies involving feminization of male or masculinization of female fish populations.¹⁴⁻¹⁹ In humans, exposure to EDCs has been proven to provoke conditions involving the reproductive,²⁰⁻²⁴ immune^{25,26} and neurological^{27,28} systems or cause developmental dysfunctions.^{29,30} Analyses have revealed that EDCs are present in all waters, including treated and untreated wastewaters, surface waters, groundwaters and even drinking waters.³¹⁻³³ Studies have confirmed that fish that live close to WWTPs, discharge points or

treatment plants, are exposed to EDCs and are already showing hormonal changes or in some cases, affected by population level decline.³⁴⁻³⁶ Additionally, a concerning factor is that EDCs are often present in the aquatic environment in the form of a mixture, showing higher toxicity compared to being on their own, due to synergistic effects.³⁷

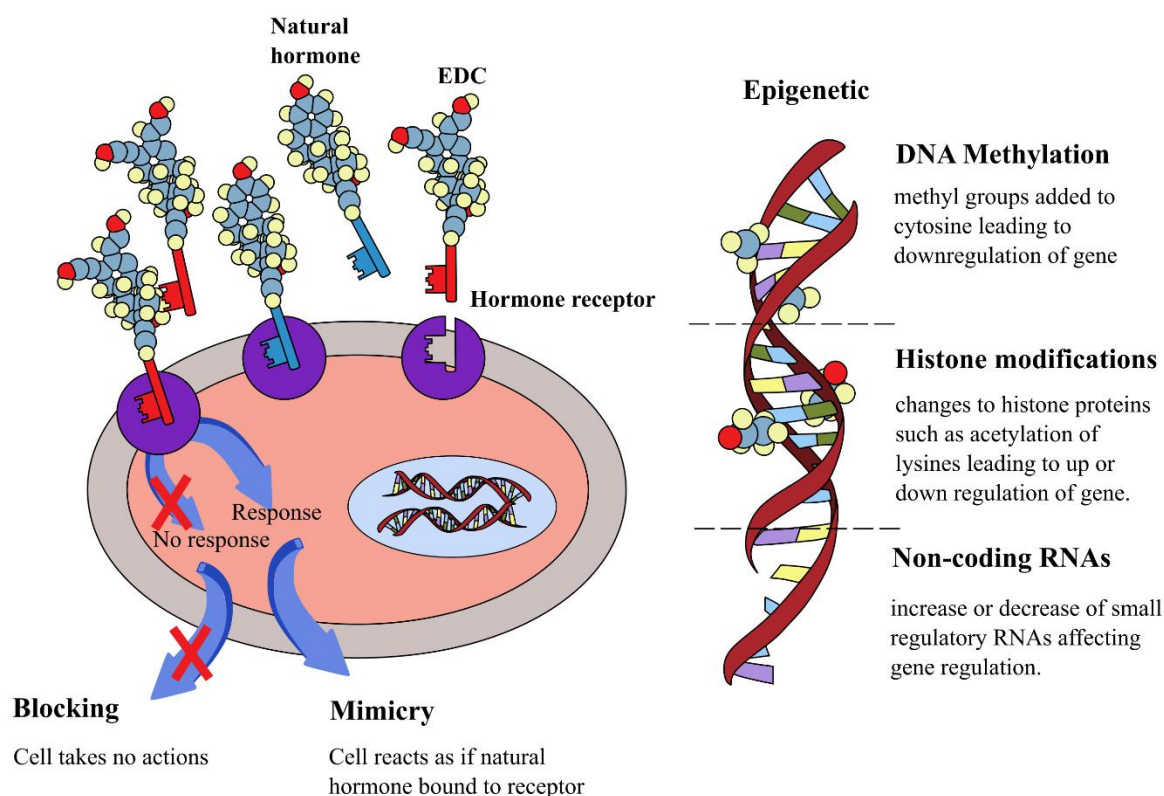


Figure 2: Mode of action of EDCs inside an organism.

Ternes *et al.*⁸ reported that in an investigation of water contamination, 32 compounds and their residues were tested and 80% of the selected compounds were found in effluents of at least one sewage treatment plant in Germany. Concerning rivers and streams, 20 compounds were detected and 4 corresponding metabolites.⁸ In a recent study of water pathways contamination,⁵ 400 UK households were investigated for their methods of pharmaceutical disposal. The participants were asked what they do with their unused or expired drugs and 63.2% replied that they throw them in the bin, 21.8% returns them to the pharmacist and 11.5% discards them into

the sink or toilet. A similar scenario was observed in Germany, where it is estimated that 16000 tonnes of pharmaceuticals are disposed every year with 60 - 80% going directly into the toilets or into household waste.⁷ In the U.S., analyses of surface and groundwater revealed more than 70 different compounds, while there is no information on the ways the compounds reached the environment nor on their eventual fate.³⁸

1.1.1. EC Priority List and Watch List

In 1996, a discussion started between the European Commission (DGXII), the European Environmental Agency, the European Centre for Environment and Health and the World Health Organisation on the concerns for aquatic life being exposed and affected by chemical pollutants and the hypothesis that human health may face similar risks. This led to further research and to a collection of data with the aim of creating a list of “suspected endocrine disruptors”. The criteria for the inclusion of substances within this list were now specified and the list was named Priority List. 564 compounds were initially suggested from publications and several organisations, a number that was later reduced to 553 which formed the initial Candidate List. In the next step, 146 of these chemicals were characterised as highly persistent and based on the available evidence of their endocrine disruption effects, 118 of them were concluded to show high and medium exposure concern.³⁹

In 2015, a new mechanism was created for providing more information and monitoring the levels of emerging contaminants as well as minimising the potential risk that they would pose to the aquatic environment. The mechanism involved the monitoring across Europe of up to a maximum of 10 chemicals (emerging contaminants) for up to four years and a new list was formed. This Watch List (**Table 1**) includes the drug diclofenac and the substance oestradiol and is built to be frequently reviewed and updated according to the levels and risks of the contaminants.⁴⁰

Table 1: Substances / group of substances suggested for the First Watch List. ⁴⁰	
Substance name	Description
Diclofenac	non-steroidal anti-inflammatory drug
17-beta-estradiol (E2), Estrone (E1)	hormone
17-alpha-ethinylestradiol (EE2)	hormone
Oxadiazon	herbicide
Methiocarb	herbicide/pesticide
2,6- <i>ditert</i> -butyl-4-methylphenol	industrial use in a variety of products
Tri-allate	herbicide
Imidacloprid, Thiacloprid, Thiamethoxam, Clothianidin, Acetamiprid	neonicotinoids, plant protection products and biocides
Erythromycin, Clarithromycin, Azithromycin	human and veterinary antimicrobials
2-ethylhexyl-4-methoxycinnamate	UV filter

1.2. Water Purification

1.2.1. Conventional wastewater treatment procedures

A typical procedure for water purification is described in **Figure 3**. In the first instance, the preliminary treatment involves raw sewage passing through the screening which removes large solids such as sanitary, car tyres etc. In the grit chamber, grit stones and sand are removed, and the water is then passed to the primary clarifier. Clarifiers are usually circular or rectangular and the purification procedure relies upon gravity. This procedure lasts for at least two hours resulting in a removal of 30 - 50% of organic load and 60% of solids. The secondary treatment then takes place where sewage goes through the aeration tank and the secondary clarifier. In the aeration tank, bacteria are mixed with the sewage and O₂ is added. These microorganisms feed on pollutants present in the sewage, leaving a more purified effluent after the procedure. A secondary clarifier follows where water is separated from any remaining sludge and then chemical procedures follow (*e.g.* chlorination) disinfecting the polluted water. It will be presented in detail in the following chapters, how conventional WWTPs are not capable of the complete removal of the aforementioned emerging contaminants. It is evident, that

conventional WWTPs present many disadvantages; apart from poor removal efficiency, the generation of toxic by-products is the major one, followed by high operational costs and large energy consumption.^{41–43}

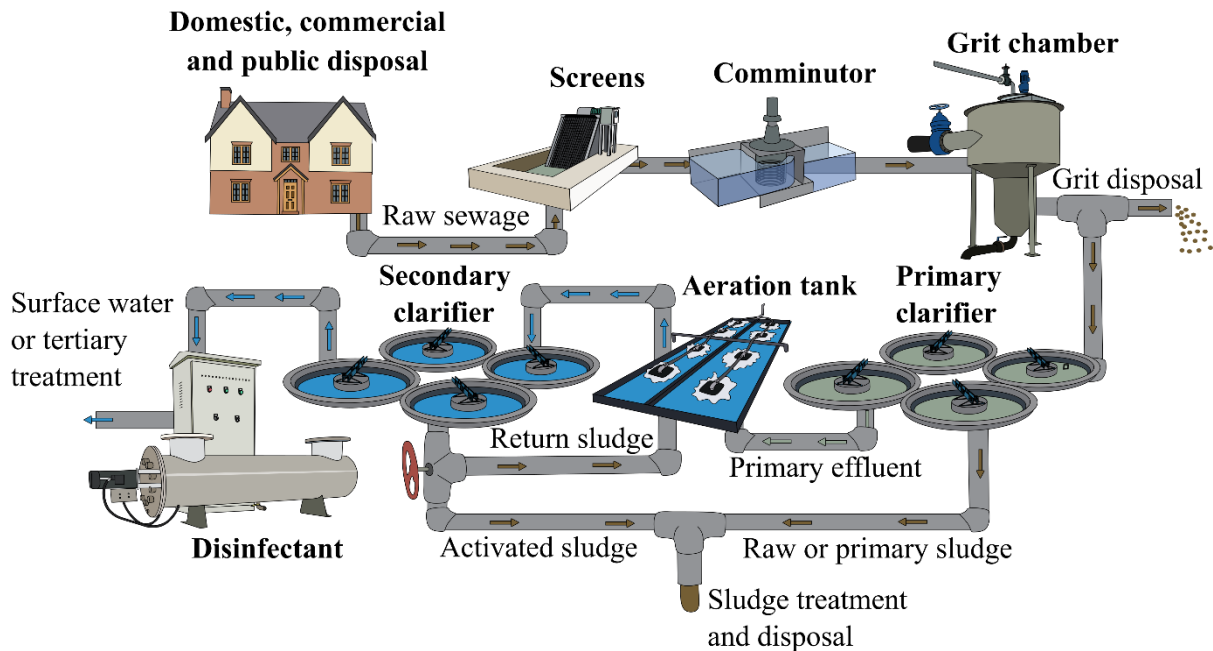


Figure 3: Primary and secondary treatment steps for water purification.

1.2.2. New techniques on wastewater treatment

The demanding solution to the problem of water contamination urges the upgrading of the existing treatment plants and has led to new ideas and experimenting. Not only new techniques are needed, but also the points where the water treatment is taking place must be of discussion. It is important that effluents from industrial facilities and hospitals are treated in source, while the contaminants are not diluted or mixed with other matters present in water. Dilution of the wastewater makes treatment more expensive and less efficient.⁴⁴

While conventional treatments (sedimentation, coagulation, sand filtration, flocculation and chlorine disinfection) have a removal efficiency of pharmaceuticals of <math><5 - 40\%</math>, nanofiltration, reverse osmosis, ozonation, activated carbon adsorption, ion exchange and

advanced oxidation/reduction processes (AO/RPs) are some of the procedures reported in the literature that are quite efficient in the removal of PPCPs.^{11,45,46}

Membrane filtration includes membrane separation systems and is often a solution for high molecular weight contaminants. Ultra-, micro- and nanofiltration, electrodialysis and reverse osmosis are some of the membrane filtration methods, with the drawbacks being the inability of treating large volumes, the severe biofouling of the membrane material and the high energy consumption because of the requirement of high operational pressures.⁴⁷ Nanofiltration and reverse osmosis have been proven to be efficient for the removal of pharmaceuticals but are highly influenced by the physicochemical properties of the contaminant (hydrophobicity, polarity, charge) and by other factors present in water: cations, natural organic matter.⁴⁸

AO/RPs have been proven to be very effective for PPCPs and require low quantities of additional chemicals but involve complex operational procedures. Throughout these processes, the decomposition of organic pollutants can be achieved through degradation mechanisms using treatments such as O₃/UV, H₂O₂/UV, O₃/H₂O₂, Fe²⁺/H₂O₂, Fe²⁺/H₂O₂/UV.⁴⁹⁻⁵¹ The formation of oxidation by-products is a major disadvantage of these techniques, the toxicity of which can sometimes be higher than the parent compound.⁴⁶ Other disadvantages include the high cost because of energy consumption and the complexity of the procedures.^{49,51}

Ozonation procedures are able to destroy some percentage of PPCPs but in some cases the oxidation may be incomplete, resulting in the formation of by-products that seem to be more toxic than the parent compounds.⁵² According to Huber *et al.* ozonation is able to oxidise a majority of some selected pharmaceuticals (including diclofenac and oestrogens) being the fastest method compared with chlorination or oxidation with ClO₂. Whereas ozonation is more efficient for some of the pharmaceuticals, resulting in the shortest half-lives of any other procedure, it is a particularly expensive method that can increase up to 40 - 50% the energy required in conventional WWTPs.^{53,54}

Ion exchange technologies have been proven to be efficient in water treatment and present a nice alternative since they do not generate any sludge. As a procedure though, it is very specific since it targets certain contaminants and it is also expensive because of the replacement of the resin after some use.⁴¹

So far, adsorption methods appear to be the most promising option for PPCPs removal, by involving mild operational conditions that are energy efficient, requiring low energy consumption and without adding any by-products to the treated water.⁵⁵ Furthermore, they present a high contaminant removal efficiency resulting in treated effluents of promising quality and provide the option of the regeneration and reuse of the adsorbent.^{43,56}

1.2.3. Adsorption

1.2.3.1. Definition

According to Faust and Aly (1986) “adsorption is a surface phenomenon that is defined as the increase in concentration of a particular component at the surface or interface between two phases”. This phenomenon occurs due to forces of attraction that occur between atoms of a solid surface and atoms of gas or liquid. The second law of thermodynamics explains adsorption as a process to reduce the free surface energy of the solid. The result is a process where a solid material (adsorbent or sorbent) is used for the removal of specific gas or liquid substances (adsorbate or sorbate). Depending on these forces of attraction, adsorption can be distinguished into physisorption, chemisorption or electrostatic sorption.^{57,58}

Physisorption is an exothermic phenomenon where weak intermolecular forces (Van der Waals) take place with no electron transfer or electron sharing between the adsorbent and the adsorbate. Due to the weak nature of the interactions, the adsorption is easily reversible by heating and the physisorbed molecule keeps its structure and identity. If desorption occurs, the molecule can be obtained in its original form without any changes to the structure. The energy

involved is of the range of 15 - 30 kJ/mol. Physisorption is a general, non-site-specific phenomenon, where the physisorbed molecules can attach to any part of the surface of the material and can form multilayers. Being an exothermic phenomenon, physisorption increases when temperature decreases and is only stable for temperatures below 150 °C.⁵⁸⁻⁶⁰

Chemisorption is an irreversible procedure where stronger interactions occur involving the transfer of electrons and the formation of chemical bonds between the adsorbent's surface and the adsorbate. The chemisorbed molecules are bound to the surface of the material at specific reactive sites, and they cover it by forming a monolayer. In this phenomenon the molecules do not keep their individuality due to the interactions with the surface and they cannot be recovered by desorption. They may break down to fragments and get trapped onto the adsorbent's surface. Chemisorption tends to increase with the increase of temperature and the energy involved is of several hundred kJ/mol, which is significantly higher than physical adsorption meaning that it can be more stable at high temperatures.⁵⁷⁻⁶⁰

Electrostatic sorption is a term used specifically for indicating the ion exchange between the contaminant's molecules and the adsorbent. It involves a solid with charged functional groups that is able to form Coulomb attractions with the adsorbed sorbate's ions.⁵⁸

1.2.3.2. Adsorption isotherms

The word isotherm derives from the two Greek words: isos, meaning equal and thermo, meaning heat. An adsorption isotherm is a curve that depicts the process of occupancy of a solid by a substance present in a mobile phase (gas or liquid), at a constant temperature and pH.⁶¹ This curve is important because it gives significant information on the mechanisms through which the substance is being attached to the solid material. It specifies the physicochemical and thermodynamic parameters such as sorption mechanisms, surface properties and adsorption capacity of the adsorbent.⁶² Adsorption isotherms are equilibrium

equations. This means that the system containing both the adsorbate and the adsorbent must be left for a sufficient amount of time to interact and reach equilibrium. The equilibrium is obtained when the adsorbent no longer interacts with the adsorbate and the adsorption and desorption rates are equal.^{63,64}

1.2.3.2.1. Classification of adsorption isotherms

An adsorption isotherm is built by plotting the amount of adsorbate onto the adsorbent (described by the letter x or Q_e) against the amount of adsorbate left in the solution (equilibrium concentration C_e). Giles *et al*, have divided the resulting graph (isotherms) into four categories, depending on their slope (**Figure 4**). This allows one to determine the ways the adsorption happens and come to valuable conclusions.⁶⁵

In the C-type adsorption isotherm (**Figure 4a**) the ratio between the equilibrium concentration and the amount of the compound trapped onto the adsorbent remains constant at any given time. This ratio (the line's slope) is called partition coefficient or distribution coefficient K_b (L/kg). This type of isotherm proposes that the adsorbate has a higher affinity towards the adsorbent rather than towards the solvent that it is diluted in.

The L-type isotherm (**Figure 4b**) describes a concentration dependant system where the slope gradient is decreasing whilst the adsorbate's concentration increases. In this system, the adsorbent is progressively saturated meaning that as the concentration of the adsorbate increases, the surface is covered, and the vacant sites are more difficult to find. This type is often used to describe systems working at low concentrations of adsorbate.

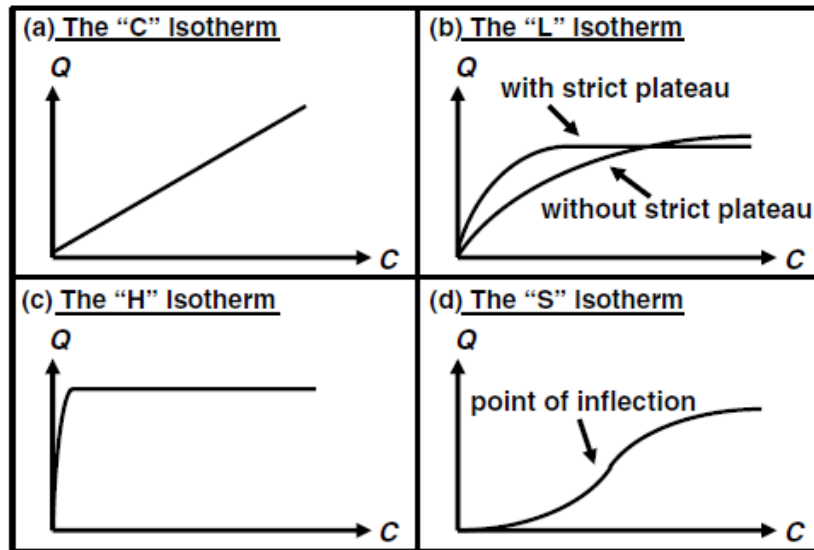


Figure 4: The four different types of adsorption isotherms according to Limousin *et al.* and Giles *et al.*^{61–65}

The H-type isotherm (**Figure 4c**) is a high-affinity isotherm where the first molecules are being adsorbed very rapidly and strongly. This curve presents a rapid rise of the initial slope showing that occupied sites can still retain adsorbate molecules, so the number of potential sites increases. When all sites are occupied and the saturation point is reached, the slope decreases. This curve suggests a very high affinity of the adsorbate towards the adsorbent.

The S-type isotherm (**Figure 4d**) the sigmoidal curve illustrates that the adsorption process is divided into two parts. The first part, before the point of inflection, is where the adsorbate has a low affinity towards the adsorbent and it takes some time to cover its surface. As soon as the surface is covered, after the point of inflection, the adsorbate covering the adsorbent's surface acts like a new adsorbent and attracts and adsorbs the rest of the adsorbate molecules (cooperative adsorption, **Figure 5**).^{60,63,66}

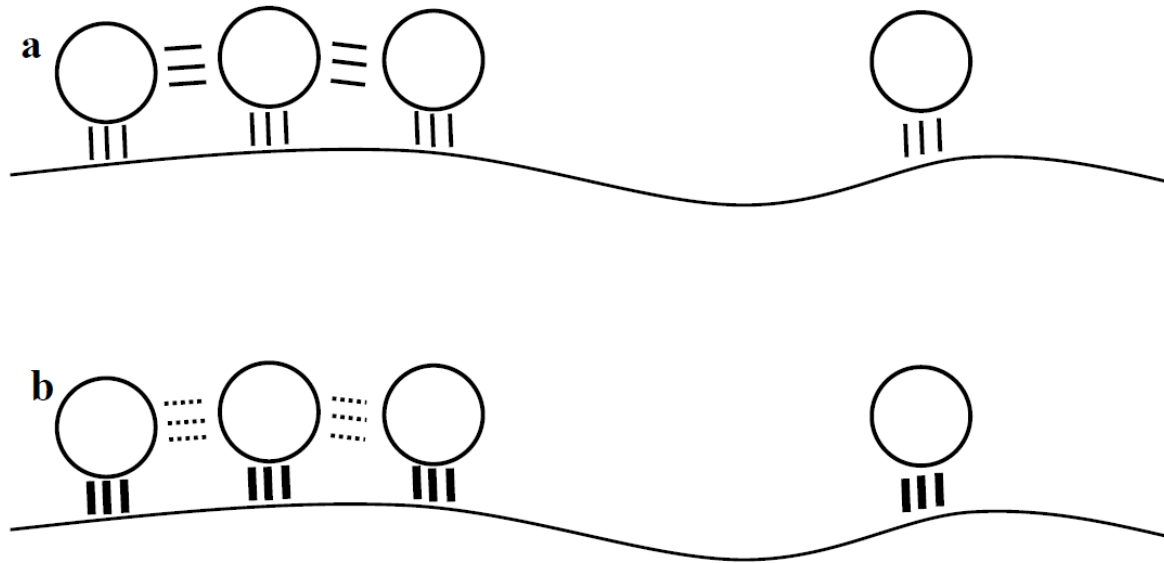


Figure 5: The adsorbent's surface and the adsorbate molecules. (a): Forces of attraction (lines) between the adsorbate molecules and the surface are equal. The molecules are adsorbed more strongly in the left position than in the right, where the only forces towards the molecule are these of the surface. This phenomenon of cooperative adsorption is described by S-type isotherms (b): Strong forces of attraction (thicker lines) between the surface and the adsorbate molecules, very weak forces (dots) between the molecules. The adsorption strength is equal between the right and the left position. This type of adsorption is described by L or H isotherms.⁶⁵

The two most well-known and widely used models for the description of solid - liquid adsorption are the Langmuir, described by the L or S type isotherm, and the Freundlich. Both models are described by two parameter isotherm equations.

1.2.3.2.2. Langmuir model

The Langmuir equation is a theoretical model which is based on the assumption that the surface of the adsorbent has a finite number of identical adsorption sites (homogenous surface in terms of binding energy), where each site is able to retain only one molecule of adsorbate. Once this site is occupied, no further adsorption can occur at this specific site. Langmuir's model assumes that the adsorption is uniform on the surface of the adsorbent resulting in the formation of a

saturated monolayer at maximum adsorption.^{67,68} This maximum adsorption is graphically depicted by a plateau which is a characteristic of Langmuir's isotherm model and means that when the saturation point is reached, no further adsorption can take place.⁶⁹ The extent of the coverage of the material's surface is highly dependent on the concentration of the adsorbate. This model also assumes that there are no interactions between the adsorbed molecules (lateral interactions) and that the adsorption is reversible.⁵⁸

In the Langmuir's equation (*Equation 1*), Q_e (mg/g) is the amount of the compound adsorbed per amount of adsorbent. Q_m (mg/g) is the maximum adsorption capacity of the material (adsorbent), K_L (L/mg) is the Langmuir adsorption equilibrium constant, and C_e (mg/L) is the concentration of the adsorbate at equilibrium. Langmuir's constant is a measure of the intensity of the adsorption process, and Q_m indicates the amount of adsorbate needed for a complete monolayer.

$$Q_e = \frac{Q_m K_L C_e}{1 + K_L C_e} \quad \text{Equation 1}$$

The above equation can be rearranged to the following linear form (*Equation 2*) which is useful for the calculation of Q_m and K_L (slope = $\frac{1}{Q_m}$, intercept = $\frac{1}{Q_m K_L}$).

$$\frac{C_e}{Q_e} = \frac{C_e}{Q_m} + \frac{1}{K_L Q_m} \quad \text{Equation 2}$$

The dimensionless constant R_L is the separation factor or Langmuir's equilibrium parameter and it indicates whether the adsorption is favourable or not (*Equation 3*).

$$R_L = \frac{1}{1 + K_L Q_m} \quad \text{Equation 3}$$

For $R_L > 1$, the adsorption is unfavourable, whereas for $0 < R_L < 1$ it is favourable. When $R_L = 0$ the adsorption is irreversible and when $R_L = 1$ the isotherm is linear.^{58,70}

1.2.3.2.3. Freundlich model

Freundlich's model describes a non-ideal, multisite, and reversible adsorption of L or H isotherm type. It is an empirical model where the adsorbent's surface is heterogeneous, which means that the binding sites on its surface are of various energies and thus affinity towards the adsorbate.⁵⁹ This type of adsorption has no restrictions in the number of layers forming onto the material's surface and it can happen in multilayers.^{63,68} Freundlich's model is characterised by the heterogeneity factor $1/n_F$, a factor that shows how favourable the adsorption is and its isotherm does not reach a plateau like Langmuir's model. Freundlich's isotherm is expressed by *Equation 4*.

$$Q_e = K_F C_e^{1/n_F} \quad \text{Equation 4}$$

where Q_e (mg/g) is the amount of compound adsorbed per amount of adsorbent, C_e (mg/L) is the equilibrium concentration and K_F and n_F are Freundlich's constants. By using the linear form of Freundlich's equation (*Equation 5*) the two Freundlich's constants can be calculated.

$$\log Q_e = \log K_F + \frac{1}{n_F} \log C_e \quad \text{Equation 5}$$

K_F ($\text{mg}^{(1-1/n)}/\text{gL}^{-1/n}$) is related to the material's adsorption capacity and can be calculated from the intercept of *Equation 5* ($\log K_F$). It represents the quantity of adsorbate adsorbed in mg/g adsorbent when C_e equals one.⁷¹ n_F is the heterogeneity factor of adsorption sites indicating the adsorption intensity and it is dimensionless. It can be calculated from *Equation 5* where the slope equals $\frac{1}{n_F}$. The slope $\frac{1}{n_F}$ gives valuable information about the adsorption processes: it specifies the heterogeneity of the adsorbent's surface becoming more heterogeneous for values closer to zero. For values above one, the adsorption is implied to be cooperative, whereas for values below one the model is better described by the Langmuir isotherm or chemisorption is implied.⁷²

1.2.3.3. Adsorption kinetics

A kinetic study examines the rate of the adsorption which can include limiting factors such as temperature and pressure conditions as well as the physicochemical properties of the adsorbent and the contaminant. The progress of the adsorption process through time is referred to as adsorption kinetics and is the determining factor for the required time for reaching equilibrium. In general, kinetic models provide useful information about the adsorption pathways and the possible mechanisms involved.^{58,73}

There are two main characteristics that are involved in the adsorption process: interparticle and intraparticle diffusion. Resistance to external diffusion/interparticle diffusion, involves the mass transfer from the bulk fluid to the external surface of the material, whereas intraparticle diffusion describes the mass transfer from the external surface of the material to the internal porous structure.⁷³

For adsorption procedures at the solid-liquid interface, the process of adsorption is generally described as a multi-step procedure, mainly involving four diffusion steps:

1. Bulk diffusion, where the adsorbate is transferred from the bulk liquid phase to the boundary layer around the adsorbent particle.
2. Film diffusion or external diffusion, where the adsorbate is transferred from the boundary layer onto the external surface of the adsorbent particle.
3. Intraparticle diffusion or internal diffusion, where the adsorbate is transferred into the interior of the adsorbent particle *via* pore or surface diffusion.
4. Adsorption and energetic interaction of the adsorbate and the adsorbent's active sites by physisorption or chemisorption *via* ion exchange, chelation and/or complexation pathways.^{58,74,75}

In general, it is assumed that the first and fourth step happen relatively fast compared to the other two and that the rate limiting steps are film and intraparticle diffusion. Usually, mass transfer within the adsorbent happens in parallel by pore and surface diffusion, processes that are difficult to differentiate.⁷⁵

In order to understand the adsorption procedure in detail there exist various mathematical models (pseudo-first order, pseudo-second order, intraparticle diffusion) that can be applied to the experimental data, giving information on the characteristics of the process. For systems that are more complex, there may exist a combination of two or more steps that are responsible for the total rate of the adsorption. After analysis with the various models, the adsorption kinetic constants can be obtained and by comparison of the R^2 values (regression correlation coefficient) the best fit model can be determined.⁵⁸ For the removal of PPCPs from water, adsorption kinetics are mostly described using the pseudo-first and pseudo-second order mathematical models.

1.2.3.3.1. Pseudo-first order model

Lagergren's model⁷⁶ is based on the assumption that the rate the solute uptake changes over time is directly proportional to the difference in the concentration of the saturated solution and the amount of solid uptake over time. This assumption can only be applied in the initial stages of the adsorption process and means that the adsorption procedure happens through diffusion through the interface. The linear form of the equation is expressed as follows (*Equation 6*):^{58,74}

$$\ln(q_e - q_t) = \ln q_e - k_1 t \quad \text{Equation 6}$$

where q_t (mg/g) is the amount of solute adsorbed per mass of adsorbent after a certain contact time t (min), q_e (mg/g) is the amount of solute adsorbed at equilibrium and k_1 (min^{-1}) is the pseudo-first order rate constant. From the plot $\ln(q_e - q_t)$ versus t the values of k_1 (slope) and $\ln q_e$ (intercept) are determined, from which the value of the maximum adsorption capacity $q_{e1,cal}$ can be calculated.

1.2.3.3.2. Pseudo-second order model

The pseudo-second order kinetic model describes adsorption processes that have as a rate limiting step chemisorption interactions. In this model, the adsorption is dependent on the adsorption capacity of the material and not on the concentration of the adsorbate that was for the pseudo-first order model. The model is described by *Equation 7*.⁷⁷

$$\frac{1}{q_t} = \frac{t}{q_e} + \frac{1}{k_2 q_e^2} \quad \text{Equation 7}$$

where q_t , q_e and t represent the same variables as for the previous model, q_t (mg/g) is the amount of solute adsorbed per mass of adsorbent after a certain contact time t (min) and q_e (mg/g) is the amount of solute adsorbed at equilibrium. k_2 (g/mg min) is the pseudo-second order equilibrium rate constant. The slope and intercept derived from the plots of t/q_t versus t are used to calculate the values of the maximum adsorption capacity $q_{e2,cal}$ and the rate constant k_2 .

1.2.3.3.3. Intraparticle diffusion

The diffusion mechanisms during the adsorption process can be identified with the intraparticle diffusion model, which considers that the predominant mechanism is intraparticle diffusion and is thus the rate controlling step. The model is described by Equation 8:⁷⁸

$$q_t = k_i t^{0.5} + I \quad \text{Equation 8}$$

where q_t (mg/g) is the amount of solute adsorbed per mass of adsorbent at time t (min), k_i (mg/g min^{0.5}) is the rate constant for the intraparticle diffusion model and I (mg/g) is the intercept which indicates the boundary layer thickness effect. The values of k_i and I can be obtained by the slope and intercept of the linear plot qt versus $t^{0.5}$. If the adsorption process involves intraparticle diffusion then the plot qt versus $t^{0.5}$ is a straight line. The I value portrays the thickness of the boundary layer; the larger its value, the greater the boundary layer effect.⁵⁸

1.2.3.3.4. Continuous packed-bed adsorption

For large-scale WWT and not small-scale lab experiments, packed-bed reactors are preferred for PPCP removal, mainly due to their simplicity and their high removal efficiency.⁷⁹

Packed-bed adsorption is a time and distance dependent process that involves a column, tightly packed with the adsorbent, through which the contaminated water passes of certain concentration and flow rate. The contaminant molecules come into contact with the material, allowing the adsorption and the mass transfer to happen.⁸⁰ Breakthrough curves are a useful outcome of the experimental packed-bed adsorption, relating the outlet to inlet contaminant concentration *versus* time or treated volume. Breakthrough curves are an essential tool for the design of large-scale packed-bed reactors.⁷⁵ The most common model used to analyse the experimental data is the Yoon-Nelson model (*Equation 9*), expressed as:⁸¹

$$C_t/C_0 = 1/[1 + \exp(K_{YN}\tau - K_{YN}t)] \quad \text{Equation 9}$$

where, C_t (mg/L) is the contaminant's concentration at time t (min), C_0 (mg/L) is the initial contaminant concentration, K_{YN} (min^{-1}) is the Yoon-Nelson rate constant and τ (min) is the time required for 50% adsorbate breakthrough. K_{YN} and τ can be calculated from the linear form of the equation (*Equation 10*) by plotting $\ln [C_t/(C_0 - C_t)]$ *versus* t .

$$\ln \left(\frac{C_t}{C_0 - C_t} \right) = K_{YN}(t - \tau) \quad \text{Equation 10}$$

The sorption capacity of the material q_0 (mg/g) can be calculated by using *Equation 11*:

$$q_0 = \frac{C_0 Q \tau}{m} \quad \text{Equation 11}$$

where Q is the flow rate (L/min) and m (g) is the mass of sorbent used in the column. This calculated value (q_0) can then be compared to the experimental one ($q_{0,exp}$), defined by

Equation 12:

$$q_{0,exp} = \frac{m_{DCF\ tot} - m_{DCF\ ads}}{m} \quad \text{Equation 12}$$

where m_{tot} (mg) is the total mass of contaminant that passed through the packed material, m_{ads} (mg) is the adsorbed contaminant mass and m (g) is the mass of sorbent used in the column.

1.2.3.4. Factors affecting adsorption

There are several factors affecting the efficiency of the adsorption process, including the physicochemical properties of the contaminants, the properties of the material used, the solvent, the pH as well as the temperature and the different operational conditions.⁸²

1.2.3.4.1. Contaminant properties

The physicochemical properties of the contaminants present in the environment play an important role in both their behaviour and on their removal, since these properties affect the fate of the contaminant in the environment.⁸³ Two important properties are water solubility, S_w , and the octanol/water partition, K_{ow} . S_w is highly dependent on the environmental conditions, such as temperature, pressure, pH, ionic strength or the existence of dissolved and suspended organic matter.⁸³ K_{ow} , is the ratio of the concentration of an organic compound in n-octanol and water at equilibrium for a specific temperature. It is used for describing the tendency of a compound to adsorb to soil and living organisms and it is related to S_w and bioconcentration factors for aquatic life. Low K_{ow} values (less than 10) mean that the organic compound is considered hydrophilic, having a high S_w .⁸³ Sorption procedures are highly dependent on the

hydrophilicity or hydrophobicity of the compound. Compounds with high K_{ow} values (greater than 10) have high sorption potential, meaning that during the primary sedimentation step, these chemicals may adsorb onto sludge.^{83,84} The volatility of the compound is another important factor since the Henry's constant can determine whether the substance can be removed from water by volatilization (compounds with $H_c \geq 10^{-3} \text{ atm mol}^{-1} \text{ m}^{-3}$).⁸⁵ For organic contaminants, adsorption happens through hydrophobic interactions whereas for polar compounds, ion exchange interactions are a possible mechanism of adsorption.⁸⁶

1.2.3.4.2. Adsorbent properties

The performance of a material (sorbent) on removing a contaminant by adsorption is highly dependent on its physicochemical properties: surface area, pore size distribution, surface charge, oxygen content.⁸⁶ An ideal candidate for contaminant adsorption should present a variety of features, with the most important being its low-cost production, its availability for purchasing and its chemical and mechanical stability. Good physicochemical properties will equip the material with high adsorption capacity, efficiency and fast adsorption kinetics, features that will vary in priority depending on the contaminant. Furthermore, the material's potential for regeneration and reuse is an extra feature that will not only reduce the operational costs but will also provide an environmentally friendly approach.⁸⁷

1.2.3.5. Materials for contaminant adsorption

There is a variety of adsorbents mentioned in the literature, with activated carbon being at the top of the list mainly owing to the material's large surface area, its surface chemistry and microporosity. Production of activated carbon is a long procedure that starts by the crushing of biomass into small particles of specific size and drying them at around 100 °C. The carbonization step follows in dry and inert atmosphere at 300 - 500 °C, leading to the formation

of biochar. The last step involves the activation of the carbonized material, by physical or chemical activation. Physical activation involves treatment of the sample with inert gases, CO₂, N₂ etc., or steam at high temperatures between 700 and 900 °C. Chemical activation involves treatment of the sample with a reagent, acid or base usually H₃PO₄ or KOH, followed by heating at 300 - 500 °C and washing for neutralising the pH. Depending on the activation, different porosities and different surface areas can be obtained of the final material. Modification steps can be added to the procedure including pyrolysis at temperatures between 550 and 900 °C.⁸⁸⁻⁹⁰ Activated carbons are reported to be very effective in contaminant adsorption from water, including PPCPs, dyes, organic pollutants and heavy metals.⁸⁸

Although activated carbon presents a good adsorption efficiency, the high cost of the material, the high energy demands for production and the high regeneration costs are a considerable drawback to its use in WWTPs.^{91,92} The demand for low-cost adsorbents has given rise to new research on non-conventional materials.^{93,94} There is a wide variety of low-cost material families presented in the literature such as clays, metal organic frameworks (MOFs), biochar, agro-industrial residues and chitosan.⁹⁵

Clays are natural phyllosilicates presenting high specific area, mechanical and chemical stability and ion exchange capacity.⁹⁶ Kaolinite, serpentine, talc, smectite, pyrophyllite and vermiculite are some of the materials belonging to this family of low-cost adsorbents. Their adsorption capacity for PPCPs is highly dependent on their chemical and pore structure.^{93,96,97}

MOFs are crystalline materials produced by bridging metal ions or clusters to organic ligands leading to the formation of one-, two- or three- dimensional networks.⁹⁸ Some of their characteristics are the large variety in size and functionality, their big surface area (1000 - 10000 m²/g), the adjustable physicochemical properties and their high pore volume.^{99,100} Although their features seem promising, not enough research has been conducted in the field of PPCPs adsorption, mainly because of the challenges they present; they are unstable in water

and there is a risk of metal leaking of the material itself, posing a secondary water contamination possibility.^{101,102}

Biochar is produced by different materials that are pyrolyzed at temperatures between 300 and 700 °C. It is a carbon-rich material that has presented high sorption capacity and affinity towards PPCPs. Compared to activated carbon, biochar is produced at lower temperatures whereas for the activation of activated carbon temperatures above 700 °C are needed.¹⁰³ Furthermore, the production of biochar produces lower CO₂ emissions as well as offering the possibility of using by-products as feedstock.¹⁰⁴

Agro-industrial residues can be used to produce biochar or activated carbon, or used directly for the removal of contaminants in water, including PPCPs.⁵¹ Cellulose is the primary component of agro-industrial residues and is the main contributor to its adsorption properties, including others such as lignin, lipids, hemicellulose, hydrocarbons, sugars, starch and proteins.^{105,106} Even though the adsorption efficiencies of these materials are not as good as activated carbon's, their high abundance, lower cost and their renewable nature make them an attractive alternative for industrial scale applications.^{107–109}

Chitosan is produced by the alkaline *N*-deacetylation of chitin found in the shells of crustaceans.^{93,110} It is a polysaccharide rich in hydroxyl and amino groups, chemically stable, showing excellent chelation behaviour and promising results in the adsorption of PPCPs.⁹⁴ Although it is a more environmentally friendly material than activated carbon, its production is quite challenging since the source of the polysaccharide and the deacetylation degree affect its adsorption properties. Another disadvantage is chitosan's chemical characteristics, preventing its use in large-scale systems because of column fouling and hydrodynamic restrictions.⁹⁴

Sporopollenin is a promising biopolymer that is ubiquitous in nature, offers low-cost production, and it is very stable both chemically and mechanically. It offers good potential as

a regenerative material and has shown good adsorption efficiency for a variety of contaminants.¹¹¹⁻¹¹⁹ Some research has been conducted on heavy metal and ions removal using sporopollenin as an adsorbent exhibiting some encouraging results¹¹¹⁻¹¹⁵ as well as pesticide and PPCPs adsorption.¹¹⁶⁻¹¹⁹

1.3 Aims and Objectives

This thesis will focus on the possibilities and the potential of sporopollenin use as an adsorbent for contaminant removal from water. The adsorption of diclofenac, triclosan, oestradiol and phosphates will be examined by analysing the adsorption kinetics and the adsorption behaviour and regenerating possibilities of the material. The aims of the thesis are to reveal the best conditions of sporopollenin exine capsules extraction regarding their adsorption efficiency targeting these four contaminants. Apart from different extractions, a variety of surface modifications will be tested in order to optimise the material for the adsorption of each individual contaminant. After specifying the optimal extraction and surface modification conditions that produce the best adsorbent, the kinetics of the adsorption procedure will be analysed under different settings. The adsorption isotherms will give an insight on the mechanisms involved in the adsorption procedure, providing information on the possible interactions between the material and the contaminant molecules. The packed-bed studies will reveal the material's potential for real world applications and will also determine its adsorption capacity for each contaminant. The possibility of regeneration/reuse of the adsorbent will also be examined, together with the appropriate regenerating agent.

2. Sporopollenin Exine Capsules

2.1. Pollens and spores

Pollen grains and spores are part of the reproductive system of flowering and non-flowering plants respectively.^{6,120} In order for the grains or spores to protect their fragile contents, nature has developed a double layered wall structure that provides protection against harmful radiation and other threats that these physiological containers may face during their journey. The inner wall is a layer rich in cellulose, pectin and other polysaccharides, and is called the intine (**Figure 6**).^{6,121} The outer wall, known as the exine, consists of a very resistant and stable organic polymer, sporopollenin.^{122,123} While the intine layer is water permeable, the exine wall is water impermeable but has apertures through which the intine is exposed and thus important nutrients are able to reach the interior.¹²⁴

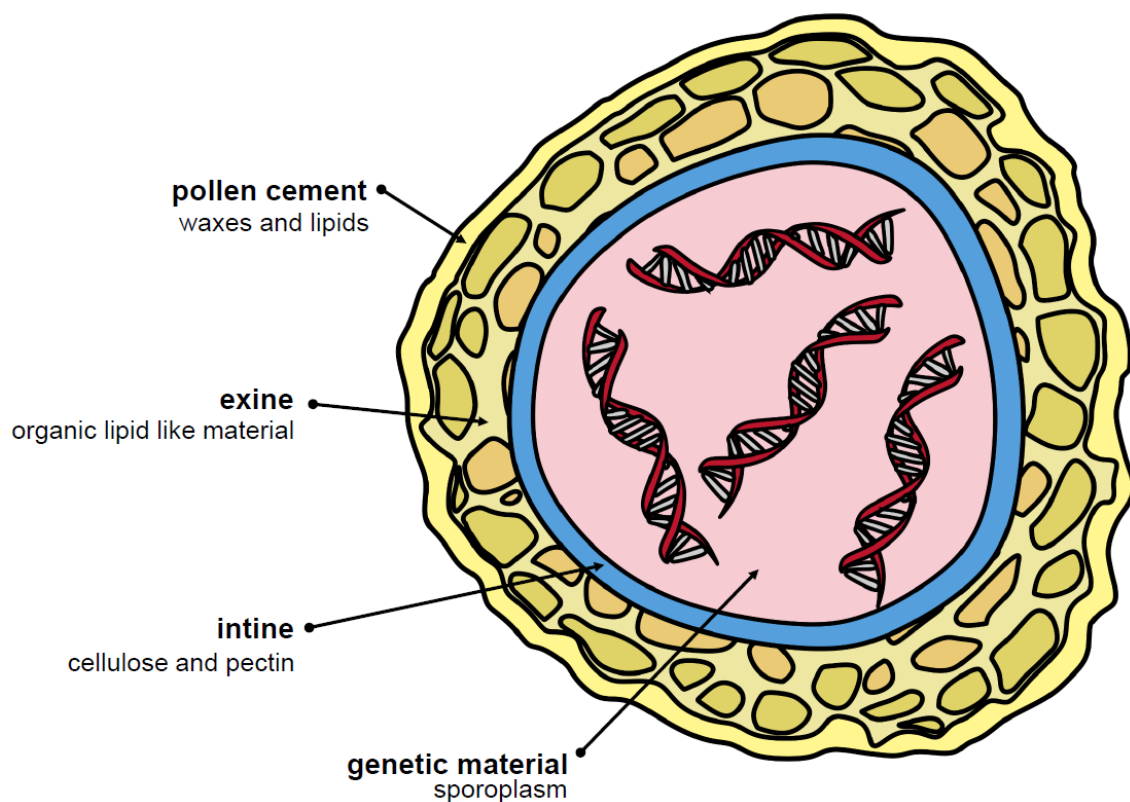


Figure 6: Schematic representation of the cross section of a *Lycopodium clavatum* spore capsule.

The morphology and size of pollen grains and spores differ from one plant species to another. This may be due to differences in the pollination procedures of each plant, leading to different surfaces depending on the pollinating agents required.¹²⁵ Their size range can vary (**Figure 7**) from 4 μm diameter for *Myosotis* (forget-me-not) to 250 μm for *Curcubita* (pumpkin).^{125,126}

2.2. Sporopollenin

Sporopollenin is the naturally occurring biopolymer which makes up the exine layer of spores of mosses, ferns, algae and fungi, and most pollen grains.¹²¹ As mentioned above, the role of this highly resistant bio-polymer is to protect the spore's contents (mainly proteins, lipids, carbohydrates and nucleic acids) from harsh environmental conditions such as UV light exposure, mechanical stress, fungal and microbial attack, desiccation and aerial oxidation.^{127,128}

Sporopollenin is extremely stable and very resistant to temperature, pressure, acid and alkali degradation.¹²⁵ Its high stability and resilience to harsh physical, biological and chemical degradation is attested by the finding of intact exines within sedimentary rocks dating back 500 million years.^{129,130} Due to the overall inertness of this biopolymer, its chemical structure has not been well characterised.^{131,132}

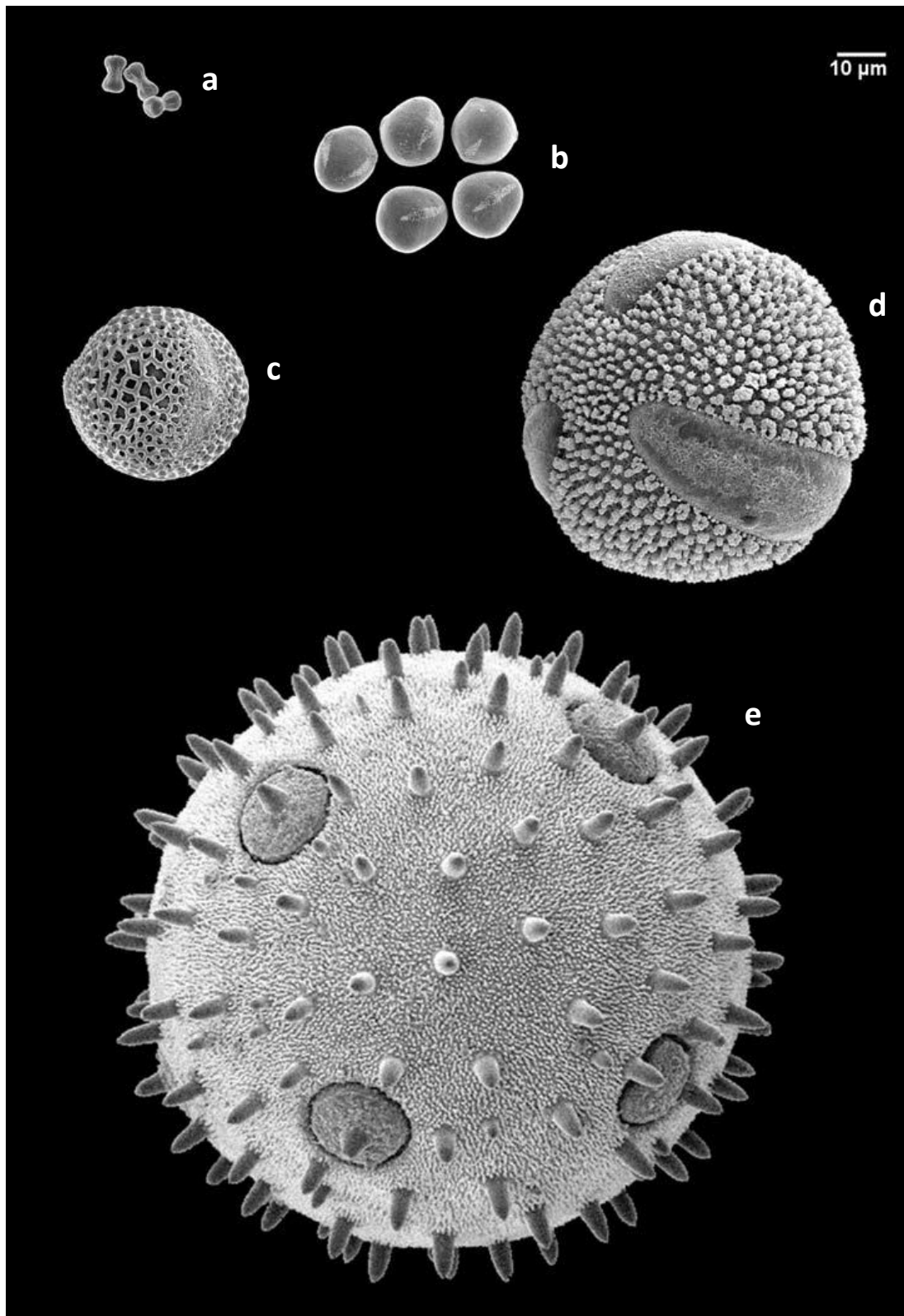


Figure 7: Size range of pollen grains and spores, **a.** *Myosotis palustris*, boraginaceae <10 µm, **b.** *Alkanna orientalis*, boraginaceae 10 - 25 µm, **c.** *Syringa vulgaris*, oleaceae 25 - 50 µm, **d.** *Plumbago auriculata*, plumbaginaceae 50 - 100 µm, **e.** *Cucurbita pepo*, cucurbitaceae >100 µm.¹³³

In early 1930s, Zetzsche *et al.* suggested that sporopollenin from *Lycopodium clavatum*, is a combination of unsaturated polymers, composed of carbon hydrogen and oxygen, of the empirical formula $C_{90}H_{144}O_{27}$.^{134,135} In 1969, Brooks and Shaw compared the infrared and elemental analyses of natural sporopollenin to a synthesized polymer derived from carotenoids and found many similarities. They proposed that the oxidative polymerisation of carotenoids and carotenoid esters leads to the final structure of sporopollenin, which is almost nitrogen free.¹²¹ This hypothesis however, was not supported in later experiments where isotopically labelled carotenoid precursors were used.^{130,136} Since then, more progress has been made, with experiments supporting catalytic enzyme reactions and a common synthetic pathway for sporopollenin of different plant families¹³⁷ suggesting that sporopollenin is an oxidative polymer of carotenoids or polyunsaturated fatty acids.^{125,138}

Although the different structures of sporopollenins derived from different plant species are still not completely known, spectroscopic and degradational studies revealed that the exhibited chemical resistance to acetolysis and high structural strength can only be attributed to a highly-cross-linked biopolymer containing a variety of functional groups¹³⁹ such as aliphatic chains, aromatic groups containing oxygen^{138,140,141,142} and hydroxyl, carbonyl/carboxyl and ether functions.^{121,143}

In 2004, Boom mentioned for the first time that sporopollenin contains *p*-coumaric and ferulic acids (**Figure 8**).¹⁴⁴ Boom isolated the exine layer from *Isoetes kilipii* megaspores and analysed it with a variety of techniques such as: direct temperature-resolved mass spectrometry, Curie-point pyrolysis-GC/MS and FT-IR. By comparing the results to the data obtained from a synthetic *p*-coumaric acid-based dehydrogenation polymer, he concluded that sporopollenin of this plant consists of polymerised *p*-coumaric acid.¹⁴⁴ In 2018, a study on the molecular structure of sporopollenin from pine pollen revealed that sporopollenin of this plant species is mainly composed of aliphatic-polyketide-derived polyvinyl alcohol parts and

7-*O-p*-coumaroylated C16 aliphatic units, crosslinked through a dioxane moiety featuring an acetal (**Figure 9**).¹⁴⁵

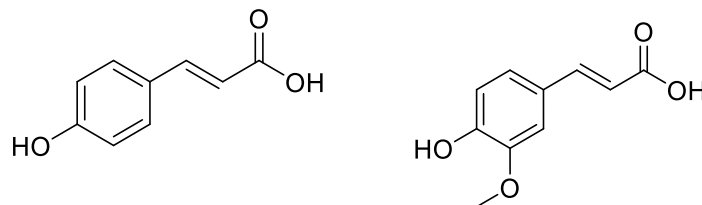


Figure 8: Chemical structures of *p*-coumaric acid (left) and ferulic acid (right).

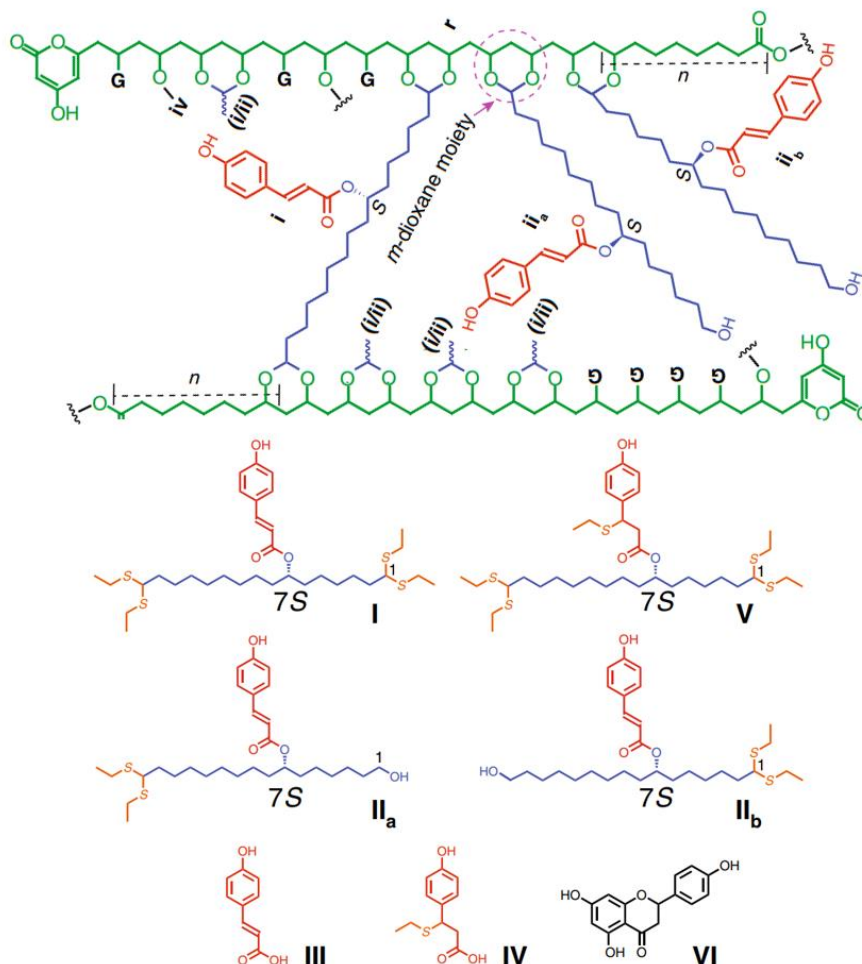


Figure 9: Chemical structure of pine sporopollenin as suggested by Li *et al.*¹⁴⁵ Thioacidolysis of pine sporopollenin gave three major (**I**, **II**_a, **II**_b) and several minor (**III**-**VI**) groups that were detected by HPLC-UV-MS.

More recently, in 2020, Mikhael *et al.* reported for the first time that sporopollenin from *Lycopodium clavatum* is a spherical dendrimer composed of a polyhydroxylated tetraketide-like monomeric main backbone with poly(hydroxy acid) networks with pseudo-aromatic α -pyrone rings. Through MALDI-TOF-MS analyses combined with ^{13}C and ^1H -NMR the team was able to reveal that this type of sporopollenin, extracted in this way, does not contain any aromatics and does not share any similarities with lignin as it was previously assumed.¹⁴⁶

2.3. Sporopollenin exine capsules

Sporopollenin capsules are extracted from pollen grains and spores using harsh conditions which result in empty exine shells that are void of any protoplasmic contents (proteins, lipids, nucleic acids and polysaccharides).¹³¹ The hollow shells, referred to in this thesis as sporopollenin exine capsules (SpECs), have high elasticity and permeability and resemble the spores from which they were extracted, in properties and morphology. Their surface is penetrated by many narrow multi directional channels that lead to the internal chamber, facilitating hydration and dehydration procedures.¹⁴⁰

These channels penetrate both walls of exine and intine and they are essential for the hydration and feeding of the sporoplasm of the living spore.¹⁴⁷ Their surface area is dependent on the plant species - pollen from *Ambrosia artemisiifolia* has a surface area of 0.623 m²/g whereas spores from *Lycopodium clavatum* have a surface area of 4 m²/g.¹⁴⁸

The extraction of SpECs includes procedures often involving a defatting process, using organic solvents, followed by acid and/or base hydrolysis (**Figure 10**). During the extraction process, all interior constituents such as saccharide material, lipids, nitrogenous materials and cellulose are removed from the capsule.¹³⁸

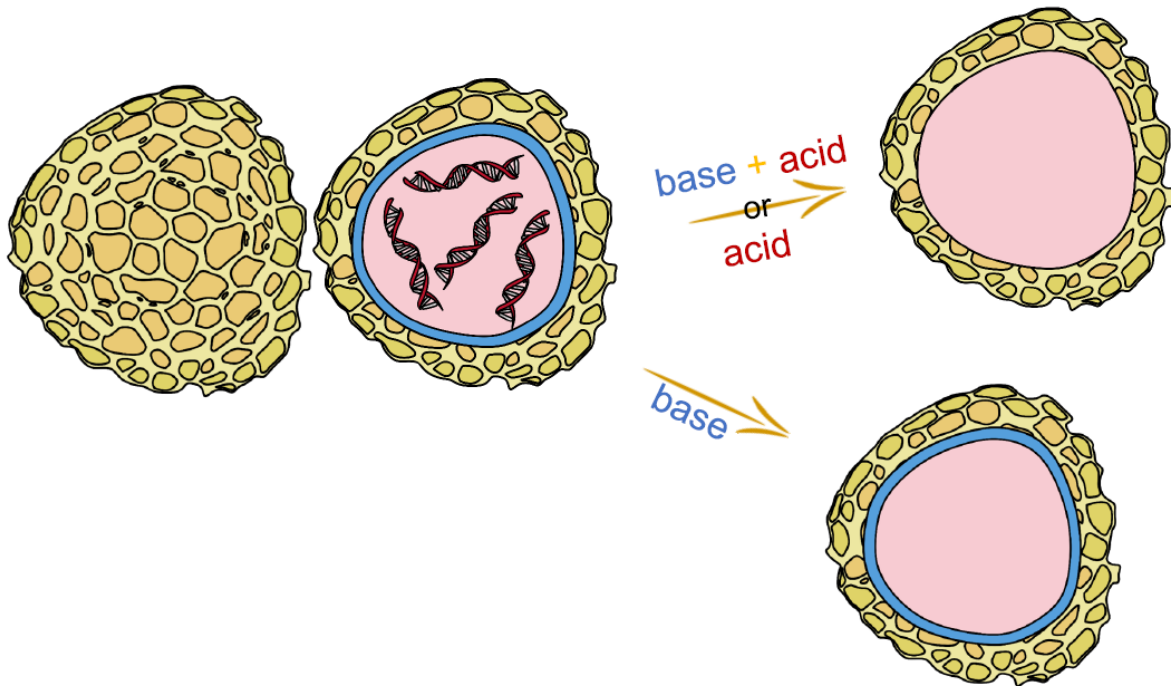


Figure 10: Spore hydrolysis procedures where the genetic material is removed and empty SpECs are produced.

The result is a nitrogen free sporopollenin shell, meaning that all proteins and nucleic acids are removed.^{131,140} Depending on the extraction procedure, a usual mass loss is around 55 - 60%, or 70 - 75% when extracting with ortho-phosphoric acid where the removal of the intine layer is more efficient.¹⁴⁷

2.3.1. *Lycopodium clavatum* SpECs

Lycopodium clavatum (*L. clavatum*) (**Figure 11**) is a plant globally spread, growing in central and south America, Europe, Africa and Asia, with the common name ‘club moss’.¹⁴⁹ Its spores are the most widely studied SpECs and have been used for many years as a base for cosmetics, herbal medicine or natural powder lubricant. This is mainly due to its low cost, its availability and its chemical stability.^{150,151}



Figure 11: *Lycopodium clavatum* plant [www.aphotoflora.com].

L. clavatum extracted SpECs have a diameter size around 25 - 30 μm and their shape is of a hemisphere ending in a trilete structure on the underside (**Figure 12a**).¹²⁶ Their morphology is similar to their parent spores, but after the extraction procedures, some of the particles might appear to be shrunk due to their hollow interior when viewed under SEM, under vacuum conditions (**Figure 12b**). This is because removal of the intine reduces the structural integrity allowing the elastic movement of the outer shell, like a balloon can be sucked-in under vacuum. SpECs are mono-dispersed particles with a rough surface that is traversed by numerous multidirectional channels (**Figure 13**).¹³¹ These channels are called muri (*pl.*) and the surface around them is called lumen. At the proximal face of the spore, there is the trilete scar made of three laesurae.¹⁵² Their total surface area has been measured to be around 4 m^2/g with a shell thickness of 2 to 3 μm .^{131,147} A variety of functional groups coat their surface including alkane, alkene, carboxylic acid, ketone, lactone and phenolic groups making them highly suitable for a variety of potential applications, including contaminant removal.

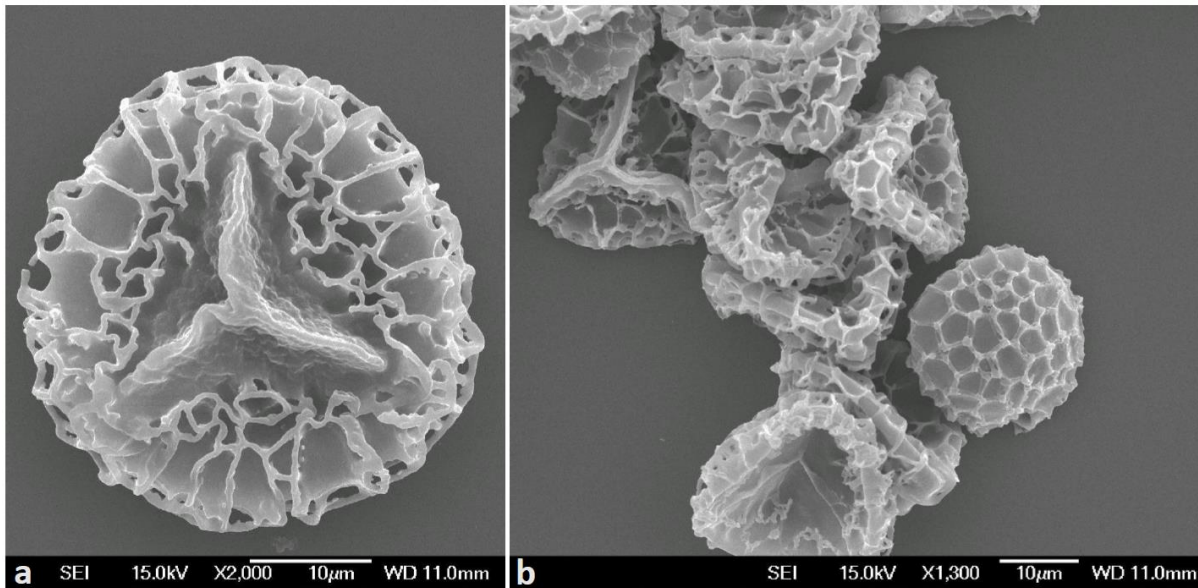


Figure 12: SEM image of *L. clavatum* SpECs where **a)** the trilete scar on the bottom of the capsule is visible and **b)** the particles appear sucked in due to the vacuum employed during SEM.

SpECs from *L. clavatum* show excellent mechanical strength and are shown to be highly resistant to chemical treatments compared with SpECs from other plant species.¹⁵³ According to Fraser *et al*, *L. clavatum* SpECs can endure extreme heating at temperatures up to 250 - 300 °C.¹⁵⁴ They have also shown great stability under high hydrostatic pressures of up to 10 GPa.¹⁵⁵

After extraction of the SpECs some fragmentation of the particles may occur, though rare.

Figure 14 presents a close-up of a fragment revealing important information on the structure of the spore. The SEM measurements revealed that the wall thickness of foot layer from observed fragments range between approximately 0.8 and 1.2 µm whilst the tectal elements protrude by as much as between 2 - 4 microns.

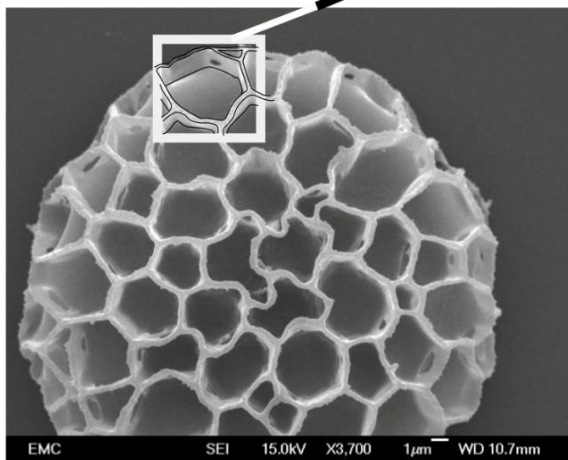
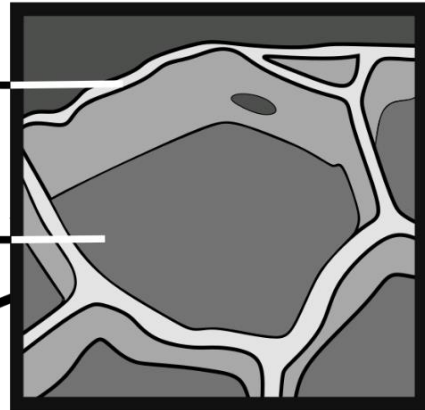
Lycopodium clavatum. morphology

Murus (pl. mura) -

Network of (sculpted) interconnected coronet like structures that make up the muri consisting only of the tectal elements of the exine.

Lumen (pl. lumina) -

Apertures in the interconnected coronet like structure that make up the muri consisting only of the foot layer of the exine.



Lycopodium clavatum. layers

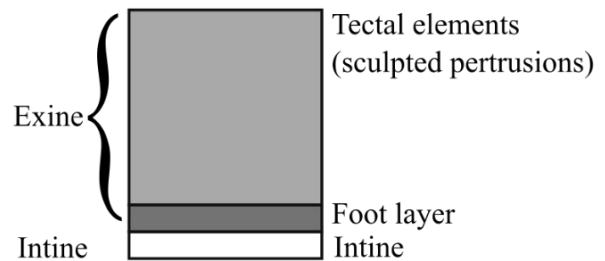


Figure 13: Morphological characteristics of a *L. clavatum* spore.

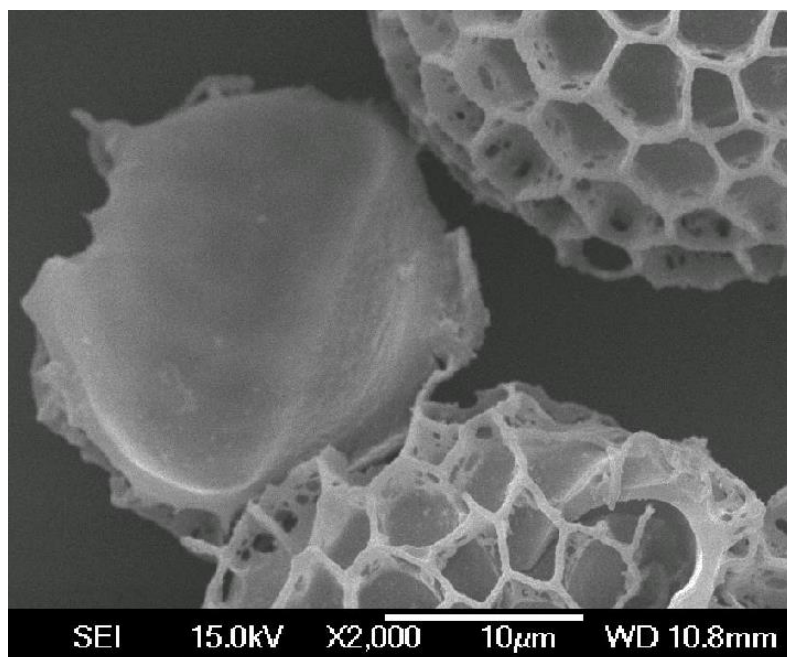


Figure 14: SEM image of a fragmented SpEC revealing the inside of the spore and providing useful information on the wall thickness and tectal elements.

2.3.2. SpECs applications

The physical and chemical properties of sporopollenin capsules make them an interesting material, reported to have been used in chromatographic applications,^{126,131,156–159,160} microcapsules for drug encapsulation and delivery,^{161–165} supercapacitor electrodes,¹⁶⁶ solid phase for peptide synthesis,¹⁶⁷ medical imaging, micro reactors for the preparation of nanoparticles and solid supports for a palladium catalyst used in Heck reactions.^{126,168}

There are many research groups that have focused their interest in using sporopollenin as a sorbent material for water purification. Sener *et al.*¹¹¹ report the efficient removal of Pb²⁺ with the use of iron-modified sporopollenin following the Freundlich isotherm model and a pseudo-second order adsorption process. More recently, Hassan *et al.* synthesised a new sorbent material: 3-aminopropyltrimethoxysilane functionalized magnetic sporopollenin-based silica coated graphene oxide and proved the successful removal of Pb(II) ions from contaminated water.¹¹² A similar sporopollenin-based material was synthesised by Markus *et al.*, magnetite-sporopollenin/graphene oxide, which was successful in adsorbing three polar organophosphorus pesticides: dimethoate, phenthoate and phosphamidon.¹¹⁶ In 2014, Çimen *et al.* reported that when sporopollenin from *L. clavatum* was modified with hydroxyphenylimino-methyl-benzoic acid, the resulting material was very efficient in adsorbing Co(II), Ni(II) and Cu(II) ions from water.¹¹³ Similarly, Sargin and Arslan¹¹⁴ reported the efficient adsorption of Cu(II) ions when modifying sporopollenin with different ratios of glutaraldehyde and chitosan. Ahmad *et al.*, successfully removed Pb(II) and As(III) ions from water by functionalising *L. clavatum* sporopollenin hydroxyethyl-piperazine.¹¹⁵ In 2018, Yaacob *et al.* synthesised magnetic sporopollenin and used it for the adsorption of lubricant oil from aqueous media.¹⁶⁹ In the same year, the same research group published their results on the synthesis of β -cyclodextrin functionalised magnetic sporopollenin and the successful

adsorption efficiency of the material against the NSAIDs indoprofen, ketoprofen, ibuprofen and fenoprofen.¹¹⁷

2.4. Aims and Objectives

In the rest of this chapter, the production of SpECs from *L. clavatum* will be discussed, following different extraction protocols from the raw spores. SEM images and IR analysis will be presented to identify possible differences between the SpECs from alternative extraction procedures. Furthermore, the analysis of SpECs having undergone a series of surface modifications either by oxidation or amination reactions or by iron loading is presented.

2.5. Raw *Lycopodium clavatum* spores

Raw *L. clavatum* spores were analysed using FT-IR spectroscopy to obtain an initial spectrum for comparison with the different extractions and modifications. All disks were created using a highly accurate balance (5 decimal places), where 1 mg of SpECs was weighed and mixed with 130 mg of KBr. All spectra were formed in Origin and normalised using second derivative methodology and finally normalised between 0 and 1 using the CH₂ peaks ($\sim 2875\text{ cm}^{-1}$). The measurements were repeated in triplicate and then normalisation was performed, leading to identical overlays.

The raw spores were also analysed using elemental combustion analysis to define the percentages of C, H and N contained (**Table 2**). Since these percentages do not add up to 100%, and based on previous studies, it was assumed that the balance element was oxygen. **Figure 15** presents the IR spectra of the raw spores, identifying all the different peaks and what they represent.

sample	C %	H %	N %
raw spores	64.99	9.61	1.37

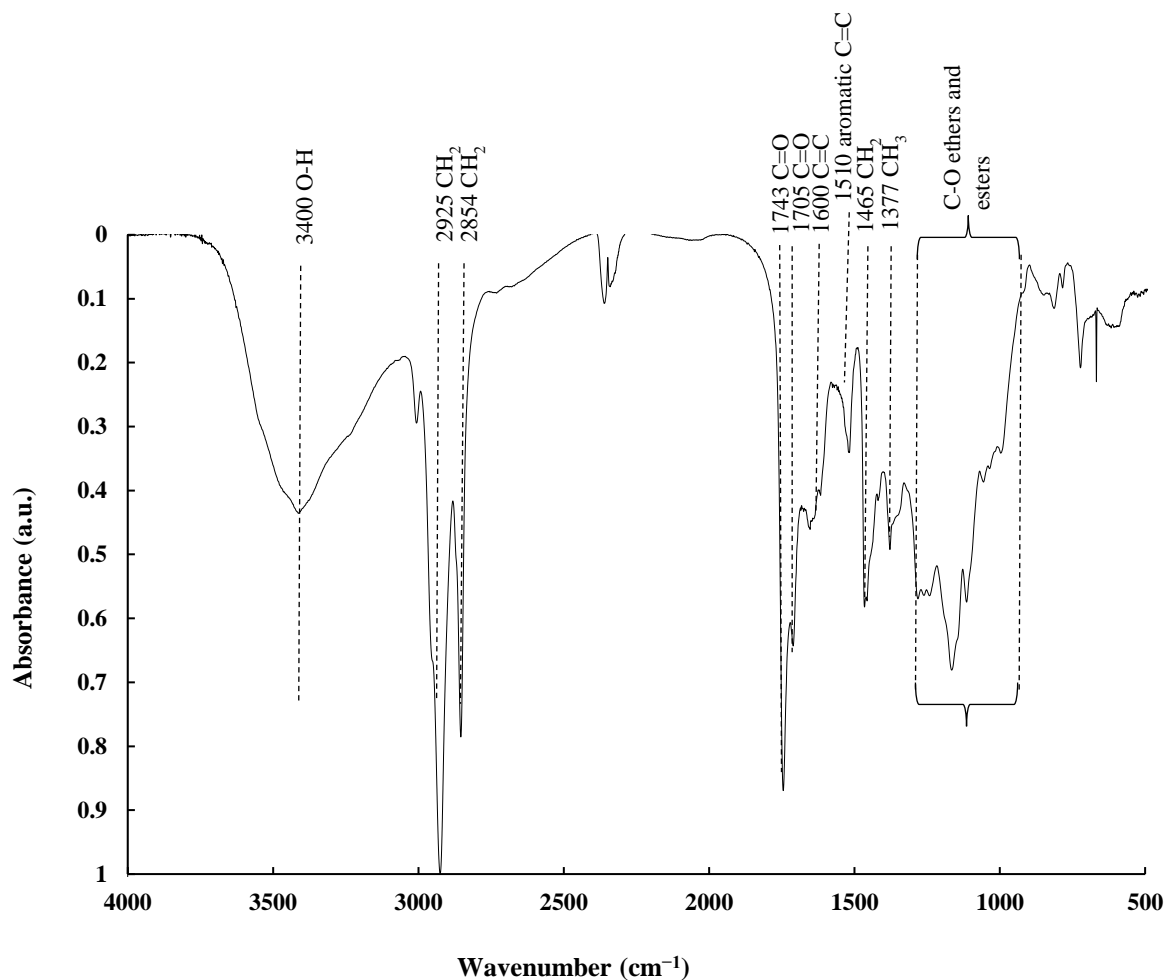


Figure 15: FT-IR spectrum of raw *L. clavatum* spores.

Lipids are believed to be present in the raw *L. clavatum* spores which have been previously identified in other species of pollens,^{170–174} characterised by the vibrational bands 1743 (C=O), 1462 (CH₂), 1240 (C-O), 1160 (C-O) and 722 cm⁻¹ (CH₂ rocking).¹⁷⁵ Unprocessed *L. clavatum* spores exhibit a band at 1743 cm⁻¹ which is likely to be assigned to the ν (C=O) of lipid esters, similar to triglycerides which also show a peak at 1743 cm⁻¹.

The broad peak centred around 3400 cm^{-1} indicates the presence of hydroxyl OH groups due to carboxylic acids, alcohols and moisture. Sharp peaks at (2925 and 2854 cm^{-1}) are associated with out of phase C-H stretching and in phase C-H stretching in methylene groups respectively.¹⁷⁰

In the first extraction [SpECs(1)], KOH extraction followed by H_3PO_4 treatment (section 8.1.1), a “defatting” processing of the raw spores was followed, involving treatment in boiling acetone. A comparison of the IR spectra of the two materials, before and after defatting, is shown in **Figure 16**. The FT-IR spectra of the defatted spores exhibit a good overlay with spectra of the raw spores, following the normalisation procedure described previously and a qualitative comparison can therefore take place, of particular functional groups of interest. They exhibit a change/depletion of all the vibrational peaks associated with lipids, suggesting that the lipids removed are part of the pollenkit having been removed by dissolution in acetone rather than by hydrolysis from the sporopollenin structure.

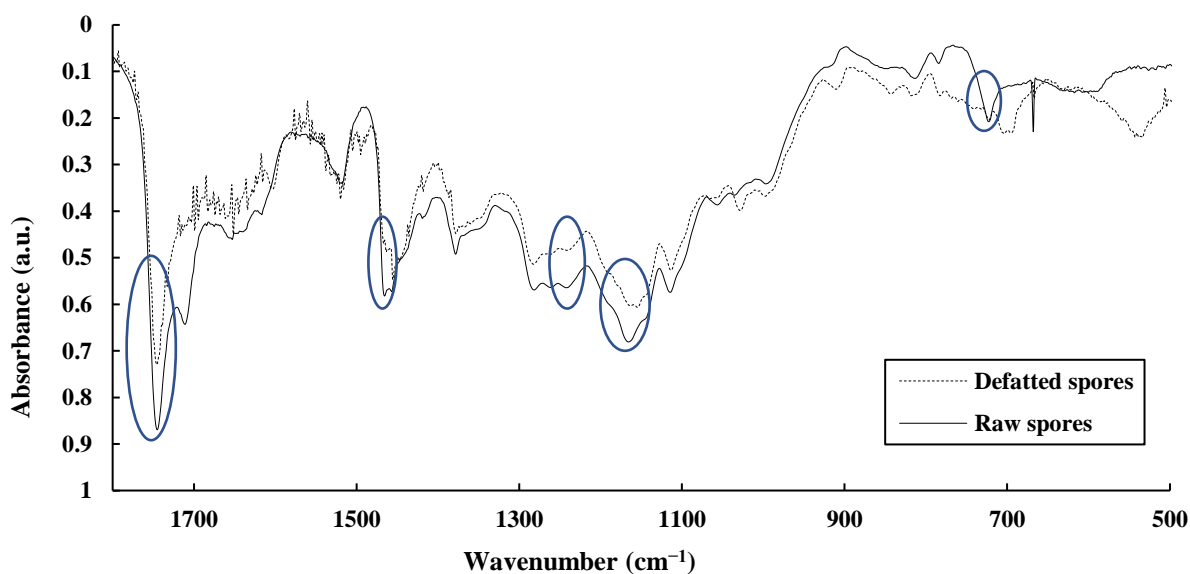


Figure 16: FT-IR spectra of raw spores and defatted spores derived from *L. clavatum*.

After the acetone treatment, the 1744 cm^{-1} peak is removed or is of depleted intensity revealing an underlying peak at 1735 cm^{-1} which may be accounted for as either esters or lactones. Interestingly, the vibrational peak at 1710 cm^{-1} which is highly associated with carboxylic acids (C=O) within the sporopollenin structure,¹⁷⁰ is entirely removed upon only acetone treatment, and yet remains present in all of the extractions (SpECs (1-3) as it will be presented in the following sections). This perhaps suggests the original 1710 cm^{-1} peak may arise from groups within the soluble pollenkit, and not the sporopollenin structure itself. However, it would further imply that although the pollenkit is removed in all the extractions [SpECs (1-3)], new carboxylic acids may be generated from the hydrolysis of esters and lactones present within the structure.

2.6. SpECs extraction

SpECs were extracted from *L. clavatum* spores following three different extraction protocols, as described in section 8.1. Each procedure resulted in SpECs of different colours (**Figure 17**) and different composition as indicated by the CHN elemental analysis (**Table 3**), with SpECs(3) presenting the highest C and H content and zero N. From this, it can be inferred that it has the lowest oxygen content, possibly from elimination reactions. SpECs(2) have a significantly lower amount of C and H, whilst retaining negligible amounts of N. The presence of larger amounts of oxygen can be implied, or more likely Na in the form of counter ions.

sample	hydrolysis	C %	H %	N %
raw spores	-	64.99	9.61	1.37
SpECs (1)	KOH - H ₃ PO ₄	66.35	8.50	0.00
SpECs (2)	NaOH	59.00	8.89	0.12 - 0.56
SpECs (3)	HCl	67.48	9.11	0.00

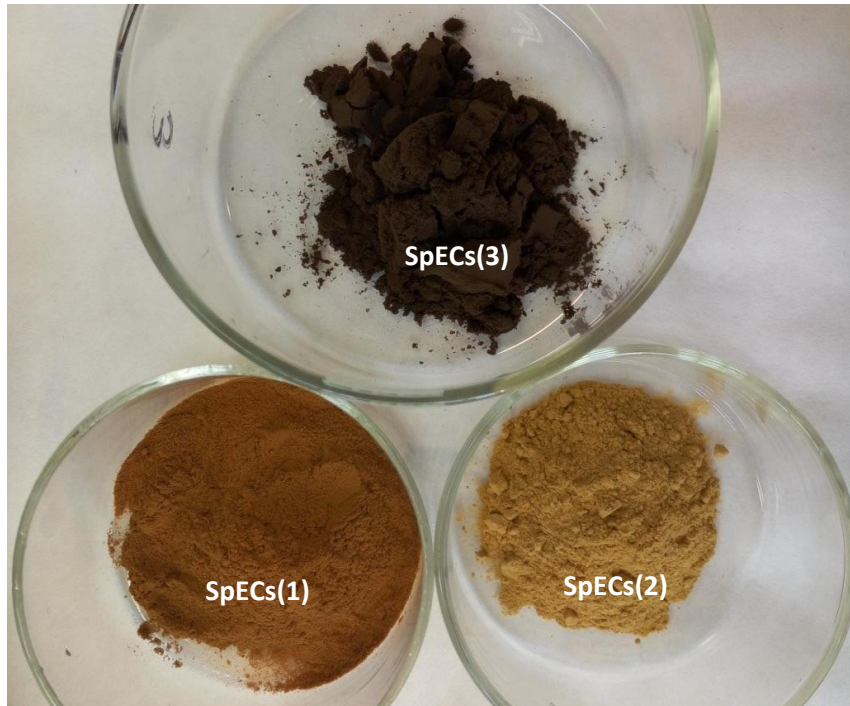


Figure 17: Extracted SpECs - the darkest colour corresponds to the HCl extraction SpECs(3), the yellow SpECs(2) are extracted *via* the NaOH hydrolysis and the brown SpECs(1) are extracted with the two step KOH/H₃PO₄ hydrolysis.

2.6.1. KOH hydrolysis - H₃PO₄ treatment [SpECs(1)]

The KOH hydrolysis followed by phosphoric acid treatment resulted in SpECs of brown colour (experimental section 8.1.1). The elemental analysis showed no evidence of nitrogen content (**Table 3**) therefore it was concluded that in this type of SpECs there is no genetic material remaining in the interior of the spore. After calculations, by the process of elimination, the oxygen content was around 25%. The SEM images showed some spore debris (**Figure 18** and **Figure 19**), indicating that the 7 days procedure might have been a little bit harsh on the spores. The extraction conditions appear to have caused some mild fragmentation of the exine shells. Exines can be seen to be “open” at the trilete scar or fragmented into a few pieces. Damage to the fine structure of the decorations of the surface is not evident, rather cracked fragments of the core exine structure has been observed.

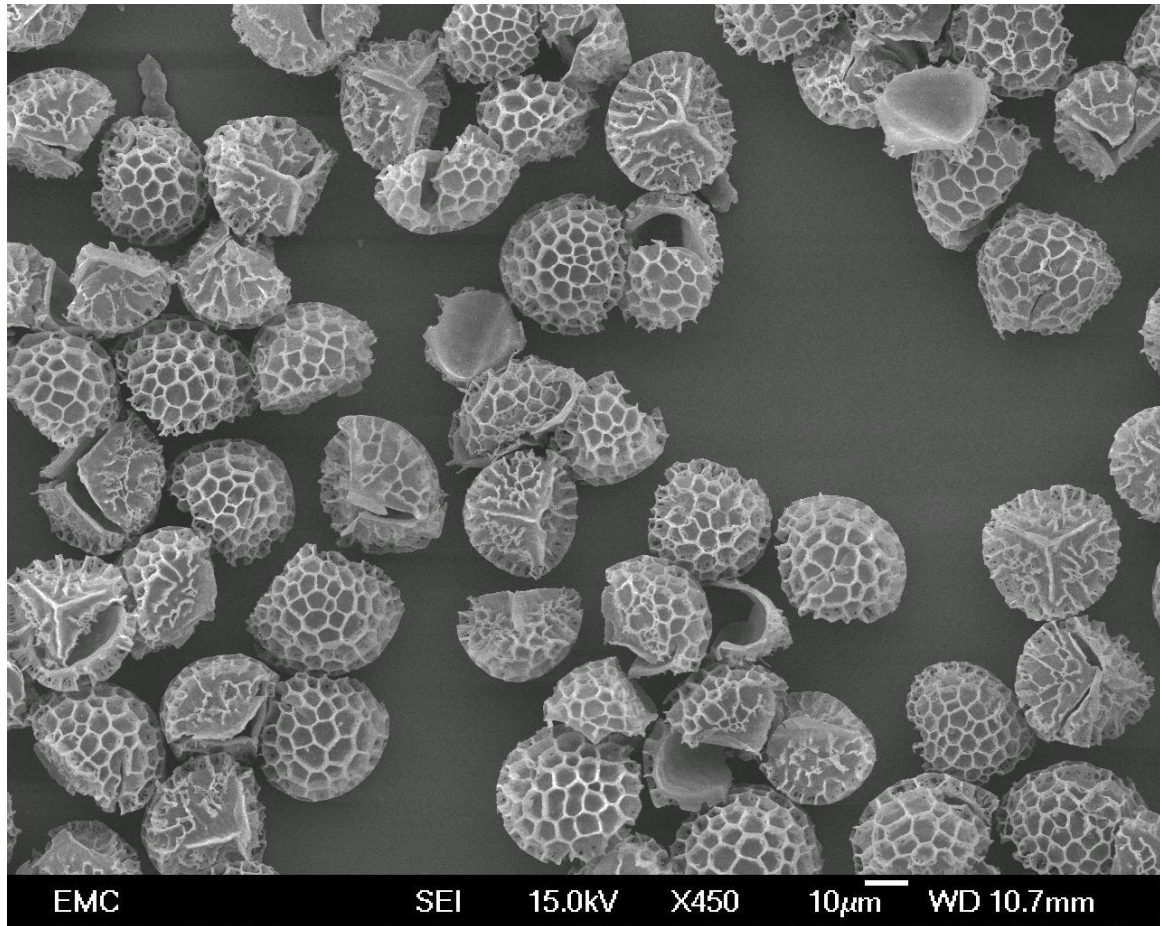


Figure 18: SEM image of KOH extracted SpECs [SpECs(1)] followed by H_3PO_4 treatment. Some fragments of the initial spores are present in the final product indicating that the hydrolysis procedure might have been harsh.

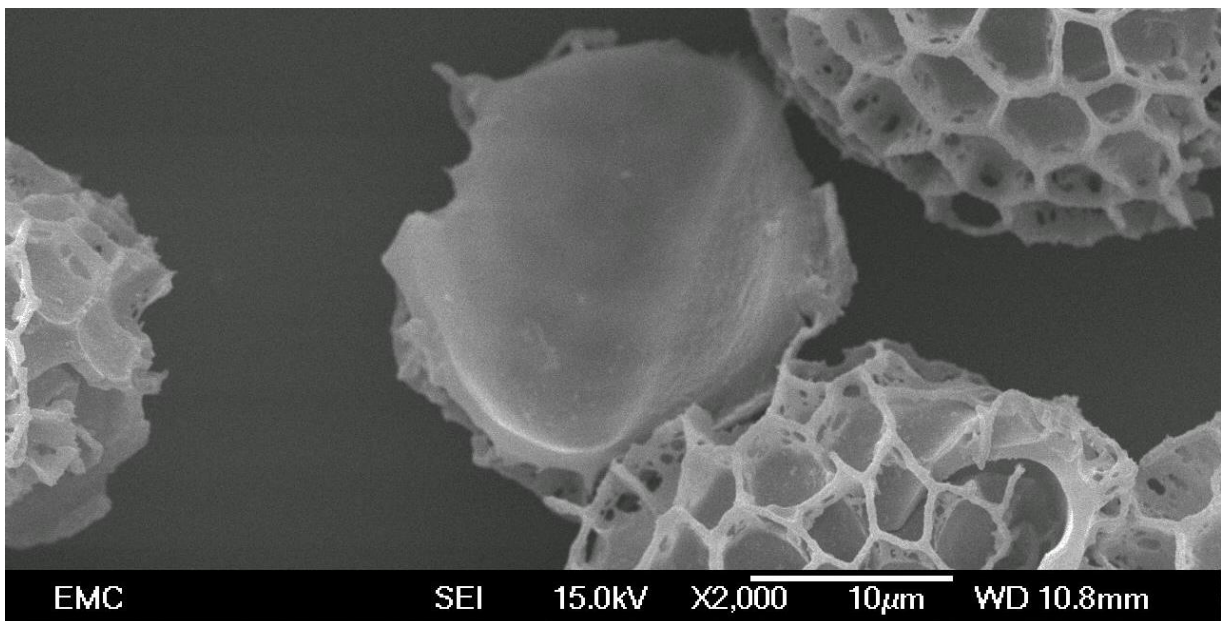


Figure 19: SEM image of KOH extracted SpECs [SpECs(1)] followed by H_3PO_4 treatment, zoomed in the area of a fragmented spore.

IR analysis

Figure 20 presents the FT-IR spectrum of SpECs(1) compared with the raw *L. clavatum* spores. The most striking observation is that this material exhibits a distinct reduction of intensity in all the peaks from functional groups in every region except for the OH stretching of hydroxyls. Such a finding might suggest that SpECs(1) is a carbonised material that is relatively featureless (of functional groups). SpECs(1) exhibit some carboxylic acid character (1710 cm^{-1}), and show no peak at 1510 cm^{-1} which is believed to represent aromatic ring modes. This is in agreement with the findings of Banoub *et al.* who concluded no aromaticity in the sporopollenin exine structure.¹⁴⁶ It should be noted however that this is only true of SpECs(1), which was the same extraction procedure investigated by Banoub *et al.* and appears not to be the case of unmodified raw spores, nor the other extractions.

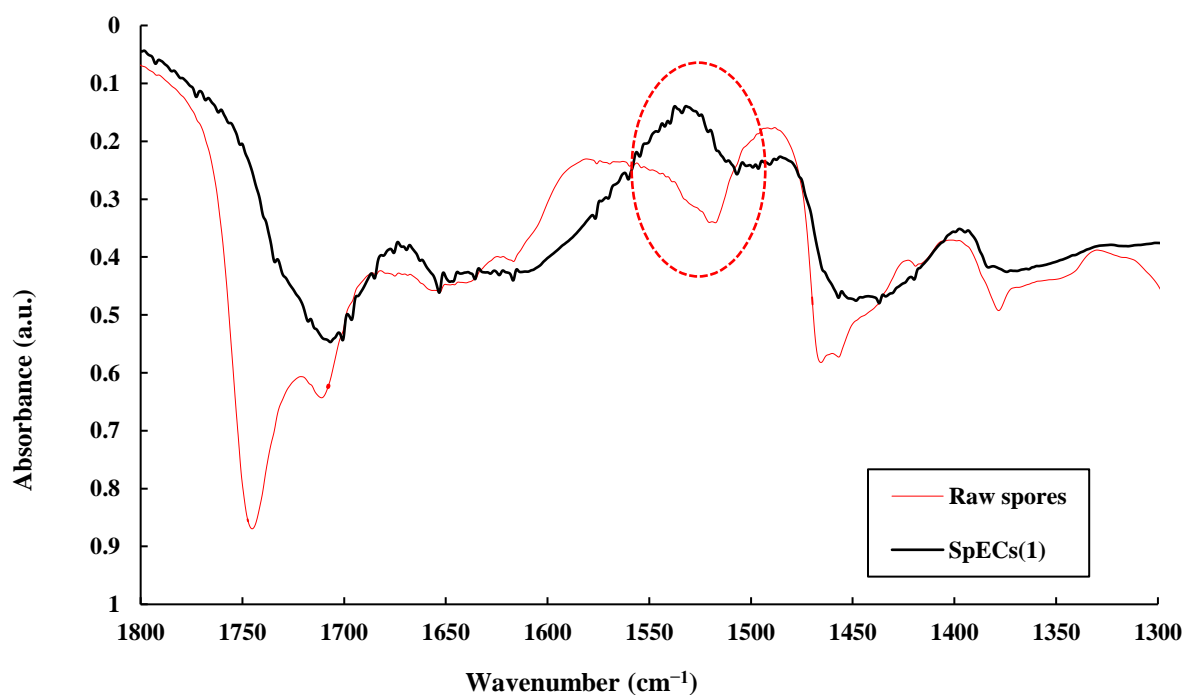


Figure 20: FT-IR spectra of SpECs(1) and raw *L. clavatum* spores. Highlighted is the removal of aromatic ring modes at $\sim 1510\text{ cm}^{-1}$.

2.6.2. NaOH hydrolysis [SpECs(2)]

Treatment of the raw *L. clavatum* spores with NaOH was performed following the protocol described in section 8.1.2 and gave a mustard yellow product, SpECs(2), with a nitrogen content of around 0.1 - 0.5% (the N% results for a small scale extraction were 0.12% while for a bigger scale the percentage was 0.56 showing that the purity of the final product depends on the scale of the extraction). The percentage of nitrogen shows that some traces are possibly left in the interior, meaning that this extraction may also contain a small amount of cellulose and pectin. The SEM images showed spores that were perfectly intact without any damage to the structure of the microcapsule exine shells (**Figure 21**). There was no evidence of cracking, “opening” at the trilete scar, nor fragmentation.

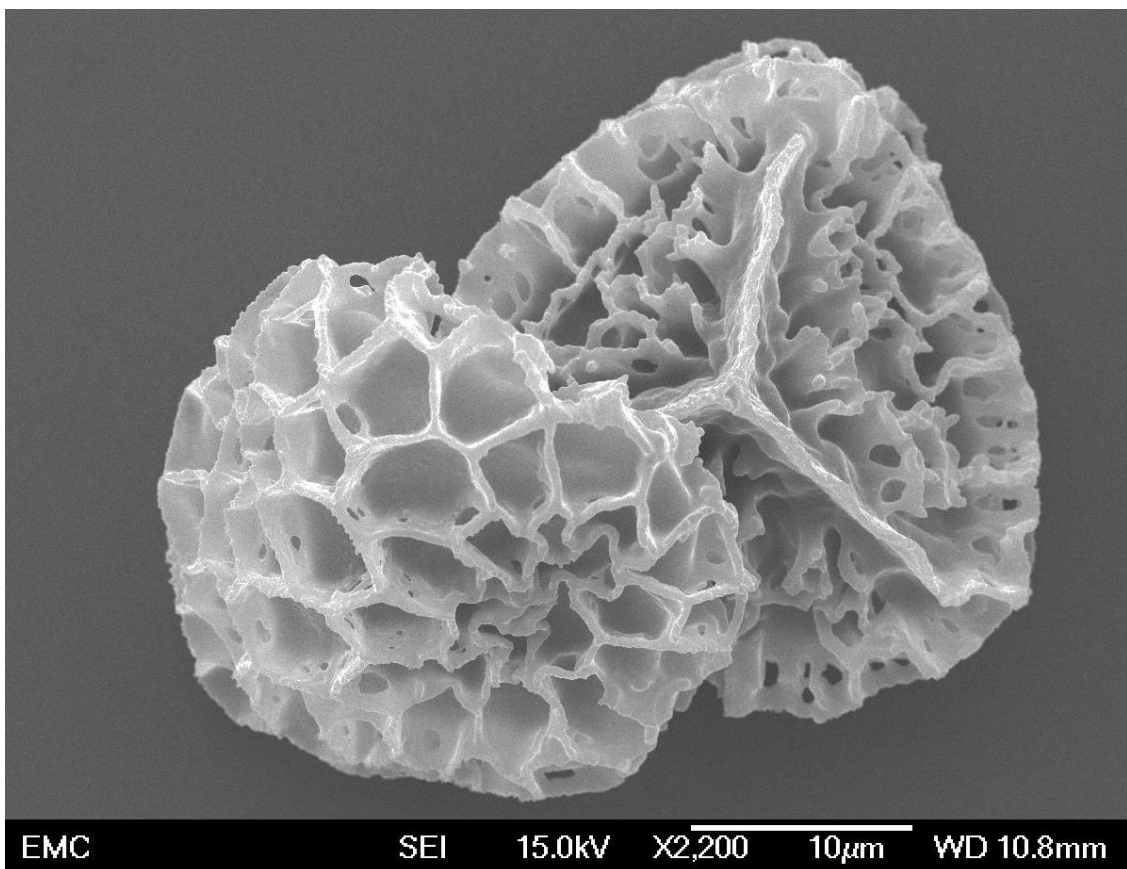


Figure 21: SEM image of NaOH extracted SpECs [SpECs(2)] showing the upper and bottom parts of two different spore particles.

However, it can be observed that the shape of the exines is imploded, such that the walls of the exine shells are sucked into the internal cavity (**Figure 22**). This is likely due to the vacuum conditions in which SEM operates. It also suggests that the intine layer of cellulosic material may have been hydrolysed in the strong basic conditions of the extraction. Microscopic images of the same extraction with SpECs being dispersed in water (**Figure 23**) showed the particles' actual shape, revealing the amazing elasticity of the material under different pressure conditions.

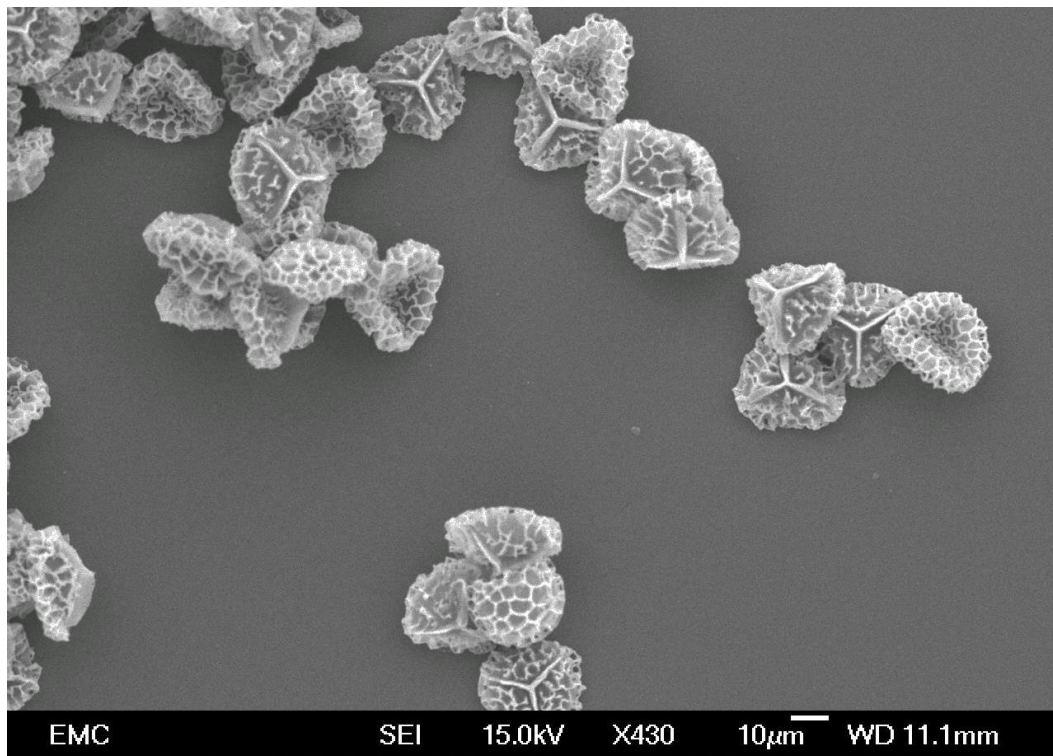


Figure 22: SEM image of NaOH extracted SpECs [SpECs(2)] showing imploded particles.

In this extraction procedure the intine is removed and this also removes a structural component that allows the exine shape to resist the strong vacuum. Nevertheless, this type of treatment appears not to damage the mura or trilete scar leaving it intact and without holes (**Figure 24**).

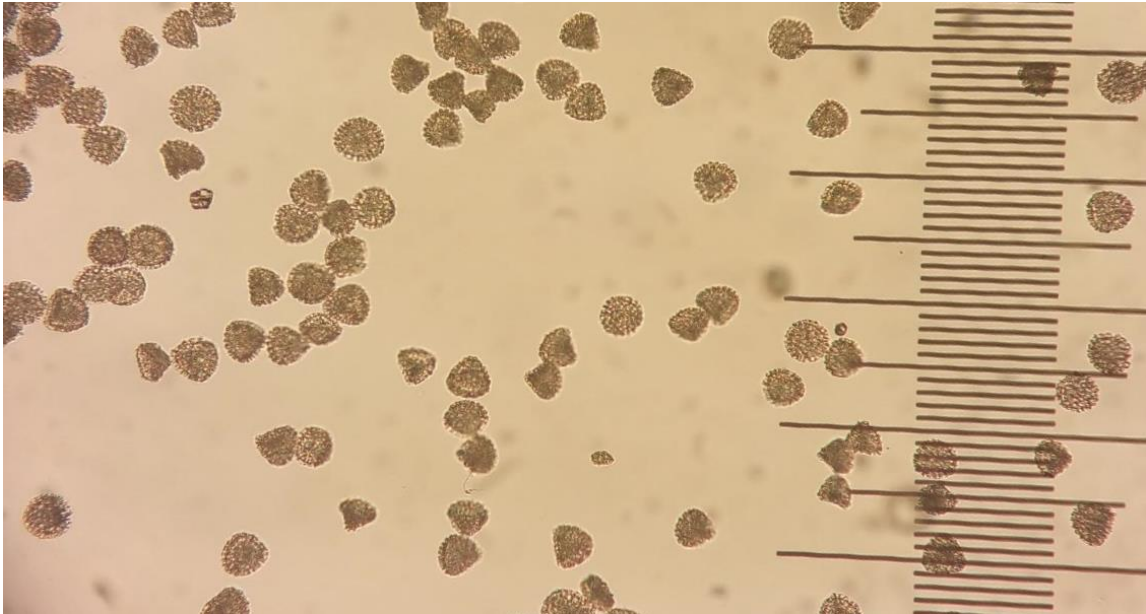


Figure 23: Microscopic image of SpECs(2) dispersed in water, showing the true size of the particles without implosion (scalebar distance between lines 10 μm).

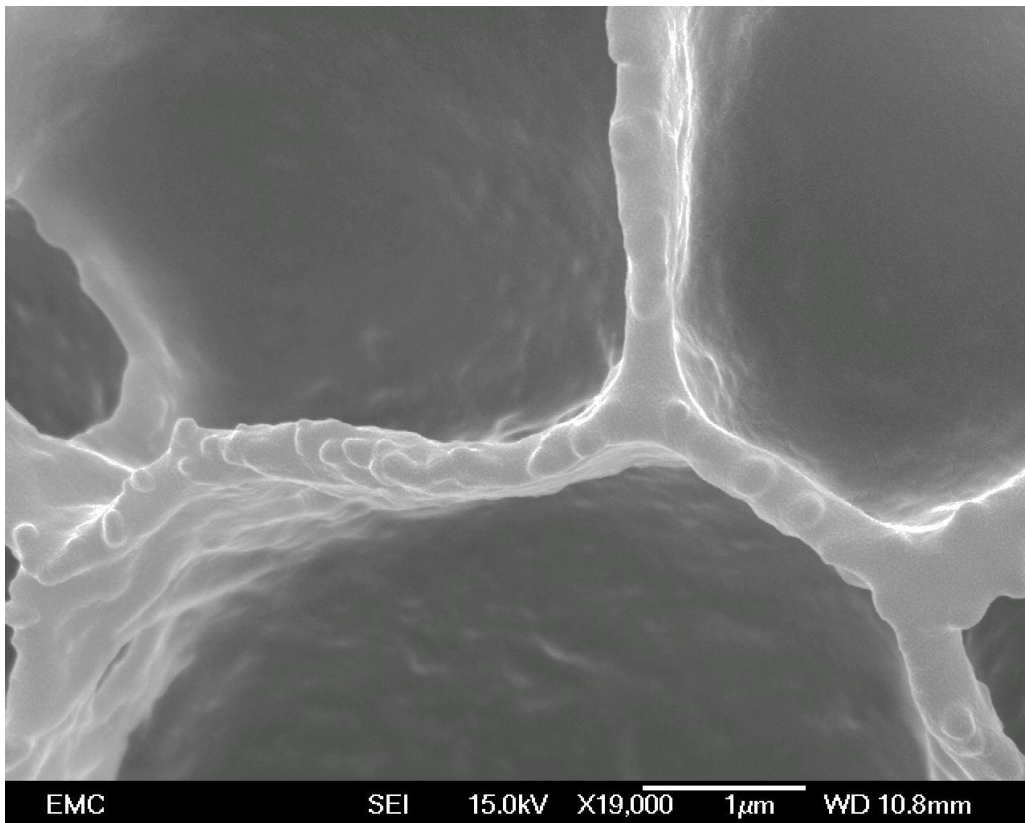


Figure 24: SEM image of SpECs(2) magnified to exhibit the mura of a shell, showing no damage on the tectal elements.

IR analysis

Figure 25 presents the FT-IR spectrum of SpECs(2) compared with raw spores. The 1743 cm^{-1} band accounting for lipid esters is reduced, however the carboxylic acid peaks $\sim 1710\text{ cm}^{-1}$ are also completely diminished. This indicates that in SpECs(2) the carboxylic acids have been replaced by sodium carboxylates. Sodium carboxylate peaks exhibit antisymmetric stretching vibrations ($\nu_{as}\text{CO}_2^-$) at 1576 and 1542 cm^{-1} and symmetric stretching vibrations ($\nu_s\text{CO}_2^-$) at 1463 and 1456 cm^{-1} .^{176,177} To confirm these carboxylate vibrations, SpECs(2) were washed using 1 M HCl and then filtered, as described below.

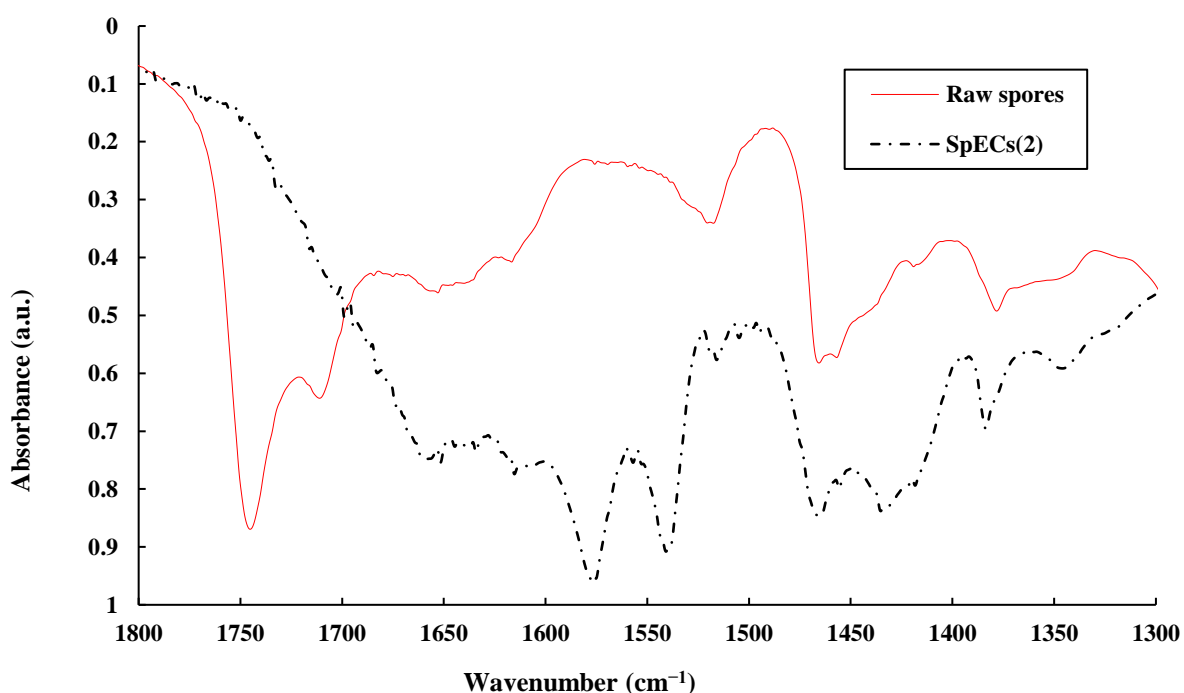


Figure 25: FT-IR spectra of SpECs(2) and raw *L. clavatum* spores.

2.6.2.1. HCl treatment of SpECs(2)

SpECs(2) were washed with $\text{HCl } 1\text{ M}$ at room temperature following the protocol described in section 8.2.2. The resulting SpECs [SpECs(2)HCl] were analysed with elemental analysis and IR spectroscopy (**Table 4**). **Figure 26** presents SpECs(2) before and after the acid rinse and

shows the loss of the sodium carboxylate vibrations, and the increase in number of carboxylic acids $\sim 1710\text{ cm}^{-1}$, which had previously been absent. This confirmed that the vibrations in the IR spectrum of SpECs(2) thought to be due to the carboxylate group, was a likely deduction.

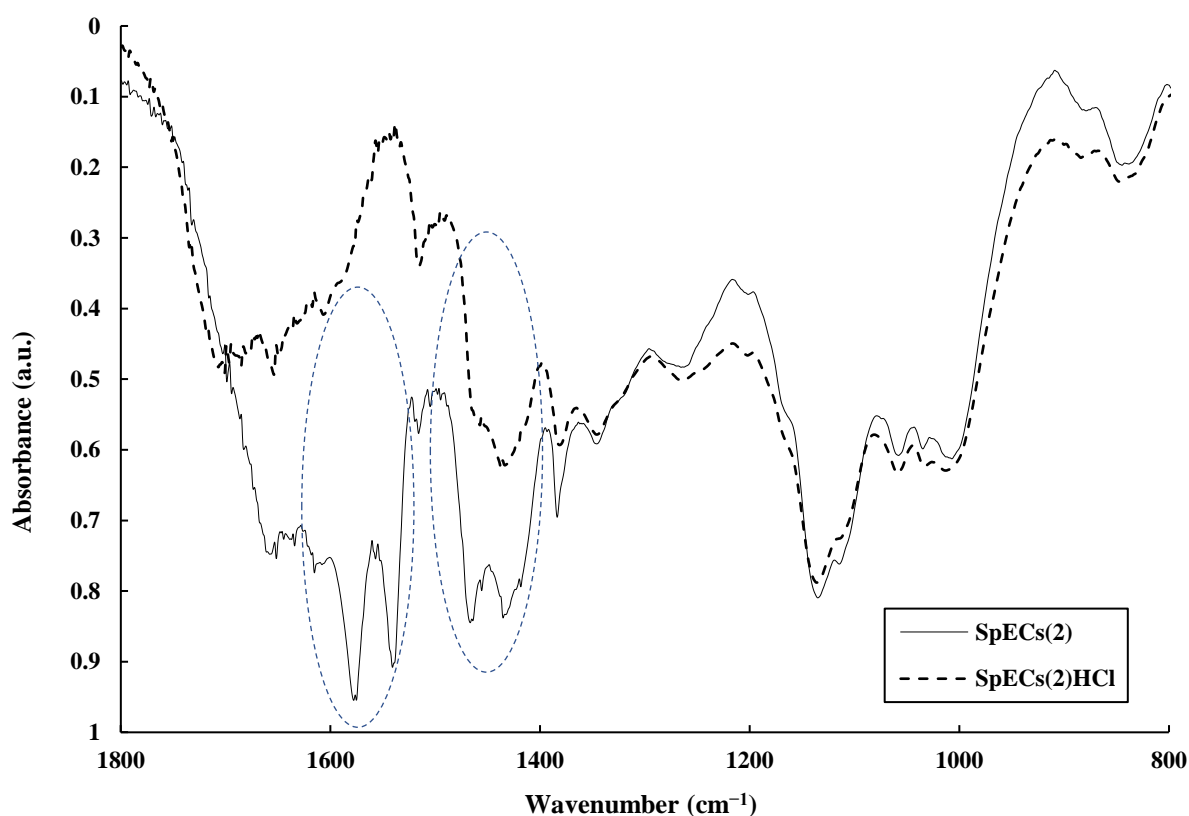


Figure 26: FT-IR spectra of SpECs(2) before and after HCl treatment [SpECs(2)HCl].

sample	treatment	C %	H %	N %
SpECs(2)	-	59.00	8.89	0.12 - 0.56
SpECS(2)HCl	HCl	60.71	8.68	0.40

2.6.3. HCl hydrolysis [SpECs(3)]

The HCl hydrolysis treatment gave SpECs of a dark brown colour, the darkest colour of the three extractions. The calculated oxygen content of these SpECs is the smallest compared to

the other two types, 23%. A possible explanation for this might be hydroxyl elimination reactions, which would form a series of double bonds, increasing possible conjugation and leading to the dark colour, but also would reduce the oxygen content.

Extraction conditions for SpECs(3) exhibit damage to the ‘decorative’ mura of the exine shells (**Figure 27**). This extraction has also led to the loss of the structural integrity provided by the trilete scar, which also seems to have been removed (**Figure 28** and **Figure 29**). There was no evidence of cracking, “opening” at the trilete scar, nor fragmentation. However, it can be noted that the shape of all of the observed SpECs has collapsed, as was seen with SpECs(2). This has allowed the wall to become concave, which completely sheds the mura from the surface.

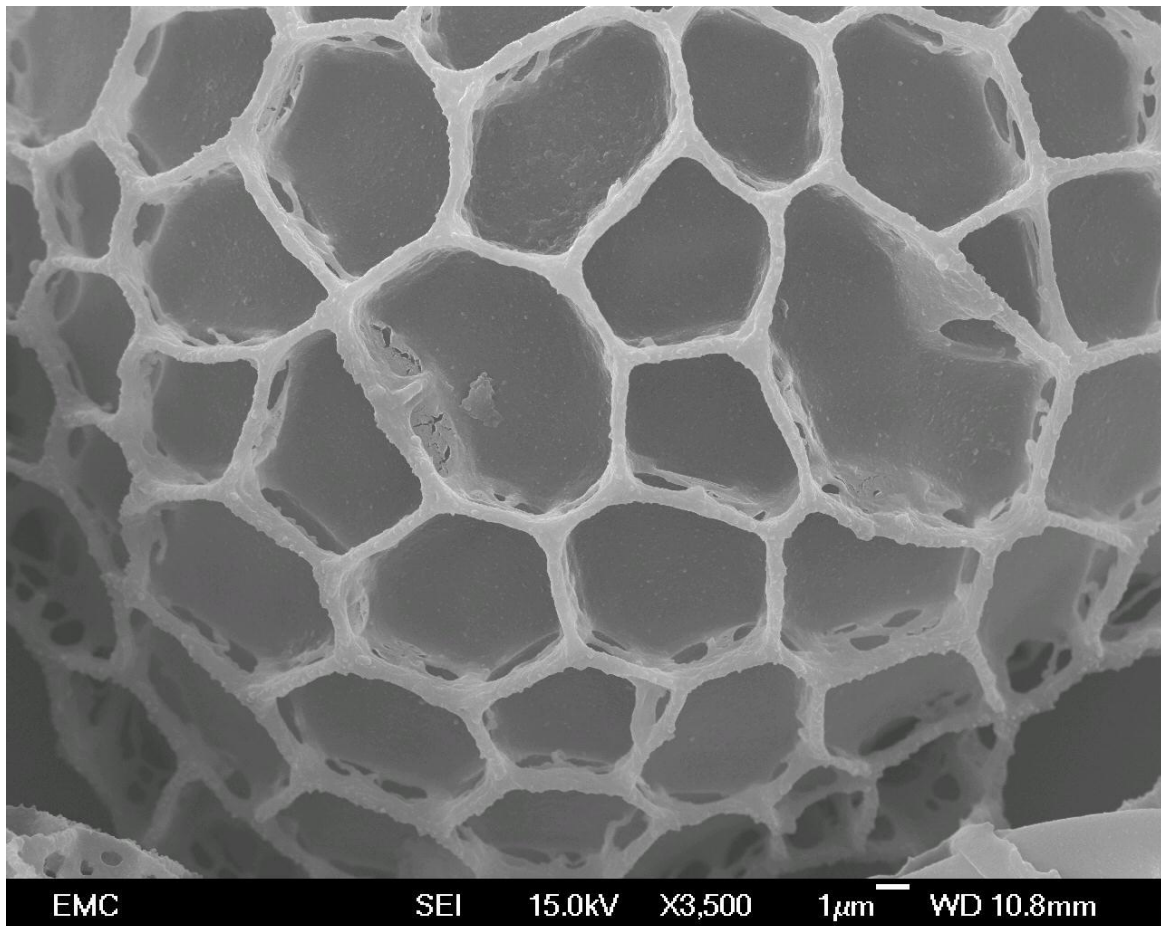


Figure 27: SEM image of SpECs(3) focused on the region of the damaged ektexine of a shell.

When SpECs particles are viewed under the microscope (**Figure 23**), they are not imploded, due to the absence of vacuum. Further to this, the damage caused to the mura of SpECs(3) appears to have occurred due to the use of vacuum and the large degree of imploding of the shape itself. It is therefore only present in extractions which have been exposed to a very strong vacuum, such that is used in SEM.

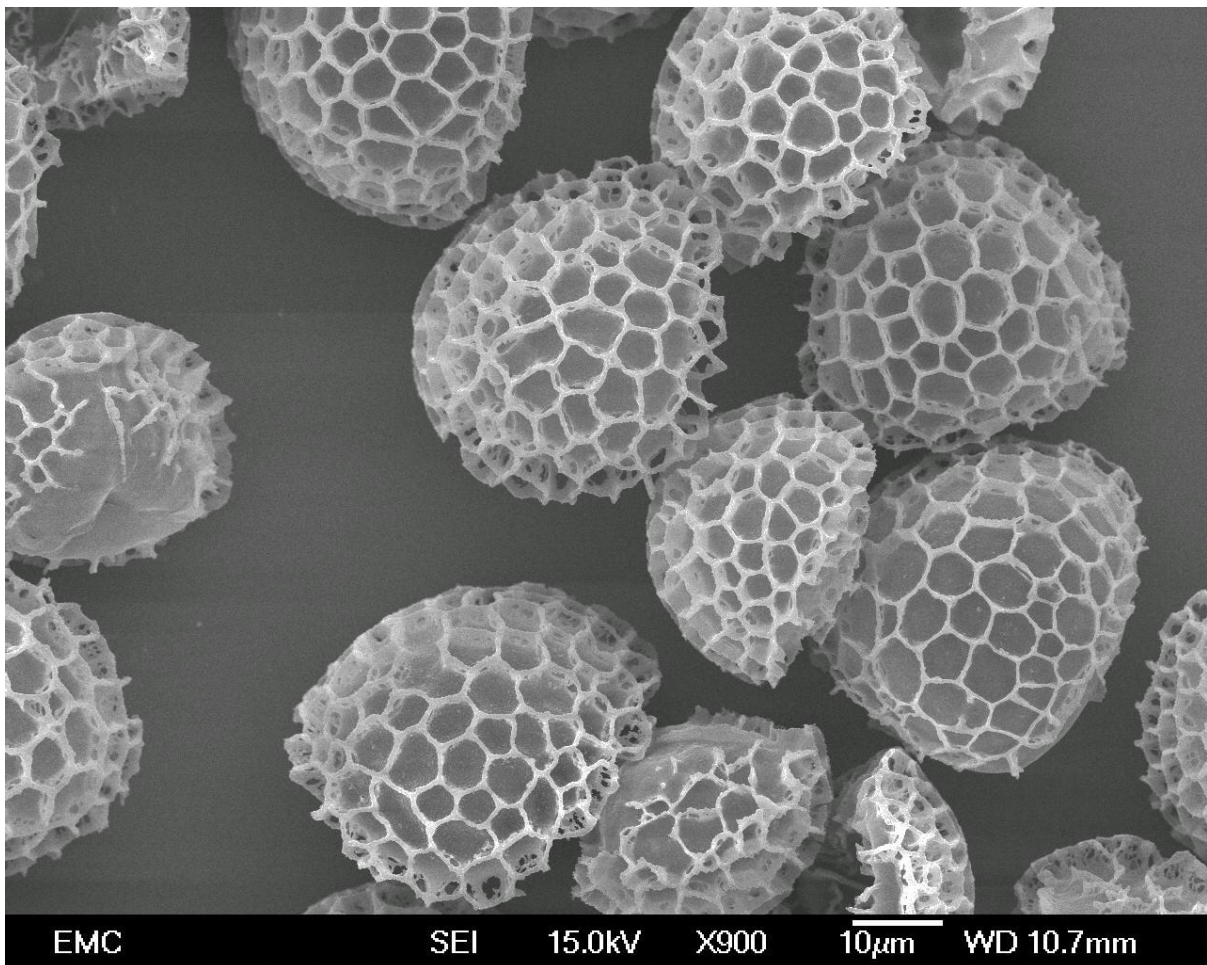


Figure 28: SEM image of HCl extracted SpECs [SpECs(3)].

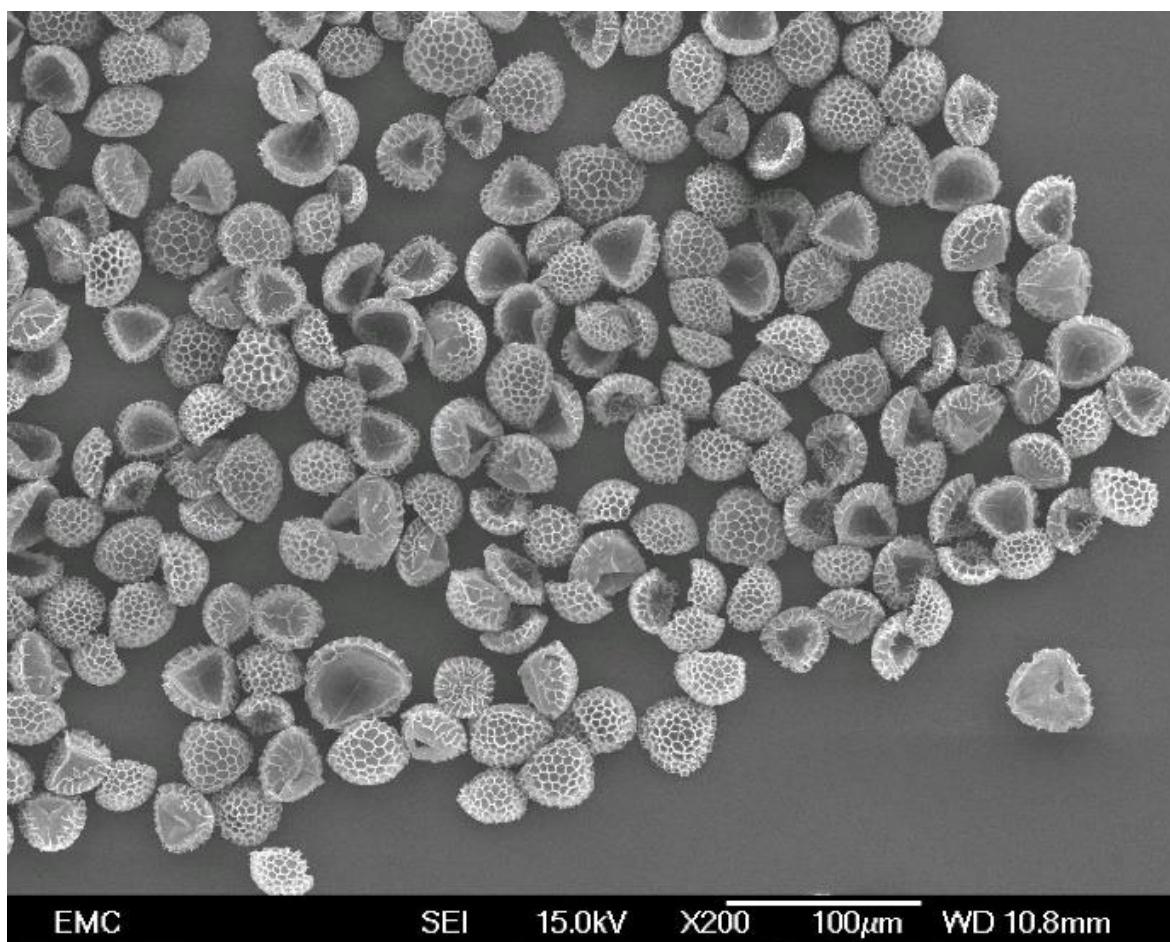


Figure 29: SEM image of SpECs(3). The trilete scar appears to be particularly vulnerable to these extraction conditions. Only this side of the exines exhibits damage to the ektexine.

IR analysis

Figure 30 presents the FT-IR spectrum of SpECs(3) compared to the one obtained by raw spores. SpECs(3) present a peak that has been shifted from the 1743 cm^{-1} , which represented lipid esters, to an increased broad peak covering $1700 - 1730\text{ cm}^{-1}$. This could be an overlap of (C=O) vibrations from both carboxylic acids and esters. Acid catalysed hydrolysis of esters could give an increased number of carboxylic acids. An increased peak at 1280 cm^{-1} which possibly accounts for C-O vibrations in ethers may have been generated by the acid catalysed dehydration of hydroxyls. Furthermore, the hydroxyl peak centred around 3400 cm^{-1} is very reduced, which might be supported by the reduced O content inferred from CHN. There is also

a large increase in the aromatic ring modes peak found at 1510 cm^{-1} which is significant, as this was entirely diminished in the SpECs(1) extraction and may be a useful adsorption site due to possible π - π interactions. There is also an increase in the alkenyl groups in the $1600 - 1650\text{ cm}^{-1}$ region which could be due to removal of hydroxyls by acid catalysed elimination reactions. Another increase in intensity is observed around 1280 cm^{-1} which is believed to be from (C-O) carboxylic acids, similar to band in the spectra of oleic (1284 cm^{-1}) and stearic acids (1297 cm^{-1}), respectively.¹⁷⁴

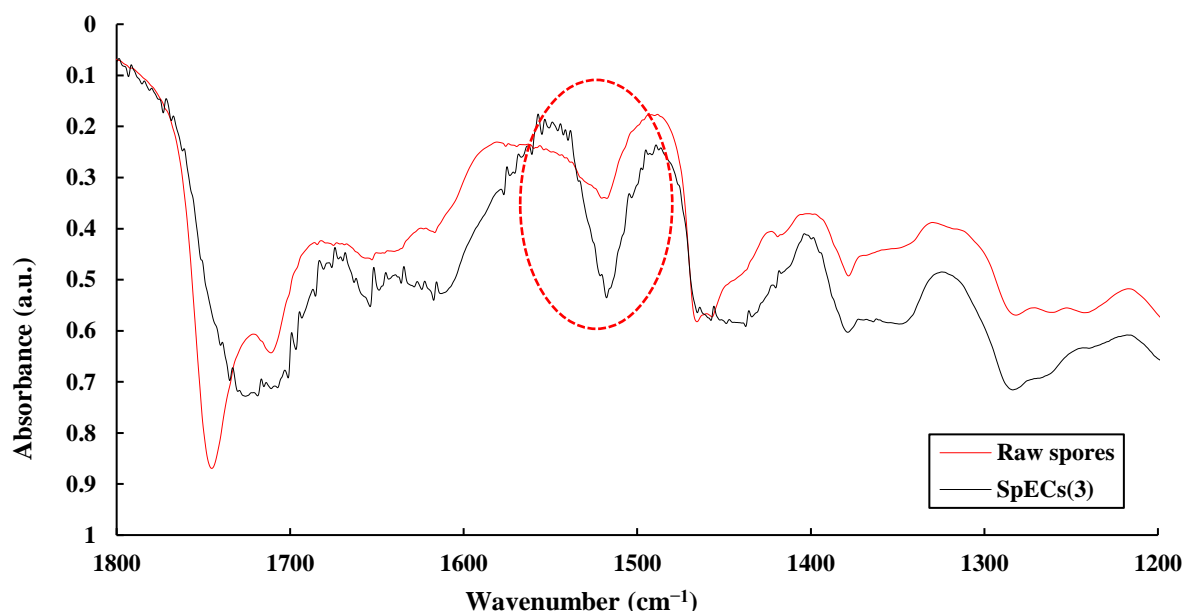


Figure 30: FT-IR spectra of SpECs(3) and raw *L. clavatum* spores. Highlighted is the significant increase in aromatic ring modes $\sim 1510\text{ cm}^{-1}$.

2.6.4. FT-IR comparison of the three extractions and the raw spores

A comparison of the different IR absorption bands observed for the different extraction methodologies is presented in **Table 5**, supplemented by comparisons with previously reported data in the literature. The aim of this collation is to try and give an accurate depiction of all the different groups that are exhibited in this material and the differences accrued due to the different extraction methodologies used in this work.

Table 5: IR analysis of the three different SpECs types and raw spores (peaks at cm^{-1}).					
raw LC	SpECs(1)	SpECs(2)	SpECs(3)	identification	Ref.
3600-2600	3600-2600	3600-2600	3600-2600	Carboxylic acid and alcohol $\nu(\text{OH})$	137,170,174,178-180
2925	2925	2925	2925	$\nu_{\text{asym}}(\text{CH}_2)$	137,170,174,178-
2855	2855	2855	2855	$\nu_{\text{sym}}(\text{CH}_2)$	137,170,174,178-
1743	-	-	1736	Lipidic esters $\nu(\text{C}=\text{O})$	170-174
-	-	-	1736	Esters $\nu(\text{C}=\text{O})$	174
1710	1708	-	1724	Carboxylic acid $\nu(\text{C}=\text{O})$	137,170-
1652	1653	1652	1654	Alkenyl $\nu(\text{C}=\text{C})$	174
1616	1617	1614	1617	Aromatic $\nu(\text{C}=\text{C})$	174
-	-	1575 and 1540	-	$\nu_{\text{asym}}\text{CO}_2^-$	176,177
-	-	1463 and 1435	-	$\nu_{\text{sym}}\text{CO}_2^-$	176,177
1516	-	1515	1509	Aromatic ring mode	181
1464	-	-	-	CH_2 deformation (lipid)	174
-	1433	-	1435	Carboxylic acid $\delta(\text{OH})$	182
1376	1387	1382	1374	$\delta_{\text{sym}}(\text{CH}_3)$	183
1344	-	1342	1341	$\Gamma_{\text{wagging}}(\text{CH}_2)$	184
1278	-	-	1280	Carboxylic acid $\nu(\text{CO})$	185
1258	1260	1260	1263	Ether $\nu(\text{CO})$	174
1240	-	-	-	Ester $\nu(\text{CO})$	172
-	1202	-	1199	Aromatic $\delta(\text{CH})$	174
1160	-	-	-	Aromatic $\nu(\text{CO})$	172
1117	1111	1123	1125	Ether or alcohol $\nu(\text{CO})$	174
1050	1059	1054	1060	Polysaccharides	174
1030	-	1033	1033	Polysaccharides	174
1007	-	1005	999	Alkenyl $\gamma(\text{CH})$	174
-	882	882	882	Unassigned	-
-	844	838	-	Aromatic $\gamma(\text{CH})$	174
826	-	-	827	Aromatic $\gamma(\text{CH})$	174
789	-	-	783	Unassigned	-
720	721	720	722	$\delta_{\text{rocking}}(\text{CH}_2)$	186

Figure 31 presents the FT-IR spectra of all three extractions compared to the raw spores. SpECs(1) exhibited fewer functional group peaks in every region except for (OH) stretching of hydroxyls. This type of SpECs still exhibits some carboxylic acid character (1710 cm^{-1}), though relatively less than the other extractions. Interestingly, it appears to show the largest peak for (OH) stretching of all the extractions, which is at odds with the understanding that phosphoric acid is often used as a dehydrating agent to catalyse elimination reaction of hydroxyl to yield alkenes.

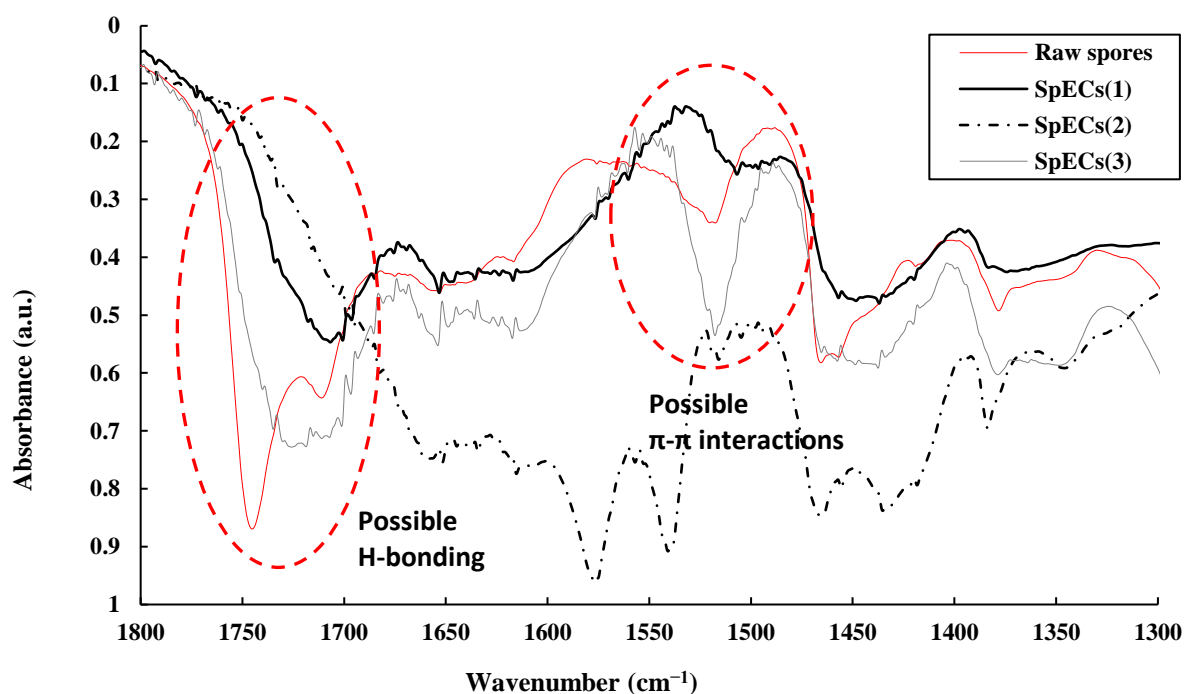


Figure 31: FT-IR spectra of the 3 SpECs types and raw *L. clavatum* spores. Highlighted are the stretching frequencies for carboxylic acids $\sim 1710\text{ cm}^{-1}$ and aromatic ring modes $\sim 1510\text{ cm}^{-1}$ as these groups represent possible adsorption sites for the contaminants.

The 1744 cm^{-1} band accounting for lipid esters is reduced in all three extractions, however the (C=O) carboxylic acid peaks $\sim 1710\text{ cm}^{-1}$ are also completely diminished in SpECs(2) which have been replaced by sodium carboxylates. In SpECs(3) the hydroxyl peak centred around 3400 cm^{-1} is the most reduced of all the extractions, which combined with the reduced oxygen

content, may indicate hydroxyl elimination reactions, which leaves a series of double bonds, accounting for the increased darkening. SpECs(3) appear to exhibit the highest proportion of both carboxylic acid groups and aromatic ring groups, which may both be important functional groups for adsorption with the four contaminants.

2.7. Surface modification of SpECs

The extracted SpECs were further treated with a series of different reagents, to produce materials with different surface chemistry and then the effects of the treatment on their IR spectra and their adsorption properties and behaviour were studied. The objective was to modify the material's surface by subjecting the SpECs to such oxidative conditions that the material would become more hydrophilic. It was believed that an increase in the number of protic sites would favour the adsorption of hydrophilic contaminants, thus oxidising procedures inspired by the existing literature for activated carbon surface modification were tested.¹⁸⁷

The oxidants tested were ammonium persulfate (APS), *tert*-butyl hydroperoxide (TBHP) and sodium hypochlorite (NaOCl). After different treatments described in section 8.2, the modified SpECs (**Figure 32**) were analysed with elemental analysis to determine the percentages of C, H and N (**Table 6**).

sample	treatment	C %	H %	N %
SpECs(3)	Extraction only	67.48	9.11	0.00
SpECs(3)BL1	NaOCl	55.35	6.54	0.00
SpECs(3)APSH1	APS 1 M 90 °C	63.36	8.15	0.00
SpECs(2)BL1	NaOCl	53.15	7.43	0.02
SpECs(2)APSH1	APS 1 M 90 °C	51.21	7.35	0.21
SpECs(2)APSR1	APS 1 M room T	52.86	7.91	1.13
SpECs(2)HCl	extraction only	60.71	8.68	0.40
SPECs(2)TBHP	<i>tert</i> -butyl hydroperoxide	57.92	8.65	1.03



Figure 32: Modified SpECs. The bleaching procedure on SpECs(2) changes the SpECs colour from yellow to white (6th vial counting from left to right). For SpECs(3) it changes the colour from dark brown to lighter brown (7th vial).

2.7.1. NaOCl treatment

Treatment with NaOCl showed to be affecting the material's colour; SpECs(2) changed from yellow to white, whilst SpECs(3) became slightly lighter. This change might indicate that the NaOCl has possibly reacted with the conjugated systems in the sporopollenin structure, affecting the double bonds and therefore removing the source of the yellow colour.

After NaOCl treatment, SpECs(3) showed a considerable reduction in their carbon and hydrogen content which implies the calculated oxygen percentage increased from approximately 23% to 38%. This large increase in oxygen might indicate the possibility of addition of Cl as well. During the HCl extraction it is suspected that many double bonds were created from elimination reactions. These double bonds could then be oxidised to give OH groups again, which can oxidise further to ketones, carboxylic acids and in some cases acetyl chloride groups, when treated with NaOCl. The same effect was observed for SpECs(2); the material's oxygen content was risen from 32% to 39%.

In this treatment, it was concluded that the freshness of the bleach used is a factor affecting the resulting product, since the protocol was repeated several times giving SpECs of different

shades of white with different adsorption properties each time. Whiter products yielded products with better adsorption properties. The concentration of bleach is the important parameter, since opened bottles or bleach older than 4 months after the production date lose their strength as concentration diminished by approximately half in this time.¹⁸⁸

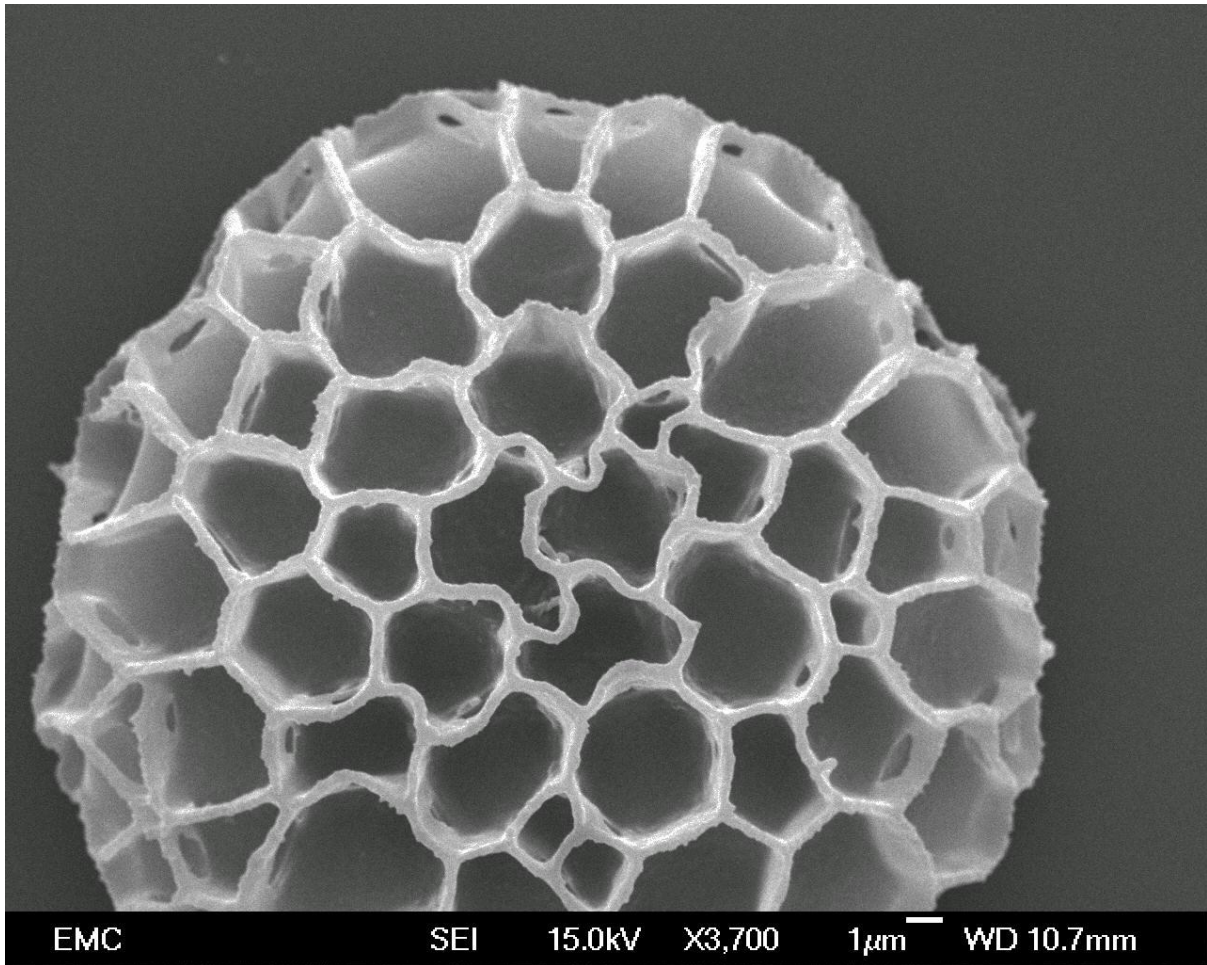


Figure 33: SEM image of SpECs(2)Bl.

Following the bleaching treatment with NaOCl, additional damage can be observed on the exine capsule surface when viewed at higher magnification. When compared with the untreated SpECs(2) (**Figure 24**), tiny holes appear homogenously over the surface of the entire material (**Figure 33** and **Figure 34**). This oxidative damage is spread across the entire capsule with no particular weak points, that might otherwise result in a breakage in the structure of the exine.

This ability of the exine to endure significant oxidative damage throughout the material without exhibiting weak points, may well be an evolved trait for the protection of the genetic material usually stored within. It also lends evidence to the efficacy of the material for antioxidant properties.

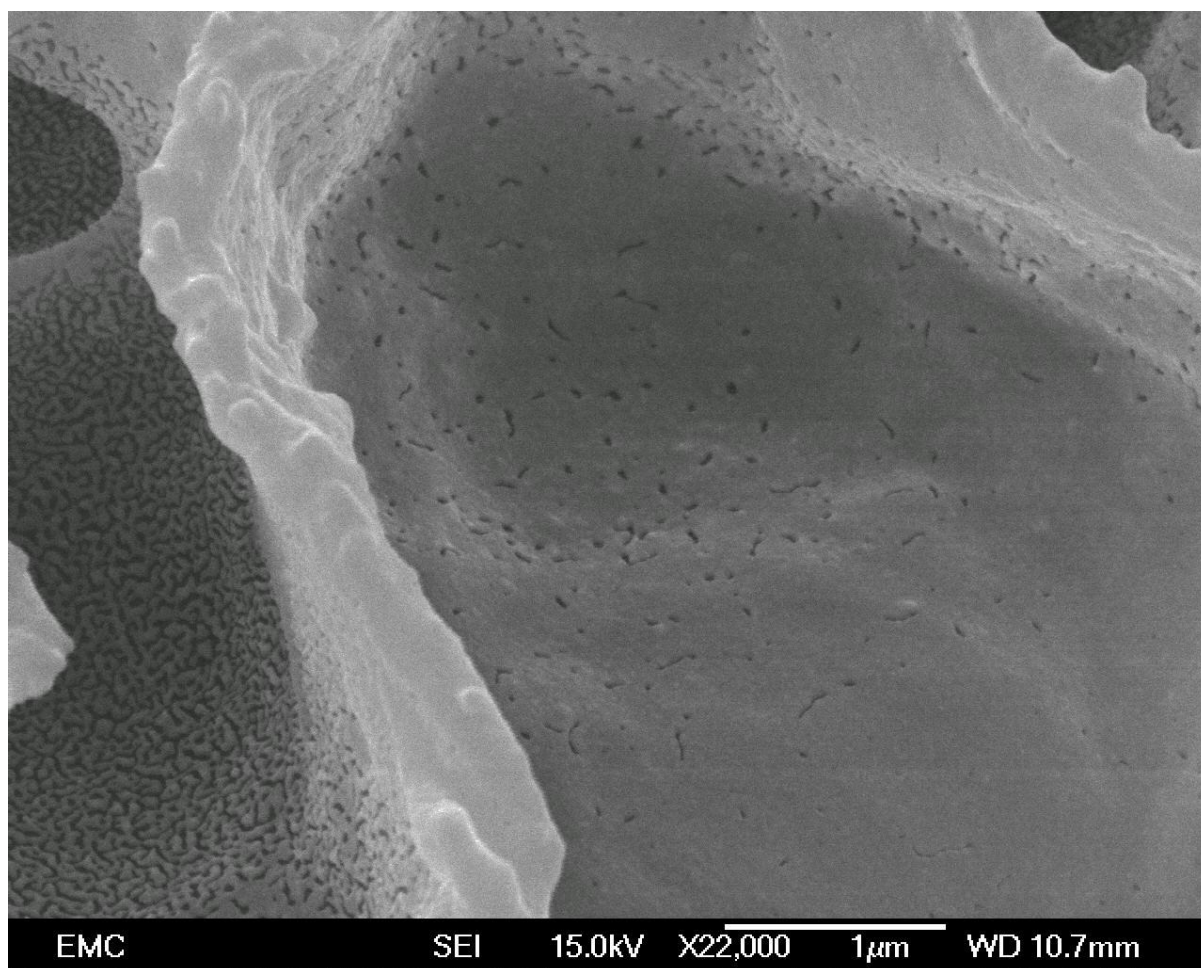


Figure 34: SEM image of SpECs(2)B1 magnified to exhibit the damage on the surface.

IR analysis

SpECs(2) were treated with NaOCl with the aim of oxidising functional groups to carboxylic acids. **Figure 35** shows the FT-IR spectra of the bleached product, SpECs(2)B1, compared to SpECs(2)HCl, exhibiting a good overlap. It is noticeable that a large increase in the stretching frequency exhibited at $\sim 1712\text{ cm}^{-1}$ which is highly associated with the carbonyls of carboxylic

acids appear to have been generated. Otherwise, the overlap of the remainder of the spectra appears very close with the original, providing reassurance that the change observed is likely a large increase in the number of carboxylic acid groups present. The CHN analysis also indicated a large increase in the relative amount of oxygens as the mass% of C and H and N decrease substantially (**Table 7**).

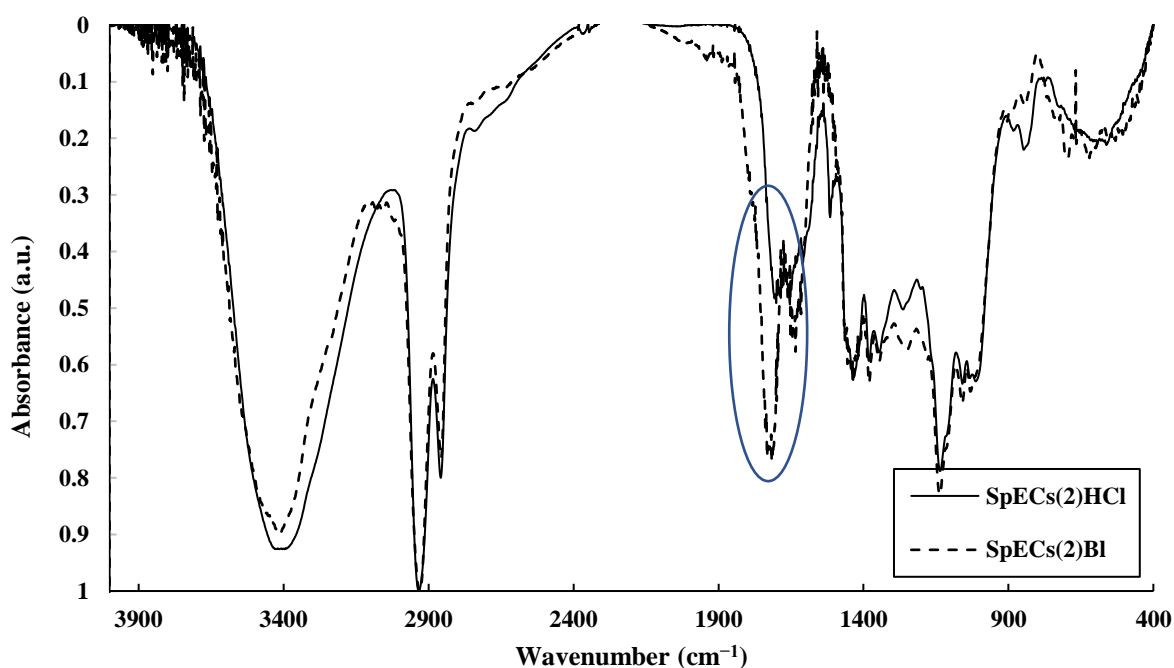


Figure 35: FT-IR spectra of NaOCl treated and HCl treated SpECs(2) [SpECs(2)Bl and SpECs(2)HCl respectively].

sample	treatment	C %	H %	N %
SpEC(2)Bl1	NaOCl	53.15	7.43	0.02
SpECS(2)HCl	HCl	60.71	8.68	0.40

2.7.2. APS treatment

The treatment with ammonium persulfate was conducted both at room temperature and at 90 °C. Different concentrations of ammonium persulfate were used (0.5 - 2 M diluted in sulfuric acid) following the procedures described in section 8.2.3. SpECs(3) showed a reduction in their hydrogen content while the calculated oxygen percentage increased from approximately 23% to 29%. The same treatment on SpECs(2) also increased the percentage of oxygen from 32% to 41% and lowered the H% by 1.5% approximately.

Treatment of SpECs(2) with ammonium persulfate at room temperature did not exhibit major differences in the elemental analysis (**Table 8**) or in the adsorption test results, whereas the same treatment at higher temperatures gave a material with much higher efficacy for adsorbing contaminants.

Table 8: Elemental analysis results for 1 M APS treated SpECs(2) at room temperature and at 90 °C.				
sample	treatment	C %	H %	N %
SpECs(2)	-	59.00	8.89	0.12 - 0.56
SpECs(2)APSH1	APS 1 M 90 °C	51.21	7.35	0.21
SpECs(2)APSR1	APS 1 M room T	52.86	7.91	1.13

After having set the temperature parameter at 90 °C, different concentrations of ammonium persulfate were tested (0.5 - 2 M) in order to determine the concentration that would create the most efficient material in terms of contaminant adsorption.

The APSH treated SpECs(2) exhibited a change in their colour, from mustard yellow it became more yellow. They also exhibited damage on their surface, a different type of damage compared to the NaOCl treated ones, which is visible in the SEM pictures **Figure 36** and **Figure 37**. There is no erosion of the shell as it was observed with the NaOCl treated SpECs(2), instead, damage appears to be greatest on the mura which appeared misshapen with far shorter

tectal elements. The integrity of the shell appears to be maintained, but again a significant number appear deflated after application of a vacuum (**Figure 38**).

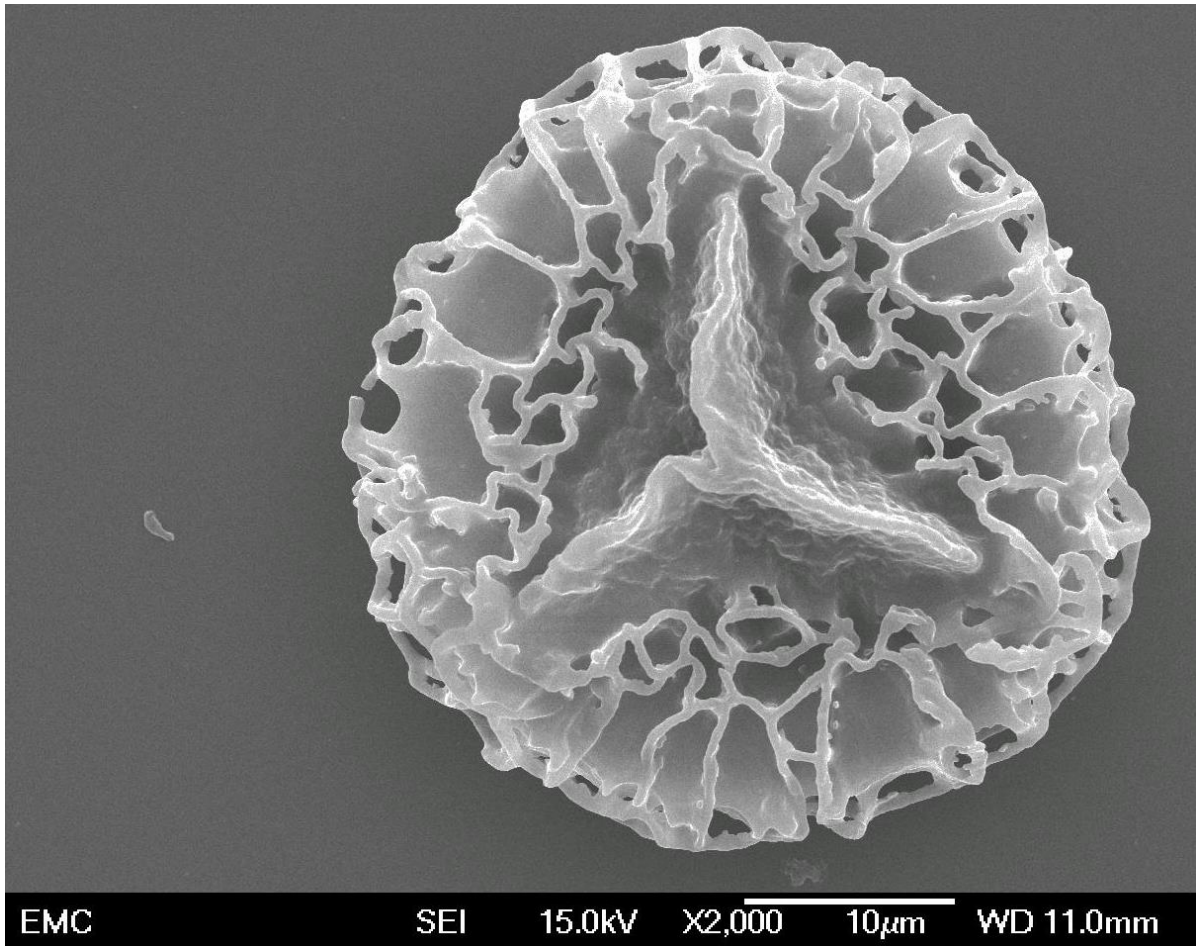


Figure 36: SEM image of SpECs(2)APSH showing the trilete scar and the damage in the decorative section of the shell.

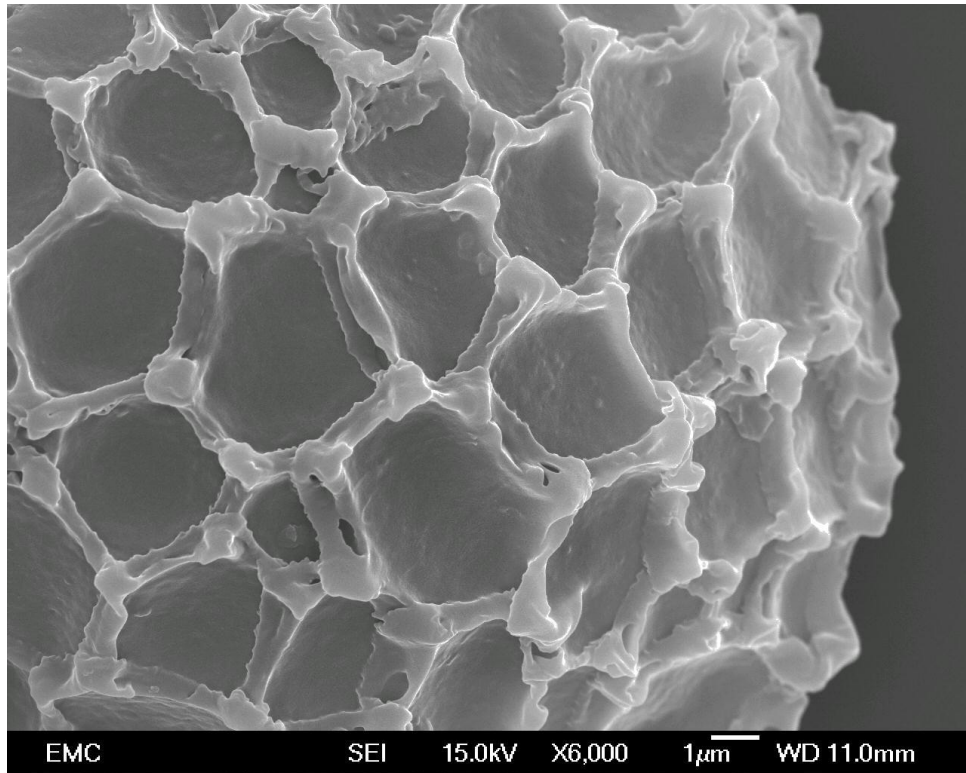


Figure 37: SEM image of SpECs(2)APSH focused on the decorative part of the shell, presenting some damage.

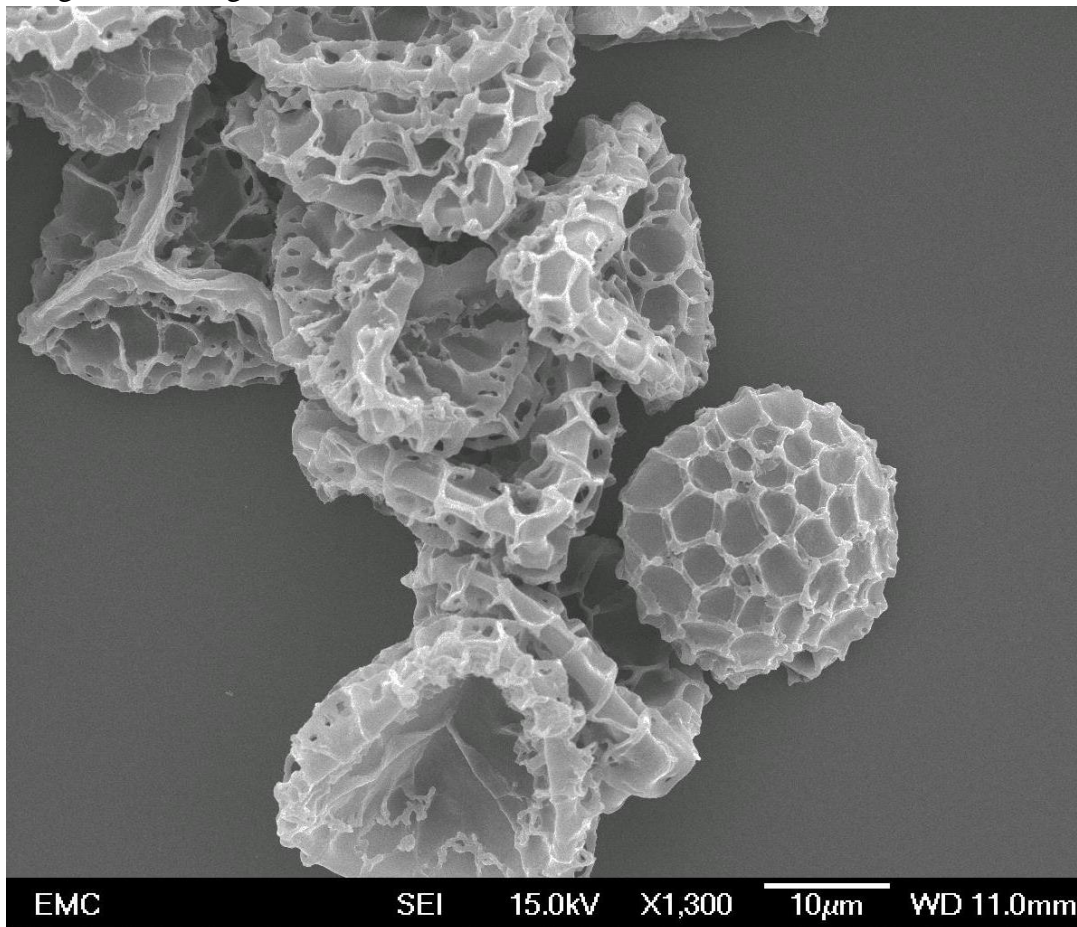


Figure 38: SEM image of SpECs(2)APSH showing collapsed spores under the vacuum.

IR analysis

Treatment with ammonium persulfate 1 M at 90°C of the SpECs(2) gave the product SpECs(2)APSH, which was compared with SpECs(2) and SpECs(2)HCl samples. There is a clear generation of carbonyls associated with vibrations from carboxylic acids using this treatment (**Figure 39**). A large peak at 1710 cm^{-1} can be attributed to the (C=O) from carboxylic acids, which may be expected due to the oxidising nature of ammonium persulfate. An increase is also seen at 1130 cm^{-1} from what is most likely to be the (C-O) vibrations of carboxylic acids. There is no overlap with possible esters and there are no carboxylates remaining.

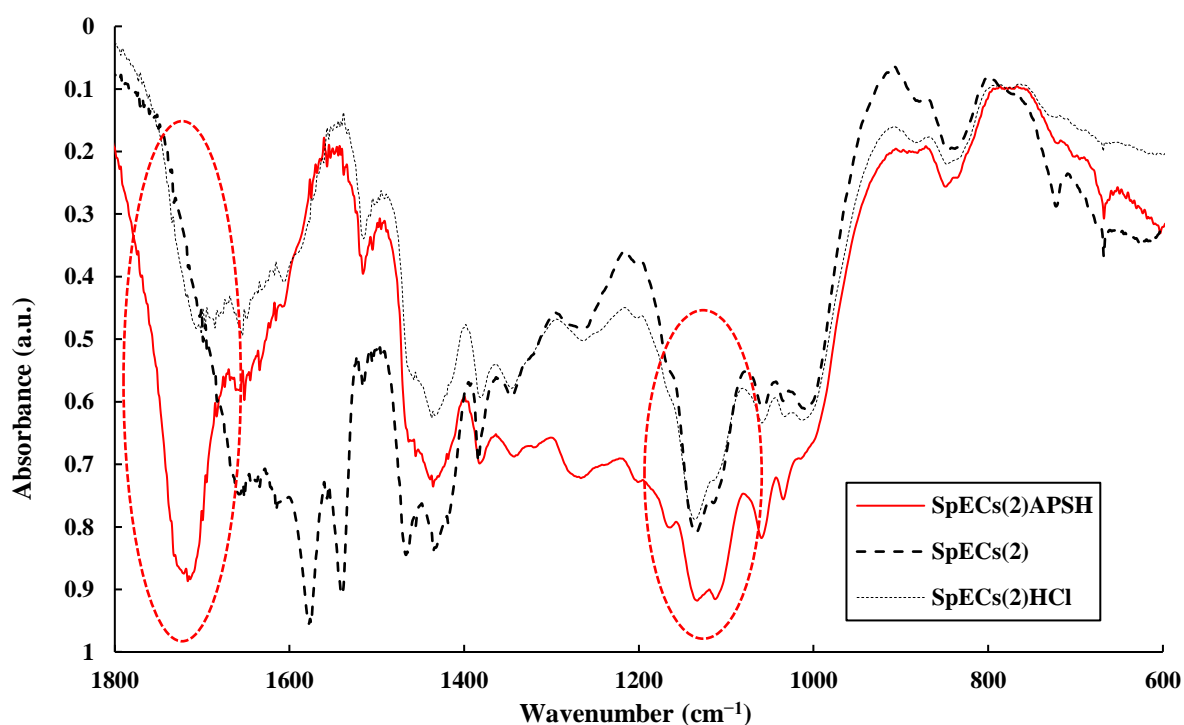


Figure 39: FT-IR spectra of SpECs(2)APSH and SpECs(2)HCl compared to SpECs(2).

2.7.3. Amination of SpECs(3)

Since it was concluded that SpECs(3) appear to have the highest abundance of carboxylic acids, an amination of these available carboxylic acids was attempted. A coupling reaction was

performed with 1,6-diaminohexane to give a functional group that can act as a hydrogen donor and may be positively charged to aid electrostatic interaction. SpECs(3) were treated with 1,6-hexanediamine following the protocol described in section 8.2.6. The resulting SpECs [SpECs(3)AM] were analysed using FT-IR and their nitrogen content was verified with elemental analysis.

Following amination, there is an increase in the region that has previously been assigned to (OH) stretching spanning $\sim 2500 - 3500 \text{ cm}^{-1}$ (**Figure 40**). This region also accounts for (N-H) stretching in primary amines. There is a clear reduction in the (C=O) peak at 1710 cm^{-1} from carboxylic acids and a large new peak formed at 1640 and 1650 cm^{-1} representing the stretching of a (C=O) from primary and secondary amides. It should also be noted that apart from these changes highlighted, the two spectra have very good overlap, which should again provide confidence with the consistency of the normalisation procedure used for the FT-IR spectra and the accuracy of the qualitative comparisons made.

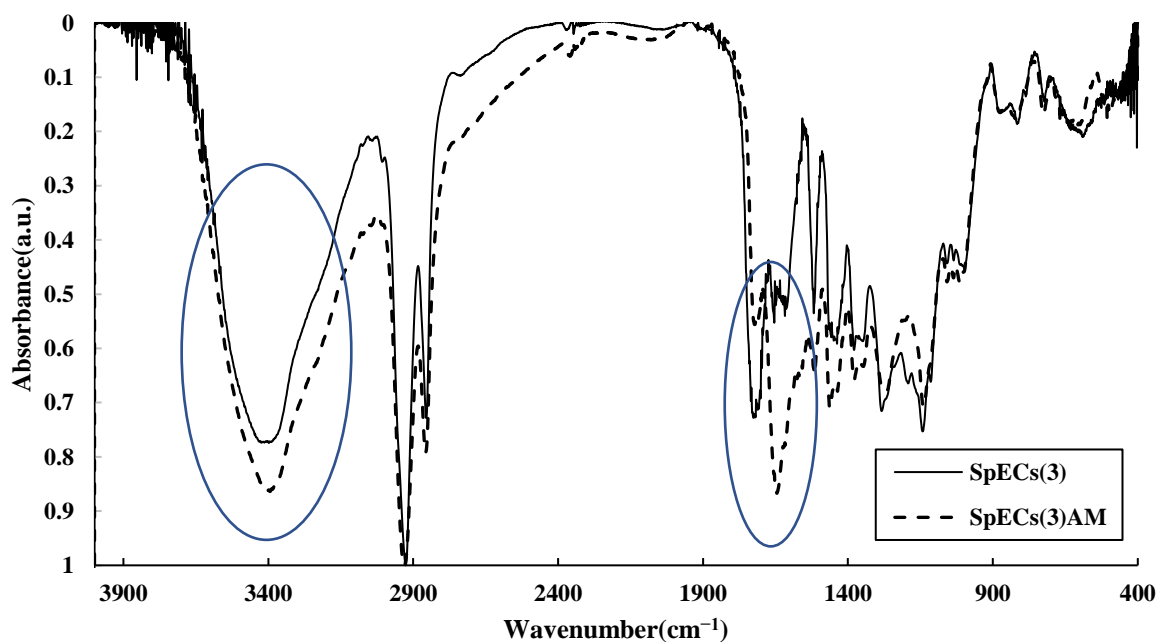


Figure 40: FT-IR spectra of SpECs(3) before and after amination (aminated form is SpECs(3)AM).

Such a result lends further weight to the previous assumption that the 1710 cm^{-1} stretching frequencies observed were indeed due to the carbonyl groups of carboxylic acids, as they have been significantly reduced whilst a new peak has emerged that is associated with the carbonyl groups of an amide, which is precisely what would be expected with a coupling reaction (**Figure 41**).

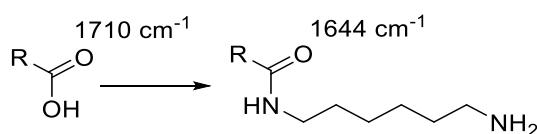


Figure 41: Carboxylic acid amination leading to the formation of a secondary amide.

From the increase in nitrogen exhibited in the CHN analysis (**Table 9**) of this product, it is clear that there has been a successful generation of amides within this material from coupling between the available carboxylic acids of the sporopollenin and the amines of the hexanediamine.

Since the molecular weight of 1,6-hexanediamine is 116 g/mol and by using the CHN data obtained both before and after amination, a calculation of the active sites per 1 g of SpECs can be performed:

- 39.8 mg of N in the sample ($1 \times 0.0398 = 39.8\text{ mg}$).
- 0.00284 mol of N in the sample ($0.0398\text{ g} / \sim 14\text{ g/mol} = 0.00284\text{ moles}$).
- Therefore 0.00142 mol of 1,6-hexanediamine ($0.00284\text{ mol} / 2 = 0.00142\text{ mol}$).
- This equates to 164 mg of 1,6-hexanediamine ($0.164\text{ g} \times 116\text{ g/mol} = 0.00142$).

In 1 g of SpECs(3)AM there exist $\sim 164\text{ mg}$ of 1,6-hexanediamine or 1.42 mmol of active sites.

The elemental analysis was repeated four months post-production in order to check the material's possible degradation. The elemental analysis results are presented in **Table 9**.

Table 9: Elemental analysis results for SpECs(3) before and after amination.

material	C%	H%	N%
SpECs(3) before amination	61.12	7.81	0.33
SpECs(3)AM fresh	61.07	8.37	3.98
SpECs(3)AM 4 months old	58.37	8.33	3.83

The elemental analysis results indicated the decrease of the carbon and nitrogen content to 95% and 96% of their original mass values respectively. Interestingly, the ratio between the carbon and nitrogen content has not changed, it has stayed steady, around 15%. While carbon and nitrogen have decreased, the hydrogen content has stayed the same, meaning that the material has possibly gained some water over time. It is concluded that the aminated SpECs were not stored properly, leading to adsorption of moisture and humidity, being evident by the elemental analysis but also on the adsorption experiment results presented in chapter 3.4.7.3.2.

2.7.4. Iron loading onto SpECs

An attempt to produce magnetic SpECs was made and thus the protocol described in section 8.2.5.4 inspired by the literature,¹⁶⁰ was followed. The original procedure describes the dissolution of the iron salts in water, followed by addition of SpECs, and finishing with the addition of ammonia solution. This simple step procedure was followed many times for all extracted SpECs but was not found to produce magnetic SpECs that would respond even to a strong magnet.

Several attempts were made, trials of altering the Fe-SpECs ratio, the ammonia solution concentration, the SpECs type or raw spores, the contact time of SpECs with the Fe salt solution and the filtration and washing step after the Fe salt contact time. No resulting material was attracted to a strong magnet until an alternative procedure was tried. SpECs were left to

sediment after the Fe loading and the Fe salt solution was removed with a pipette, followed by dropwise addition of concentrated ammonia solution. The microscopic image of the resulting material showed SpECs particles possibly surrounded by newly formed particles, assumed to be some form of iron oxide (**Figure 42** and **Figure 43**). SpECs loaded with Fe salts in ethanolic solution and under vacuum were tested as well. A portion was left stirring with different concentrations of ammonia solution (1, 2 and 3 M). The resulting materials showed some response towards a strong magnet. The same protocol was repeated with the Fe salt solution in water and the mixture was left under vacuum overnight, however the resulting material did not show any magnetic response.

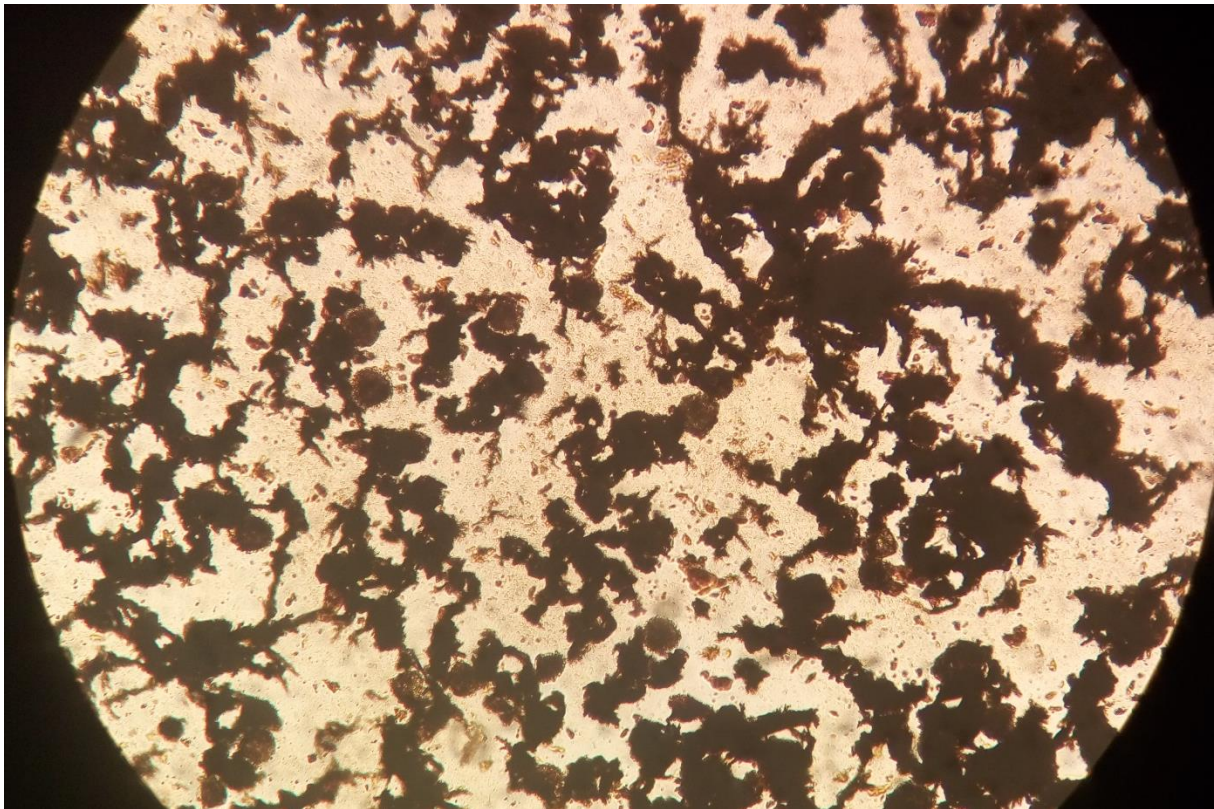


Figure 42: Microscope image of raw spores surrounded by newly formed particles after the magnetic procedure (lens 20 x 0.40).

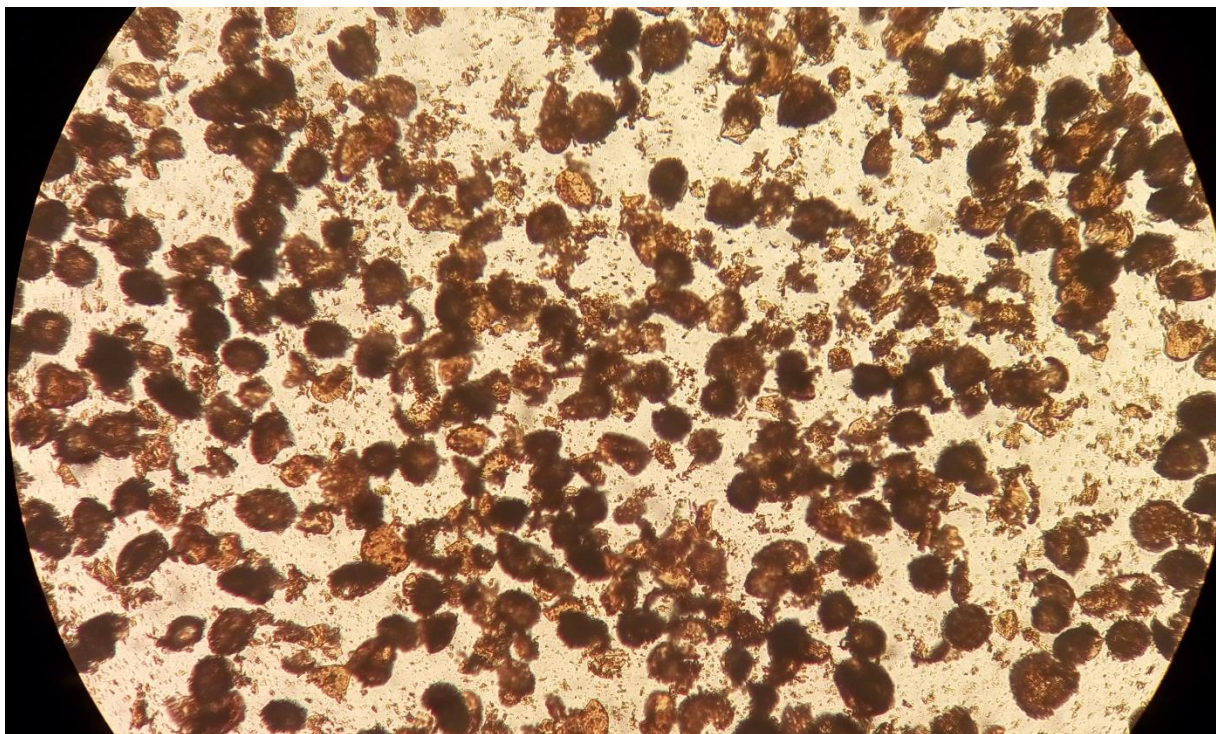


Figure 43: Microscope image of SpECs(3) surrounded by newly formed particles after the magnetic procedure (lens 20 x 0.40).

The protocol was therefore adapted, by omission of the final oxidising step to produce a nonmagnetic, iron loaded product (experimental section 8.2.5). First, the iron salts were diluted in a solution following the addition of the SpECs, either under vacuum or without. Two different solvents were tested, water and acetone, so that the best loading conditions would be determined. Elemental and ICP-OES analysis followed each procedure to show the iron loading percentages.

The different extracted SpECs were treated with $\text{FeCl}_3 \cdot 6\text{H}_2\text{O}$ and $\text{FeCl}_2 \cdot 4\text{H}_2\text{O}$ in different solvents: water or acetone, with and without the application of vacuum. The differences in the loading protocol produced SpECs with different Fe loadings, according to the ICP-OES analysis.

2.7.4.1. Iron loading on SpECs(1)

As detailed previously, SpECs(1) displayed damage after their extraction, in the form of cracking and fragmentation of shells. The fragmentation only appeared to be large pieces as smaller debris were not observed. The cracking of shells provided an opportunity for examining the inner surface of the iron loaded SpECs(1) (M20, 3.3% Fe loading). It was observed that there was a significant amount of material on the inside surface of the broken fragment of the iron loaded exines compared with the fragments that were not iron loaded (**Figure 44**). This may give indication of where the iron prefers to attach, as far less was observed on the outer surfaces. This may also explain why loading with the use of vacuum yielded a higher Fe% than when no vacuum was used.

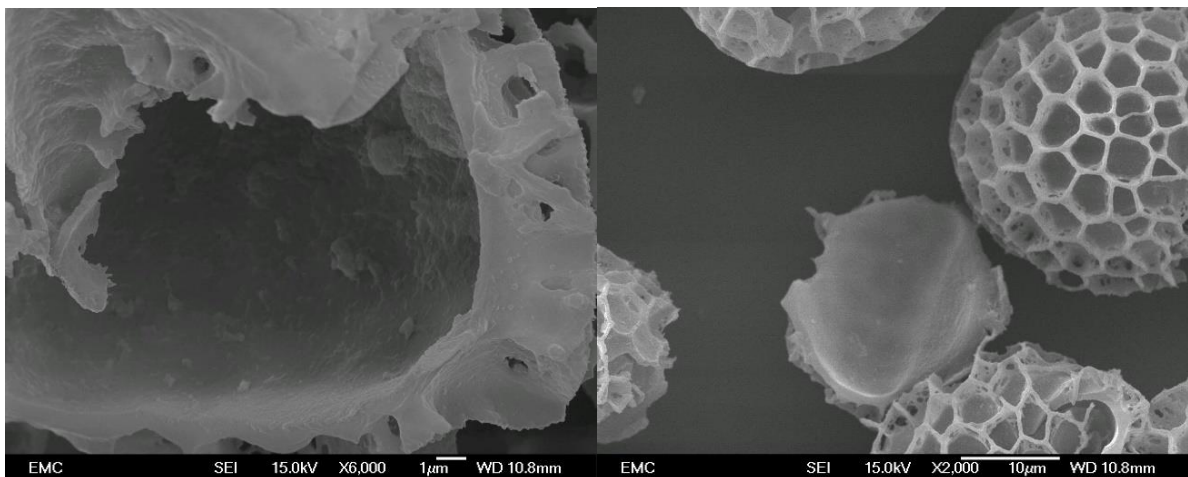


Figure 44: Comparison between inner fragments of iron loaded (left) and unloaded SpECs(1) (right).

Iron loading of SpECs(1) in acetone [M18SpECs(1)] gave the highest Fe percentage, (11.6% Fe loading, **Table 10**) compared to the water loading. As **Figure 45** shows, the iron loading is visible on the surface of SpECs(1) as well.

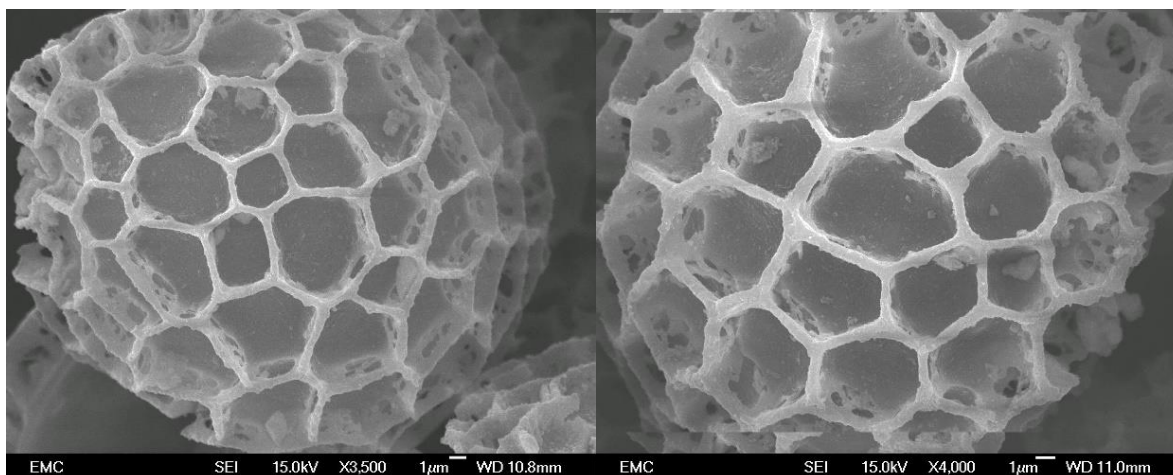


Figure 45: SEM images of iron loaded SpECs(1) in acetone under vacuum.

Table 10: Elemental analysis results for C, H, N content and ICP-OES analysis for Fe of SpECs(1) before and after Fe loading.

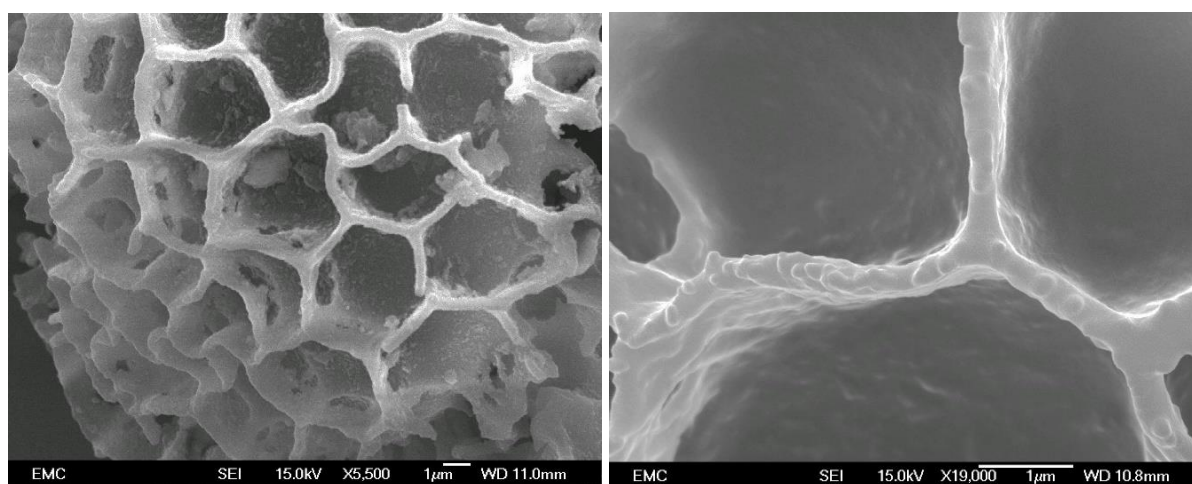
sample	Fe loading conditions	%C	%H	%N	%Fe
SpECs(1)	-	58.65	7.24	0.12	-
M09SpECs(1)	in water	58.78	7.47	0.00	1.668
M20SpECs(1)	in water + vac	55.50	7.01	0.17	3.328
M18SpECs(1)	in acetone + vac	46.96	6.16	0.15	11.57

2.7.4.2. Iron loading on SpECs(2)

Iron loading of SpECs(2) in acetone (M17, 9.9% Fe loading, **Table 11**) and unloaded SpECs(2) exhibited a similar comparison as observed for SpECs(1), displaying the presence of a material on the surface of the iron loaded SpECs(2) [M17SpECs(2)], that is not present in the unloaded samples (**Figure 46**). SpECs(2) presented a 3.3% of iron loading in water and a much higher loading of 9.9% when using acetone as a solvent.

Table 11: Elemental analysis results for C, H, N content and ICP-OES analysis for Fe of SpECs(2) before and after Fe loading.

sample	Fe loading conditions	%C	%H	%N	%Fe
SpECs(2)	-	59.00	8.89	0.56	-
M11SpECs(2)	in water	51.94	7.68	0.91	2.930
M21SpECs(2)	in water + vac	53.19	7.42	1.11	3.382
M17SpECs(2)	in acetone + vac	44.40	6.77	0.92	9.914

**Figure 46:** SEM images of iron loaded (left) and unloaded SpECs(2) (right).

2.7.4.3. Iron loading on SpECs(3)

Iron loaded SpECs(3) prepared in acetone (M19, 8.4 Fe%, **Table 12**) exhibited a large amount of iron debris on the outer surface when compared with unloaded SpECs(3) samples and a much greater degree visible on the outside (**Figure 47**, **Figure 48** and **Figure 49**) than the other iron loaded extractions, despite having a lower overall Fe%. This might indicate that the inner surface of this extraction is less appealing to the iron molecules. As with SpECs(1), SpECs(3) presented the highest Fe loading, 8.4%, when treated in acetone and under vacuum.

Table 12: Elemental analysis results for C, H, N content and ICP-OES analysis for Fe of SpECs(3) before and after Fe loading.

sample	Fe loading conditions	%C	%H	%N	%Fe
SpECs(3)	-	60.10	7.57	0.17	-
M10SpECs(3)	in water	60.02	7.45	0.15	0.632
M23SpECs(3)	in water + vac	60.06	7.60	0.11	1.765
M19SpECs(3)	in acetone + vac	51.11	6.23	0.00	8.356

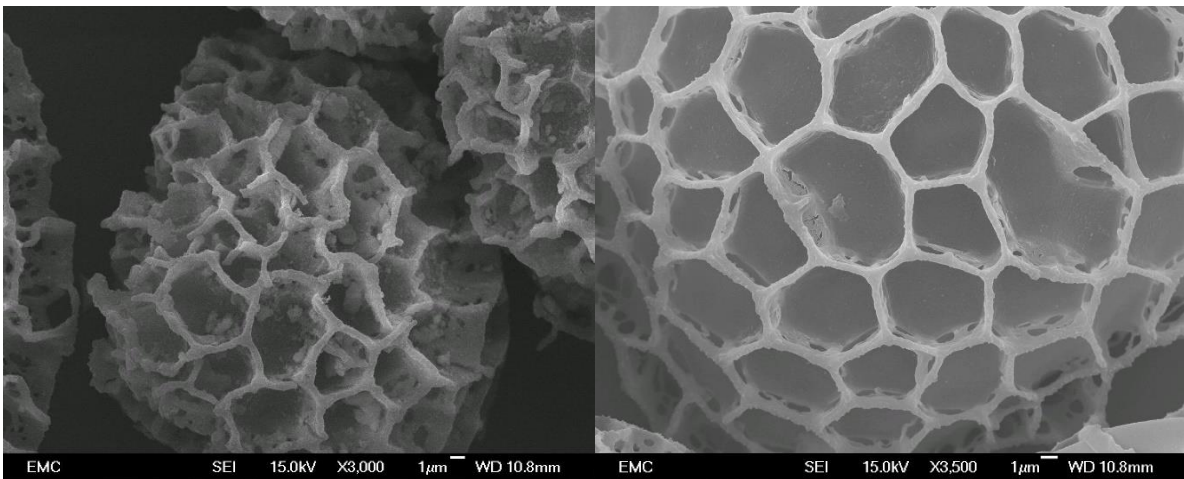


Figure 47: SEM images of iron loaded SpECs(3)M19 (left) and unloaded ones (right).

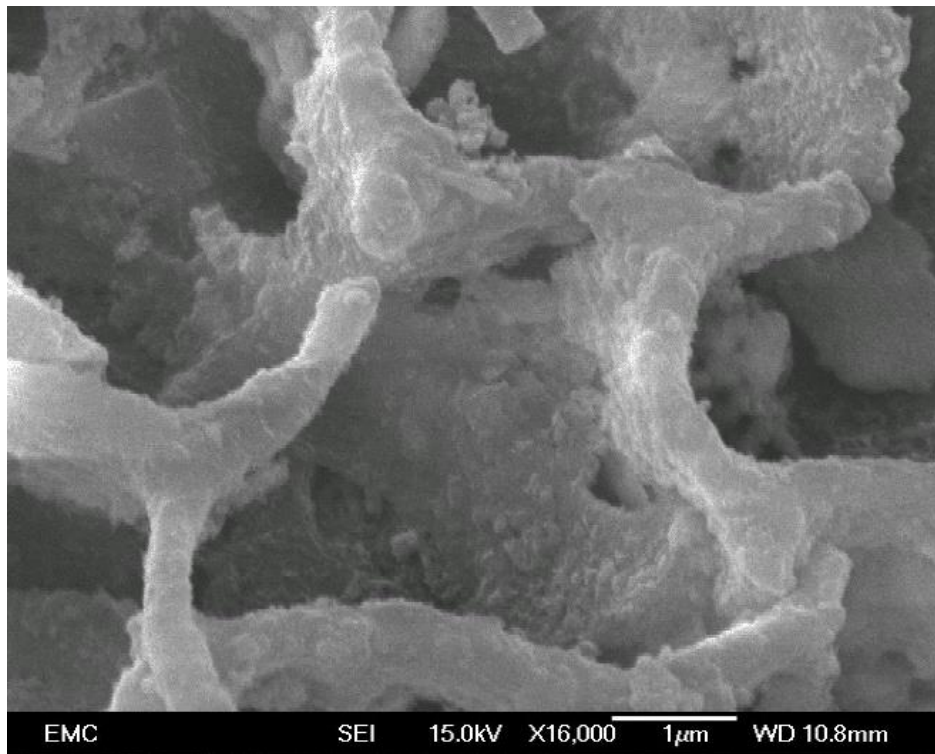


Figure 48: SEM image of iron loaded SpECs(3) focused on the surface of the capsule.

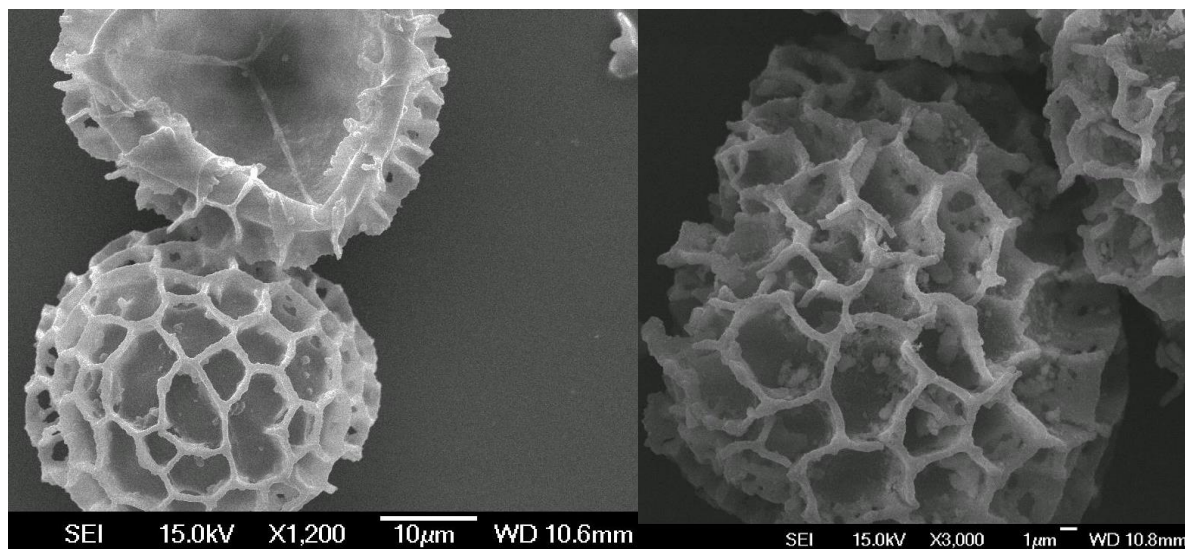


Figure 49: SEM image of iron loaded SpECs(3) showing the loading of the iron molecules on the surface of the capsule.

2.8. SpECs surface analysis - Boehm titration

The Boehm titration was first introduced for the analysis of the surfaces of carbon black and activated carbon.¹⁹¹ Boehm suggested that when a material's surface carries functional groups containing oxygen, the quantities of these groups can be measured based on their different pKa values. Bases of different strength can neutralize oxygen groups of different acidities (**Figure 50**). Since the dissociation constants of carboxyl groups, lactones (after hydrolysis) and phenols are quite different, it has been proven that an accurate way of their determination would be their neutralization behaviour. The traditional procedure involves treatment of the material with a selection of three different bases followed by filtration. The resulting solution is then collected and titrated with a selected base.

The modified Boehm titration procedure involves mixing the material with a basic aqueous medium followed by filtration. Instead of titrating the resulting solution, the treated material is collected, dried and analysed for its Na content. The three different bases proposed are sodium hydroxide (NaOH), sodium carbonate (Na₂CO₃) and sodium bicarbonate (NaHCO₃). The strongest base of all three, NaOH, can neutralize all Brønsted acids, which means that in

sporopollenin it will neutralize phenols, lactone groups and carboxylic acids (**Figure 50**). Na_2CO_3 can neutralize lactones and carboxylic groups and NaHCO_3 will only neutralize carboxylic acids.

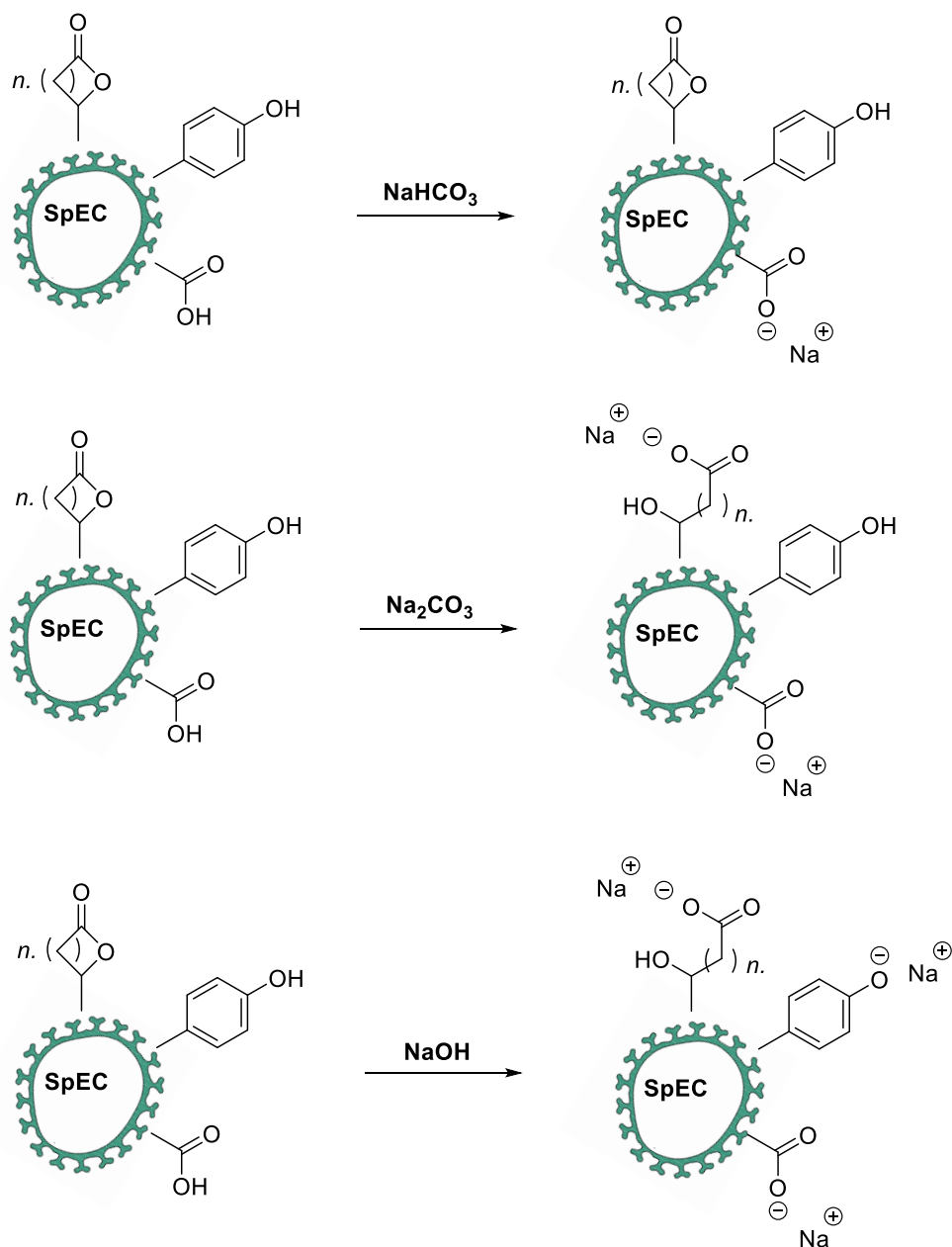


Figure 50: Reactions between the different bases and the different functional groups present on the surface of SpECs.

The surfaces of the extracted SpECs were thus analysed using the modified Boehm titration where SpECs were treated with aqueous solutions (0.1 M) of the three bases (NaOH, NaHCO₃ and Na₂CO₃) for 24 hours (see section 8.3.1). After filtration, washing and drying, the loaded SpECs were analysed for their Na content using ICP-OES analysis and the results are presented in **Table 13**.

Table 13: Sodium loading for different types of SpECs. Each analysis was performed in triplicate.			
sample	Na (ppm)	Na % w/w	*10 ⁻³ mmol/g SpEC
SpECs(1)	503.16	0.050	21.88
SpECs(1) NaOH	3261.40	0.326	141.80
SpECs(1) Na ₂ CO ₃	1907.06	0.191	82.92
SpECs(1) NaHCO ₃	1072.18	0.110	46.62
SpECs(2)	1967.97	0.197	85.56
SpECs(2) NaOH	4233.90	0.423	<u>184.08*</u>
SpECs(2) Na ₂ CO ₃	8617.03	0.862	374.65
SpECs(2) NaHCO ₃	4096.64	0.410	178.12
SpECs(2)APSH	47.76	0.005	2.08
SpECs(2)APSH NaOH	29940.79	2.994	1301.77
SpECs(2)APSH Na ₂ CO ₃	23617.90	2.362	1026.87
SpECs(2)APSH NaHCO ₃	13885.82	1.390	603.73
SpECs(3)	59.49	0.006	2.59
SpECs(3) NaOH	15387.59	1.539	<u>669.03*</u>
SpECs(3) Na ₂ CO ₃	16534.65	1.653	718.90
SpECs(3) NaHCO ₃	5529.52	0.550	240.41

*It is suspected that these values are artificially low due to extraction of these groups into solution when the strongest base (NaOH) was used.

The content of acidic groups was calculated for each type of SpECs. The carboxylic acid groups was determined from the NaHCO₃ results. The lactones were determined by subtracting the NaHCO₃ results from the Na₂CO₃. The Na₂CO₃ result was then subtracted from the NaOH and the amount of phenolic groups was calculated (**Table 14**). **Figure 51** presents a comparison of the IR spectra of the three extractions and the APS modified SpECs(2), zoomed in the region

of 1710 cm^{-1} vibration for a carbonyl peak associated with carboxylic acids. The IR data appeared to be in ordered agreement with the number of carboxylic acids determined by the modified Boehm titration.

Table 14: Content of acidic functional groups for each SpECs type.

Type of SpECs	Acidic group (mmol/g SpEC)			Total
	Carboxylic	Lactone	Phenolic	
SpECs(1)	0.046	0.036	0.059	0.120
SpECs(2)	0.178	0.193	?*	0.100
SpECs(2)APSH	0.603	0.422	0.276	1.300
SpECs(3)	0.240	0.478	0.00*	0.666

*It is suspected that these values are artificially low due to extraction of these groups into solution when the strongest base (NaOH) was used.

The results obtained from SpECs(3) and their carboxylic content however are not in agreement with the calculated results obtained from the amination experiments. Boehm titration gave quite a low number, 0.238 mmol/g, whereas the amination calculations implied that the carboxylic groups are most probably around 1.42 mmol/g.

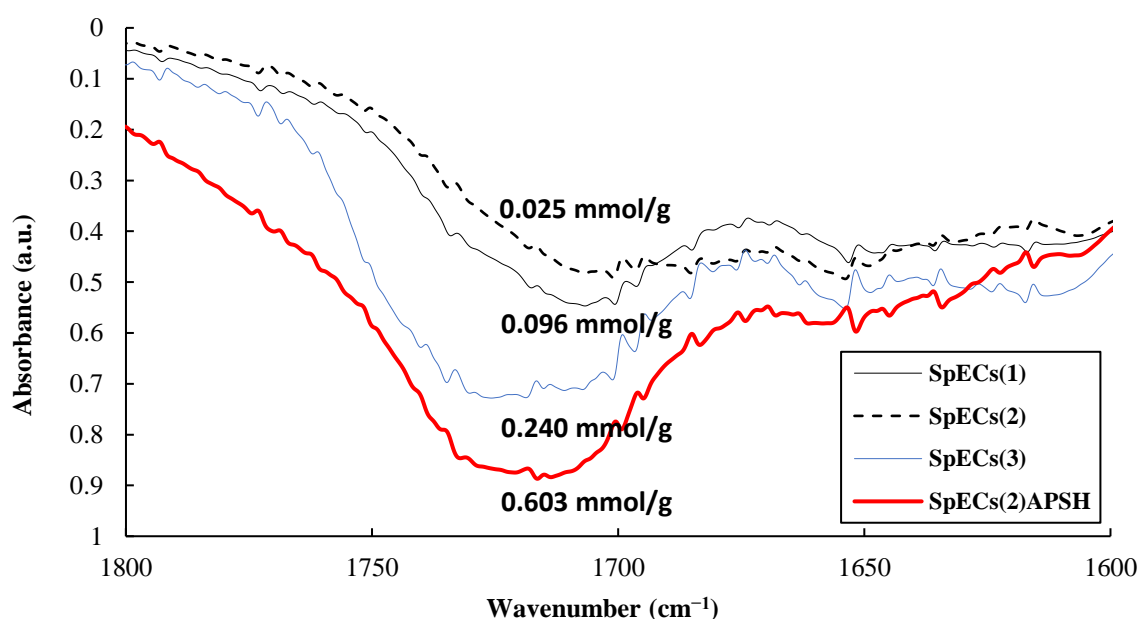


Figure 51: FT-IR spectra of SpECs and the ammonium persulfate treated SpECs(2), focused in the 1710 cm^{-1} vibration for a carbonyl peak associated with carboxylic acids.

The FT-IR and Boehm analyses have indicated that the different extraction procedures give SpECs with different acidic group loadings. SpECs(1) have the lowest total amount of acidic groups and they are the only type in which the phenolic content is more than the carboxylic acids and the lactone groups. SpECs(2) have given questionable results since their total amount of acidic groups was lower than the sum of all the individuals. They show a higher content of carboxylic acid and lactone groups which is quite interesting, considering that both SpECs(1) and SpECs(2) are extracted using bases (KOH and NaOH respectively) so one would expect that their acidic group content would be the same. The surface modification of SpECs(2) treated with ammonium persulfate has resulted in SpECs with 1.3 mmol/g acidic groups, with carboxylic groups occupying half of the quantity (0.6 mmol/g). Unfortunately, the comparison to SpECs(2) would not be valid since the results for these type of SpECs are questionable. It should be noted here that these results can not be taken as quantitatively accurate, since the treatment with the different types of bases over the 24 hours, sometimes gave solutions of brown colour, meaning that there was likely material extracted from the SpECs during the treatment, altering their surface and properties. Therefore, the results obtained should be considered more qualitative or indicative that the relative order of increasing number of carboxylic acids is in agreement with expectations and with FT-IR results, but not be considered quantitatively accurate measurements.

2.9. Conclusions

L. clavatum raw spores were treated following three extraction procedures and SpECs(1 - 3) were produced. After extraction, some further modifications of the material were performed, and the resulting SpECs were analysed with elemental analysis, FT-IR and SEM imaging.

SpECs(1), extracted with KOH followed by phosphoric acid, were of brown colour and some debris was noticed in the SEM images, indicating that the 7 days procedure was harsher on the

spore grains. IR analysis suggested that SpECs(1) is more like a carbonised material that is relatively featureless with regard to functional groups. It exhibited evidence of some carboxylic acid groups, but the fewest among the extractions, and no peak for the aromatic ring modes. The relative featureless material may have implications for its performance as an adsorbent.

NaOH extracted SpECs(2) were of mustard yellow colour and presented some remnants of nitrogen content. IR analysis revealed that in SpECs(2) the carboxylic acids had been replaced by sodium carboxylates, which could be converted back to the protic form by an HCl wash.

HCl extracted SpECs(3) were of dark brown colour and SEM images revealed some damage to the 'decorative' mura of the exine shells, but this damage is believed to occur due to the sudden sucking in of the walls under the vacuum of SEM. This damage was not observed when viewed only by light microscopy. IR analysis and comparison to the raw spores showed an increased number of carboxylic acids and a significant increase in aromatic rings, which could both provide promising adsorption sites. The alkenyl groups were also increased, that could be due to removal of hydroxyls by acid catalysed elimination reactions.

NaOCl oxidation treatment of SpECs(2) and SpECs(3) had as a result a large increase in oxygen content, inferred from the decrease in C, H and N of the elemental analysis. SEM images revealed that this treatment damaged the exine surface across the entire capsule with no particular weak points nor the presence of any debris. It was also concluded that the concentration of the NaOCl solution was an important parameter, since opened bottles or bleach older than 4 months after the production date lose their strength and have no effect on SpECs. FT-IR revealed a very large increase in the stretching frequency of $\sim 1710\text{ cm}^{-1}$, associated with carboxylic acid groups.

APSH treatment of SpECs(2) and SpECs(3) exhibited a reduction in their carbon and hydrogen content while the calculated oxygen percentage increased. After treatment, a slight change in

their colour was observed and SEM images revealed some damage on the surface; whereas the shell was intact, the damage appeared to be greatest on the mura which appeared misshapen with far shorter tectal elements. As with the NaOCl oxidation, FT-IR analysis confirmed a clear generation of new carbonyl groups associated with carboxylic acid stretching frequency $\sim 1710\text{ cm}^{-1}$.

Amination of SpECs(3) was successful and was confirmed by the increase in nitrogen in the CHN elemental analysis, and by FT-IR analysis where a new amide C=O stretching frequency was observed, that increased whilst the C=O stretching frequency of carboxylic acids, decreased. This treatment also revealed that due to the amount of nitrogen added by a peptide coupling reaction, the carboxylic groups that were present on the surface of the SpECs(3) material were at least 1.42 mmol/g.

The iron loading procedure gave maximum loadings for all SpECs, when performed in acetone under vacuum. SpECs(1) presented the highest Fe percentage, (11.6% Fe) and SEM images revealed that a significant amount of material was located on the inside surface of broken SpECs(1) fragments. SpECs(2) presented 9.9% Fe and SpECs(3) presented a 8.4 Fe%, located on their outer surface.

Boehm titration confirmed that the different extraction procedures give SpECs with different acidic group loadings. SpECs(1) presented the lowest total amount of acidic groups and they were the only type in which the phenolic content is more than the carboxylic acids and the lactone groups. SpECs(2) presented questionable results since their total amount of acidic groups was lower than the sum of all the individuals. They showed a higher content of carboxylic acid and lactone groups and their surface modification when treated with APS resulted in SpECs with 1.3 mmol/g acidic groups, with carboxylic groups occupying half of the quantity (0.6 mmol/g). SpECs(3) appeared to not contain any phenolic groups and the majority of their acidic content was lactone groups. The results obtained from SpECs(3) and

their carboxylic content are not in agreement with the calculated results obtained from the amination experiments. Boehm titration gave quite a low number, 0.238 mmol/g, whereas the amination calculations inferred that the carboxylic groups are most probably around 1.42 mmol/g. It should be noted that these results may not be very reliable, and that they should be considered as a qualitative indication that the relative order of increasing number of carboxylic acids is in agreement with expectations and with FT-IR results.

3. Diclofenac

3.1. Introduction

Diclofenac (DCF) is a synthetic, non-steroidal anti-inflammatory drug (NSAID), present in many pills and creams as the active compound. It is an anti-arthritic, analgesic, anti-pyretic and anti-rheumatic compound, mainly used for the treatment of inflammations and painful conditions and can be bought without prescription for either human or veterinary use.^{4,192,193}

DCF is a phenylacetic acid derivative introduced to the market around 1970. It has weak acidic properties ($pK_a \sim 4$) and it is usually presented in the monosodium salt form (**Figure 52**). It exhibits medium solubility in water, 2.37 mg/L and a $\log K_{ow}$ of 4.51.¹⁹⁴ Its functional groups, aromatic amine and carboxylic acid, make the compound act as either proton donor or acceptor giving Lewis acid-base characteristics.¹⁹⁵

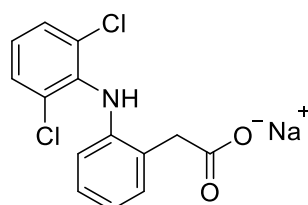


Figure 52: Structure of diclofenac in the monosodium salt form.

The estimated global consumption of DCF per year from both human and veterinary use is near 1,000 tons.¹⁹⁶ DCF acts as a cyclooxygenase (COX) inhibitor in mammalian species. COX enzymes are the catalysts in the synthesis of prostaglandins whose main role is pain mediation, but they are also involved in other biochemical functions such as blood flow regulation and kidney function. Several studies report that some side effects of DCF consumption can be connected with prostaglandin synthesis inhibition.¹⁹⁷

After consumption, DCF is not completely metabolised in either the human or the animal body. In humans, it is partially metabolised to a range of by-products that are either hydroxylated, methoxylated or conjugated with acyl glucuronide, the predominant ones being the 4'-hydroxydiclofenac and 5-hydroxydiclofenac (**Figure 53**).¹⁹⁸ When used in the tablet form, DCF stays in the human system for 2 hours. After 2 hours, 65 - 70% of the compound will be excreted through urine in metabolite form, and 20 - 30% of the initial dose excreted in the faeces. Other products containing DCF (gels or creams, eye drops or injections), are expected to produce the same metabolites as the oral form but in different amounts.⁷ Gels and creams (topical application of the compound) have been proven to be the main contributor to water contamination, since only 6 - 7% of the active ingredient is adsorbed, leaving the remaining 93% prone to washing from the skin and ending up in water.¹⁹⁹

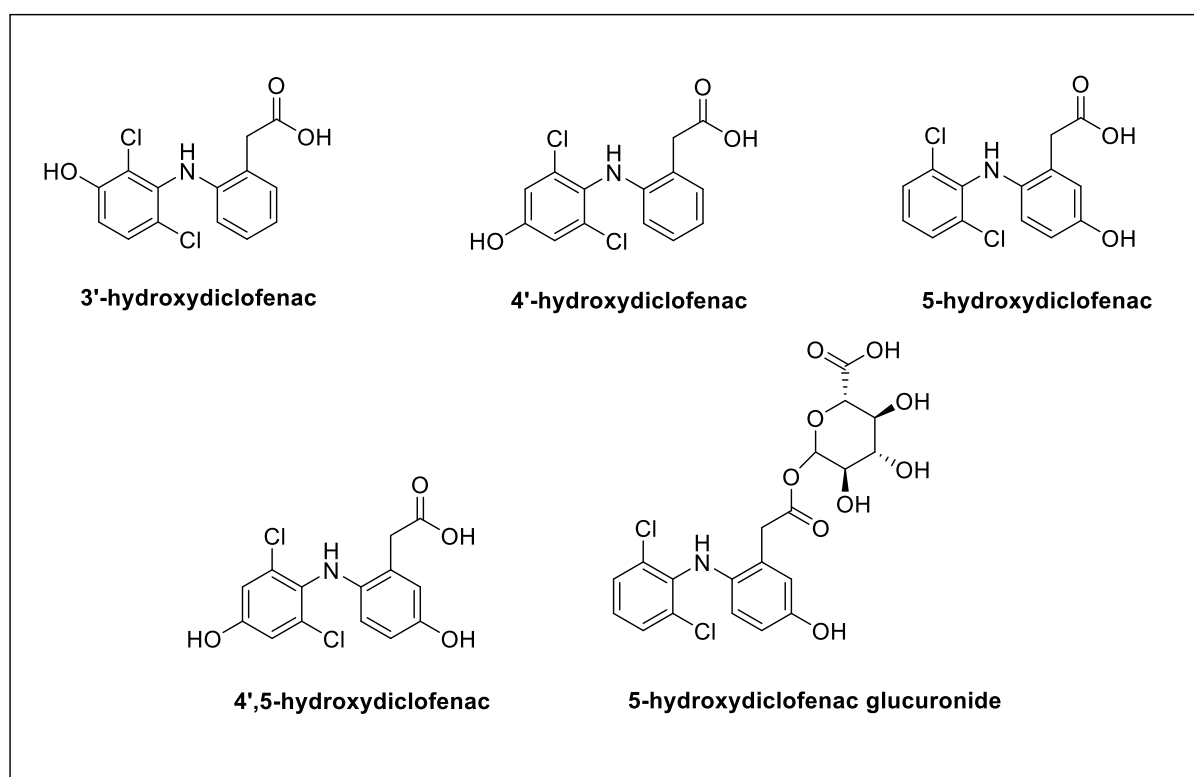


Figure 53: The principal metabolites of DCF following oral consumption by humans.

Many factors have contributed to the increase in the levels of DCF detected in the environment, such as the rise in its use, the inefficiency of WWTPs for DCF removal, or the discharge of untreated wastewater directly into the environment.²⁰⁰⁻²⁰² Some of the different pathways that have led to DCF entering the aquatic system, are due to the direct disposal of effluents, deriving from either hospitals, houses or municipal effluents.²⁰³ Conventional WWT procedures are incapable of complete removal of DCF, placing it in the category of the most persistent toxic waste.¹⁹⁴ This persistence is also enhanced by the fact that DCF is hydrophobic and a relatively stable compound, but under sunlight exposure and in aqueous solution DCF is photodegradable, producing a series of by-products (mainly carbazoles) by losing a chlorine atom with release of hydrochloric acid (**Figure 54**).

Even though efforts have been made to reduce the use of DCF and replace it with naproxen,²⁰⁴ globally, the concentrations of both DCF and its by-products in surface waters have been reported to be 0.7 ng/L - 4.4 µg/L whereas for wastewater, the concentrations can reach up to 8.5 µg/L.¹⁹³ Various areas around the globe have reported the presence of DCF in marine/coastal environments such as the North Atlantic and North Pacific oceans, with concentrations ranging from a few ng/L to around 460 ng/L for the North Atlantic coast and 843 ng/L for the North Pacific ocean.^{205,206} In German rivers the mean concentration of DCF has been reported to be 0.15 µg/L with a peak concentration of 1.2 µg/L. In Switzerland, DCF concentrations in rivers and lakes have been reported in the range of 1 ng/L - 0.37 µg/L and higher in effluents from sewage treatment plants (0.3 - 0.9 µg/L). In Brazil, the concentration range is 3.3 - 785 ng/L²⁰⁷ whereas in the Middle East region DCF concentrations have reported to be as high as 3 µg/L.²⁰⁸ Even in remote locations around the world such as Antarctica, DCF has been detected in relatively high levels (15.09 µg/L).²⁰⁹

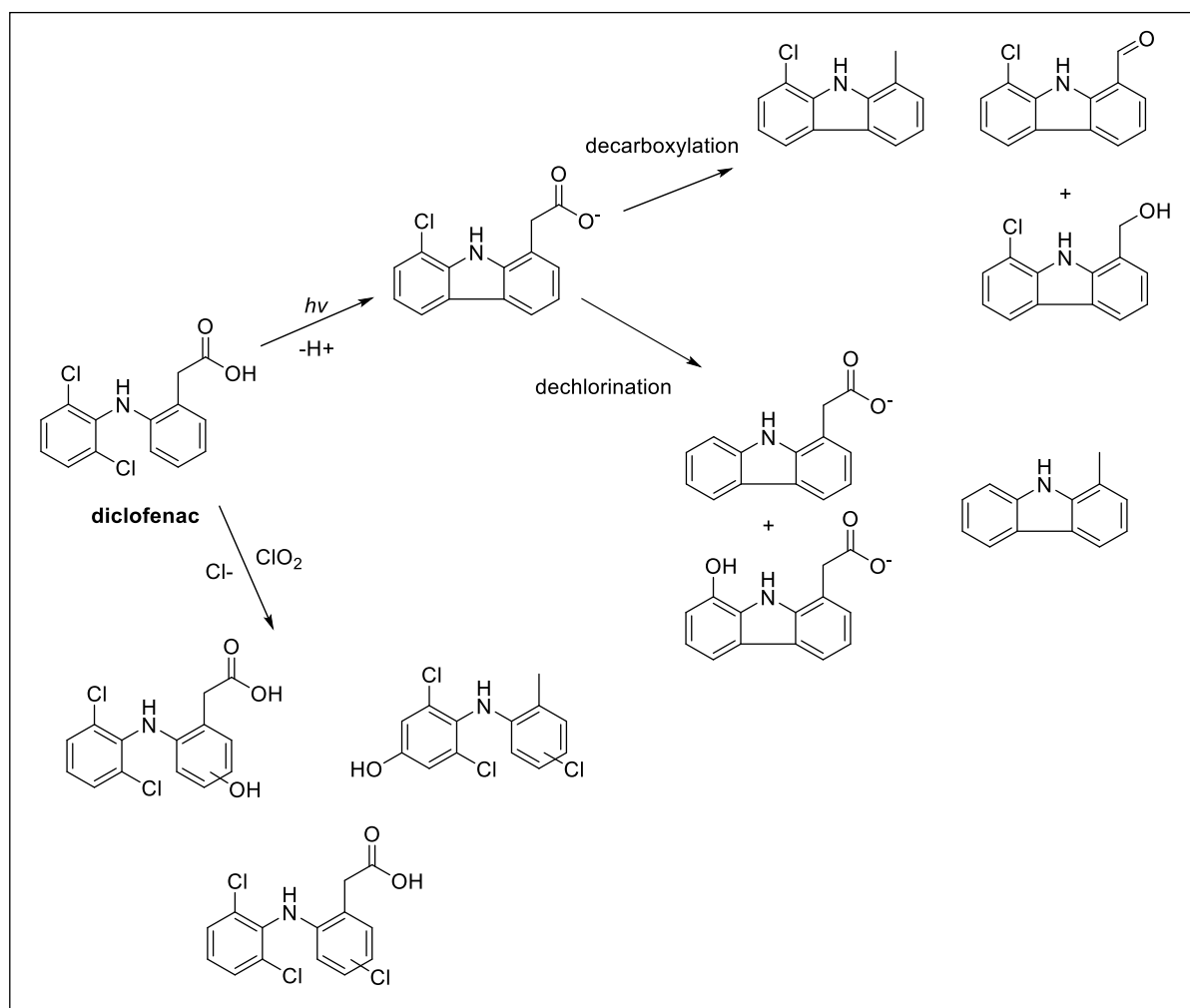


Figure 54: By-products after photolysis or chlorination of DCF.^{71,194,195}

Although DCF has been reported to have relatively low toxicity for fish and algae, there are observations of histopathological effects and bioaccumulation of DCF after chronic exposure, at concentrations around 1 - 5 $\mu\text{g/L}$. Studies on the acute exposure of fish (*Oryzias latipes*) and crustaceans (*Daphnia magna* and *Moina macrocopa*) confirmed a low toxicity, whereas studies on the chronic exposure of the rainbow trout (*Oncorhynchus mykiss*) at low concentrations of DCF (1 $\mu\text{g/L}$) exhibited histopathological effects.^{210,211} Studies in amphibians (*Limnodynastes peronii*, *Lithobates catesbeianus* and *Xenopus laevis*) showed that DCF had a teratogenic effect on their organs, viscera and tail axis.^{212,213} It has been shown that DCF (at concentrations between 125 and 250 $\mu\text{g/L}$) is able to also affect the larval development and

swimming performance of *Trachycephalus typhonius* and *Physalaemus albonotatus*.¹⁹⁶ Of particular concern is the bioaccumulation of DCF in fish bodies, leading to a potentially secondary poisoning risk for fish-eating birds.⁷ Three Asian vulture species (*Gyps bengalensis*, *G. tenuirostris* and *G. indicus*) have been reported to be near extinction due to their consumption of cattle carcasses previously treated with DCF,²¹⁴⁻²¹⁶ this has also been found to be the case for African vultures (*G. coprotheres*).²¹⁷ There are relatively few studies focused on the effects of DCF on marine organisms, however, a recent study on *Gasterosteus aculeatus* exposed to 3.82 µg/L for one month, provoked a decline in its population due to mortality of the adult fish.²¹⁸ In humans, even at low levels (1 µg/L), it has been stated that a continuous DCF daily intake can cause renal lesions and cytotoxicity to the liver and kidneys.⁴ In the U.K., 155 people older than 19 years old have reported adverse effects since 1979, 5% of which had a fatal outcome.²¹⁹

Due to its toxicity and the inefficiency of currently available methods for reducing concentrations by water purification, DCF has been included in the watch list of contaminants regulated by 2013/39/EU Water Framework Directive (WFD).^{1,199,220} In this watch list, the environmental quality standard for DCF was set at 0.1 µg/L for inland surface waters, including rivers and lakes, and 0.01 µg/L for other coastal surface waters.²²¹ These ecosystems are particularly vulnerable due to the considerable concentrations of DCF from WWTP outfalls coupled with the direct contributions from catchment areas.²²²

The majority of DCF entering the environment passes *via* WWTP outputs, where the extent of the molecule's degradation depends on the technologies used. Since DCF is not susceptible to biodegradation, its removal rates are often low even when biological treatments are used.¹⁹⁴ Its resistance to treatments such as activated sludge processes, sludge ozonation, advanced oxidation processes and biological nutrient removal is a problem reported in many publications.^{194,223} It has been reported that technologies like sorption onto sludge²²⁴ or

biodegradation by activated sludge^{7,225,226} have not been highly effective for DCF removal, whereas studies into adsorption on granular activated carbon have suggested highly promising results (approximately 99.7% of DCF removal).²²⁷ According to Homlok *et al.* irradiation technologies are very effective since they are able to achieve a complete mineralisation of the molecule.¹⁹² Other reported effective methods are chlorine or chlorine dioxide oxidation, however both methods include the drawbacks of creating by-products.²²⁷ In a recent study investigating the effects of chlorination processes, 14 structures of DCF's degradation by-products were isolated, with toxicities ranging from slight to severe.²²⁸ Other studies have shown that adsorption processes for water treatment are quite efficient against pharmaceutical compounds, especially DCF.^{229–233} Activated carbon is one of the most commonly tested materials for adsorption of pharmaceuticals. The list of tested biomass waste used for the production of activated carbon for the purposes of DCF removal includes olive and peach stones, cocoa shell, orange peel and potato peel, chicken feathers and palm kernel shells.^{1,3–5,7,8,234–236} Other materials tested for DCF adsorption are hydrogels,²³² activated cokes,²³⁷ covalent organic frameworks,²³⁸ metal organic frameworks,²³¹ nanocellulose,²³⁹ TiO₂,²⁴⁰ and biochars.²⁴¹

As described above, it is clear that current methods for removal of DCF from wastewater streams are not optimal and therefore new purification procedures are needed, involving new materials that are both efficient and environmentally friendly.

3.2. Aims and objectives

In this chapter, the adsorption of DCF onto SpECs extracted from *L. clavatum* will be studied. Different extraction protocols and post treatments will be tested, in order to identify the most efficient type and conditions. The term efficient describes a material that exhibits good adsorption properties, quick and low-cost production protocol, reusability, adsorption stability

and environmentally friendly production conditions. New treatments of SpECs will be applied and tested, to study the feasibility to ameliorate the material's surface by chemical treatment for enhancing the adsorption properties toward DCF.

3.3. Diclofenac detection and quantification

A stock solution of DCF sodium salt was prepared in milliQ water and was further diluted into eight standard solutions over a range of concentrations from 0.5 $\mu\text{g/mL}$ (1.6 μM) to 10 $\mu\text{g/mL}$ (31 μM). Each solution was prepared in triplicate and their absorbance was measured at a wavelength of 275 nm, at room temperature. Baseline calibration was performed using blank solutions of milliQ water, meaning that a concentration of 0 $\mu\text{g/mL}$ gave absorbance values of zero with no deviation from this value. A calibration curve was created (**Figure 55**), and *Equation 13* was used for the calculation of DCF's concentration (x) in all of this chapter's adsorption experiments (LOD = LOQ = 0.006 $\mu\text{g/mL}$).

$$y = 0.0312x + 0.0056$$

Equation 13

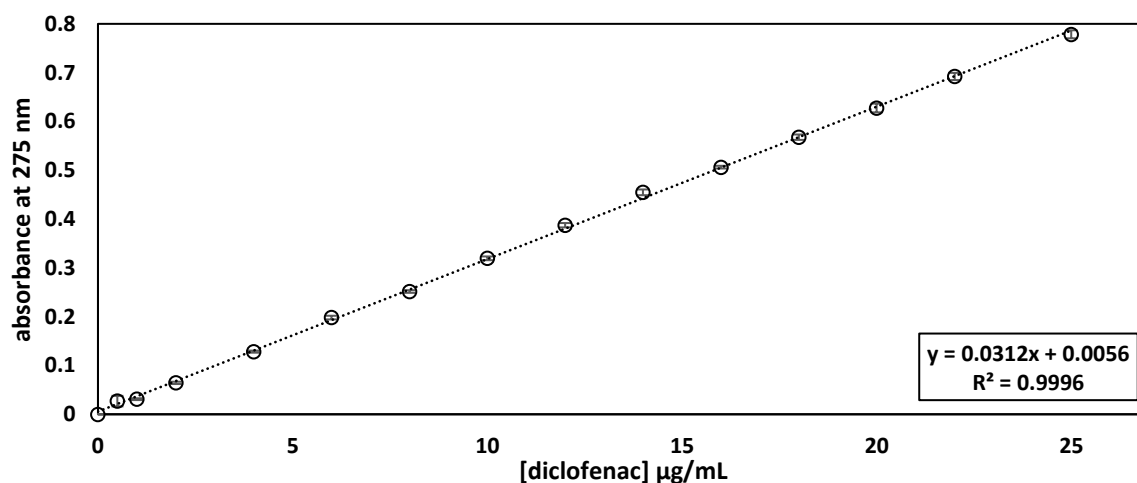


Figure 55: DCF reference curve at the concentration region of 0 - 25 $\mu\text{g/mL}$ at 275 nm detection wavelength ($n=3$).

3.4. Diclofenac adsorption experiments

The influence of contact time on DCF adsorption was examined, by following the procedure described in the experimental section 8.4.2. Briefly, a solution of known DCF concentration ($6\ \mu\text{g}/\text{mL}$) was mixed with 20 mg of the adsorbent material (different types of SpECs) for different periods of time, at room temperature (**Figure 56**).

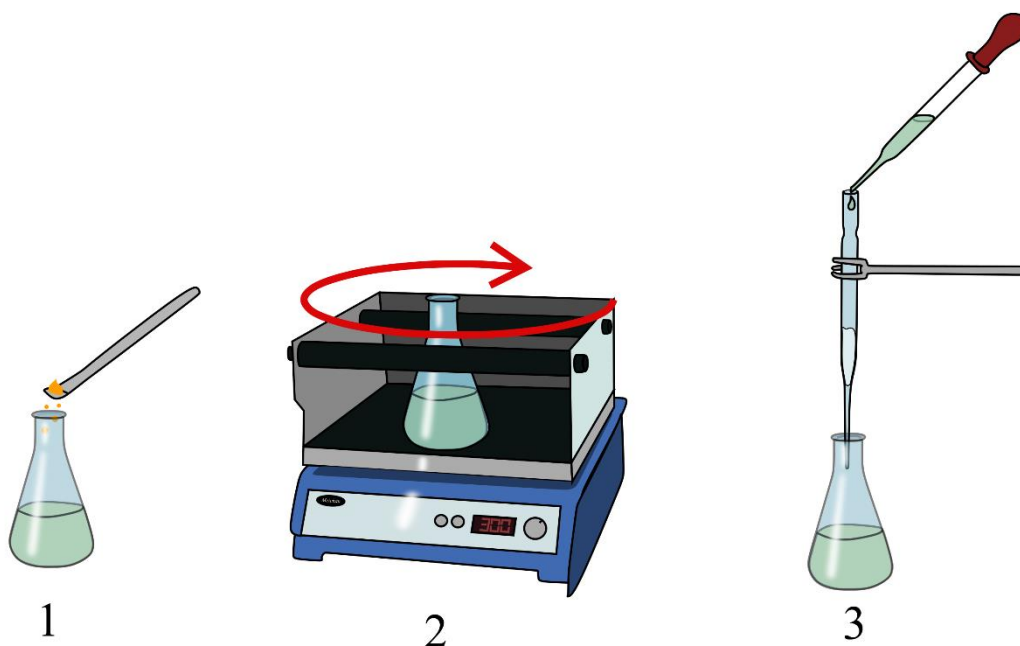


Figure 56: Experimental setup for the adsorption experiments describing the three-step procedure: 1) SpECs are added to the contaminant solution, 2) the suspension is shaken in the orbital shaking for a period of time, 3) the suspension is filtered through a pipette equipped with cotton wool.

The mass of SpECs, the volume and the concentration of the solution were kept constant (20 mg, 5 mL and $6\ \mu\text{g}/\text{mL}$ respectively) and the pH of both the initial solution and the final solution were measured to be six. After filtration, the resulting solution was analysed for its DCF content and the final DCF concentration was compared with the initial concentration. The adsorption percentage was calculated with *Equation 14*.

$$\% DCF ads. = \frac{(C_0 - C_{eq}) 100}{C_0} \quad \text{Equation 14}$$

where C_0 is the initial and C_{eq} is the final DCF concentration.

3.4.1. Cotton interference in diclofenac adsorption experiments

During the DCF adsorption experiments, the final solution was separated from the SpECs by filtration through a cotton wool plug. Since the cellulose in cotton wool could conceivably act as an adsorbent for DCF, experiments were undertaken to show that this method would not affect the results.

- a solution of known concentration of DCF (6 $\mu\text{g/mL}$) was filtered through a glass pipette plugged with cotton wool. The absorbance of the solution was measured before and after the filtration (the experiment was repeated three times).
- a solution of known concentration of DCF (6 $\mu\text{g/mL}$) was mixed with SpECs in two separate vials. In the final step before measuring the absorbance, one sample was filtered through the cotton wool plug, and the other was centrifuged (the experiment was repeated three times). The absorbance of the final solutions was measured and the averages are presented in **Table 15**.

Absorbance before cotton wool filtration	0.205 ± 0.001
Absorbance after cotton wool filtration	0.220 ± 0.009
Absorbance after SpECs treatment and filtration	0.079 ± 0.004
Absorbance after SpECs treatment and centrifuge	0.072 ± 0.010

It is evident that cotton wool had no adsorption capacity for DCF since the difference in the absorbance increased, 0.015 and 0.007 which translated into 0.28 and 0.03 $\mu\text{g/mL}$ respectively.

In order for the experimental results to be more accurate, blanks (SpECs + milliQ water, filtration through cotton) were prepared for every measurement and the blank's absorbance was subtracted from every sample for all of the subsequent experiments.

3.4.2. Diclofenac adsorption onto SpECs derived from different plants

The influence of contact time upon DCF adsorption was examined, from 1 hour to 67 hours of contact time. A graph of DCF adsorption% against time was created by plotting the percentage of adsorption against the different contact times. SpECs from three different plants (*Secale cereale*, *Helianthus annuus* and *L. clavatum*) were compared for their DCF adsorption efficiency (**Figure 57**). All SpECs were extracted by following the same protocol, HCl hydrolysis described in the experimental section 8.1.3.

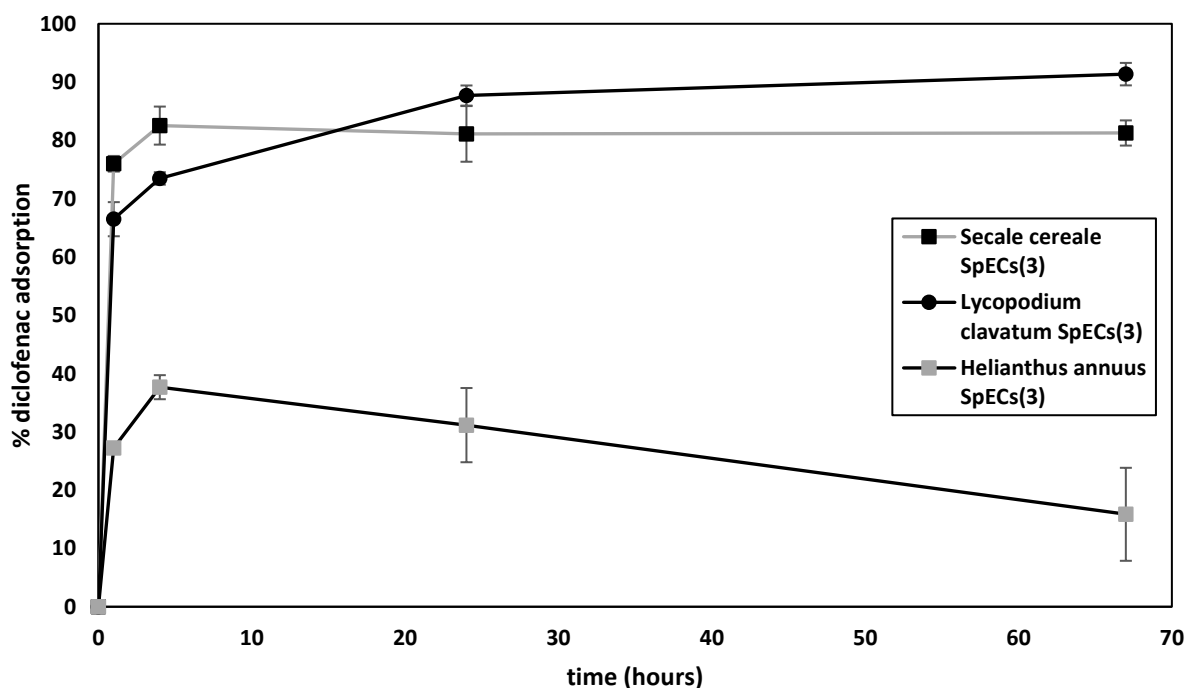


Figure 57: Effect of contact time on DCF adsorption for SpECs derived from rye (*Secale cereale*), sunflower pollen (*Helianthus annuus*) and *L. clavatum* spores by HCl extraction protocol [SpECs(3)] (DCF concentration: 6 mg/L, n=3).

The performance of the three SpECs extraction types was tested with DCF adsorption at different contact times and is presented in **Figure 59**. Raw unprocessed spores exhibited poor adsorption efficiency. One explanation for this result can be that raw pollens and spores contain lipids from the pollenkit on their surface, making the material significantly more hydrophobic than extracted SpECs. The hydrophobic surface of raw spores impedes contact with water ('wettability') and this can reduce the material's adsorptive properties.

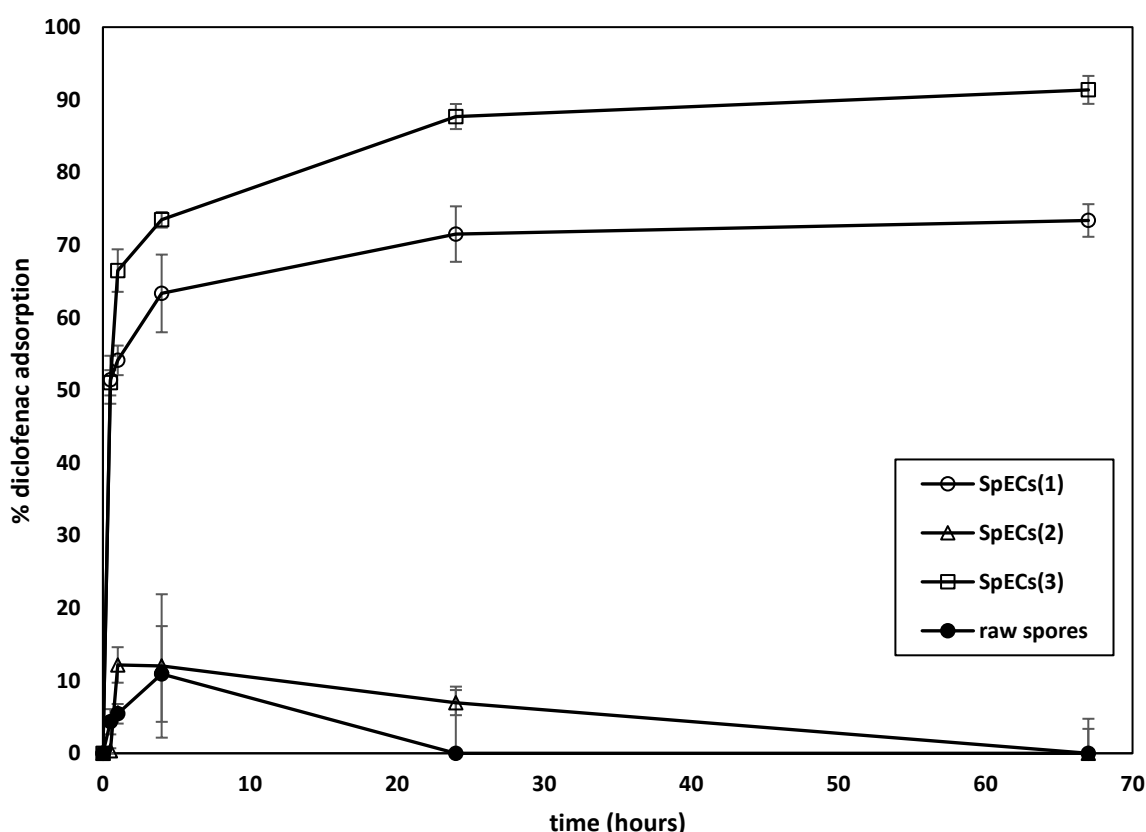


Figure 59: Effect of contact time on DCF adsorption for different *L. clavatum* SpECs types and raw spores, (DCF concentration: 6 mg/L, n=3).

SpECs(2) were extracted by base hydrolysis in which the raw *Lycopodium* spores were treated with NaOH and exhibited a similarly poor adsorption efficiency. A possible explanation for their poor performance might be that this extraction protocol results in SpECs with a surface loaded with carboxylic acids from pre-existing functional groups or newly created carboxylic

acids from hydrolysis reactions which are converted into the negatively charged carboxylates ($\text{COO}^- \text{Na}^+$).

The presence of $\text{COO}^- \text{Na}^+$ was confirmed by the IR analysis of the material which showed that in SpECs(2) the carboxylic acids have been replaced by sodium carboxylates. Sodium carboxylate peaks exhibit antisymmetric stretching vibrations ($\nu_{as}\text{CO}_2^-$) at 1576 and 1542 cm^{-1} and symmetric stretching vibrations ($\nu_s\text{CO}_2^-$) at 1463 and 1456 cm^{-1} . To confirm these carboxylate vibrations, SpECs(2) was washed and filtered using 1 M HCl. The resulting SpECs [SpECs(2)HCl] were analysed with elemental analysis (**Table 16**) and IR. **Figure 60** shows SpECs(2) before and after the acid treatment, exhibiting the removal of the sodium carboxylate vibrations and a rise to the number of carboxylic acids $\sim 1710 \text{ cm}^{-1}$, which had previously been absent. This confirmed that the vibrations in SpECs(2) that were suspected of being sodium carboxylates was likely accurate. This extraction appeared to be the least capable of adsorbing DCF probably due to the charge repulsion between the material's surface and DCF's carboxylate groups. This is because both the material and the DCF are negatively charged, so they repel one another.

Table 16: Elemental analysis results for SpECs(2) and HCl treated SpECs(2)HCl.

sample	treatment	C %	H %	N %
SpECs(2)	-	59.00	8.89	0.12 - 0.56
SpECs(2)HCl	HCl	60.71	8.68	0.40

SpECs(1), were treated with acid following the base hydrolysis step producing SpECs with a neutral surface and therefore the material does not suffer from the repellent interactions that were observed between SpECs(2) and DCF. SpECs(1) presented better adsorption properties for DCF compared to SpECs(2), reaching 40% DCF removal after four hours of contact time. As described in the previous chapter though, SpECs(1) use the harshest chemical procedure

which leads to a more carbon-rich material presenting fewer surface functional groups, such as carboxylic acids.

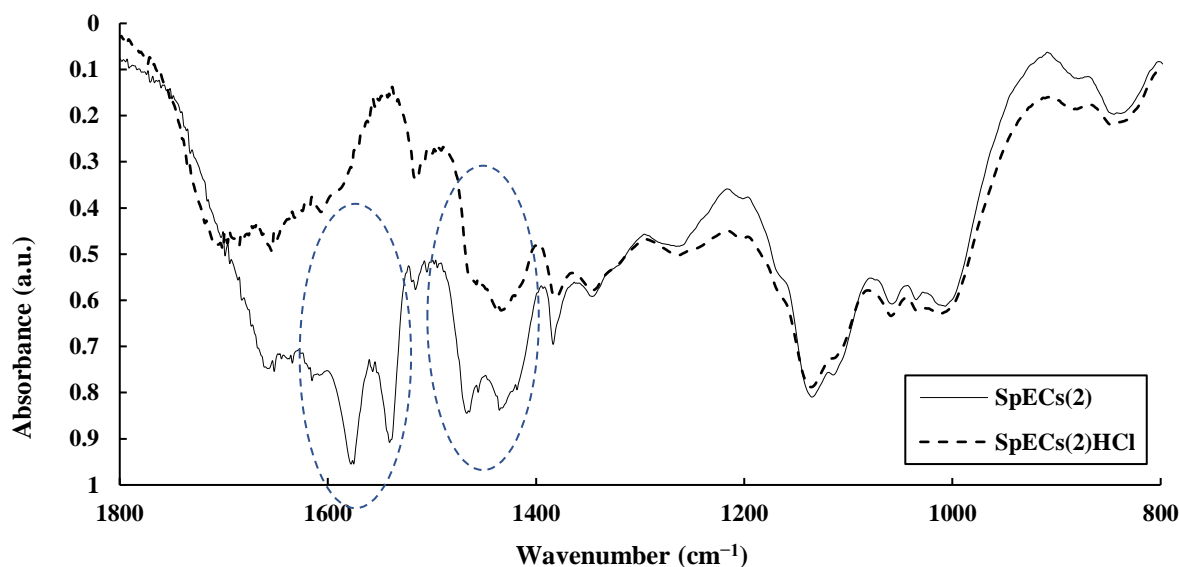


Figure 60: FT-IR spectra of SpECs(2) before and after HCl treatment [SpECs(2)HCl].

SpECs(3) exhibited the best DCF adsorption performance, with almost 90% of DCF adsorbed when equilibrium is reached after 24 hours. This extraction process only involves acid treatment resulting in SpECs with no remaining genetic residues (no nitrogen was present when analysed with elemental analysis). SpECs(3) exhibited the fastest adsorption rate of DCF, removing 65% of DCF in only one hour. According to the IR analysis presented in the previous chapter (2.6.4), when comparing the intensity of the 1710 cm^{-1} (C=O) carboxylic acid peak of the different extractions (**Figure 61**), it was observed that there is a correlation between DCF adsorption efficiency and the carboxylic acids available on the sorbent material. The bigger the 1710 cm^{-1} peak, the greater the affinity for DCF adsorption. SpECs(3) have the highest relative abundance of carboxylic acid character and they have showed the highest adsorptivity of the

group. They also present the highest 1510 cm^{-1} peak believed to represent aromatic ring modes, it may be that further adsorption is achieved by π - π interactions.

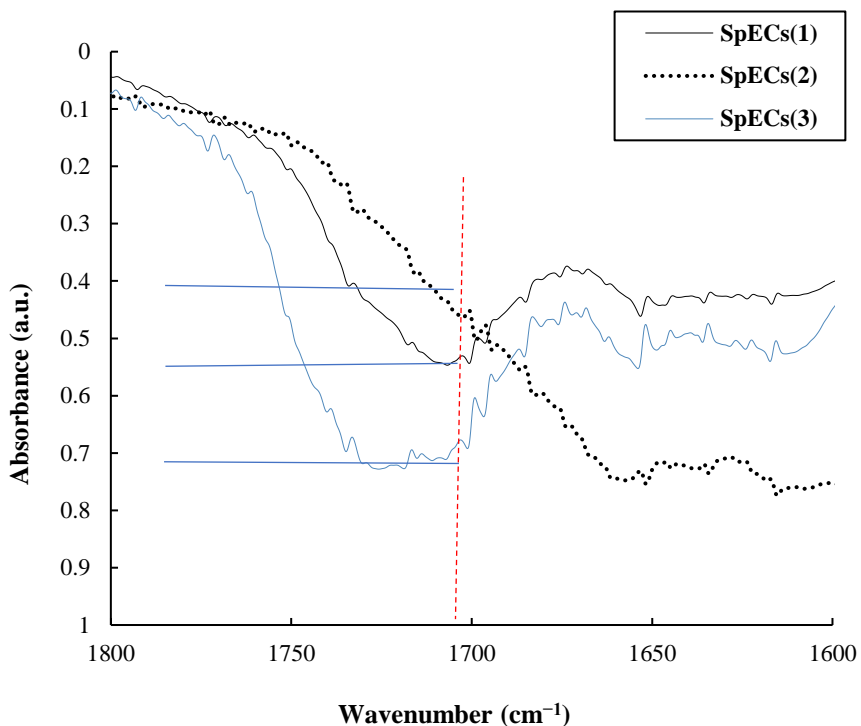
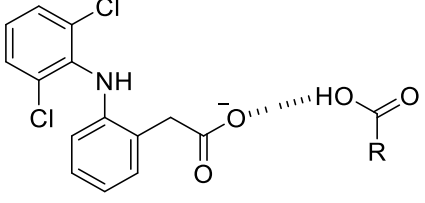
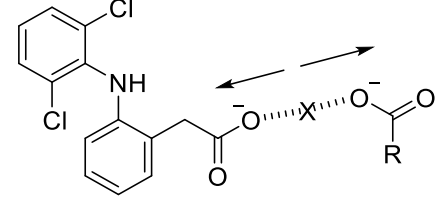
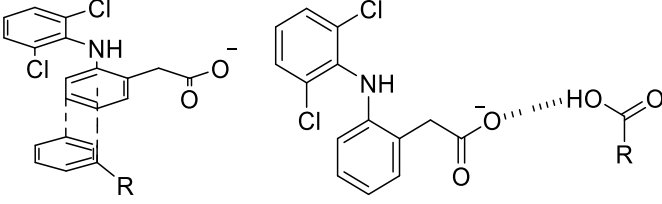


Figure 61: Extract from the IR spectra of the three different extracted SpECs, zoomed in the region around the 1710 cm^{-1} peak.

Table 17 presents the DCF adsorption percentages obtained after one hour of contact time for the different tested SpECs and the raw spores. It also includes the possible dominant interactions between the material and the DCF molecules that may account for the observed differences in adsorption efficiencies between extractions. A schematic of the possible interactions is also presented in **Figure 62**.

Table 17: DCF adsorption performance of SpECs and raw spores after one hour of contact time and their possible adsorption mechanisms.		
type	possible dominant interactions	ads. % after 1 h
raw spores	hydrophobic polar DCF gives poor interaction	4%
SpECs(1)	Hydrogen bond donor  DCF as acceptor for hydrogen bonding	54%
SpECs(2)	Electrostatic interactions (repulsion)  Charge repulsion reduces adsorption potential	12%
SpECs(3)	Hydrogen bond donor and π - π interactions  π - π interactions DCF as acceptor for hydrogen bonding	65%

Π - π interactions are almost certainly present in all materials, but were highlighted in SpECs(3) as they display a noticeable increase in the 1510 cm^{-1} band over the other materials. **Table 17** expresses what might be the dominant interactions leading to the differences observed, for example it would be possible for SpECs(2) to present some π - π interactions if it were not for the charge repulsion effects. As stated in **Table 17**, the ability of SpECs to remove DCF from water increases in the order: raw spores < SpECs(2) < SpECs(1) < SpECs(3), with SpECs(3) being the most efficient type by removing 65% of the contaminant in one hour.

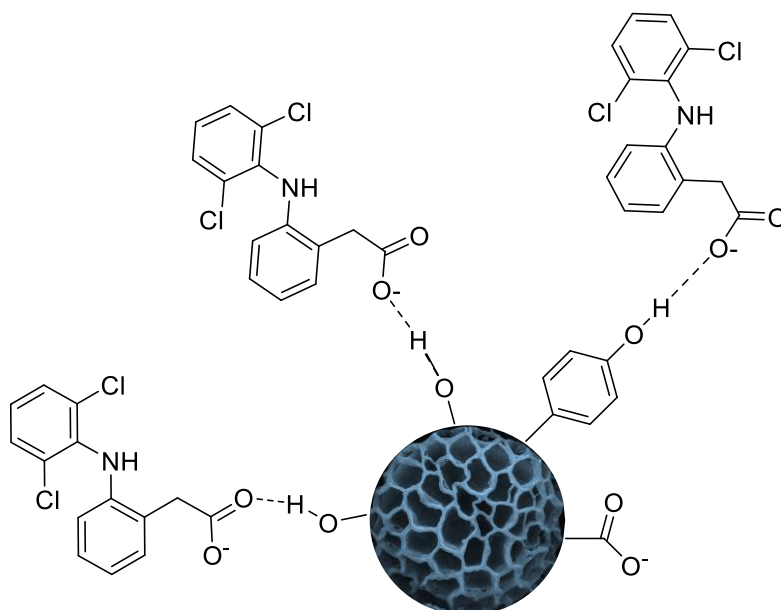


Figure 62: Schematic representation of possible adsorption interactions between DCF and the functional groups on the surface of SpECs.

3.4.3.1. Effect of drying conditions on the adsorption efficiency of SpECs(3)

The drying conditions after the extraction procedure were examined in order to assess whether the drying process influences the adsorptive properties of the resulting material. After extraction, SpECs(3) were either air dried (following the standard protocol), dried in a vacuum desiccator for five days, or in an oven at 100 °C for four days. Their DCF adsorption performance is presented in **Figure 63**.

The vacuum-desiccator drying did not exhibit significant changes in the adsorption efficiency of the SpECs. Oven drying at 100 °C deteriorated the material's adsorption properties by lowering the adsorption efficiency from 90% to 40%. The increased heating appears to have resulted in the reduction of the functional groups on the SpECs surface. **Table 18** presents the possible adsorption mechanisms between the two materials and the DCF molecules, together with their adsorption performance after one hour of contact time.

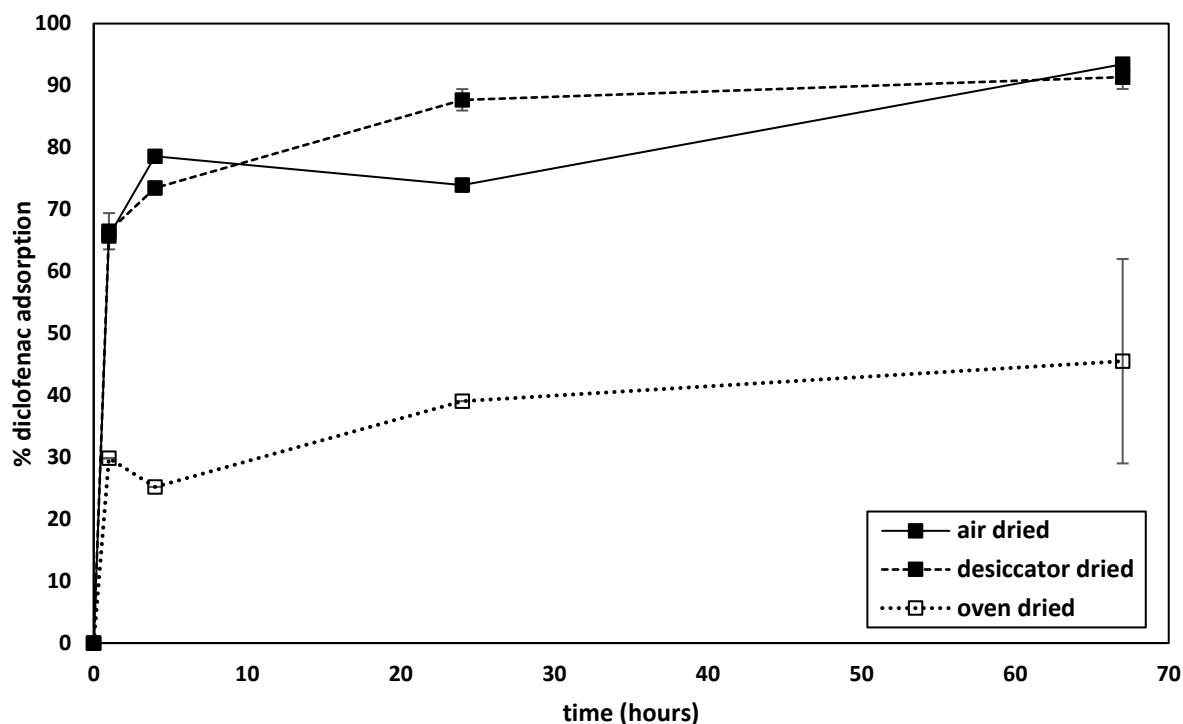


Figure 63: Effect of drying procedures for SpECs(3) on DCF adsorption. Air dried at the pump (air dried), dried under vacuum in a desiccator (desiccator dried) and dried into an oven at 100 °C (oven dried), (DCF dose: 6 mg/L, n=3).

IR analysis of SpECs(3) dried in the desiccator and SpECs(3) dried in the oven (**Figure 64**) showed clear differences within the (OH) peak region (centred around $\sim 3400\text{ cm}^{-1}$), ester and carboxylic acid (C=O) region ($1700 - 1750\text{ cm}^{-1}$) and the aromatic ring modes peak at 1510 cm^{-1} . Although it can be suggested that some moisture loss may happen that leads to a reduction of the OH band, it is unlikely that this is the only change happening. Moisture retention is believed to be minimal for this extraction as it is by far the most hydrophobic of all extractions. It has been suggested by the literature that π - π interactions play an important role in DCF adsorption,^{237,242} such interactions may have been affected by the reduction in the aromatic ring modes peak (1510 cm^{-1}). The reduction in such ring modes may be due to autoxidation reaction due to four days spent in a hot oxygen environment.

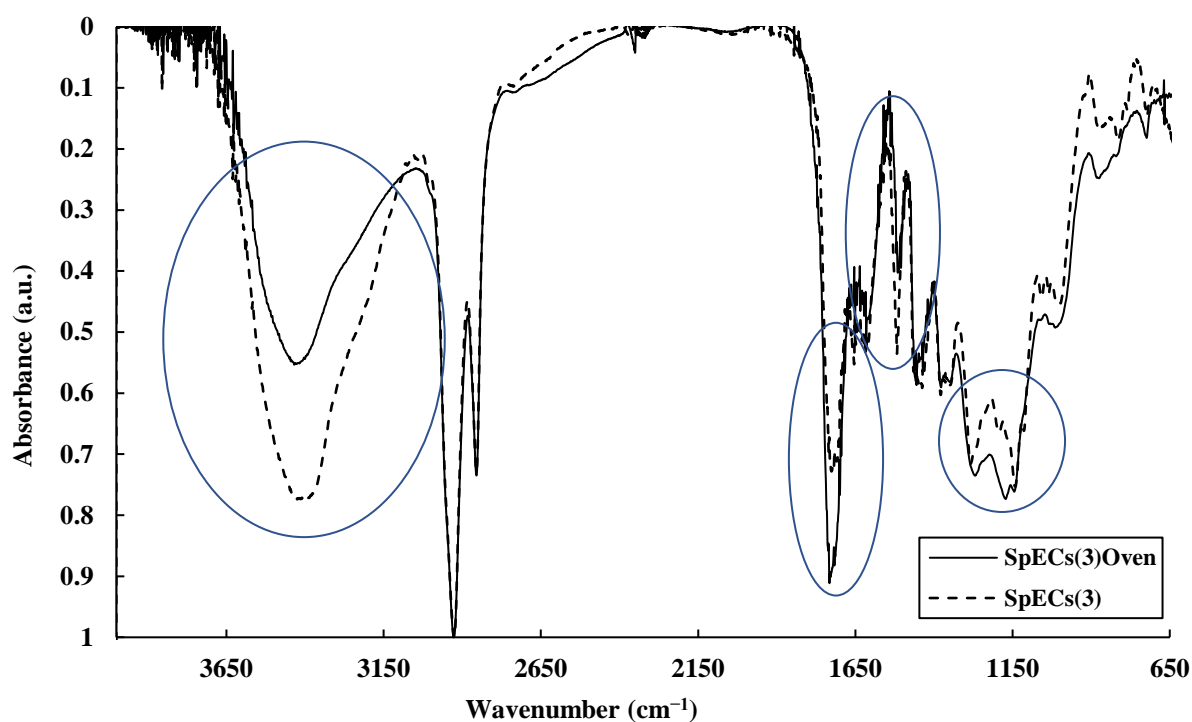
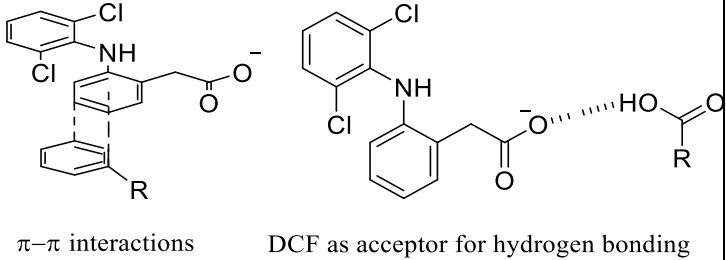
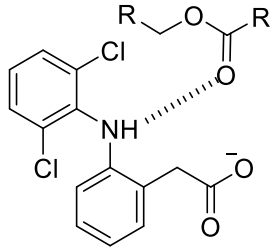


Figure 64: FT-IR spectra of SpECs(3) dried in a desiccator and SpECs(3) oven dried.

Of note is an increase in the carbonyl vibration region, however it appears there is a subtle shift in the peak to 1732 cm^{-1} thought to derive from (C=O) ester vibrations as well as an increase in intensity of peaks between $1170 - 1270\text{ cm}^{-1}$ believed to represent potential (C-O) stretching in esters and ethers. As this is accompanied by a dramatic decrease in hydroxyls (3400 cm^{-1}), it may be possible that a “Fischer-type” esterification reaction is occurring between carboxylic acids and hydroxyls, catalysed by a dehydration reaction. This reduction in carboxylic acids, would indicate the importance of this functional group to act as a hydrogen bond acceptor for the adsorption of DCF. As an ester can participate in hydrogen bonding mechanisms as a hydrogen acceptor but not as a hydrogen donor, it may also imply that the dominant mechanism of adsorption of DCF is that the secondary amine of DCF behaves as a proton donor. However, as the nitrogen is less electronegative than oxygen, there is a weaker dipole and therefore a weaker hydrogen bond is formed than if there was a proton available on a carboxylic acid.

Table 18: DCF adsorption performance of SpECs(3) and SpECs(3) oven dried, after one hour of contact time and their possible adsorption mechanisms.		
material	possible interactions	ads. % after 1 h
SpECs(3)	<p>Hydrogen bond donor and π-π interactions</p>  <p>π-π interactions DCF as acceptor for hydrogen bonding</p>	66%
SpECs(3) oven dried	<p>Hydrogen bond acceptor</p>  <p>DCF as donor for hydrogen bonding</p>	30%

3.4.3.2. Effect of wettability of SpECs on the adsorption of DCF

In order to test whether the hydrophobicity of the material was a factor affecting DCF adsorption, wettability tests were carried out, where instead of using dry SpECs, the material was left to soak in milliQ water for 15 days.

The DCF adsorption results of the wet SpECs were compared to those of the dried ones are presented in **Figure 65**. In general terms, in all samples there were small differences of the range of 10% between dry and wet material. SpECs(2) and SpECs(1) showed slightly better adsorption capacity when dry and the same results were obtained for SpECs(3) as well. SpECs(2)APSH1 gave opposite results: wet SpECs of this form adsorbed 10% more DCF than the dried ones, reaching equilibrium after 24 hours.

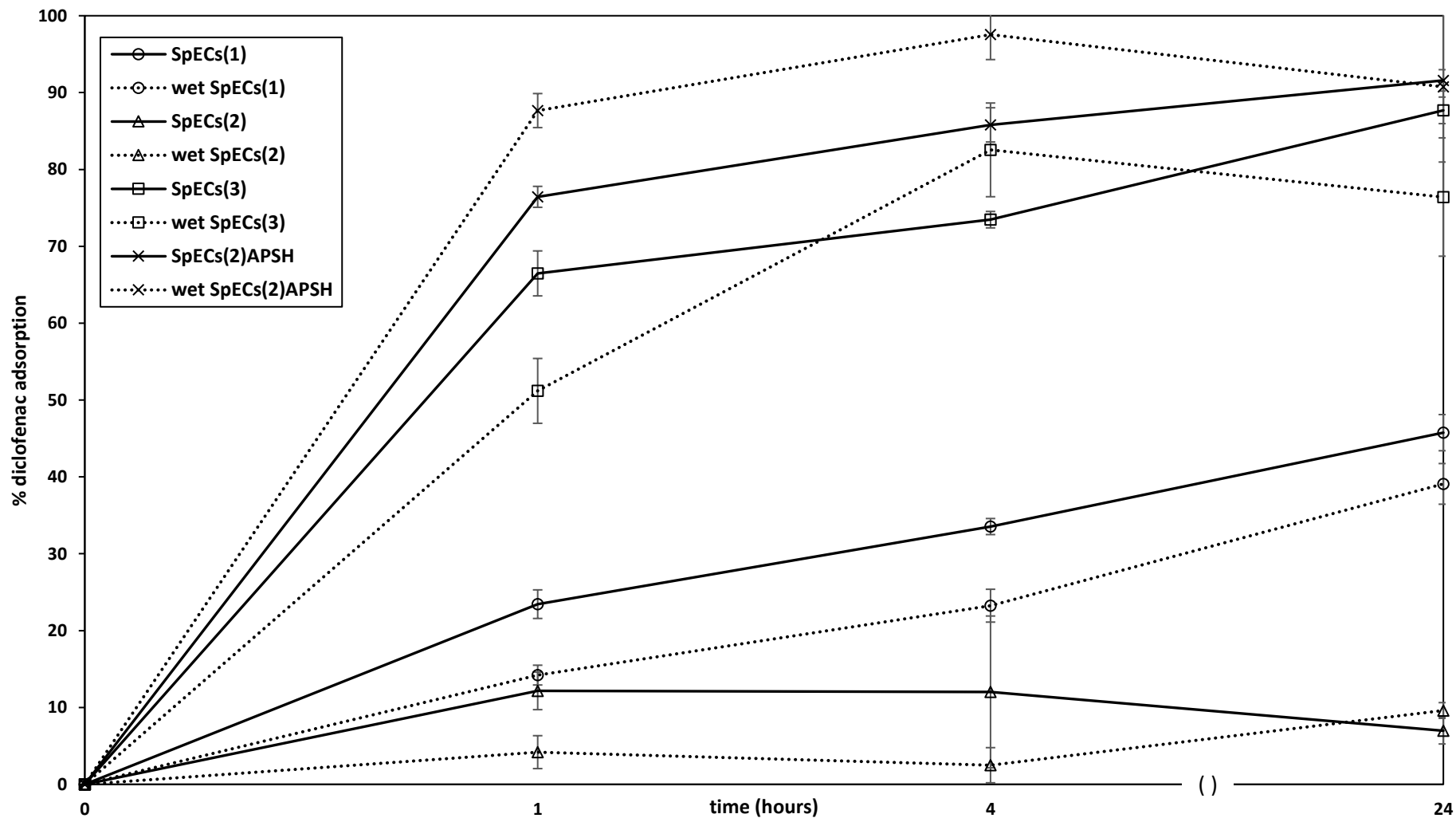


Figure 65: Comparison of DCF adsorption behaviours of dried and wet SpECs. SpECs(2)APSH accounts for SpECs(2) treated with ammonium persulfate, treatment that will be further analysed in the following sections (DCF dose: 6 mg/L, n=3).

3.4.4. Diclofenac adsorption onto modified SpECs

Due to the trend of increasing carboxylic acids correlating with a higher rate and capacity for DCF adsorption, some surface treatments of the extracted SpECs were proposed. SpECs(2) exhibited the poorest DCF adsorptive properties, for this reason, they were chosen to undergo a series of surface modifications to test whether their adsorption efficiency could be improved. Sodium hypochlorite (NaOCl), *tert*-butyl hydroperoxide and ammonium persulfate were used as oxidising agents to modify available primary hydroxyls, ketomethyls, aldehydes and remaining esters to carboxylic acids, with the aim to further improve adsorptivity. Alkenes too may be oxidatively cleaved or converted to alcohols *via* epoxidation, which could be further modified into more carboxylic acids and ketones.

Another proposed treatment was the coupling of 1,6-diaminohexane with available carboxylic acids of SpECs(3) to produce a material that can give attractive electrostatic interactions and can also be a hydrogen donor.

3.4.4.1. Diclofenac adsorption onto ammonium persulfate treated SpECs(2)

Following the different protocols described in section 8.2.3, SpECs(2) were treated with ammonium persulfate (APS) of differing concentrations (0.5 - 2 M, diluted in sulfuric acid) either with heating at 90 °C or at room temperature. APS is a relatively mild oxidant that is expected to oxidise some of the functional groups on the SpECs surface and possibly enhancing DCF adsorptive efficiency. The SpECs obtained were analysed with FT-IR and their adsorption performance against DCF was tested (**Figure 66**).

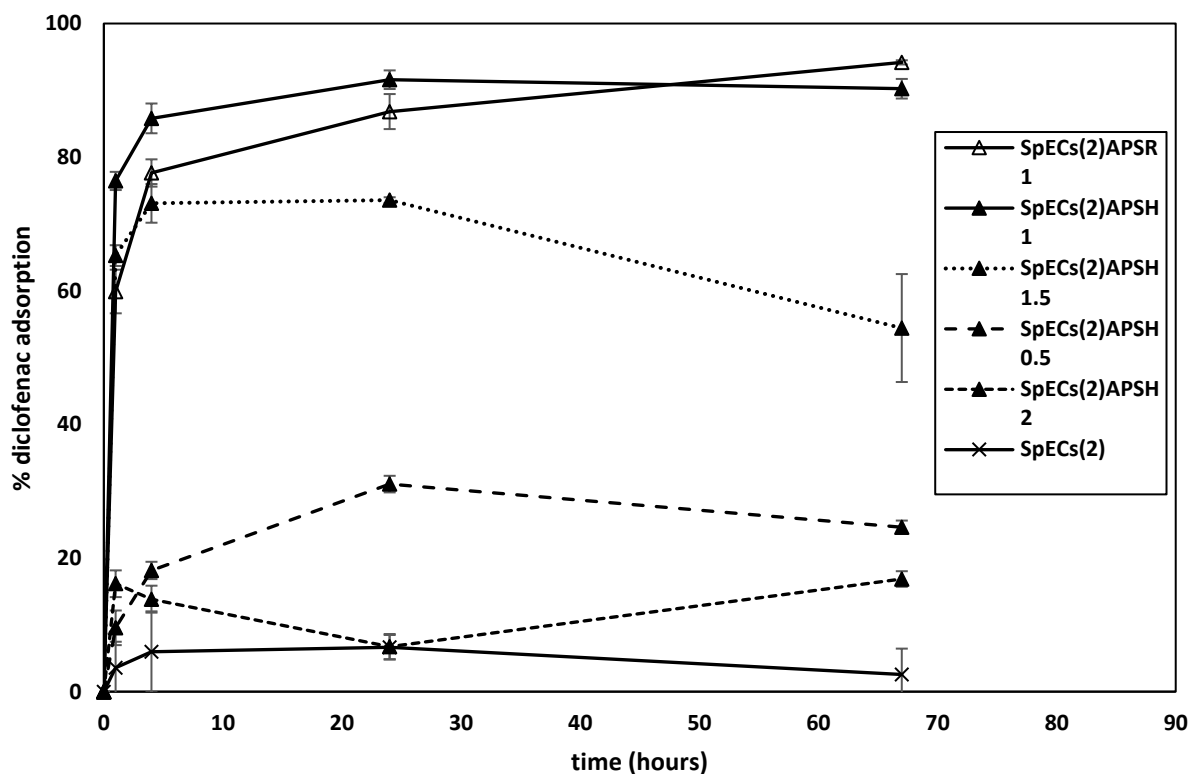


Figure 66: Effect of time for DCF adsorption on modified SpECs(2) treated with different concentrations of ammonium persulfate (APSR1: 1 M ammonium persulfate at room temperature, APSH1: 1 M ammonium persulfate at 90 °C, APSH1.5: 1.5 M ammonium persulfate at 90 °C, APSH0.5: 0.5 M ammonium persulfate at 90 °C, APSH2: 2 M ammonium persulfate at 90 °C) (DCF dose: 6 mg/L, n=3).

The treatment with concentrated APS (2 M) at 90 °C slightly improved the adsorption efficiency of SpECs(2) compared with the non-treated ones, and the same seemed to have occurred for the dilute solution of APS (0.5 M). One would expect that the higher the oxidant concentration, the higher the amount of the formed oxygen surface groups and the higher the adsorption capacity of the material.

The APS concentrations that improved the adsorption efficiency of SpECs(2) were 1.5 M and 1 M, with the latter being the most effective [SpECs(2)APSH1]. The DCF adsorption percentages obtained from SpECs(2)APSH1 were much higher than the ones obtained from the untreated SpECs(2). In only one hour, SpECs(2)APSH1 removed 75% of DCF, reaching a maximum adsorption of 90% in 24 hours. The same treatment was performed with APS 1 M

at room temperature, presenting DCF adsorption percentages slightly lower than those obtained by the treatment at 90 °C.

Oxidative treatment at 90 °C seemed to be more effective, since it produced SpECs with better DCF adsorption performance than the ones oxidised at room temperature. It should also be noted that the treatment as outlined in section 8.2.3, involved the use of sulfuric acid and will have also protonated the carboxylate groups that were likely causing a repellent effect. However, this is true for all of the APSH treatments, and whilst this must be considered, it is not the only effect at play as there were clear differences between the different conditions aforementioned.

IR analysis

The APS treatment experiments showed that an increase in the DCF adsorption efficiency of the SpECs is possible. Treatment of SpECs(2) with 1 M APS at 90 °C resulted in a significant increase of the material's adsorption efficiency, comparable to and exceeding that of the SpECs(3). FT-IR analysis of the material showed a clear generation of carboxylic acids; in **Figure 67** a large peak at 1710 cm^{-1} can be attributed to the (C=O) from carboxylic acids, which may be expected due to the oxidising nature of APS. An increase is also seen at 1130 cm^{-1} from what are most likely to be the (C-O) vibrations of carboxylic acids. There is no overlap with possible esters and there are no carboxylates remaining. From this, it can be inferred that hydrogen bonding between the carboxylic acid groups from the APS modified SpECs and the DCF molecules predominate π - π adsorption mechanisms, particularly as the 1510 cm^{-1} aromatic ring modes peak has decreased in this material.

Figure 68 presents the FT-IR of DCF overlaid with SpECs(2)APSH whereas **Figure 69** shows the FT-IR of SpECs(2)APSH and SpECs(2)APSH after having adsorbed DCF. There is not any increase in the regions of highest intensity for DCF, as the relative amount of DCF to

SpECs is very small (30 μg DCF on 20 mg SpECs). However, there are differences in the regions which are expressed by carboxylic acid stretches, OH (3400 cm^{-1}), C=O (1710 cm^{-1}) and C-O (1130 cm^{-1}), which are the proposed groups of interaction with the adsorbed molecules.

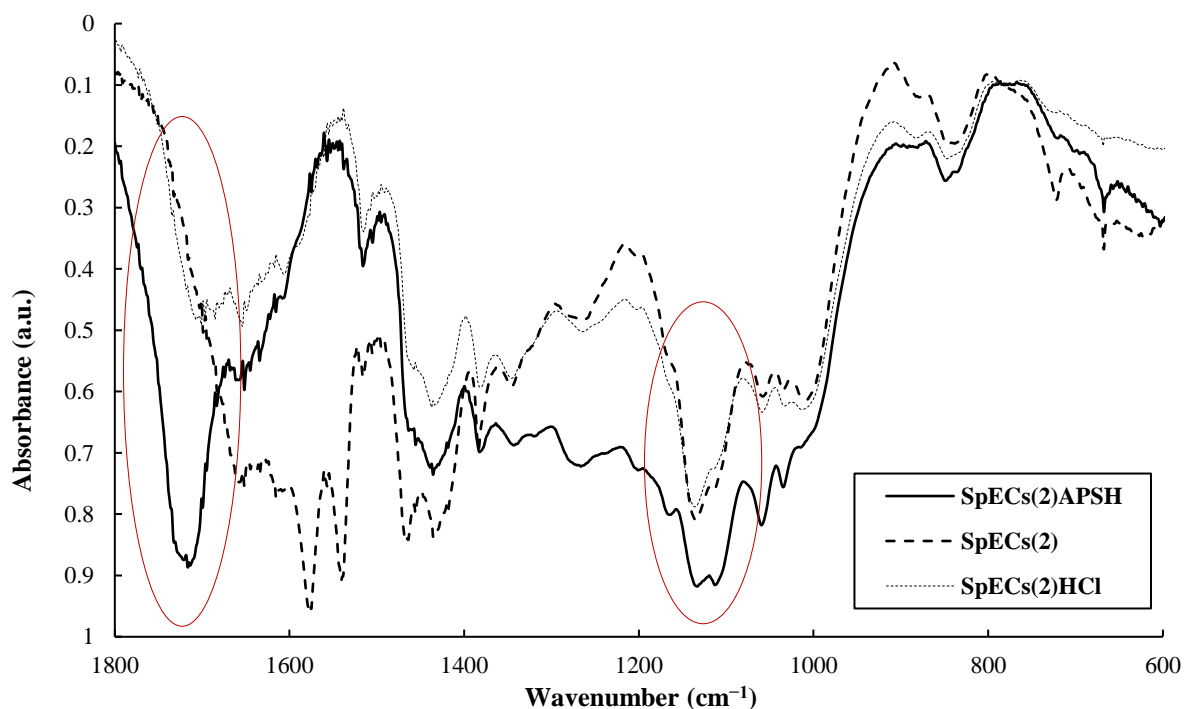


Figure 67: FT-IR spectra of SpECs(2), SpECs(2) HCl treated and SpECs(2)APSH. Comparisons between SpECs(2)HCl and SpECs(2)APSH is more accurate for the region around 1600 cm^{-1} because of the absence of the carboxylates peak.

The differences in the spectra (**Figure 69**) are most clear at 3300 cm^{-1} and 1130 cm^{-1} , regions that account for O-H and C-O vibrations respectively. This clear increase in intensity after DCF adsorption is due to a well-known signature of hydrogen bonding and bridging groups. According to Bratos and Marechal,^{243,244} the band assigned to hydrogen bonds is shifted to lower frequencies and strongly broadened when compared to free hydrogen stretching bands. The strong increase in the intensity of the infrared bands is many hundreds of times greater than the number of bonds for which they account.^{245,246} Such differences in the IR spectra of

the material may give indication that DCF is adsorbed onto the surface of SpECs *via* hydrogen bonding.

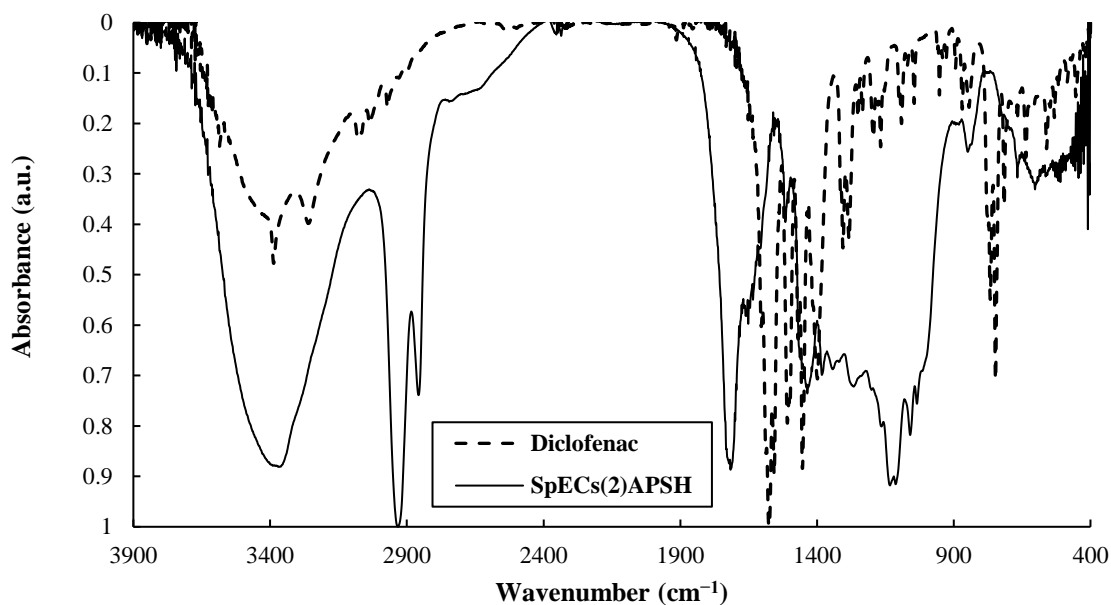


Figure 68: FT-IR spectra of DCF on its own and SpECs(2)APSH.

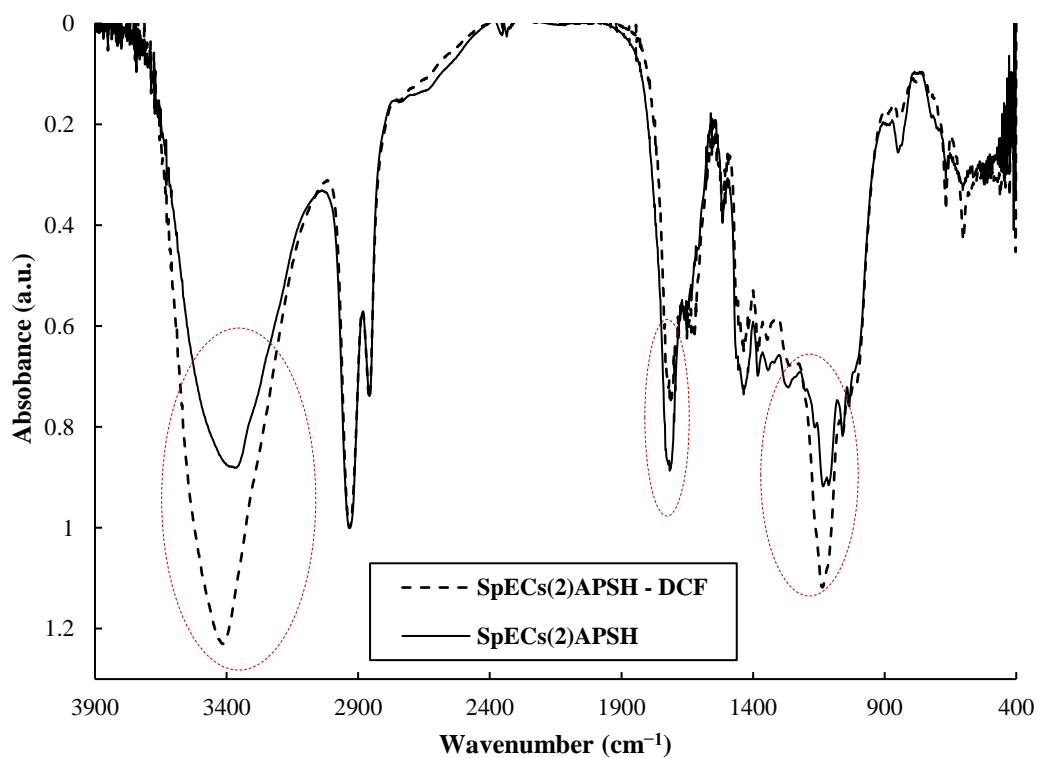


Figure 69: FT-IR spectra of SpECs(2)APSH1 and SpECs(2)APSH1 loaded with DCF.

3.4.4.2. Diclofenac adsorption onto HCl treated SpECs(2)

Following the results obtained with APS, it was anticipated that other modifications could increase the adsorptivity of SpECs. SpECs(2) were treated with 9 M HCl at room temperature for three hours, following the protocol described in section 8.2.2. The aim of doing this was to protonate the carboxylate groups on the surface of the base-hydrolysed SpECs and test their DCF adsorption efficiency in comparison to the acid-hydrolysed SpECs [SpECs(3)]. The results (**Figure 70**, SpECs(2)HCl) were unsurprisingly similar to those obtained from SpECs(1), a result that was expected, since the SpECs(1) extraction procedure involves a base hydrolysis followed by an acid treatment, which is similar to the production procedure of SpECs(2)HCl.

Once SpECs(2) were washed with HCl to protonate the carboxylates to the neutral -COOH, there was an improvement in adsorptivity. However, there are fewer carboxylic acids exhibiting within FT-IR for this material compared to the number present in SpECs(3), and so its adsorption efficiency did not reach the performance of SpECs(3). **Figure 71** shows the FT-IR of SpECs(2) obtained before and after the HCl treatment exhibiting the removal of the sodium carboxylate vibrations. Adsorption then improved as the electrostatic repulsion is removed (**Table 19**), but still remains fairly poor, since the material exhibits a low number of carboxylic acid groups $\sim 1710\text{ cm}^{-1}$.

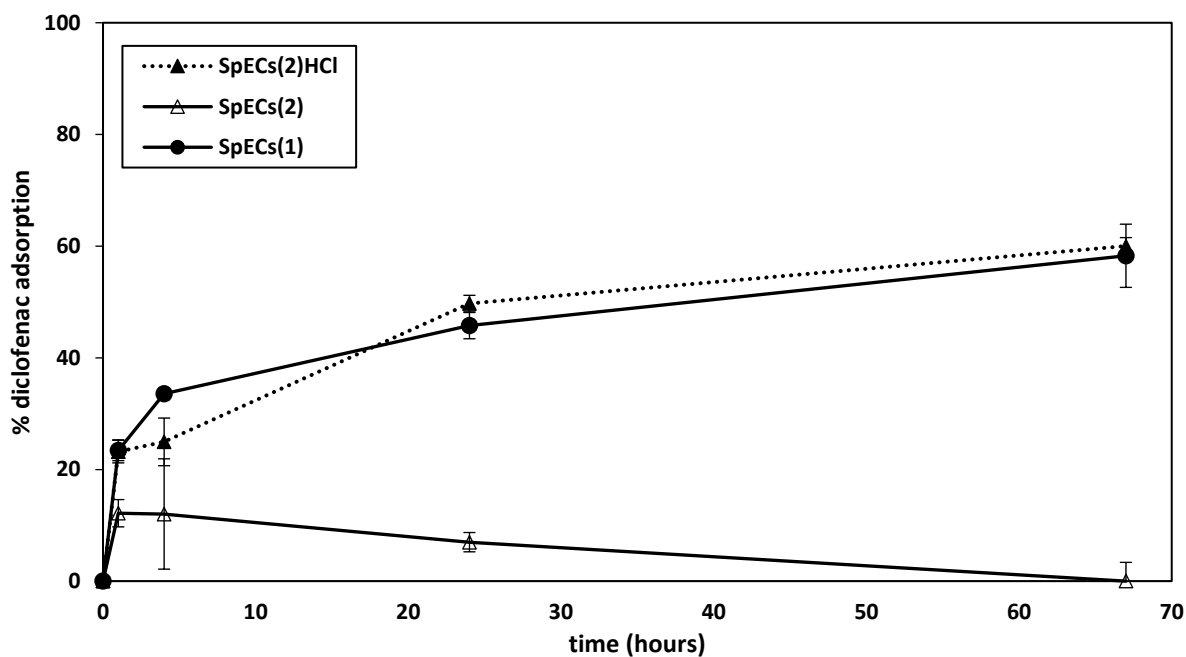


Figure 70: Effect of time on DCF adsorption for unmodified and modified SpECs(2) compared to SpECs(1). SpECs(2)HCl: treatment with HCl 1 M, (DCF dose: 6 mg/L, n=3).

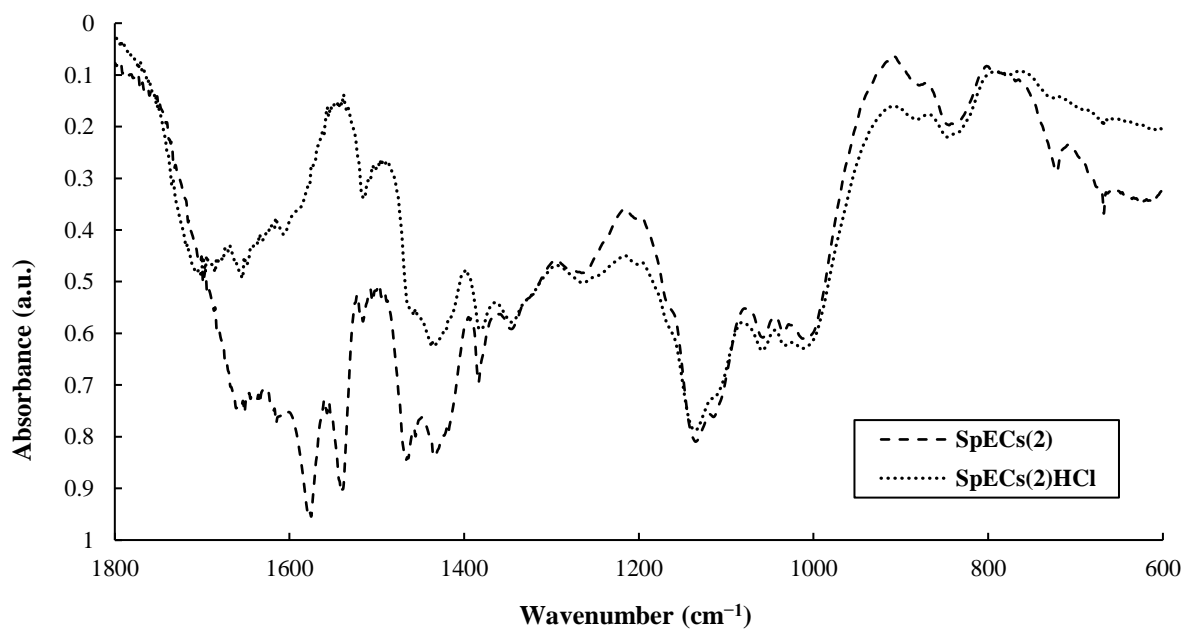
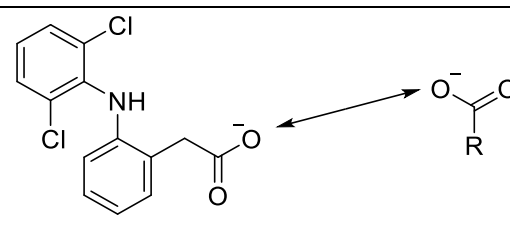
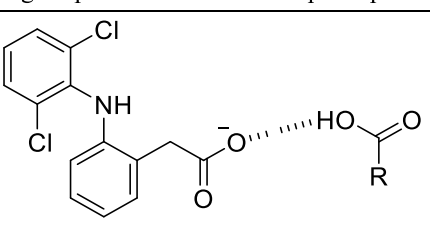


Figure 71: FT-IR spectra of SpECs(2) and SpECs(2)HCl.

Table 19: DCF adsorption performance of SpECs(2) and SpECs(2)HCl, after one hour of contact time and the possible adsorption mechanisms.			
material	possible interactions		ads. % after 1 h
SpECs(2)	electrostatic interaction (repulsion)	 <p>Charge repulsion reduces adsorption potential</p>	12%
SpECs(2) HCl	Hydrogen bond donor	 <p>DCF as acceptor for hydrogen bonding</p>	26%

3.4.4.3. Diclofenac adsorption onto TBHP treated SpECs(2)

Treatment of SpECs(2) with *tert*-butyl hydroperoxide (TBHP) 70% at room temperature for three hours, didn't have any significant improvement on their DCF adsorption efficiency. In fact, the treatment seemed to have decreased the little adsorption ability that SpECs(2) presented previously [Figure 72, SpECs(2)TBHP]. Further investigation is needed on this material since the IR spectra obtained were not conclusive.

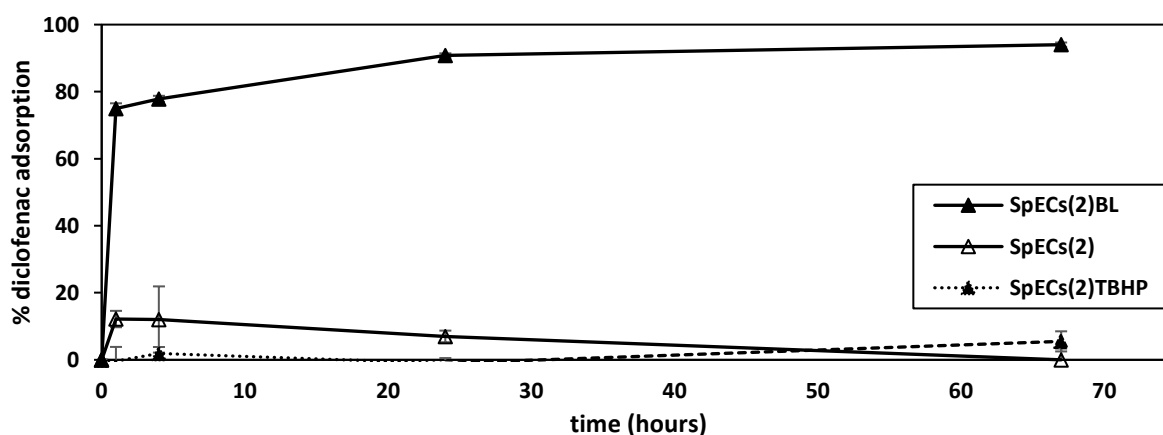


Figure 72: Effect of time on DCF adsorption for unmodified and modified SpECs(2). Different treatments at room temperature: SpECs(2)BL: NaOCl 14%, SpECs(2)TBHP: 70% *tert*-butyl hydroperoxide (DCF dose: 6 mg/L, n=3).

3.4.4.4. Diclofenac adsorption onto NaOCl treated SpECs(2)

The best results for DCF adsorption on SpECs(2) were obtained after treating SpECs(2) with 14% NaOCl at room temperature for one hour [Figure 73, SpECs(2)BL]. The colour of the SpECs changed from yellow to white and their DCF adsorption performance went from 0% to 90% after 24 hours of contact time. The change in colour possibly indicates that NaOCl is able to further oxidise colour bearing groups, oxidising the aromaticity and leading to a whitened product.

IR analysis revealed that the aromatic ring modes group at 1510 cm^{-1} has been completely depleted in the bleached product. Figure 73 presents a comparison between the IR spectra of SpECs(2)Bl and SpECs(2)HCl, where a large number of carboxylic acids appears to have generated (C=O stretching frequency exhibited at $\sim 1712\text{ cm}^{-1}$).

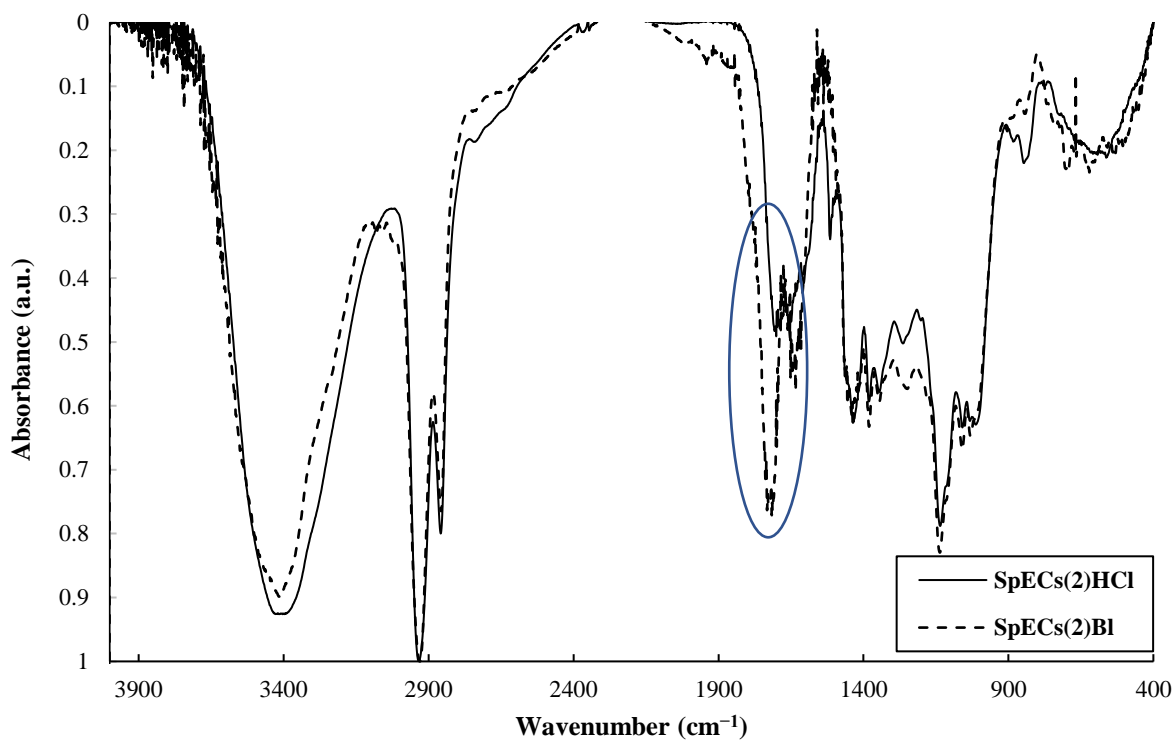


Figure 73: FT-IR spectra of SpECs(2)HCl and SpECs(2)Bl.

The CHN analysis also indicated a large increase in the relative number of oxygens as the mass% of C and N decreased substantially (**Table 20**). Since this is accompanied by a dramatic improvement in the adsorption capacity for the material, it has been assumed that the carboxylic acids were responsible for this improvement.

sample	treatment	C %	H %	N %
SpECs(2)	-	59.00	8.89	0.12 - 0.56
SpECS(2)HCl	HCl	60.71	8.68	0.40
SpECs(2)Bl	NaOCl	53.15	7.43	0.02

3.4.4.5. Diclofenac adsorption onto oxidised SpECs(3)

Treatment with sodium hypochlorite (14% aq. NaOCl) and ammonium persulfate (APS 1 M) both exhibited improved DCF adsorption efficiency over SpECs(2). The same treatments were therefore applied to SpECs(3) in order to examine whether the already good adsorption properties could be further improved. SpECs(3) were oxidised with NaOCl following the same procedure as used for SpECs(2) (section 8.2.1) and their DCF adsorption efficiency was tested. The same experiment was conducted for SpECs(3) oxidised with APS 1 M. The results are presented and compared in **Figure 74**.

The APS treatment was not effective in the case of SpECs(3); it significantly reduced their adsorption properties and converted them into a poor material for DCF adsorption. Their adsorption capacity decreased from ~80% to almost zero. It is unclear what occurred that may have led to this result, particularly as the FT-IR gave a very similar result to that of sample SpECs(3)Bl. Unfortunately, FT-IR analysis did not yield any clues to any major differences between the two materials (**Figure 75**) and further investigation would be needed since no conclusions can be made together with the elemental analysis results (**Table 21**). **Figure 76** shows a comparison with SpECs(3) and SpECs(3)Bl. The areas highlighted show the depletion

of aromatic ring modes (1510 cm^{-1}) and increase in carboxylic acids (1710 cm^{-1}) following NaOCl treatment. This might add further evidence that the significant mechanism of adsorption is H-bonding and not π - π interactions.

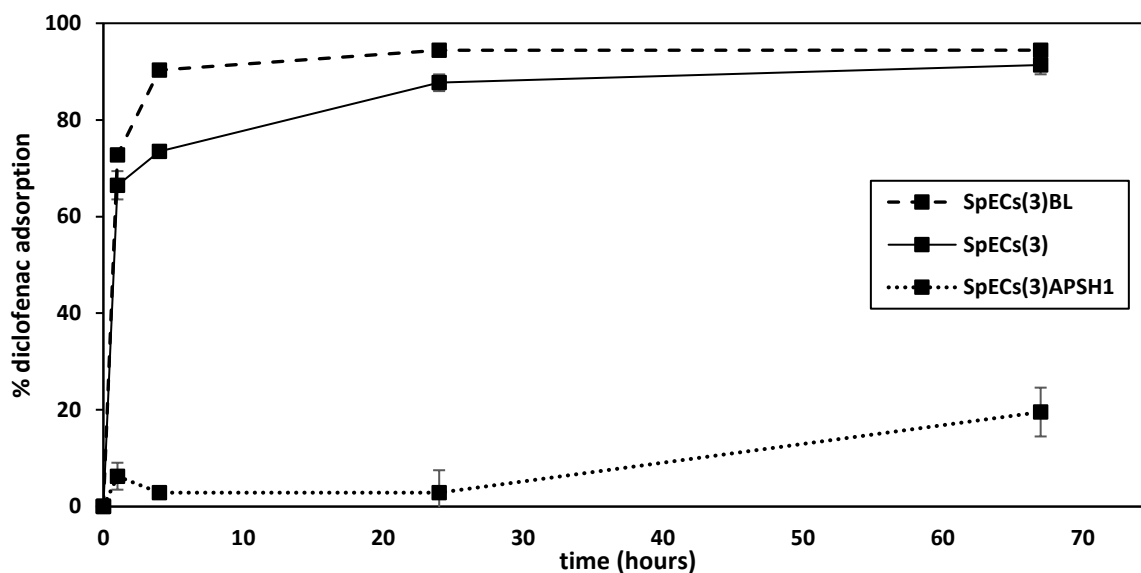


Figure 74: Effect of time on DCF adsorption for modified SpECs(3). Different treatments: SpECs(3)BL: 14% NaOCl at room temperature, SpECs(3)APSH1: 1 M ammonium persulfate at 90 °C (DCF dose: 6 mg/L, n=3).

In this treatment, it seems that the freshness of the bleach used is a factor affecting the resulting product, since the protocol was repeated several times producing SpECs of different shades of white and different adsorption properties each time. The concentration of bleach is the important parameter, since opened bottles or bleach older than four months after the production date lose their strength.¹⁸⁸ Unfortunately, treatment with NaOCl was not reliable on giving consistent results since repeated treatments on both SpECs(2) and SpECs(3) could not give materials presenting similar DCF adsorption performance to the ones presented above.

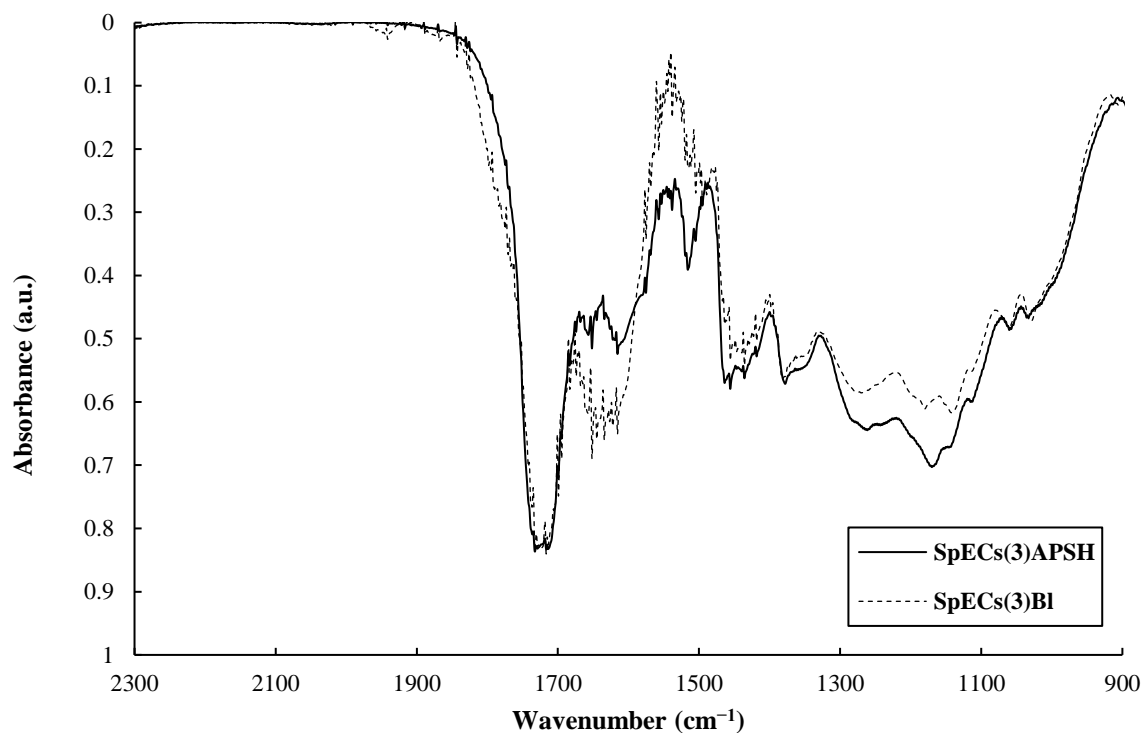


Figure 75: FT-IR spectra of APS treated SpECs(3) [SpECs(3)APSH] compared to NaOCl treated SpECs(3) [SpECs(3)BI].

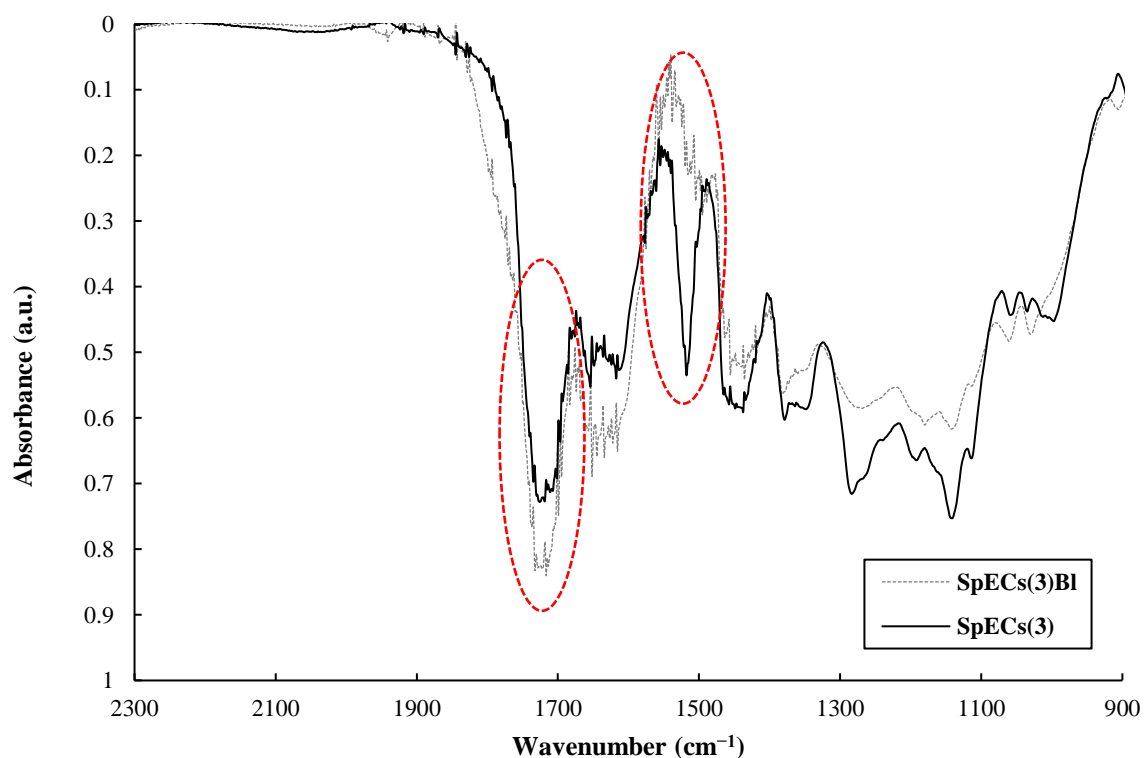


Figure 76: FT-IR spectra of NaOCl treated SpECs(3) [SpECs(3)BI] compared with SpECs(3). Highlighted areas of interest are the complete depletion of the aromatic ring modes (1510 cm⁻¹) and the increase in carboxylic acids ~1710 cm⁻¹.

Treatment with NaOCl made SpECs(3) slightly more efficient; after four hours of contact time DCF adsorption increased from 75% to 90%. Elemental analysis showed a difference in the carbon content (**Table 21**) implying that the oxygen content has increased, and that this difference enhanced the material's adsorption efficiency.

Table 21: Elemental analysis results for SpECs(3) and modified SpECs(3).				
material	C %	H %	N %	material description
SpECs(3)	67.07	8.82	0.00	HCl extraction
SpECs(3)APSH	63.36	8.15	0.00	ammonium persulfate treatment
SpECs(3)BL	55.26	6.53	0.00	NaOCl treatment

3.4.4.6. Comparison on SpECs(2)APSH, SpECs(2)Bl, SpECs(3) and SpECs(3)Bl

Between the initial extractions it was concluded that SpECs(3) presented the best properties for adsorption of DCF, both in terms of adsorption speed but also adsorption percentages. SpECs(3) performance was compared to the three modified SpECs that presented a good DCF adsorption behaviour and the results are presented in **Figure 77**.

It is evident from **Figure 77** that bleached SpECs(3) [SpECs(3)Bl] yielded the best DCF adsorption performance, reaching 90% DCF adsorption at four hours of contact time. All types presented similarly good performances, with the unmodified SpECs(3) giving the lowest adsorption percentages. When considering the ideal candidate however, the speed, cost and environmental impact of the methodologies employed is of prime importance. Bearing these factors in mind it may well be argued that the simple acid hydrolysis that yielded SpECs(3) was a very promising candidate for DCF adsorption, only marginally behind the bleaching methodologies mentioned but with a more facile and environmentally friendly production.

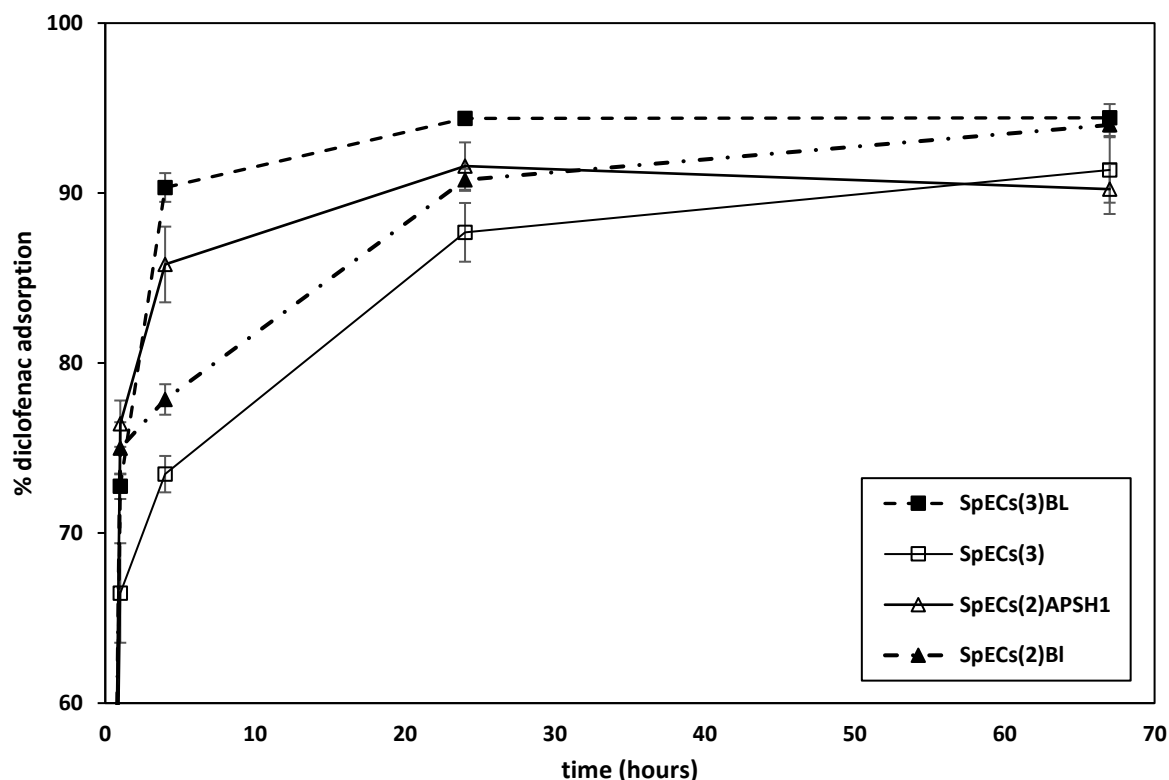


Figure 77: DCF adsorption performances of SpECs(3), NaOCl treated SpECs(3) [SpECs(3)BI], NaOCl treated SpECs(2) [SpECs(2)BI], and ammonium persulfate 1 M treated SpECs(2) [SpECs(2)APSH1] zoomed in the region of 60 - 100% adsorption ($n = 3$, DCF 6 $\mu\text{g/mL}$).

3.4.4.7. Diclofenac adsorption onto aminated SpECs(3)

After concluding that out of the three extractions SpECs(3) presented the best performance for DCF adsorption, it was decided to further modify the material in order to test whether the efficiency could be further improved and whether the time to reach equilibrium could be made significantly shorter.

From the previous tests it was concluded that DCF appears to be behaving primarily as a hydrogen bond acceptor, due to the ionized carboxylate group in the sodium salt of DCF. For this reason, conversion of the available carboxylic acids of the material was suggested in order to give a positively charged group so that the material might act like an anion exchange resin, retaining the DCF molecules through an electrostatic interaction as well as an H-bonding

interaction. A coupling reaction with 1,6-diaminohexane would give such an ammonium ion functional group which can act as both a hydrogen donor and is positively charged to aid electrostatic interaction (**Figure 78**).

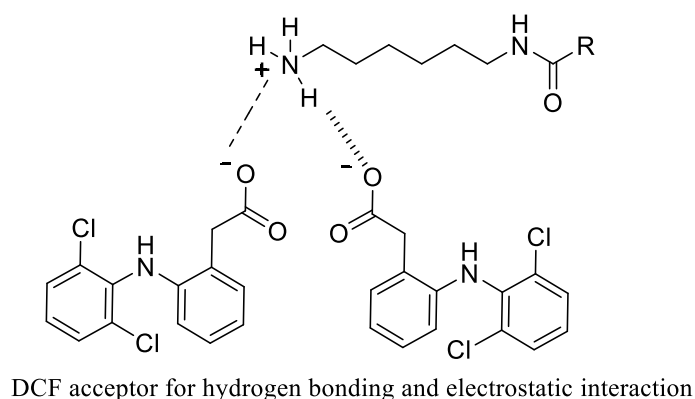


Figure 78: Possible electrostatic and hydrogen bonding interactions between DCF and the aminated SpECs (R = the SpECs polymer).

SpECs(3) were aminated with 1,6-diaminohexane following the protocol described in section 8.2.6 and previously described in the literature.¹⁸⁹ The resulting SpECs [SpECs(3)AM] were analysed with elemental analysis to confirm the increase in their N content (from 0.33% it has risen to 3.98% after the amination reaction, **Table 22**).

Table 22: Elemental analysis results for SpECs(3) before and after amination.			
material	C%	H%	N%
SpECs(3)	61.12	7.81	0.33
SpECs(3)AM	61.07	8.37	3.98

The resulting SpECs [SpECs(3)AM] exhibited a dramatic reduction in the contact times needed for the majority of DCF to be retained on the material, being noticeably faster compared with all other treatments. **Figure 79** shows the comparison of the DCF adsorption for the untreated SpECs(3) and SpECs(3)AM. It is evident that while the material had a good adsorption

efficiency before any treatment, after amination, the contact time needed for complete DCF removal was far shorter. In only 30 seconds equilibrium was reached, in which 90% of the DCF was adsorbed. After one minute, all of the DCF had been retained on SpECs(3)AM, whilst previously, a maximum of 90% was achieved in 65 hours of contact time.

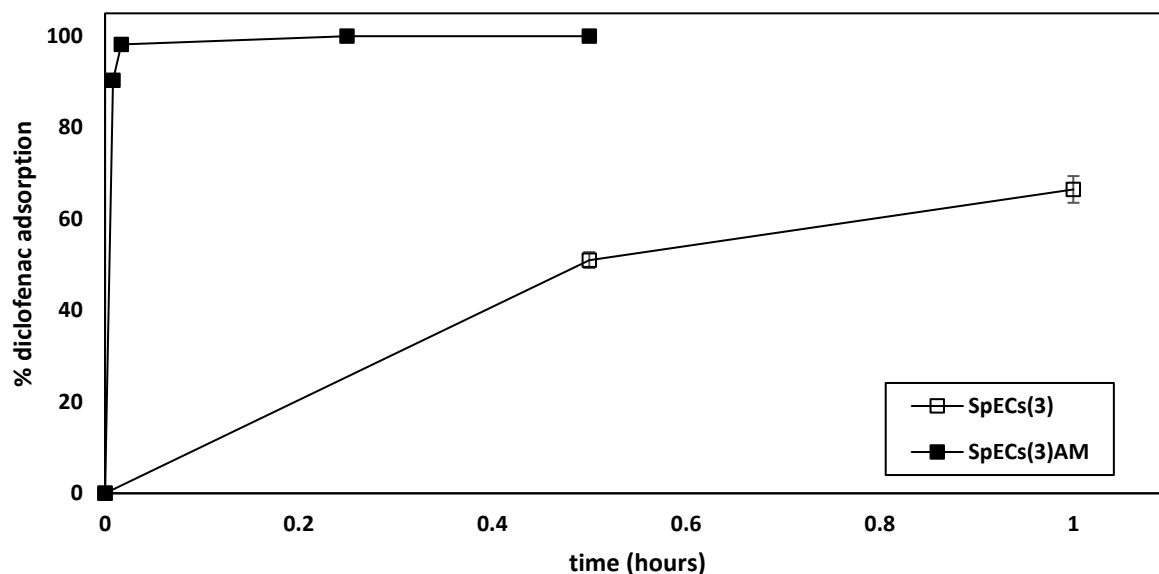


Figure 79: DCF adsorption; comparison between SpECs(3) and SpECs(3)AM (DCF dose: 6 mg/L, n=3).

The results of this treatment have given the best overall adsorption of DCF, and by far the quickest. The resulting SpECs while being positively charged, were more attractive to the DCF molecules, making the process of adsorption much faster. The opposing charges from the positively charged primary amine, acting as a hydrogen donor and the negatively charged carboxylic acids on DCF, acting as hydrogen acceptor, had as a result the increase in the material's adsorption efficiency. Apart from this, more protons were introduced on the material's surface, further increasing the binding sites for the DCF molecules and facilitating the adsorption possibly *via* H-bonding (**Figure 80**).

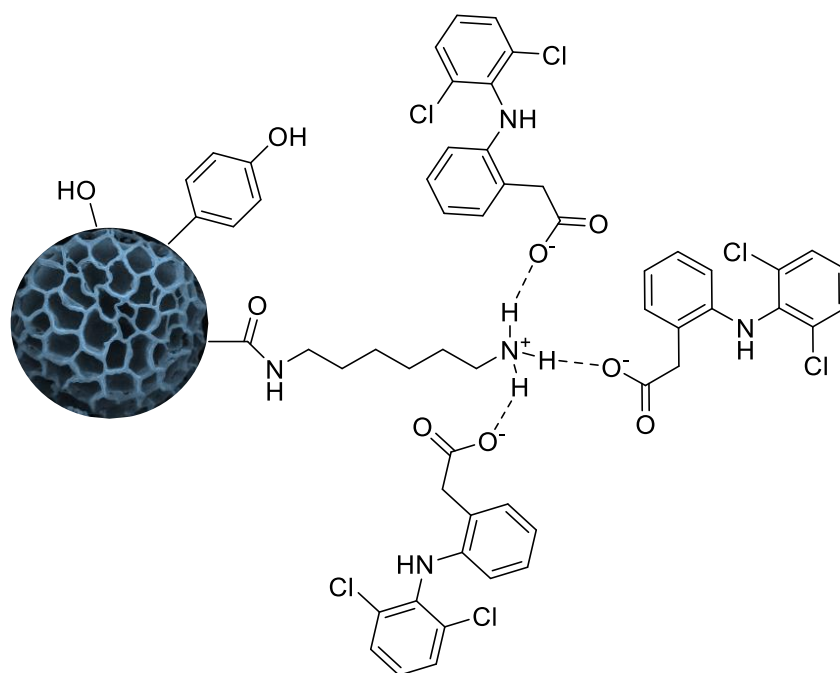


Figure 80: Schematic representation of possible adsorption forces between DCF and the surface of aminated SpECs(3).

Figure 81 presents a comparison of the DCF adsorption performances for the different SpECs types (modified and unmodified) for up to one hour of contact time. It is evident that the best adsorption properties were presented by the aminated SpECs(3), far better compared to the APS treated SpECs(2). Whereas the treatment with APS was able to improve the adsorption efficiency of the material and make it reach higher adsorption percentages, the amination of SpECs(3) both improved their efficiency as well as significantly reduced the contact time needed for equilibrium to be reached.

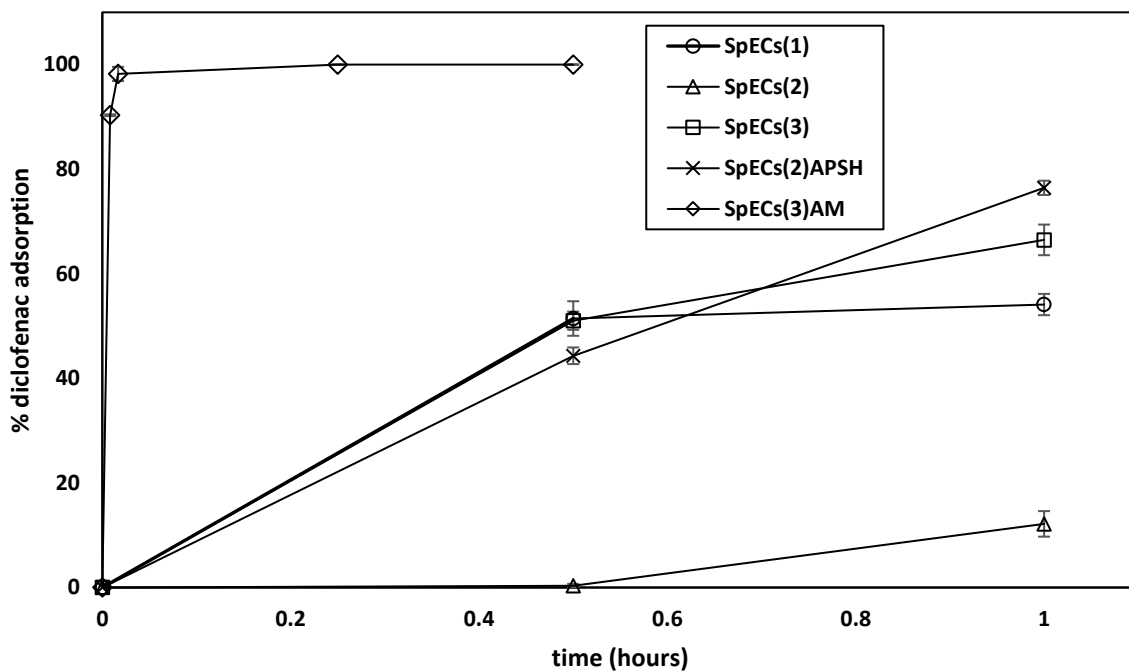


Figure 81: Effect of contact time on DCF adsorption, graph zoomed in the region of 0 - 1 hour of contact time (DCF dose: 6 mg/L). Comparison between the adsorption efficiencies of the different SpECs types and the most efficient modified SpECs (DCF dose: 6 mg/L, n=3).

3.4.5. Diclofenac adsorption kinetics

In order to investigate the adsorption mechanisms of DCF on the different SpECs types, pseudo-first order and pseudo-second order kinetic models were applied to the experimental data, to further explore the potential rate controlling steps. According to Simonin,²⁴⁷ a common mistake in most studies is the inclusion of data that are close or at equilibrium, altering the results of the analysis, reducing the accuracy of fit to the pseudo-first model and leading to conclusions that the pseudo-second model is a better fit. In order to avoid that, all data close to equilibrium will not be taken into account in this analysis and for this reason the SpECs(3)AM data analysis will not be possible, since equilibrium was reached too quickly to collect data points.

3.4.5.1. Pseudo-first order model

The pseudo-first order model or Lagergren's model⁷⁶ is generally applicable in the initial stage of the adsorption and is based on the assumption that the rate of adsorption is dependent on the concentration of the adsorbate. The linear form of the equation is expressed as follows (*Equation 15*):^{58,74}

$$\ln(q_e - q_t) = \ln q_e - k_1 t \quad \text{Equation 15}$$

where q_t (mg/g) is the amount of solute adsorbed per mass of adsorbent after a certain contact time t (min), q_e (mg/g) is the amount of solute adsorbed at equilibrium and k_1 (min^{-1}) is the pseudo-first order rate constant.

From the plot $\ln(q_e - q_t)$ versus t (**Figure 82**) the values of k_1 (slope) and $\ln q_e$ (intercept) were determined, from which the value of the maximum adsorption capacity $q_{e1,cal}$ was calculated. The experimental maximum adsorption capacity was calculated using *Equation 16*.

$$q_{e1,exp} = [DCF] * \frac{V}{m_{SpECs}} \quad \text{Equation 16}$$

where $[DCF]$ ($\mu\text{g/mL}$) is the concentration of DCF in the solution, V (mL) is the volume of the solution and m_{SpECs} (mg) is the mass of the SpECs used.

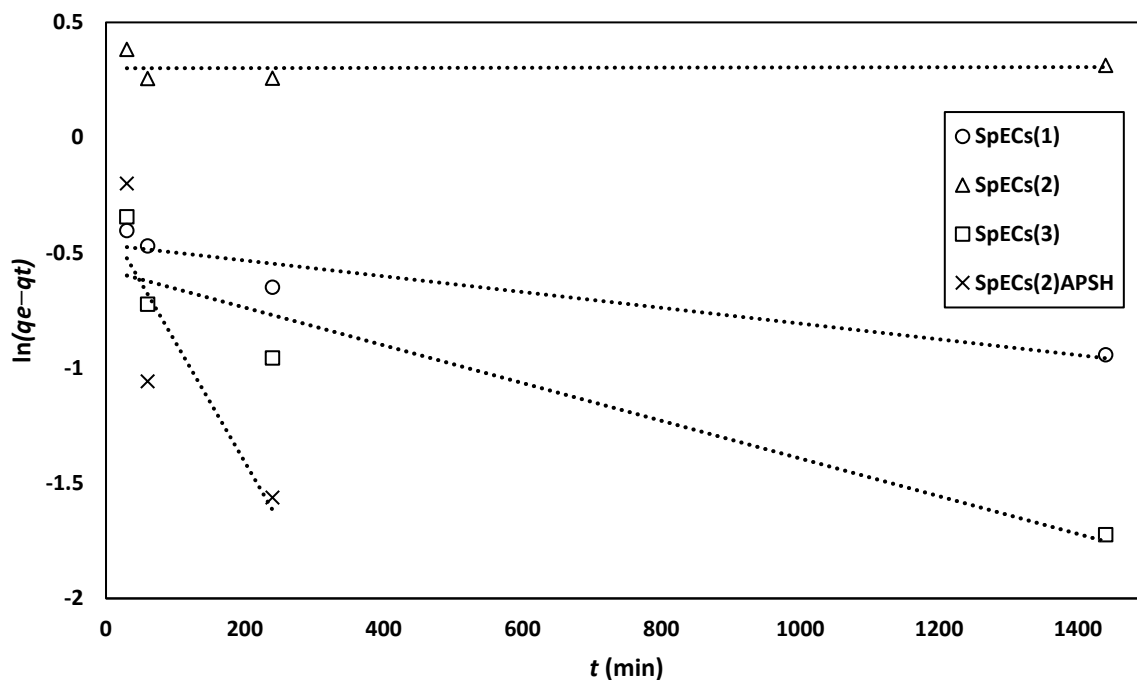


Figure 82: Kinetic investigation on the adsorption of DCF by different types of SpECs described by the pseudo-first order model.

All calculated values are summarised in **Table 23**, where it can be observed that for some SpECs the values of the correlation coefficient (R^2) are close to 1, whereas for others, the values are very low, indicating that this model was not suitable for them. SpECs(1) gave the highest R^2 value, 0.908, and the values of the experimental ($q_{e1,exp}$) and calculated ($q_{e1,cal}$) maximum adsorption capacity were close, 1.425 and 1.592 mg/g respectively, suggesting that this model was suitable for the adsorption of the DCF molecules onto the SpECs(1) surface. SpECs(3) presented a good R^2 value (0.8915), with the experimental and calculated values of the maximum adsorption capacity being close (1.448 and 1.775 mg/g respectively), indicating that the pseudo-first order model might be suitable to describe the adsorption process for this type of SpECs and that the procedure might involve diffusion-controlled phenomena. SpECs(2)APSH presented similar values for the experimental and calculated adsorption capacity, 1.471 and 1.444 mg/g respectively, but a lower R^2 value (0.7358) compared to the previous SpECs. SpECs(2) presented a very low R^2 value (0.0016), concluding that the

pseudo-first order model was not suitable to describe the DCF uptake. Analysis with the pseudo-second order model gave a better insight onto which model describes the uptake of DCF by which material.

3.4.5.2. Pseudo-second order model

The pseudo-second order model describes adsorption processes that involve chemisorption and is expressed as (Equation 17):⁷⁷

$$\frac{1}{q_t} = \frac{t}{q_e} + \frac{1}{k_2 q_e^2} \quad \text{Equation 17}$$

where q_t (mg/g) is the amount of solute adsorbed per mass of adsorbent after a certain contact time t (min), q_e (mg/g) is the amount of solute adsorbed at equilibrium, while k_2 (g/mg min) is the pseudo-second order equilibrium rate constant. The slope and intercept derived from the plots of t/q_t versus t (**Figure 83** and **Figure 84**) were used to calculate the values of the maximum adsorption capacity $q_{e2,cal}$ and the rate constant k_2 which are presented in **Table 23**.

The analysis using the pseudo-second order model gave higher R^2 values compared to the pseudo-first order model. The R^2 values were very close to unity for the majority of SpECs apart from SpECs(2) which gave a value of 0.7906, which was better than the value given by the pseudo-first model (0.0016). As both models did not give satisfactory values for both the R^2 and the maximum adsorption capacity it was concluded that SpECs(2) is not the best candidate for DCF adsorption. As with the previous model, SpECs(1) gave the highest R^2 value, 0.9997. The difference between the experimental and calculated maximum adsorption capacity values though was higher (1.425 and 1.050 mg/g respectively) compared to the previous model.

Maybe DCF adsorption from SpECs(1) can be described by both models since they both gave good values. It can be concluded that the adsorption of DCF by SpECs(3) and SpECs(2)APSH is described by the pseudo-second model since both types presented high R^2 values (0.9995 and 0.9924 respectively) combined with experimental and calculated maximum adsorption capacity values that were in close agreement.

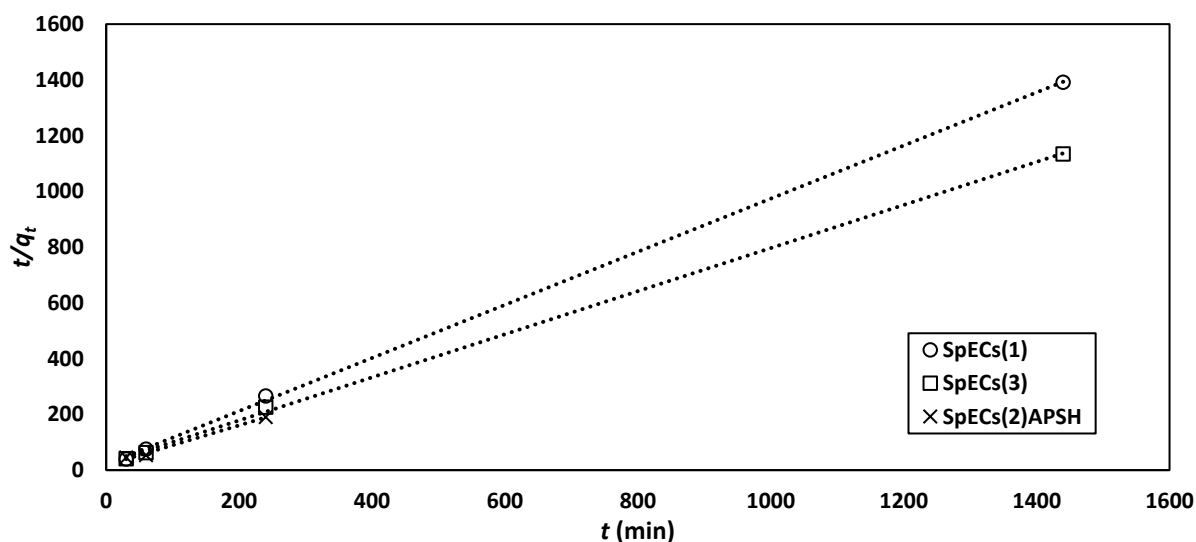


Figure 83: Kinetic investigation on the adsorption of DCF by different types of SpECs described by the pseudo-second order model.

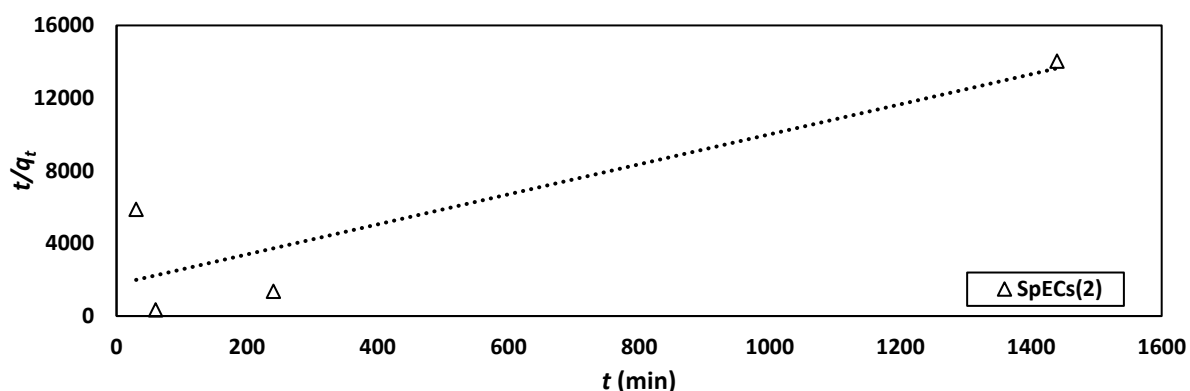


Figure 84: Kinetic investigation on the adsorption of DCF by SpECs(2) described by the pseudo-second order model.

The adsorption of DCF by SpECs was best described by the pseudo-second order model after excluding all the data points close to equilibrium. All tested SpECs presented similar values of maximum adsorption capacity, around 1.4 mg/g. Comparison to other materials found in literature tested for DCF adsorption showed that the values obtained (1.3 - 1.8 mg/g) were relatively low. Magnetic covalent organic frameworks presented the highest value of maximum adsorption capacity, 337 mg/g,²⁴⁸ whereas magnetic chitosan particles showed an adsorption capacity of 187 mg/g at a pH 4.²⁴⁹ Another study on chitosan-based magnetic composite particles with core-brush topology testing DCF adsorption at various temperatures and pHs gave values ranging from 95 - 110 mg/g.²⁵⁰ At pH 6 and at 25 °C, organophilic bentonites showed values in the range of 5.5 - 38.7 mg/g.¹⁹³ Carbide derived carbons produced at temperatures between 800 - 1400 °C gave a $q_{e2,cal}$ range of 250 - 350 mg/g.²⁵¹ The values for zeolitic imidazole frameworks were between 31 - 44 mg/g for a temperature range of 20 - 40 °C.²⁵² Isabel grape bagasse presented a lower value, 4.96 mg/g for an initial DCF concentration of 5 mg/L.¹⁰⁸ However, the experimental conditions were not identical to the ones used above, and were often not indicative of real world conditions. Also, the majority of the studies existing in the literature on DCF adsorption conclude that the adsorption kinetics are best described by the pseudo-second order model which as mentioned previously, it is often a false result. Since adsorption studies tend to take into account all experimental data points, including the ones close to or even at equilibrium, the results can be highly inaccurate and can lead to false conclusions according to Simonin.²⁴⁷

The initial rate of sorption h (mg/g min) was also calculated using *Equation 18*:²⁵³

$$h = k_2 q_e^2 \qquad \text{Equation 18}$$

The values of h (**Table 23**) showed a big variation between the different types of SpECs, with SpECs(2) giving the slowest adsorption rate, 0.0006 mg/g min, confirming that this type is not the best candidate for DCF adsorption. After their treatment with APS though, their initial rate of sorption increased from 0.0006 to 0.055 mg/g min, which was the highest value obtained. SpECs(1) and SpECs(3) presented similar values, ~0.04 mg/g min.

Table 23: Kinetic parameters for DCF adsorption by different SpECs described by different models.				
model/ parameter	adsorbent			
	SpECs(1)	SpECs(2)	SpECs(3)	SpECs(2)APSH
$q_{e,exp}$ (mg/g)	1.425	1.471	1.448	1.471
pseudo-first order				
$q_{e1,cal}$ (mg/g)	1.592	1.350	1.775	1.444
k_1	0.0003	4.00E-06	0.0008	0.0052
R^2	0.908	0.0016	0.8915	0.7358
pseudo-second order				
$q_{e2,cal}$ (mg/g)	1.050	0.121	1.294	1.404
k_2	0.04262	0.03915	0.02512	0.02789
h (mg/g min)	0.0470	0.0006	0.0421	0.0549
R^2	0.9997	0.7906	0.9995	0.9924

3.4.5.3. Intraparticle diffusion model

This model describes adsorption as a multi-step procedure, involving four diffusion steps: bulk diffusion, film diffusion, intraparticle diffusion and the adsorption of the contaminant molecules at the adsorbent's surface *via* ion exchange, chelation and/or complexation pathways.⁷⁴ Intraparticle diffusion can be quite a slow process, described by *Equation 19*:⁷⁸

$$q_t = k_i t^{0.5} + I \quad \text{Equation 19}$$

where q_t (mg/g) is the amount of solute adsorbed per mass of adsorbent at time t (min), k_i (mg/g min^{0.5}) is the rate constant for intraparticle diffusion model and I (mg/g) is the intercept which indicates the boundary layer thickness effect. The values of k_i and I can be obtained by the slope and intercept of the linear plot qt versus $t^{0.5}$ (**Figure 85**).

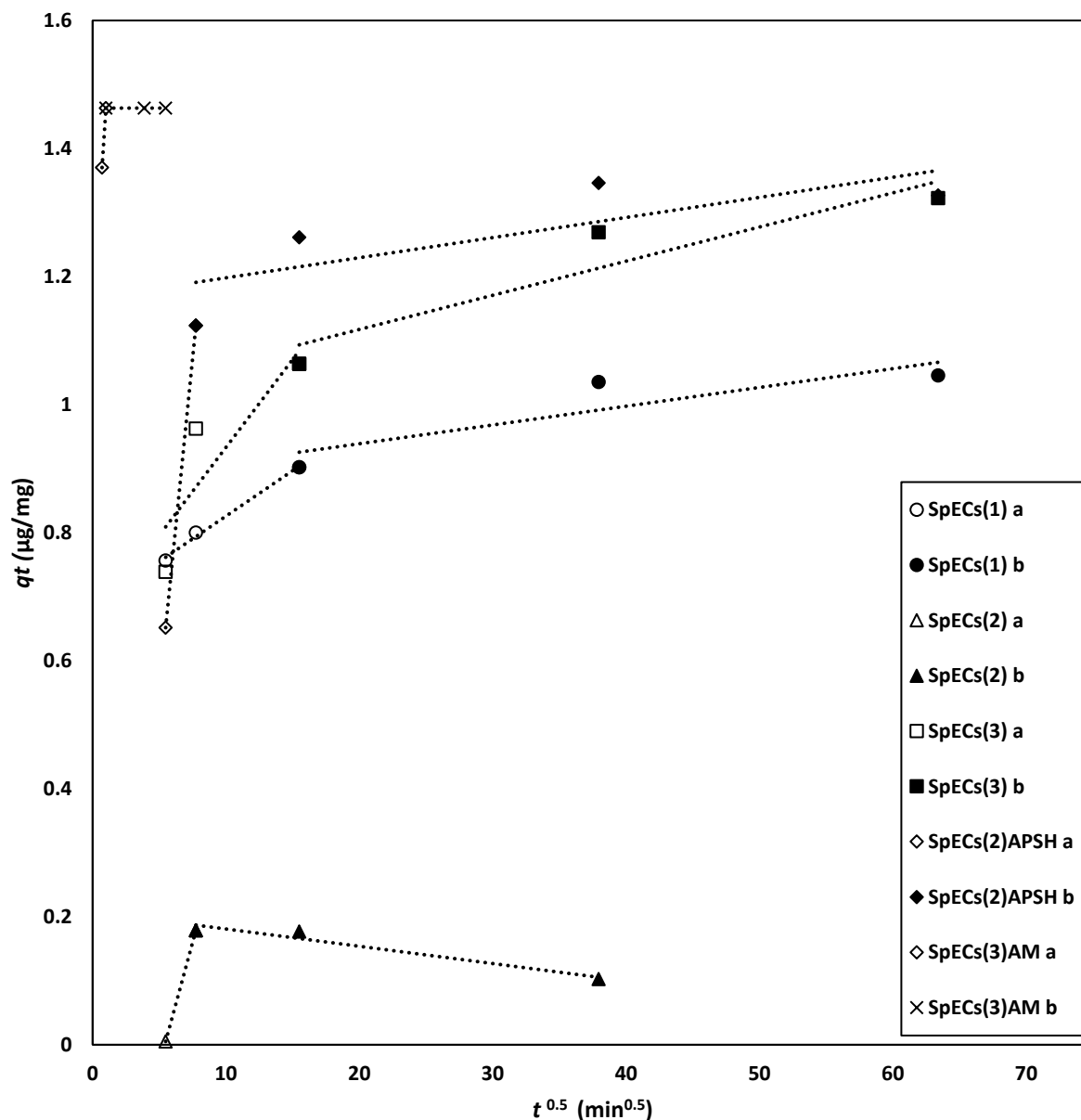


Figure 85: Intraparticle diffusion model for the adsorption of DCF onto different types of SpECs where (a) represents the first diffusion step and (b) represents the second diffusion step.

All the plots for the different SpECs types showed multilinearity, suggesting that during the sorption process, two different steps take place and that intraparticle diffusion is not the only rate-controlling step. The first linear part of the plots describes the migration of the DCF molecules from the solution to the SpECs surface *via* film diffusion, whereas the second part corresponds to the intraparticle diffusion, where the DCF molecules are gradually entering the pores of the SpECs with rate constants and intercepts presented in **Table 24**. All plots showed similar characteristics, while none passes through origin, a finding that means that film diffusion and intraparticle diffusion happen simultaneously during the process of adsorption²⁵⁴⁻²⁵⁶ of DCF onto the different SpECs types.

It is evident from **Figure 85** that the adsorption of DCF (q_t) is increasing with the increase of contact time, with the removal mostly taking place at the first step of the diffusion process. Analysis of the two steps **Table 24** showed that for the majority of the SpECs the first step presented a faster adsorption rate k_i and the second step followed with a much slower k_i , at $\sim 0.003 \text{ mg/g min}^{0.5}$. Such a finding can be explained by the fact that at the beginning of the adsorption, there exists a great number of empty sites available on the surface of the material, a number that decreases with time. In addition, after the first sites are occupied, there may exist repulsion forces between the adsorbed contaminant molecules and the ones in solution, preventing the latter from binding on the sorbent and thus slowing down the process.

The parameter I provides useful information on the effect that the boundary layer has on the adsorption process and is initially zero for $t = 0$. SpECs(1), SpECs(3) and SpECs(2)APSH presented similar I values for the first step, ~ 0.67 which during the next step it increased to ~ 1 showing that after the initial adsorption of the first DCF molecules on the surface of the SpECs, the effect of the boundary layer increased. SpECs(3)AM presented a high I value for the first step of the diffusion process which was further increased during the second step (from 1.146 to 1.463), showing that this type had already an increased boundary layer effect even at the

beginning of the adsorption process. SpECs(2) was the only type that presented a decrease in its I value, from 0.41 during the first step it decreased to 0.21, meaning that the effect of the boundary layer was decreasing with time, possibly indicating that a formation of multilayers of DCF molecules is happening on the surface of the material, facilitating the further adsorption of the free DCF molecules.

Table 24: Intraparticle diffusion parameters for DCF adsorption by different SpECs involving steps a and b.				
adsorbent	step	k_i (mg/g min^{0.5})	I	R^2
SpECs(1)	a	0.014	0.684	0.994
	b	0.003	0.880	0.774
SpECs(2)	a	0.077	0.414	1
	b	0.003	0.208	0.950
SpECs(3)	a	0.028	0.659	0.753
	b	0.003	1.167	0.610
SpECs(2)APSH	a	0.028	0.659	1
	b	0.005	1.011	0.873
SpECs(3)AM	a	0.318	1.146	1
	b	0.00	1.463	0.916

3.4.6. Diclofenac adsorption isotherms

The linear forms of the Langmuir²⁵⁷ and Freundlich²⁵⁸ models were used (*Equation 20* and *Equation 21* respectively) in order to investigate the distribution of the adsorbed DCF molecules between the aqueous phase and the SpECs particles.

$$\frac{C_e}{Q_e} = \frac{C_e}{Q_m} + \frac{1}{K_L Q_m} \quad \text{Equation 20}$$

$$\log Q_e = \log K_F + \frac{1}{n_F} \log C_e \quad \text{Equation 21}$$

where C_e (mg/L) is the concentration of the adsorbate at equilibrium, Q_e (mg/g) is the amount of contaminant adsorbed per amount of adsorbent, K_L (L/mg) is the Langmuir adsorption equilibrium constant and Q_m (mg/g) is the maximum adsorption capacity of the material. K_F ($\text{mg}^{(1-1/n)}/\text{gL}^{-1/n}$) and n_F are Freundlich's constants.

The experimental procedure described in section 8.4.3 was followed, where 5 mL portions of DCF solutions of different concentrations (0.5 - 90 $\mu\text{g/mL}$) were mixed with 20 mg of SpECs and were agitated for 24 hours at room temperature. After filtration, the resulting solutions were analysed for their DCF content and the linear forms of the models were plotted using Excel (**Figure 86**, **Figure 87** and **Figure 88**). Q_e was calculated with *Equation 22*.

$$Q_e = \frac{(C_0 - C_e)V}{m} \quad \text{Equation 22}$$

where C_0 is the initial DCF concentration, V is the volume of the solution used and m is the mass of the adsorbent. Q_m was calculated from the slope of the Langmuir plot and K_L was calculated from the intercept. K_F was determined from the intercept of the Freundlich plot and n_F was calculated from the slope. All the parameters for both models (Langmuir and Freundlich) are presented in **Table 25**.

model/parameter		SpECs(1)	SpECs(2)	SpECs(3)	SpECs(2)APSH	SpECs(3)AM
Langmuir	Q_m (mg/g)	3.414	0.548	13.889	500	5.828
	K_L (L/mg)	0.097	0.01	0.106	0.0005	1.05
	R^2	0.732	0.072	0.874	0.045	0.965
Freundlich	K_F ($\text{mg}^{(1-1/n)}/\text{gL}^{-1/n}$)	2.024	0.002	1.106	4.011	3.819
	$1/n_F$	0.468	0.68	0.878	0.999	0.064
	R^2	0.953	0.446	0.81	1	0.955

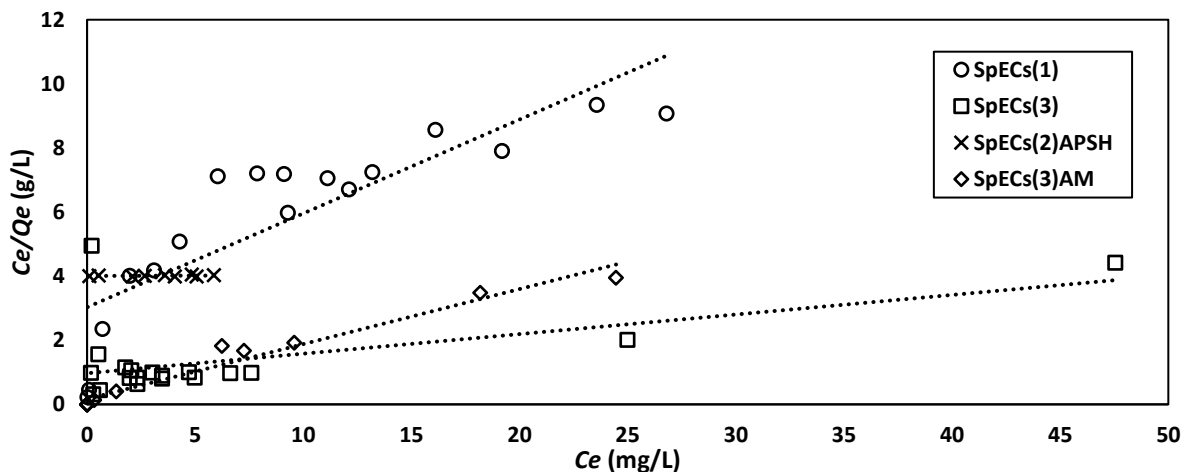


Figure 86: Langmuir linear adsorption isotherms for DCF uptake by different types of SpECs.

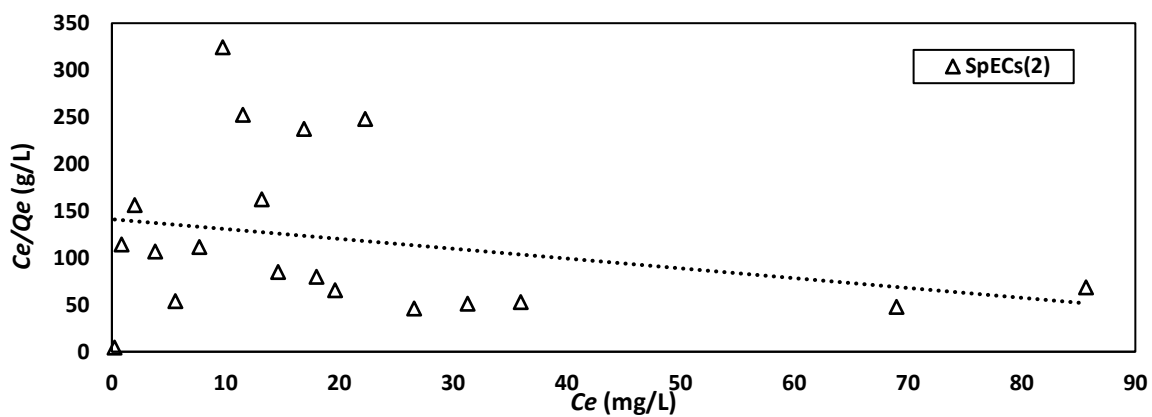


Figure 87: Langmuir linear adsorption isotherm for DCF uptake by SpECs(2).

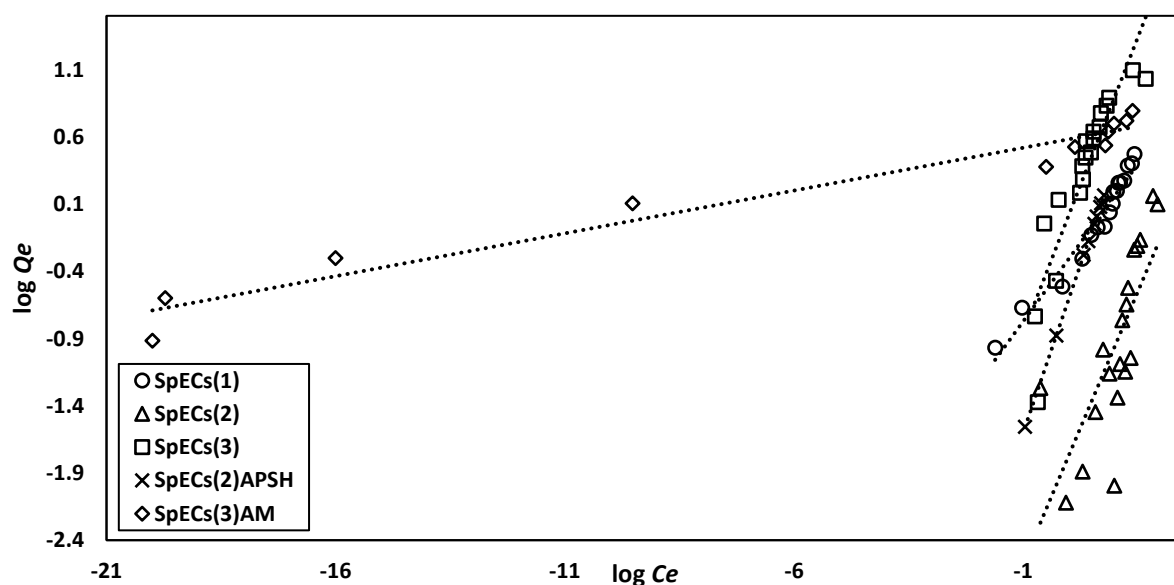


Figure 88: Freundlich linear adsorption isotherms for DCF uptake by different types of SpECs.

The isotherm analysis of the DCF adsorption showed that for the majority of the tested SpECs the Freundlich model presented a better fit to the experimental data. SpECs(1) gave a R^2 value of 0.953 for the Freundlich model whereas SpECs(2)APSH presented a R^2 value equal to one. As mentioned in the introduction, the Freundlich model describes a multisite and reversible adsorption procedure, where the adsorbent's surface is heterogeneous. This means that the active sites on the surface of SpECs(1) and SpECs(2)APSH are of various energies and thus affinity towards the DCF molecules, and adsorption takes place by creating multilayers on the surface of the material.

SpECs(3) and SpECs(3)AM gave results that were able to be described by both models according to the R^2 values obtained. In both models, SpECs(3) presented R^2 values that were close to each other (0.81 for Freundlich and 0.87 for Langmuir), whereas SpECs(3)AM gave values that were close to unity; 0.96 for Freundlich and 0.97 for Langmuir. The Langmuir model describes a homogenous contaminant adsorption, where each active site of the adsorbent's surface can only be occupied by one molecule of pollutant and maybe that is the case for both SpECs(3) and SpECs(3)AM. SpECs(2) did not give satisfactory R^2 values either using the Langmuir model or the Freundlich; 0.072 and 0.446 respectively.

In the Langmuir model, Q_m indicates the amount of adsorbant needed for a complete monolayer over the sorbent surface. Interestingly, SpECs(3) presented a much higher Q_m value compared to their aminated form, suggesting that their surface has more active sites of possible DCF binding than the aminated form. The actual number of amines present in SpECs(3)AM is limited by the original number of carboxylic acids available in SpECs(3), meaning that it is possible that SpECs(3)AM is a material with fast DCF adsorption efficiency but with fewer available binding sites.

As the Freundlich model does not include such a parameter for the maximum adsorption capacity of the material, an indication of the adsorption capacity of the adsorbent can be the

factor K_F . K_F is related to the material's adsorption capacity; the greater the K_F value is, the more efficient the material is against the contaminant in target. SpECs(2)APSH presented the highest K_F value between the tested SpECs. This confirmed that the surface oxidation worked and that the procedure made the material more efficient whilst untreated SpECs(2) exhibited a far lower value (4.011 and 0.002 $\text{mg}^{(1-1/n)}/\text{gL}^{-1/n}$ respectively).

The $1/n_F$ value included in the Freundlich model is another important factor that provides useful information about the characteristics of the adsorption process. The highest $1/n_F$ value was presented by SpECs(2)APSH and was almost one (0.999) indicating the cooperative adsorption of DCF, possibly forming multi-layers on the surface of the material. SpECs(1) and SpECs(3)AM presented a $1/n_F$ value that was lower than one, fact that implies that the adsorption of the DCF molecules is mainly happening through chemisorption. SpECs(3)AM presented a value closer to zero meaning that their surface is more heterogeneous compared to the other two types.

Comparison to other materials already tested in the literature showed that SpECs(3) presented better Q_m values for DCF adsorption compared to magnetic chitosan particles,²⁴⁹ with the latter having a Q_m value of 10 mg/g when analysed with the Langmuir model. SpECs(3) gave a value of 14 mg/g, value which is close to the one reported in the literature for organophilic bentonites (13.3 mg/g).¹⁹³ Activated carbon and porous carbons with metal azolate frameworks analysed with the Langmuir model gave greater values of 79 and 503 mg/g respectively²⁵⁹ whereas titanate nanosheet-pozollan nanocomposites gave values at around 80 mg/g.²⁶⁰ Magnetic covalent organic frameworks gave results that were better described by the Freundlich model, presenting a K_F value of 335 $\text{mg}^{(1-1/n)}/\text{gL}^{-1/n}$,²⁴⁸ much higher than the value of 4.01 $\text{mg}^{(1-1/n)}/\text{gL}^{-1/n}$ obtained by SpECs(2)APSH.

3.4.7. Diclofenac packed-bed studies

In order to test the DCF adsorption efficiency of the different SpECs under flow conditions, packed-bed experiments were conducted. The procedure described in section 8.9 was followed, where a glass column (30 cm × 2.5 cm) was tightly packed with a layer of SpECs of fixed mass and height. A solution of known DCF concentration was passed through the SpECs layer under gravity, until the complete saturation of the material. Different initial DCF concentrations were tested, as well as different SpECs masses and flow rates. The flow rate was altered under gravity by adjusting the column's tap. All data obtained were analysed with the Yoon-Nelson model (*Equation 23*), expressed as:⁸¹

$$C_t/C_0 = 1/[1 + \exp(K_{YN}\tau - K_{YN}t)] \quad \text{Equation 23}$$

where, C_t (mg/L) is the contaminant's concentration at time t (min), C_0 (mg/L) is the initial contaminant concentration, K_{YN} (min^{-1}) is the Yoon-Nelson rate constant and τ (min) is the time required for 50% adsorbate breakthrough. K_{YN} and τ can be calculated from the linear form of *Equation 24* by plotting $\ln(C_t/(C_0 - C_t))$ versus t .

$$\ln\left(\frac{C_t}{C_0 - C_t}\right) = K_{YN}(t - \tau) \quad \text{Equation 24}$$

The sorption capacity of the material q_0 (mg/g) can be calculated by using *Equation 25*:

$$q_0 = \frac{C_0 Q \tau}{m} \quad \text{Equation 25}$$

where Q is the flow rate (L/min) and m (g) is the mass of sorbent used in the column.

This calculated value (q_0) can then be compared to the experimental one ($q_{0,exp}$), defined by

Equation 26:

$$q_{0,exp} = \frac{m_{DCF\ ads}}{m} \quad \text{Equation 26}$$

where $m_{DCF\ ads}$ (mg) is the adsorbed DCF mass and m (g) is the mass of sorbent used in the column. $m_{DCF\ ads}$ was calculated using *Equation 27*.

$$m_{DCF\ tot} = m_{DCF\ el} - m_{DCF\ ads} \quad \text{Equation 27}$$

where $m_{DCF\ tot}$ is the total amount (g) of DCF that passed through the column and $m_{DCF\ el}$ is the amount (g) of DCF eluted. $m_{DCF\ tot}$ and $m_{DCF\ el}$ were calculated using *Equation 28* and *Equation 29*:

$$m_{DCF\ tot} = V_{tot} * C_0 \quad \text{Equation 28}$$

$$m_{DCF\ el} = C_{el} * V_{el} \quad \text{Equation 29}$$

where V_{tot} is the total volume of the contaminant solution that passed through the column, C_0 is the initial concentration of the contaminant, C_{el} is the concentration of the eluted solution after passing through the column and V_{el} is the volume of the eluted solution.

The SpECs bed was covered with low iron sand to keep the particle bed tightly packed. The sand layer was checked individually for its DCF adsorption ability by passing through a solution of known DCF concentration (10 mg/L) and by comparing the initial and final concentration (C_f and C_0 respectively). The results presented in **Table 26** confirmed that sand had no adsorption efficiency over DCF.

fraction	volume (mL)	C_f (mg/L)	C_0 (mg/L)
1	5	10.238	10.258
2	5	10.208	10.258
3	15	10.268	10.258
4	20	10.089	10.258
5	20	10.268	10.258
6	20	10.298	10.258
7	50	10.149	10.258
8	60	10.208	10.258
9	60	10.208	10.258
10	90	10.238	10.258
11	150	10.298	10.258
12	150	10.238	10.258

Initially, before the breakthrough point, while the effluent's DCF content was low, the effluent was collected in fractions of 5 mL. Later in the experiment when the DCF concentration increased and was more stable, the fractions were collected in larger volumes (50 to 100 mL) and analysed with a UV-Vis spectrometer. The treated volume was plotted against the recovered DCF concentration divided by the initial DCF concentration and the breakthrough curves were formed in Excel.

3.4.7.1. Breakthrough curves for SpECs(3)

The first set of experiments involved changes in the initial contaminant dose to set the conditions for all experiments. In the first experiment, 1 g of SpECs(3) (2 cm high) was packed under 5 g of low iron sand (1.5 cm high) and a solution of DCF 10 mg/L passed through at a flow rate of 2 mL/min. In the second experiment, 1 g of SpECs(3) (2 cm high) was packed under 4.5 g of low iron sand (1.5 cm high) and a solution of DCF 60 mg/L passed through at a flow rate of 1.8 mL/min. The results obtained were plotted in the form of breakthrough curves (**Figure 89**) and the data were analysed with the Yoon-Nelson model (*Equation 23*).

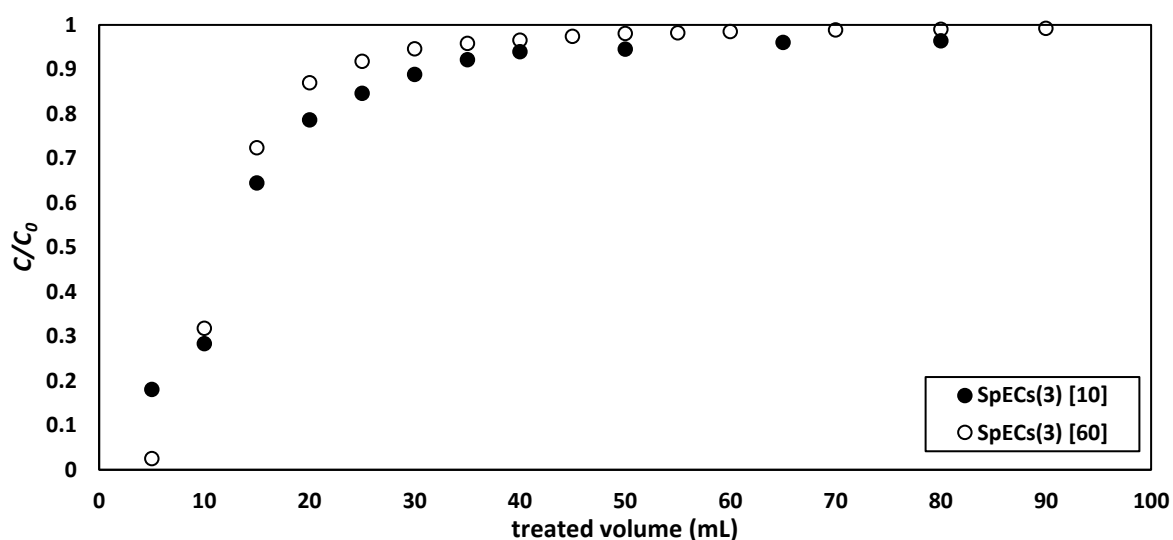


Figure 89: DCF breakthrough curves for 1 g packed SpECs(3) at 10 mg/L DCF initial concentration (C_0) and 2 mL/min flow rate (SpECs(3)[10]) and 1 g packed SpECs(3) with 60 mg/L DCF initial concentration and 1.8 mL/min flow rate (SpECs(3)[60]).

Although the concentration of the DCF solution was six times higher in the second experiment, the breakthrough curves obtained from both experiments exhibited strong resemblance, showing that the contaminant's concentration did not affect the material's saturation point. A small difference of 5 mL of treated volume can be observed in the graph for the breakthrough point ($C/C_0 = 0.5$) which is reached 5 mL earlier for the higher concentration.

The analysis using the Yoon-Nelson model indicated that the higher dosage (60 mg/L initial DCF concentration) had a better fit, with a high R^2 value and experimental values that are in close agreement to the calculated ones (**Table 27**). More specifically, the maximum adsorption capacity values were 0.79 mg/g for the calculated and 0.62 mg/g for the experimental, whereas the breakthrough time was 8.63 minutes for the calculated and 8.84 minutes for the experimental. On the contrary, the low dosage experiment did not give satisfactory results with the Yoon-Nelson analysis. The values of the maximum adsorption capacity were not close with the calculated being 0.065 mg/g and the experimental being 0.15 mg/g.

initial [DCF]	flow rate (mL/min)	K_{YN} (min ⁻¹)	τ (min)	τ_{exp} (min)	R^2	q_0 (mg/g)	$q_{0,ex}$ (mg/g)
10 mg/L	2.06	0.1223	3.298	5.974	0.736	0.065	0.15
60 mg/L	1.77	2.7037	8.625	8.838	0.957	0.788	0.62

Even though the higher dosage gave better fitting to the Yoon-Nelson model, it was decided to conduct all packed-bed experiments at the lower contaminant dose, 10 mg/L, since this is a more realistic concentration, closer to the values that are encountered in real wastewater samples. As mentioned in the introduction, the reported values of DCF present in wastewater effluents can reach concentrations up to 8.5 $\mu\text{g/L}$.¹⁹³ Since such a concentration is considered very low for a packed-bed experiment setup and would require the use of large quantities of water, it was decided to conduct the experiments at the concentration of 10 mg/L to save water as well as time. The flow rate on the other hand, together with the packed-bed's mass were variants that needed further investigation.

Figure 90 shows the breakthrough curves for DCF adsorption by SpECs(3) where 3 g of SpECs(3) (6.5 cm high) were packed under 6 g of low iron sand (1.5 cm high). A solution of

DCF 10 mg/L passed through the SpECs bed at two different flow rates: 0.8 and 0.5 mL/min, with the two breakthrough curves not presenting major differences when compared to each other.

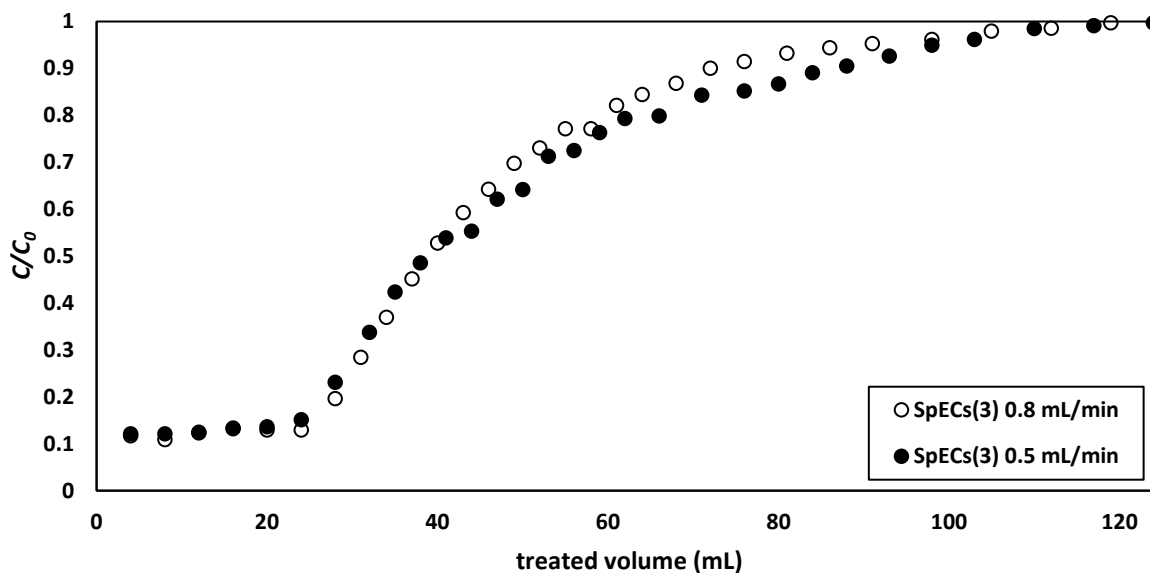


Figure 90: Breakthrough curves for 3 g packed SpECs(3) and DCF at 10 mg/L initial concentration (C_0) and two different flow rates: 0.8 mL/min and 0.5 mL/min.

Both experiments presented a good fit when analysed with the Yoon-Nelson model (**Table 28**) with both R^2 values being close to 0.97. A noticeable difference between the two flow rates was that the slower flow rate presented a higher breakthrough time τ , at 75.4 minutes, whereas the flow rate at 0.8 mL/min presented a τ at 52.2 minutes. Such a finding was expected since a slower flow rate would slightly increase the time needed to reach the 50% C/C_0 point. Both calculated values (τ) were in accordance with the experimental ones (τ_{exp}). The maximum adsorption capacities were similar for both flow rates, around 0.13 mg/g, values that were in agreement with the experimental ones. This experiment shows that a difference of 0.3 mL/min in the flow rate does not have a big impact on the adsorption of DCF by SpECs(3), apart from the breakthrough time that presented a difference of almost 20 minutes when the flow rate was slower.

Table 28: Yoon-Nelson model parameters for DCF adsorption (C_0 at 10 mg/L) by SpECs(3) (3 g) at two different flow rates.

flow rate (mL/min)	K_{YN} (min^{-1})	τ (min)	τ_{exp} (min)	R^2	q_0 (mg/g)	$q_{0,ex}$ (mg/g)
0.5	0.0353	75.368	73.3	0.966	0.12687	0.133
0.8	0.0524	52.193	50.8	0.976	0.14057	0.134

3.4.7.2. Breakthrough curves for SpECs(2)APSH

A similar experimental procedure was followed for the oxidised form of SpECs(2) [SPECS(2)APSH], where the glass column was packed with 0.5 g SpECs(2)APSH (0.8 cm high) covered with 2 g of low iron sand (0.4 cm high). The adsorption of DCF (initial concentration 10 mg/L) was tested under two different flow rates, 1.5 and 3.0 mL/min. The effluent was initially collected in fractions of 5 mL and later in bigger volumes (20 - 150 mL) and analysed for its DCF content. The treated volume was plotted against the recovered DCF concentration divided by the initial DCF concentration and the breakthrough curves were formed in Excel (**Figure 91**).

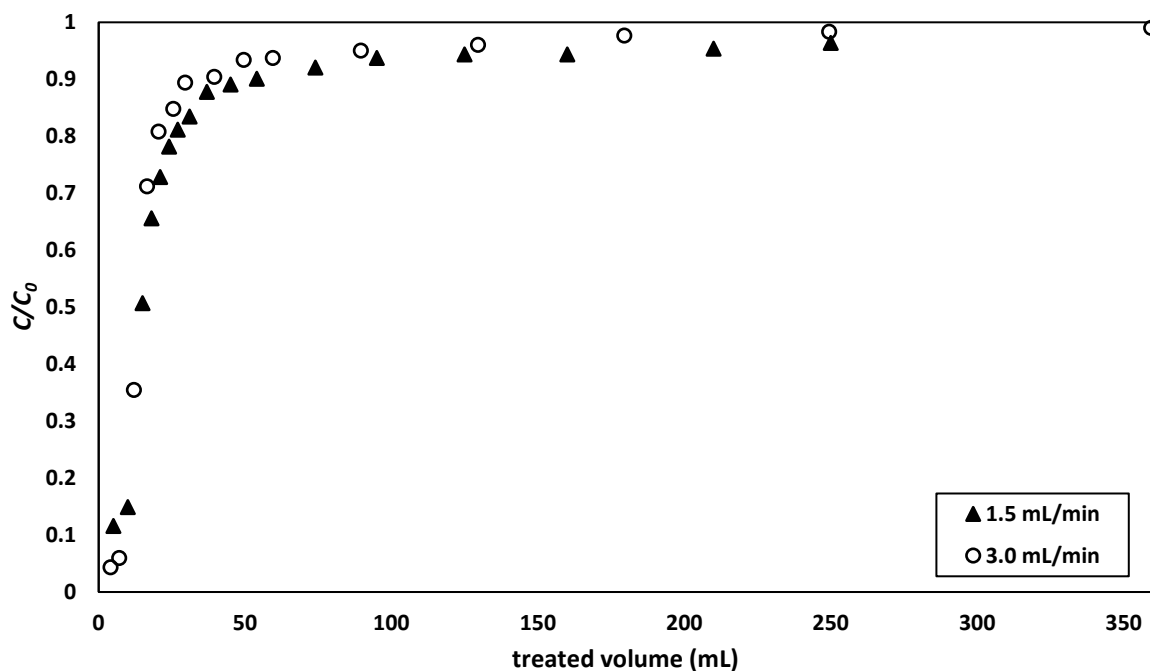


Figure 91: DCF breakthrough curves for 0.5 g packed SpECs(2)APSH at 10 mg/L DCF initial concentration (C_0) and two different flow rates: 1.5 mL/min and 3.0 mL/min.

As it can be seen in **Figure 91**, the material reached its saturation point after around 50 mL of treated DCF solution with the two different flow rates giving similar results. It is also evident that the breakthrough point, where half of the initial DCF concentration was able to pass through the packed-bed, occurred at around 13 mL for the faster flow rate and at 15 mL for the slower one. Both findings indicated that whereas the oxidised SpECs(2) had shown a good adsorption efficiency against DCF under the previous setup in the previous kinetic experiments (chapter 3.4.4.1) the material is not as efficient under the packed-bed setup, since it requires long contact times with the contaminant solution in order to interact and adsorb the DCF molecules.

The collected data were analysed with the Yoon-Nelson model and both flow rates presented a good agreement between calculated and experimental values (**Table 29**). It was proven that the difference in the flow rate had an impact on the breakthrough point, with the τ value going from 12 minutes down to 6 minutes when the flow rate changed from 2 to 3 mL/min. The adsorption capacity of the SpECs(2)APSH was not affected by the flow rate, with both flow rates presenting similar values, 0.32 mg/g. Such a value is relatively low, finding that confirms that the packed-bed setup is not ideal for this type of SpECs. Since the adsorption capacity is strongly dependant on the bed height and the influent concentration, a different experimental setup with bigger bed volume and possibly lower DCF concentration might have given better results and enhance the material's efficiency for DCF adsorption. It was concluded that under the tested conditions SpECs(2)APSH was not an ideal candidate for DCF adsorption.

flow rate (mL/min)	K_{YN} (min^{-1})	τ (min)	τ_{exp} (min)	R^2	q_0 (mg/g)	$q_{0,exp}$ (mg/g)
1.5	0.1237	11.85	15.5	0.753	0.320	0.312
3.0	0.4734	6.01	5.5	0.811	0.324	0.254

3.4.7.2.1. Regeneration and reusability of SpECs(2)APSH

After the completion of the breakthrough curves, the packed SpECs(2)APSH were washed with milliQ water in order to check if the adsorbed DCF could be easily desorbed. **Figure 92** shows the breakthrough curve derived from the previous experiment (full circles) and the region of the milliQ water washings after reaching the breakthrough point (empty circles). It is evident that initially a small amount of DCF came out as ‘dead volume’ since some DCF solution would have stayed trapped between the SpECs but after this initial point it is obvious that no amount of DCF was able to desorb from the packed SpECs and contaminate the pure water passing through.

After the water washings, the packed material was washed with absolute ethanol in order to desorb all of the adsorbed DCF. The recovery rates were tested together with the reusability of the SpECs; the packed SpECs(2)APSH were washed with a continuous flow of pure ethanol, until the ethanolic effluent contained no DCF. In total, 110 mL of pure ethanol was used in order to completely remove all the adsorbed DCF, quantity that was calculated to be around 0.5 mg. At the end of the washing the ethanolic solution was coming out of the column as blank, indicating that no more DCF could be removed. The comparison between the calculated amount of adsorbed DCF against the amount of recovered DCF (**Table 30**) gave the recovery percentages that were high, suggesting that absolute ethanol was an efficient solvent for the regeneration of the packed SpECs.

The reusability of the regenerated SpECs(2)APSH was tested for two more cycles under the same experimental setup as before; the DCF solution passed through the packed-bed until the complete saturation of the material, the material was then washed with absolute ethanol until the complete removal of the contaminant and then reused.

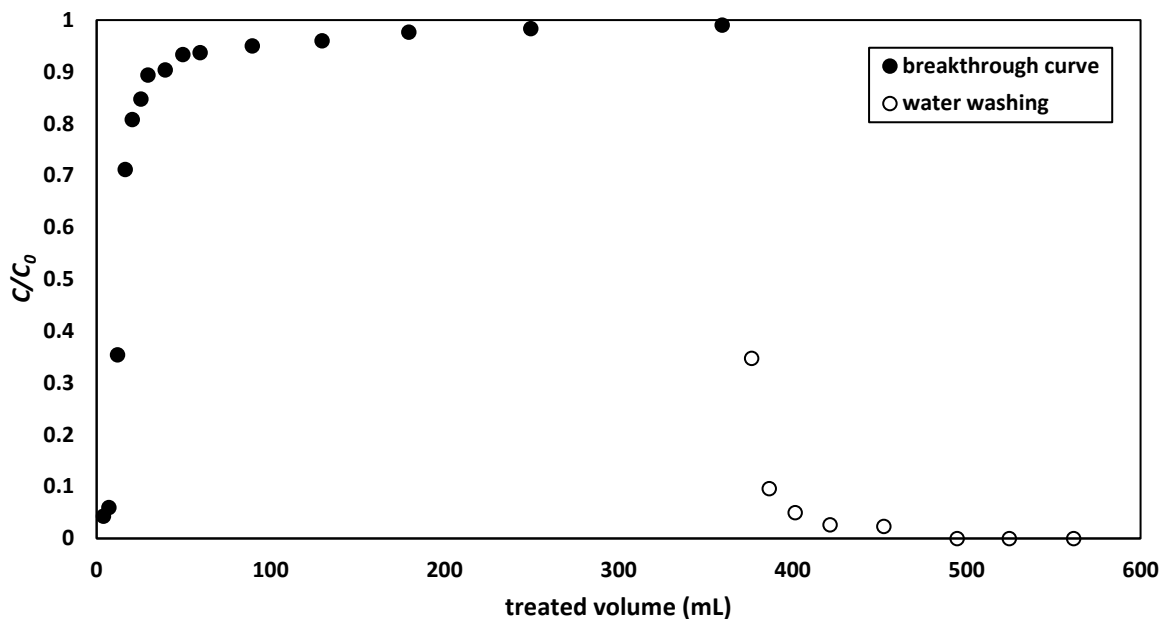


Figure 92: Breakthrough curve for SpECs(2)APSH and DCF adsorption, followed by washing of the packed-bed with milliQ water after reaching the saturation point.

flow rate	adsorbed DCF (mg)	recovered DCF (mg)	% DCF recovery
1.5 mL/min	0.500	0.448	89.6
	0.600	0.598	99.7
	0.597	0.471	78.9
3.0 mL/min	0.560	0.468	83.6
	0.745	0.695	93.3
	0.630	0.579	91.9

Figure 93 shows the breakthrough curves for all the three cycles at the flow rate of 1.5 mL/min, whereas **Figure 94** presents the breakthrough curves for the flow rate of 3 mL/min. In both graphs it can be observed that the material behaves similarly in all three cycles, with the first cycle being slightly less efficient compared to the previous two. This can be attributed to factors such as inadequate packing of the SpECs bed, meaning that holes exist between the packed particles, allowing the DCF molecules to pass through the column without interacting with the

material. After each washing, the solvent passing through is able to push the particles and pack them tighter, having as a result a slightly better performance in the reuse cycles.

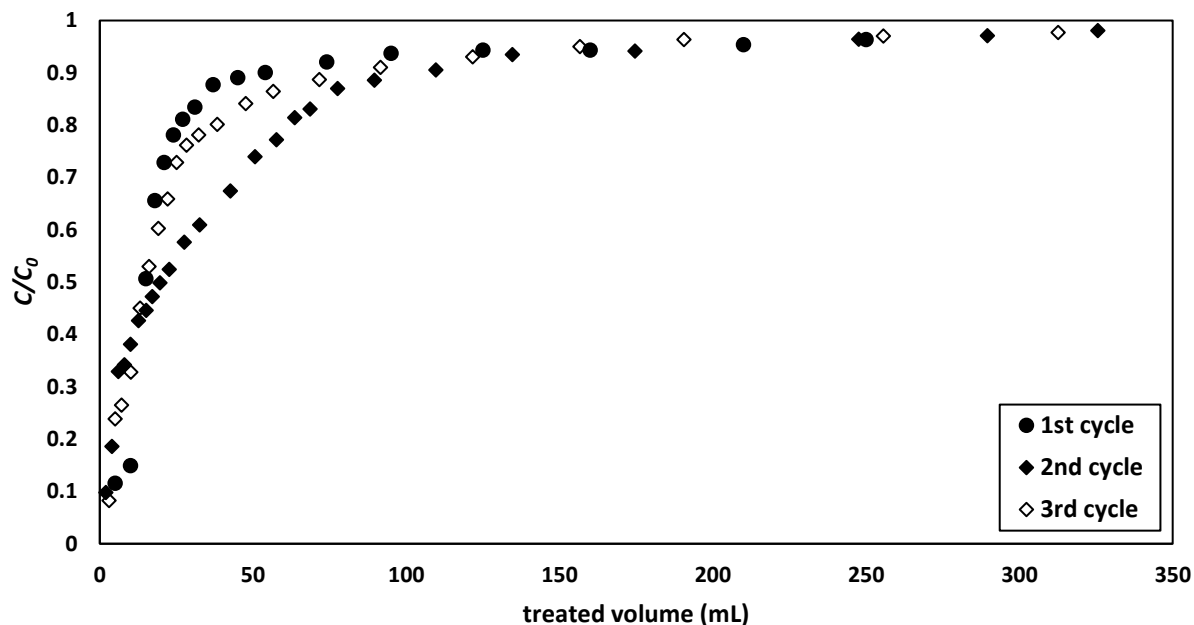


Figure 93: Breakthrough curves for DCF adsorption at a flow rate of 1.5 mL/min for three cycles of SpECs(2)APSH reuse.

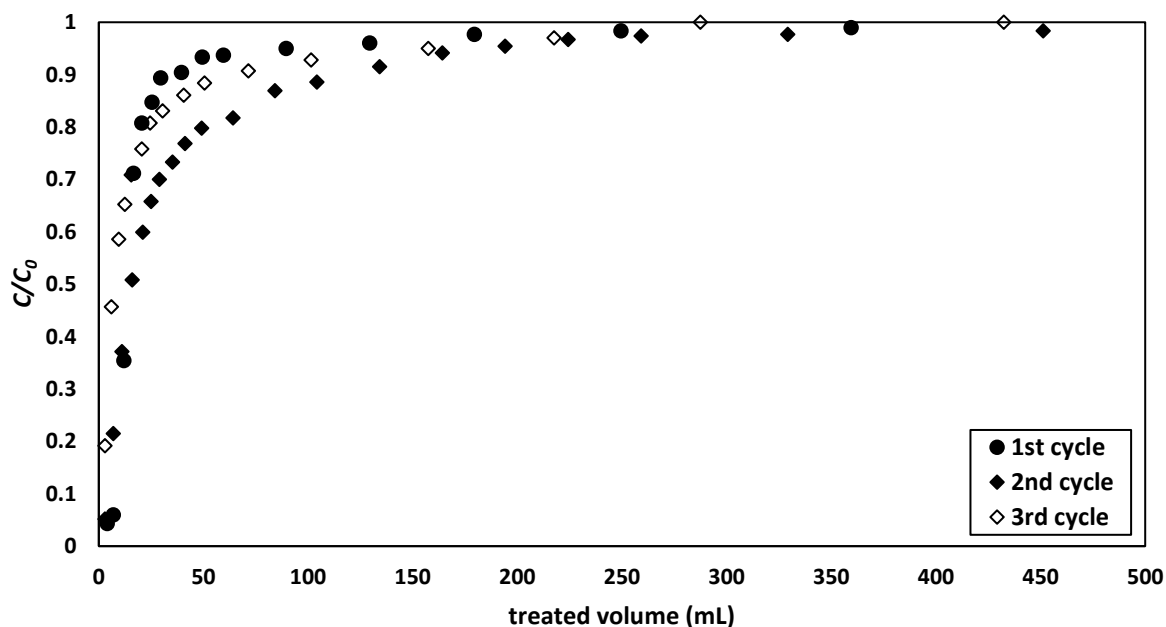


Figure 94: Breakthrough curves for DCF adsorption over three cycles of SpECs(2)APSH use and regeneration (flow rate = 3 mL/min).

The total adsorption capacity of the material after each cycle was compared against that of the first cycle and the results are presented in **Figure 95**. SpECs(2)APSH presented similar $q_{0,exp}$ values between the regenerating cycles (1 - 1.2 mg/g for the slow flow rate and 1.1 - 1.5 mg/g for the faster one) values that compared to the ones obtained from the first cycle are much higher (**Table 31**). Such a result confirms that during the first cycle, the material was not packed very well, whereas after the solvent washings and reuse, the packing was better, leading to higher and consistent adsorption capacities.

flow rate	K_{YN} (min^{-1})	τ (min)	τ_{exp} (min)	R^2	q_0 (mg/g)	$q_{0,exp}$ (mg/g)
1.5 mL/min	0.124	11.853	10.5	0.753	0.32	0.31
1st reuse	0.023	12.283	15.5	0.788	0.34	1.20
2nd reuse	0.018	22.656	11.2	0.738	0.61	1.94
3 mL/min	0.473	6.006	5.5	0.811	0.32	0.25
1st reuse	0.029	22.017	5.4	0.682	1.21	1.49
2nd reuse	0.036	28.675	3.1	0.684	1.55	1.26

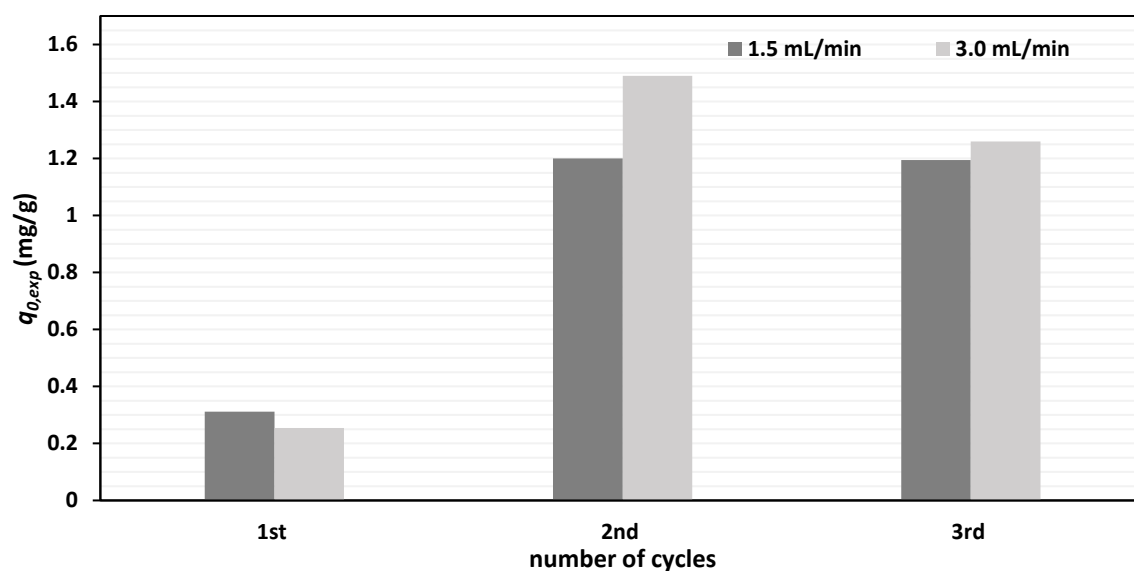


Figure 95: Comparison of the DCF adsorption capacity ($q_{0,exp}$) of SpECs(2)APSH, at two flow rates, over three cycles of use and regeneration.

3.4.7.3. Breakthrough curves for SpECs(3)AM

The same experimental procedure was followed for the aminated form of SpECs(3) [SPECs(3)AM], described in section 8.9, where the glass column was packed with 0.2 g SpECs(3)AM (0.5 cm high) covered with 2 g of low iron sand (0.5 cm high). The adsorption of DCF was tested under two different flow rates, 2.0 and 3.0 mL/min and the initial DCF concentration was 10 mg/L. Initially, the effluent was collected in fractions of 5 mL whilst later in bigger volumes (20 - 150 mL). The collected effluent was analysed for its DCF content and the treated volume was plotted against the recovered DCF concentration divided by the initial DCF concentration for the construction of the breakthrough curves (**Figure 96**).

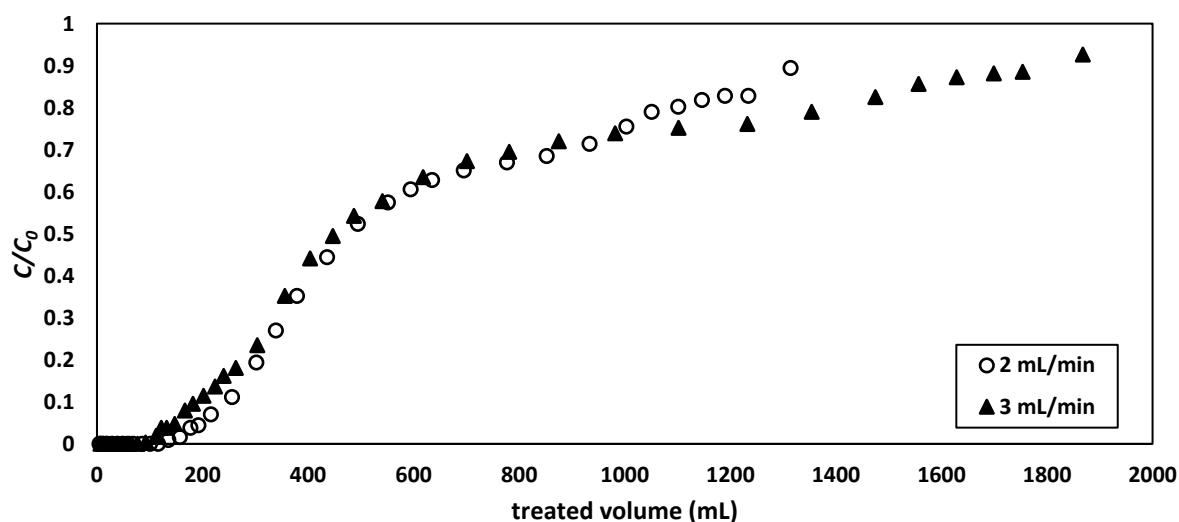


Figure 96: Breakthrough curves of 0.2 g packed SpECs(3)AM and DCF at 10 mg/L initial concentration at two different flow rates: 2.0 and 3.0 mL/min.

It is evident from **Figure 96** that for both flow rates the material did not reach its saturation point even after 1.5 and 1.8 L of treated volume. The breakthrough point, where half of the initial DCF concentration was able to pass through the packed-bed, occurred at ~450 mL of treated volume for the faster flow rate and at ~500 mL for the slower one. To put some context to such a result; it would mean that in a larger scale and before reaching the breakthrough point,

1 kg of the aminated SpECs(3) would be able to equivalently treat 320,000 litres of contaminated water at a concentration of ~0.07 mg/L of DCF, value that was the reported concentration in hospital effluents.²⁶¹ It would therefore also be able to treat 2.5 million litres of wastewater at a concentration of 0.0088 mg/L, an earlier stated concentration.¹⁹³ The Massachusetts Water Resources Authority²⁶² reported annual water consumption of hospitals ranging from 15 million gallons (~68 million L) to 145 million gallons (~660 million L), of which approximately 42% is for sanitary purposes.²⁶³ This would mean that the range of aminated SpECs(3) required annually for treating these hospitals would be from ~90 kg - 860 kg.

It is clear that the amination procedure not only increased the material's efficiency for DCF adsorption, but it also made the contact time smaller, a fact that was observed in the kinetic experiments as well. The collected data were analysed with the Yoon-Nelson model and the results are presented in **Table 32**.

flow rate (mL/min)	K_{YN} (min^{-1})	τ (min)	τ_{exp} (min)	R^2	q_0 (mg/g)	$q_{0,exp}$ (mg/g)
2.0	0.014	283.5	230	0.815	27.42	29.9
3.0	0.019	184.4	135	0.761	26.75	33.2

Both flow rates presented Yoon-Nelson values that were in close agreement with the experimental ones. SpECs(3)AM showed a higher maximum adsorption capacity compared to the untreated material, SpECs(3); 1 g of packed SpECs(3) presented 0.065 mg/g maximum adsorption capacity at a flow rate of 2 mL/min (**Table 27**) whereas 0.2 g of SpECs(3)AM presented a value of 27.4 mg/g at the same flow rate, proving that the amination created a much more efficient material. The change in flow rate did not have a noticeable impact on the maximum adsorption capacity since the calculated values for both flow rates were around

27 mg/g. The only difference observed when changing the flow rate to a faster one was the decrease in the value of the breakthrough point, possibly because of the lower residence time of the DCF molecules in the adsorbent bed.

Using this information and the previously determined moles of active sites present within 1 g of SpECs(3) (1.42 mmol), the moles of active sites that have been occupied can be calculated.

- Moles of DCF that reacted with 200 mg of SpECs(3)AM - ($0.0332 \text{ g} / 296.148 \text{ g/mol} = 0.0112 \text{ mmol}$)
- Number of moles of hexamethylenediamine in 200 mg of sample - ($1.42 \text{ mmol} / 5 = 0.284 \text{ mmol}$)
- Number of available sites taken by DCF - ($0.0112 \text{ mmol} / 0.0284 \text{ mmol} * 100 = 39.4\%$)

In conclusion, approximately 39.4% of the calculated moles of active sites have been occupied.

3.4.7.3.1. Regeneration and reusability of SpECs(3)AM

After the completion of the breakthrough curve, the regeneration and reusability of the packed SpECs(3)AM was also tested. The packed SpECs were washed with milliQ water to check if the adsorbed DCF could be easily desorbed. **Figure 97** overlays the previously created breakthrough curve and the region of the milliQ water washings after the saturation point. It is clear that the adsorbed DCF molecules are strongly attached to the SpECs(3)AM particles and water cannot remove them from the adsorbent.

After the elution of milliQ water, the packed SpECs(3)AM were washed with absolute ethanol in order to remove all of the adsorbed DCF and test the reusability of the material. The packed-bed was washed with a continuous flow of pure ethanol until the ethanolic effluent contained no DCF. A total of approximately 1.3 L of pure ethanol was required in order to

completely remove all of the adsorbed DCF, indicating the difficulty of detaching the adsorbed DCF molecules from the packed-bed of SpECs(3)AM.

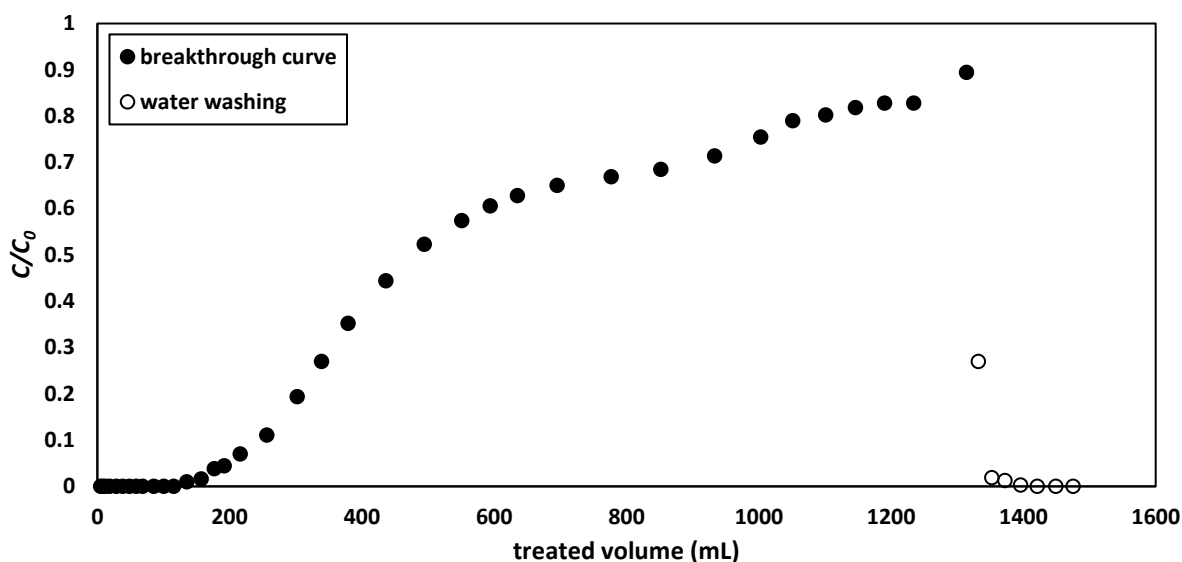


Figure 97: Packed SpECs(3)AM washed with milliQ water after the completion of the DCF breakthrough curve.

By the end of the ethanol washings, the ethanol solution was coming out free from DCF, meaning that all of the adsorbed DCF had been removed (approximately 6 mg). The values of the recovered DCF was compared to the adsorbed DCF and the recovery percentages are presented in **Table 33**. The recovery rates were high, suggesting that absolute ethanol was an efficient solvent for the regeneration of the packed SpECs(3)AM, however a very large volume was required, making it not a viable solution for the regeneration of the material.

experiment	adsorbed DCF (mg)	recovered DCF (mg)	% DCF recovery
2.0 mL/min	5.973	5.968	99.9
3.0 mL/min	6.639	6.405	96.5

The reusability of the regenerated SpECs(3)AM was tested for one more cycle, following the previous experimental conditions. **Figure 98** shows the breakthrough curves for the two cycles performed at the flow rate of 2 mL/min, whereas **Figure 99** presents the breakthrough curves for the faster flow rate, 3 mL/min. It is evident from these graphs that the material does not behave as well during a second cycle of use, presenting a significant decrease in its adsorption efficiency. In both flow rates, the point of 50% adsorbate breakthrough decreased from around 400 mL of treated volume to 200 mL, showing the earlier saturation of the material. It is possible that something is blocking the active sites of the material, either gasses, water or ethanol, possibly introduced during the washing step, having as a result the reduction of its adsorption capacity.

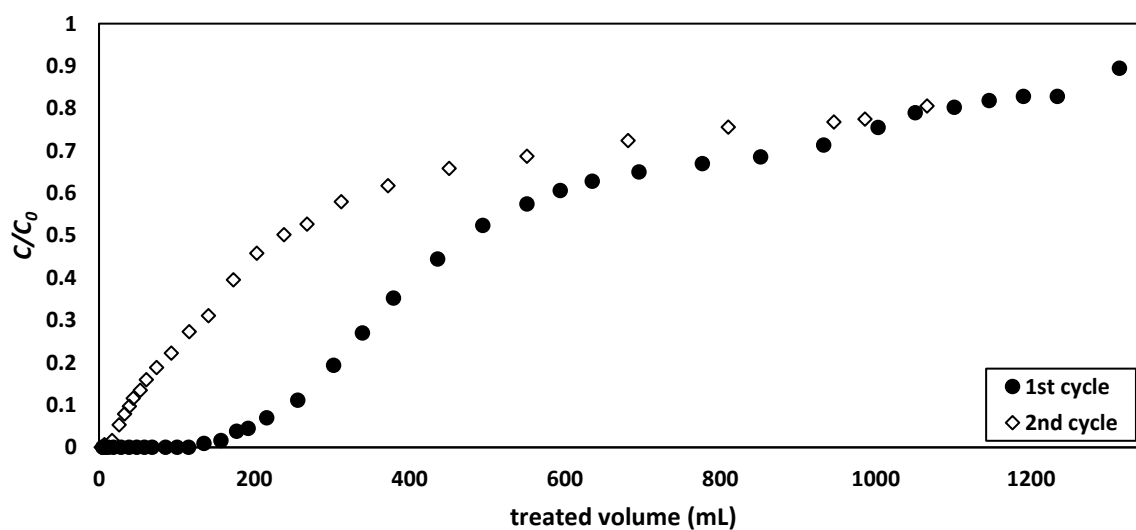


Figure 98: Breakthrough curves for DCF adsorption at a flow rate of 2 mL/min for two cycles of SpECs(3)AM use.

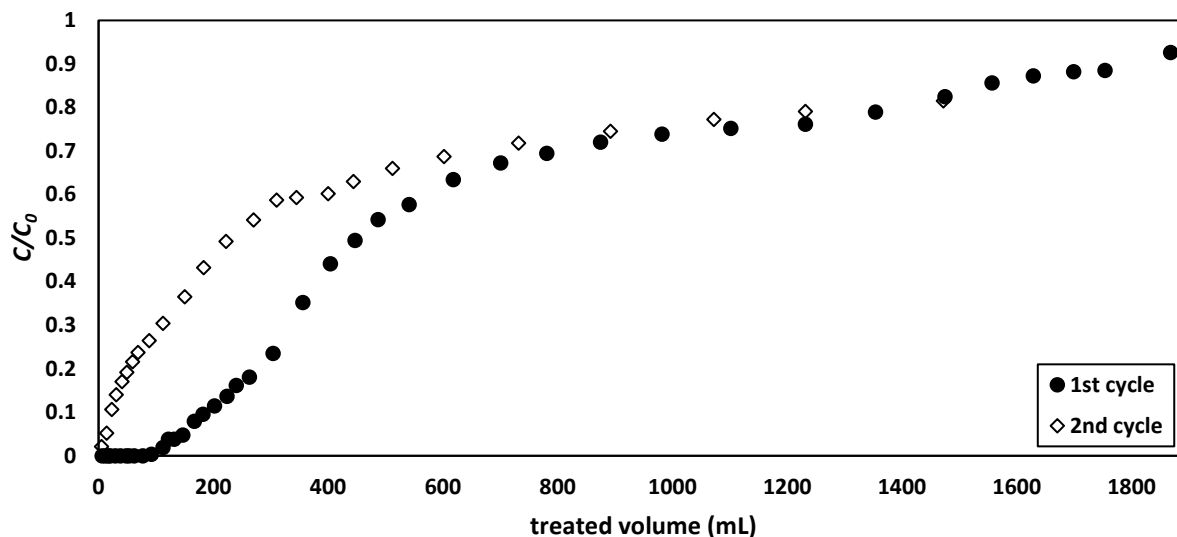


Figure 99: Breakthrough curves for DCF adsorption at a flow rate of 3 mL/min for two cycles of SpECs(3)AM use.

The experimental maximum adsorption capacity ($q_{0,exp}$) showed a decline between the two cycles of use, starting from 30 mg/g for the slow flow rate and going down to ~20 mg/g during the second cycle (**Figure 100**). A similar result was obtained for the faster flow rate as well, with the $q_{0,exp}$ value starting at ~33 mg/g and going down to 22 mg/g, both showing a decline of 33%.

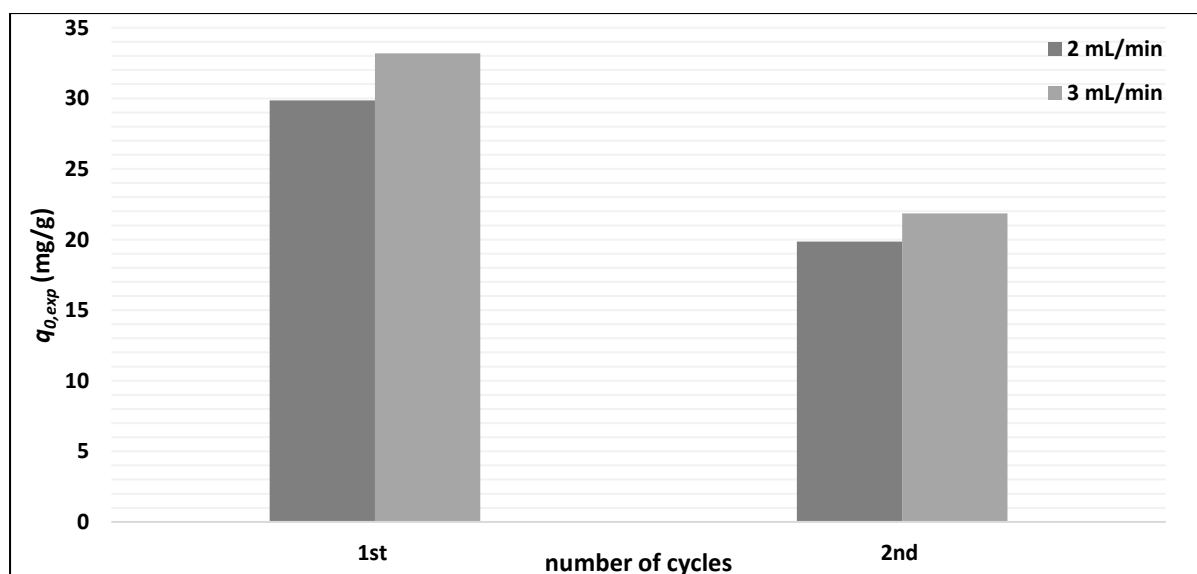


Figure 100: Comparison of the DCF adsorption capacity of SpECs(3)AM between each cycle of use.

Analysis with the Yoon-Nelson model (**Table 34**) confirmed this decline in maximum adsorption capacities which was accompanied by a decline in the values of the breakthrough point. The second cycle also presented a much lower τ compared to the first cycle, confirming the material's loss of efficiency. At this stage it was unclear if the regeneration method chosen played a role in the loss of efficiency, or whether the storage conditions of the material was a factor.

Table 34: Comparison of the Yoon-Nelson model parameters for SpECs(3)AM (0.2 g) and DCF adsorption (10 mg/L initial concentration) at two different flow rates and for two cycles of use.

flow rate	K_{YN} (min^{-1})	τ (min)	τ_{exp} (min)	R^2	q_0 (mg/g)	$q_{0,exp}$ (mg/g)
2 mL/min	0.014	283.5	230	0.815	27.42	29.9
1st reuse	0.019	142.9	122	0.707	13.98	19.9
3 mL/min	0.019	184.4	135	0.761	26.75	33.2
1st reuse	0.023	87.26	62	0.731	12.81	21.9

3.4.7.3.2. Effect of the age of SpECs(3)AM on their DCF adsorption efficiency

As previously stated, SpECs(3)AM exhibited a reduction in their adsorption efficiency upon recycling and reuse. During this time, evidence was also obtained that the age of the material (time since production) might have played a role on its efficiency to adsorb DCF. A study was therefore undertaken in which SpECs(3)AM of different ages, stored in screw cap amber vials in a drawer away from sunlight, were tested using the same packed-bed system described above. The glass column was packed with 0.2 g SpECs(3)AM (0.5 cm high) covered with 2 g of low iron sand (0.5 cm high). The adsorption of DCF was tested under two different flow rates, 2.0 and 3.0 mL/min and the initial DCF concentration was 10 mg/L. **Figure 101** shows the breakthrough curves obtained from the same material as used in the previous experiments, but 20 days post-production instead of the 10 days above.

It is evident that in the 20 day aged experiment SpECs(3)AM exhibited poorer results, with the 50% adsorbate breakthrough point appearing at a treated volume of 300 mL instead of 500 mL or 135 minutes instead of 284 min. Such a result could possibly be attributed to absorbed humidity on the material's aminated groups or to possible surface oxidation preventing the active sites from binding with the DCF molecules. As explained before, the opposing charges from the positively charged aminated SpECs act as a hydrogen donor and the negatively charged carboxylic acids of DCF act as hydrogen acceptor. If the material loses its charge due to auto oxidation then the performance is lost.

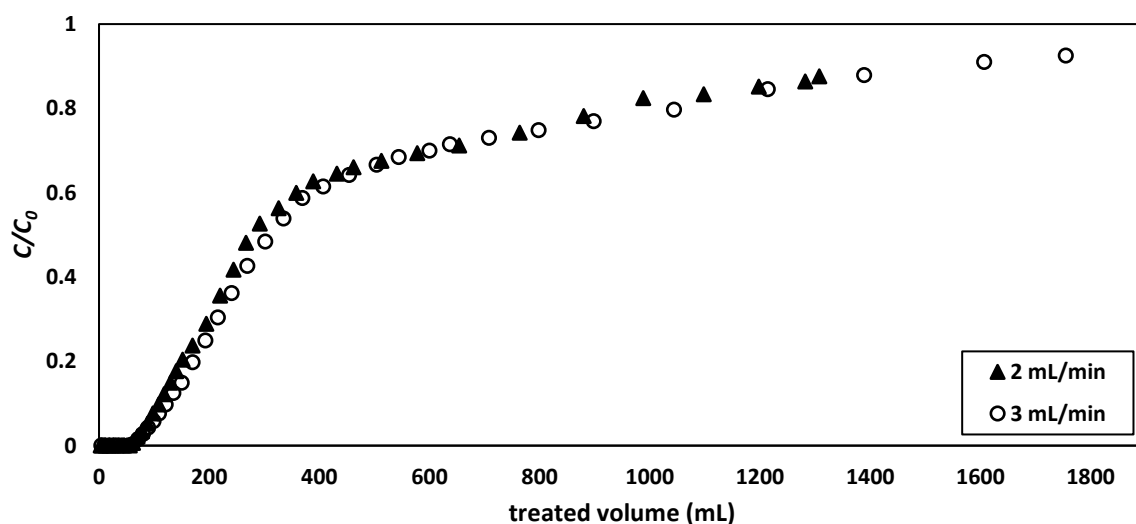


Figure 101: Breakthrough curves of SpECs(3)AM (0.2 g) for DCF adsorption (10 mg/L) at two different flow rates, conducted 20 days after the amination reaction.

The same breakthrough curve experiment was conducted for SpECs(3)AM, 15 days post-production, 3 months and 3.5 months post-production, in order to determine if a continued decline in the material's adsorption efficiency occurs (**Figure 102**).

It is evident from **Figure 102** that the decline in the DCF adsorption efficiency of SpECs(3)AM is related to the age of the material. The first two experiments were conducted 5 days apart, with the first one presenting a nice breakthrough curve and the second presenting different

results with a lower adsorption capacity. 15 days after amination, SpECs(3)AM presented a breakthrough curve that was similar to the one obtained 20 days after amination, suggesting that during this period of 15 - 20 days the decline in the material's adsorption efficiency did not worsen. The maximum DCF adsorption capacity showed a decline of 24% in the first 5 days but then was stable for the next 5 days (**Table 35**). After 3 and 3.5 months, the decline of the material's DCF adsorption efficiency was notable; the breakthrough point appeared at 50 mL of treated volume and the maximum adsorption capacity was 64% and 71% less compared to the initial $q_{0,exp}$. The DCF adsorption efficiency of SpECs(3)AM decreased as time passed after amination, indicating that adsorption of a competing molecule occurred in the meantime or oxidation of its surface took place.

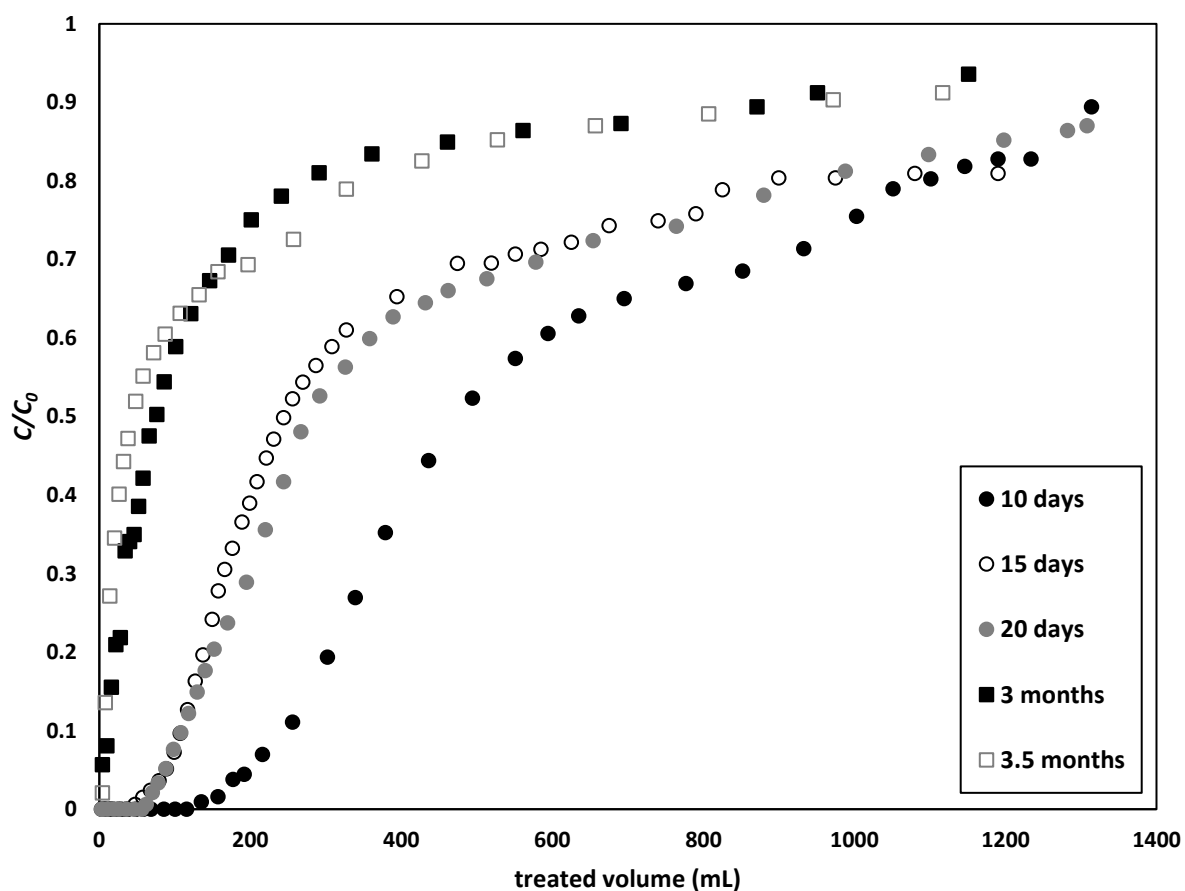


Figure 102: Comparison of breakthrough curves obtained for DCF (10 mg/L) elution, after different periods of time since the production of SpECs(3)AM. Sample was stored in a tightly closed amber vial, placed in a drawer away from sunlight exposure.

Table 35: Comparison of maximum adsorption capacities of SpECs(3)AM depending on the date of use after production.

period after amination	10 days	15 days	20 days	3 months	3.5 months
$q_{0,exp}$ (mg/g)	29.86	22.70	23.74	10.63	8.73

3.5. Conclusions

Diclofenac is a non-steroidal anti-inflammatory drug (NSAID), present in many pills and creams mainly used for the treatment of inflammations and painful conditions. The increase of its levels detected in the environment can be mainly attributed to the inefficiency of WWTPs and the discharge of untreated wastewater directly into the environment deriving from either hospitals, houses or municipal effluents. Although DCF has been reported to have relatively low toxicity for fish and algae, there are observations of histopathological effects and bioaccumulation of DCF after chronic exposure at concentrations around 1 - 5 $\mu\text{g/L}$. In humans, even at low levels (1 $\mu\text{g/L}$), it has been stated that a continuous DCF daily intake can cause renal lesions and cytotoxicity to the liver and kidneys.

The adsorption efficiencies of the three basic SpECs types together with some modified forms were tested for DCF. The adsorption kinetics revealed that there are some important factors that can affect the material's efficiency such as the drying procedure, the degree of surface oxidation or the surface modification. Drying at high oven temperatures, resulted in a decrease in the adsorption efficiency, making the air-drying procedure preferable. Pre-wetting of SpECs showed no improvement on their adsorption efficiency proving that their hydrophobicity does not prevent the DCF molecules from reaching the possible binding sites of the material's surface. Between the three basic SpECs types, SpECs(3) gave the best adsorption performance whereas between the different modifications SpECs(3)AM presented the fastest adsorption; after one minute of contact time all quantity of DCF was adsorbed. The aminated SpECs while being positively charged were more attractive to the DCF molecules, making the adsorption

much quicker whereas the opposing charges from the positively charged primary amine and the negatively charged carboxylic acids on DCF had as a result the increase in the materials adsorption efficiency. The speed of adsorption may also be the most important factor in making this material suitable for real world conditions.

The adsorption of DCF by SpECs was best described by the pseudo-second order model after excluding all the data points close to equilibrium, meaning that data obtained from SpEC(3)AM could not be analysed. The tested SpECs presented similar values of maximum adsorption capacity in the range of 1.3 - 1.8 mg/g. Comparison to other materials found in literature tested for DCF adsorption showed that the values obtained were relatively low, (magnetic covalent organic frameworks presented the highest value of 337 mg/g,²⁴⁸ magnetic chitosan particles gave a value of 187 mg/g,²⁴⁹ organophilic bentonites showed values in the range of 5.5 - 38.7 mg/g,¹⁹³ and Isabel grape bagasse presented the lowest value of 4.96 mg/g¹⁰⁸) however the experimental conditions were not identical to the ones used above.

Intraparticle diffusion analysis revealed that during DCF adsorption all tested SpECs involve multiple diffusion steps (film diffusion and intraparticle diffusion) that happen simultaneously. During the first step, SpECs(3)AM presented the highest adsorption rate (0.318 mg/g min) meaning that out of all tested SpECs, SpECs(3)AM is possibly the one with the most available active sites for DCF to bind.

Adsorption isotherm analysis showed that for the majority of SpECs the Freundlich model presented a better fit to the experimental data, apart from SpECs(3) and SpECs(3)AM whose results were able to be described by both models. SpECs(2)APSH presented the highest K_F value, 4.011 mg^(1-1/n)/gL^{-1/n} as well as the highest $1/n_F$ value (0.999), indicating the cooperative adsorption of DCF, possibly forming multi-layers on the surface of the material. SpECs(3) presented the highest Q_m value, 13.889 mg/g. Comparison to other materials already tested in the literature showed that SpECs(3) presented higher Q_m values compared to magnetic

chitosan particles,²⁴⁹ (10 mg/g) and similar values for organophilic bentonites (13.3 mg/g).¹⁹³ Activated carbon and porous carbons with metal azolate frameworks gave greater values of 79 and 503 mg/g respectively²⁵⁹ whereas titanate nanosheet-pozollan nanocomposites gave values at around 80 mg/g.²⁶⁰ Magnetic covalent organic frameworks gave results that were better described by the Freundlich model, presenting a K_F value of $335 \text{ mg}^{(1-1/n)}/\text{gL}^{-1/n}$,²⁴⁸ much higher than the value of $4.01 \text{ mg}^{(1-1/n)}/\text{gL}^{-1/n}$ obtained by SpECs(2)APSH.

Packed-bed studies were performed for SpECs(3), SpECs(3)AM and SpECs(2)APSH, for different flow rates and the breakthrough curves were formed and analysed with the Yoon-Nelson model. SpECs(2)APSH presented average results ($q_{0,exp}$ at 0.25 - 0.31 mg/g) mainly due to the fact that the SpECs bed was not tightly packed, a fact that was confirmed by the higher $q_{0,exp}$ values obtained from the regenerating cycles (1 - 1.2 mg/g for the slow flow rate and 1.1 - 1.5 mg/g for the faster one). SpECs(3)AM showed a higher maximum adsorption capacity compared to the untreated SpECs(3); SpECs(3) presented 0.065 mg/g maximum adsorption capacity at a flow rate of 2 mL/min whereas SpECs(3)AM presented a value of 27.4 mg/g at the same flow rate. Unfortunately, the packed-bed study showed that whereas SpECs(3)AM was the most efficient SpECs type of all, its reuse did not give as good results with the procedure tested. Furthermore, the material presented a decrease in its adsorption efficiency with time, indicating that there might be an 'expiry date' for its use which was around 15 days postproduction when stored carefully.

Packed-bed studies are a very accurate way of studying the behaviour of a material and predicting its potential in a bigger scale use. In a theoretical scenario where a small water treatment setup would be built outside hospitals filtering their effluents, a cartridge containing 1 kg of SpECs(3)AM would be able (in terms of capacity) to equivalently treat 320,000 litres of contaminated water at a concentration of $\sim 0.07 \text{ mg/L}$ of DCF (value that was the reported concentration in hospital effluents²⁶¹) before reaching the breakthrough point. It would

therefore also be able to treat 2.5 million litres of wastewater at a concentration of 0.0088 mg/L (reported wastewater value¹⁹³). The Massachusetts Water Resources Authority²⁶² reported annual water consumption of hospitals ranging from 15 million gallons (~68 million L) to 145 million gallons (~660 million L), of which approximately 42% is for sanitary purposes.²⁶³ This would mean that the range of SpECs(3)AM required annually for treating these hospitals would be from ~90 - 860 kg.

In conclusion, it is worth mentioning that an efficient adsorbent apart from a good adsorption capacity should also present easy and environmentally friendly production, low-cost procedures and good reusability. As stated above, some of the materials presented in the literature gave better numbers when tested for their adsorption performance but without stating details about the rest of the criteria. SpECs derived from *L. clavatum* were proven to be a potent candidate for DCF adsorption, with SpECs(3) presenting the best results under different experimental conditions. Modifications of the SpECs surface ameliorated their adsorption properties, especially when treated with ammonium persulfate or after amination. SpECs presented a very good adsorption capacity with fast adsorption rates which together with their low-cost production, their environmentally friendly nature and their reusability potential, they make a very promising adsorbent material for real-world applications.

4. Triclosan

4.1. Introduction

Triclosan (5-chloro-2-(2,4)-dichlorophenoxy-phenol, TCS) is a synthetic, broad spectrum antimicrobial agent found in a variety of commercial products of daily use such as household cleaning products, detergents, hand soaps, skin creams, shampoos, deodorants, toothpastes, plastic toys and kitchenware as well as textiles.^{264–266} It was first introduced into the health care industry in the early 1970's as a preservative, or as an antiseptic factor due to its efficacy at low concentrations to inhibit bacterial fatty acid biosynthesis. TCS (**Figure 103**) is active against both Gram-positive and Gram-negative bacteria, with its antibiotic and antimycotic properties making it a key ingredient in a large number of products.²⁶⁷ It is estimated that in 1998 the global production of TCS exceeded 1,500 tons, where more than 43% of the total production was used in Europe and the US.²⁶⁸

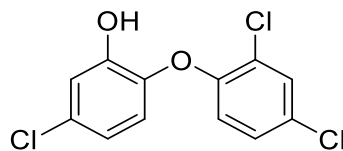


Figure 103: Chemical structure of triclosan.

TCS is a halogenated aromatic hydrocarbon, with functional groups such as phenolic, diphenyl ether and polychlorinated biphenyl substructures.²⁶⁹ It is a stable, lipophilic compound of non-volatile nature (5.3×10^{-4} Pa at 20 °C) with a $\log K_{OW} = 4.8$ at pH 7 indicating its high adsorption potential.⁸⁴ Even though it shows low solubility in water ($S_w = 10$ mg/L at 20 °C), it has been reported to be present in wastewater and surface water at concentrations ranging from 9 ng/L to 6.7 $\mu\text{g/L}$.³⁸ Due to its low hydrophilicity, it can easily accumulate in organic

tissue and travel through the food chain, it has been reported to bioaccumulate in aquatic organisms such as fish (*Danio rerio*, *Cyprinus carpio*, *Gibelion catla*)^{266,270,271} and algae (*Cladophora spp.*, *Nannochloris sp.*).^{272,273} TCS is structurally similar to the structures of polychlorinated bisphenyls (PCBs), bisphenol A (BPA), dioxins and thyroid hormones meaning that it presents similar toxic chemical properties.^{84,274} Once TCS is released into the aquatic system and under sun light exposure can be oxidised and produce several types of polychlorinated dibenzo-*p*-dioxins (**Figure 104**) specifically at high pH levels.²⁷⁵ Since it is an aromatic compound with high chlorine content, it is resistant to degradation and persistent to the environment.²⁷⁴

Being a broad-spectrum bactericide agent that has been used for more than 50 years, it can affect sensitive species and non-target components of the aquatic environment.²⁷⁶ Recent studies have shown the presence of TCS in both aquatic and terrestrial ecosystems, detecting its bioaccumulation in snails (*Helisoma trivolis*), algae (*Cladophora spp.*),²⁷⁷ fish (*Abramis brama*)²⁷⁸ and marine mammals (*Tursiops truncatus*).²⁷⁹ TCS has not shown any acute toxicity to mammals, but it has proven toxic for aquatic organisms such as rainbow trout (*Oncorhynchus mykiss*) (LC₅₀ = 0.35 mg/L), *Daphnia magna* (EC₅₀ = 0.39 mg/L) and algae (*Scenedesmus sub.*) (EC₅₀ = 1.5 µg/L).²⁶⁷ Wilson *et al.* showed that TCS can influence algal communities in their structure and function while being in environments that are WWTP effluent receptors.²⁸⁰ The effects of TCS uptake by sensitive species have been the study of many researchers, concluding that TCS is one of the most toxic antibacterial compounds, since it can be hazardous to the aquatic environment at concentrations as low as 0.3 mg/L. It has been shown to cause teratogenic responses in zebrafish (*Danio rerio*) embryos, with hatching delay and mortality at concentrations above 0.7 mg/L. It has also been proven that it affects the developmental stages of rainbow trout (*Oncorhynchus mykiss*) at concentrations below 0.071 mg/L.²⁸¹

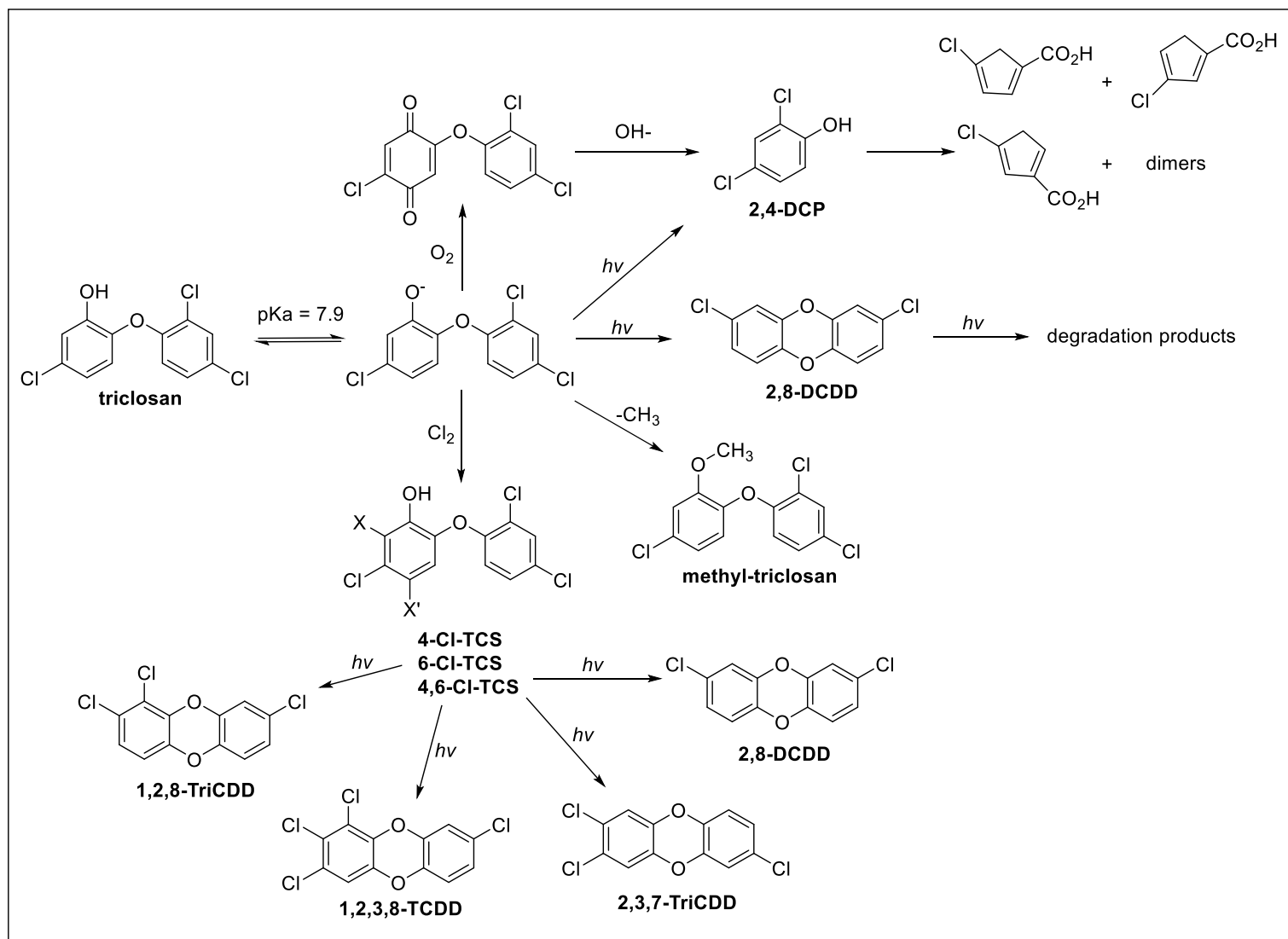


Figure 104: TCS by-products after ozonation, methylation, chlorination and photolysis.

The potential of TCS being an endocrine disruptor has been the focus of many researchers, since it has presented some oestrogenic activity.^{282,283} In fish, TCS has some weak androgenic effects²⁸⁴ while in rats, it demonstrates antiandrogenic effects.²⁸⁵ Depending on tissues, cell types and species, TCS has (anti)oestrogenic and (anti)androgenic effects and can act as a thyroid-disrupting compound, making it a non-steroidal estrogen.²⁸⁶⁻²⁸⁹

The cycle of TCS entering the waterways starts from products of daily use being washed down the drain, making TCS a water-borne anthropogenic contaminant. The water entering WWTP contains up to 96% of the compound leading to influent concentrations in the range of 1 - 10 mg/L.²⁹⁰ While in the WWTPs, 79% of the total quantity is biodegraded, 15% is adsorbed onto biosolids and 6% is discharged into surface water.²⁶⁸

TCS can convert into other by-products; during the biological treatment it can be methylated and form methyltriclosan,²⁹¹ whilst during the disinfection treatment it can interact with free chlorine and form chlorinated derivatives like chlorodioxins, chlorophenol, *p*-hydroquinone, 2,4-dichlorophenol and chloroform,²⁹² which are even more harmful to the environment due to their higher lipophilicity and their resistance to degradation.^{268,293} Both TCS and its chlorinated derivatives are difficult to remove with conventional treatments leading to their presence in the effluents of the WWTP. Whilst in surface waters, both TCS and its chlorinated derivatives can undergo photolysis and can be converted into 2,4-dichlorophenol, polychlorodibenzo-*p*-dioxins and oligomerisation products, known for their carcinogenic properties and their high persistence in the environment.^{292,294-296} In the U.S. TCS is amongst the seven most frequently detected contaminants in surface and stream water.²⁹⁷ Significant levels of TCS have been detected in humans across the world, in samples such as urine, plasma and breast milk²⁶⁹ indicating that the effects of long-term exposure have to be evaluated. The use of TCS is forbidden in Japan and Canada, whereas in Europe it is classified under the category of dangerous irritant to the environment and aquatic life.²⁶⁸

In conclusion, TCS is a compound of potential environmental concern because it can affect aquatic and terrestrial organisms, it can cause antimicrobial resistance, it is environmentally persistent and can bioaccumulate. Furthermore, TCS has estrogenic and androgenic effects, it disrupts thyroid function, disturbs endobiotic and xenobiotic metabolism and can cause liver fibrosis and carcinogenesis in a variety of organisms.

Recent studies have focused in removing TCS from water through adsorption technologies by testing materials such as montmorillonite,²⁹⁸ laccase nanofibers,²⁹⁹ biosolid amended soils,³⁰⁰ kaolinite, carbon nanotubes^{265,275} and silt loam.³⁰¹ The chemical composition and surface properties of the material together with its porosity, are factors that affect the effectiveness of the adsorption process, demanding more research into new promising materials.

4.2. Aims and objectives

In this chapter, the adsorption of TCS onto SpECs extracted from *L. clavatum* will be studied. The three different extracted SpECs will be tested in order to identify the most efficient type and analyse the adsorption processes. The term efficient describes a material that exhibits good adsorption properties, quick and low-cost production protocol, reusability, adsorption stability and environmentally friendly production. After examining the adsorption kinetics for TCS and identifying the most suitable SpECs type, the material's behaviour will be further examined using packed-bed studies.

4.3. Triclosan detection and quantification

A stock solution of TCS in ethanol was prepared and made into further dilutions in milliQ water, giving a range of TCS solutions with concentrations from 0 to 15 µg/mL. In the high concentration adsorption experiments, TCS detection and quantification was conducted with an Agilent Technologies HPLC system equipped with a Phenomenex Gemini column (5 µm,

C18, 150 x 4.60 mm), having as a mobile phase milliQ water and acetonitrile. The gradient was 0-10 min 80:20 H₂O:MeCN, 10-20 min 100% MeCN, 20-22 min 80:20 H₂O:MeCN and the TCS peak appeared at a retention time ~15:20. The data acquisition and analysis was performed with the Laura software. All of the standard solutions were prepared in triplicate and two reference curves were built, one at 220 nm detection wavelength (**Figure 105**) and another at 280 nm (**Figure 106**), in order to test which of the two wavelengths gave the best limit of detection and limit of quantification.

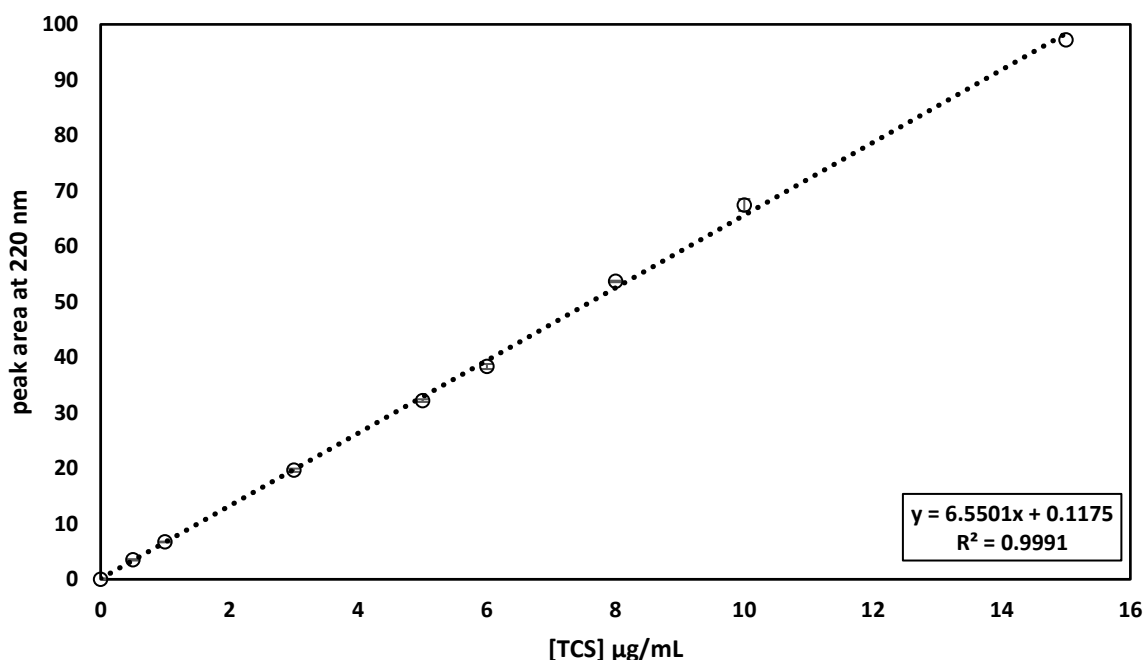


Figure 105: TCS reference curve at the concentration region of 0 - 15 µg/mL at 220 nm detection wavelength (n=3).

For the detection wavelength at 280 nm, the LOD and LOQ were calculated to be 0.354 µg/mL whereas for the detection wavelength at 220 nm, the LOD and LOQ were lower: 0.118 µg/mL. The 220 nm wavelength was chosen for the analysis of all TCS solutions of the following experiments and *Equation 30* was used for the calculation of TCS concentration (x).

$$y = 6.55x + 0.1175$$

Equation 30

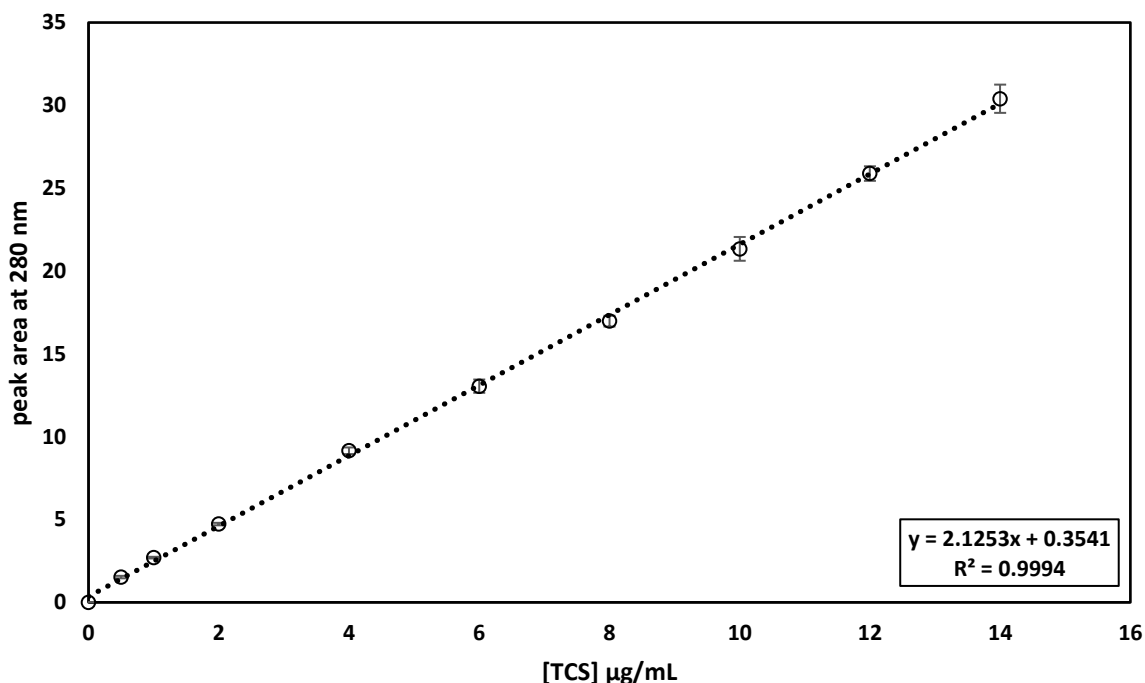


Figure 106: TCS reference curve at the concentration region of 0 - 15 µg/mL at 280 nm detection wavelength (n=3).

For the TCS adsorption experiments that were undertaken at environmentally relevant concentrations, the detection and quantification was conducted with a Shimadzu HPLC-ESI-MS/MS system at the negative mode equipped with a Shim-pack GISS-HP C18 Shimadzu column (3 µm, C18, 100 x 3.0 mm), with the oven temperature set at 40 °C. The mobile phase was LC-MS grade water spiked with 0.1% formic acid and LC-MS grade acetonitrile. The gradient was 0-0.1 min 100% H₂O, 0.1-3.0 min 70:30 H₂O:MeCN, 3.0-4.2 min 100% MeCN, 4.2-6.0 min 70:30 H₂O:MeCN giving a retention time around 3:30. The data acquisition and analysis was conducted with the LabSolutions software. All standard solutions were prepared in triplicate and a reference curve was built (**Figure 107**) with an LOD and LOQ of 0.59 ng/mL.

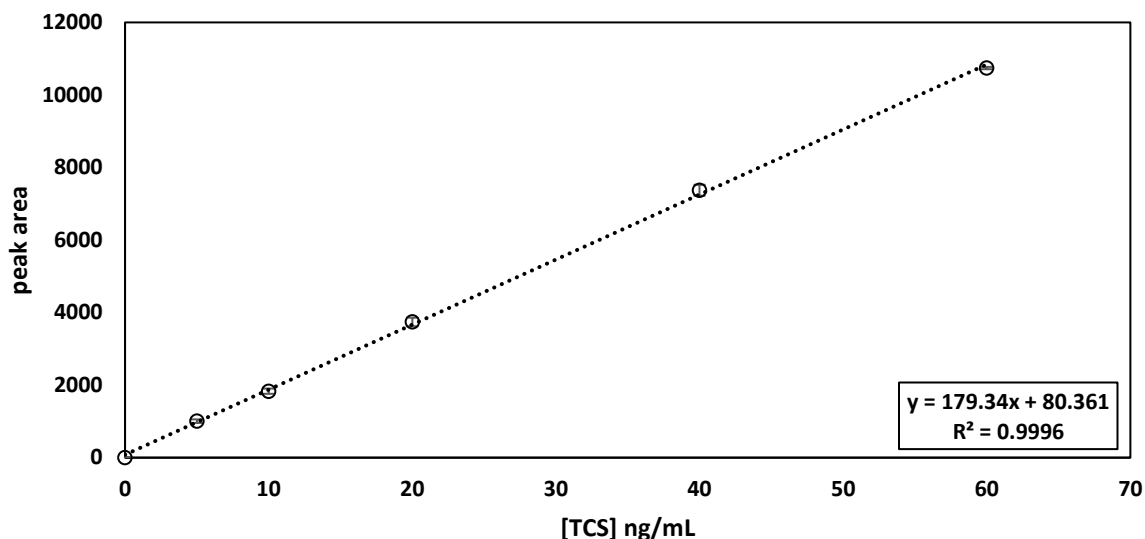


Figure 107: TCS reference curve at the concentration range of 0 - 60 ng/mL (n=3).

For the calculation of TCS concentrations (x) in the lower concentrations range, *Equation 31* was used:

$$y = 179.34x + 80.361 \quad \text{Equation 31}$$

4.4. Triclosan adsorption experiments

The adsorption of TCS on the different SpECs was examined following the protocol described in section 8.5.2 (**Figure 108**); briefly, 5 mL of a 6 $\mu\text{g/mL}$ TCS solution was left in contact with 20 mg of the adsorbent material (different types of SpECs) for different periods of time under shaking with the orbital shaker. After filtration, the TCS concentration of the resulting solution was quantified and compared against the initial concentration and the adsorption percentage was calculated with *Equation 32*.

$$\% \text{ TCS ads.} = \frac{(C_0 - C_{eq}) 100}{C_0} \quad \text{Equation 32}$$

where C_0 is the initial and C_{eq} is the final TCS concentration.

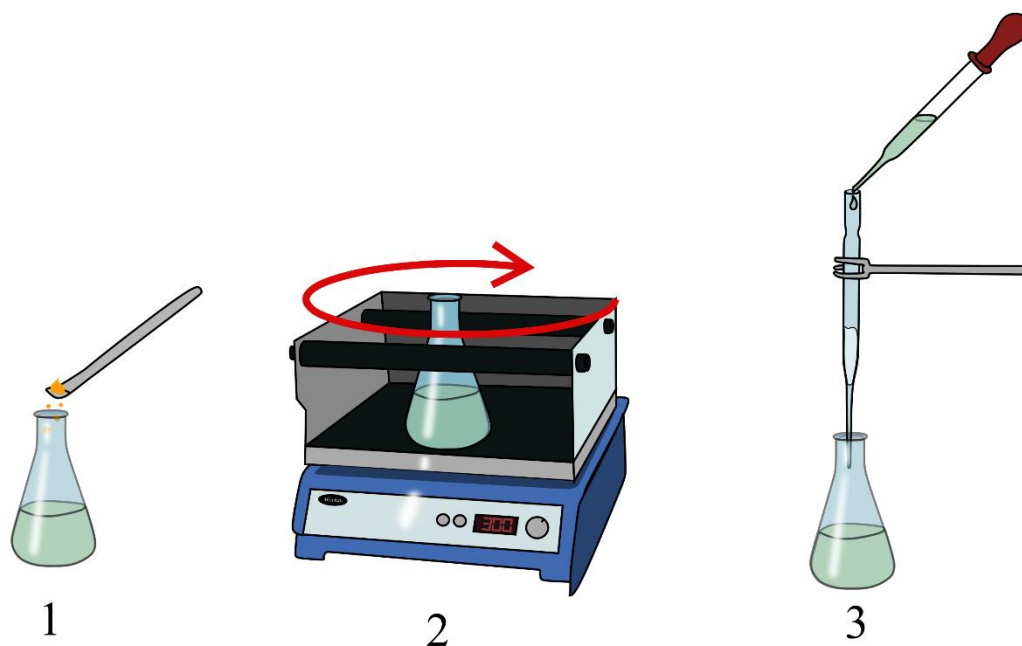


Figure 108: Experimental setup for the adsorption experiments describing the three-step procedure: 1) SpECs are added to the contaminant solution, 2) the suspension is shaken in the orbital shaking for a period of time, 3) the suspension is filtered through a pipette equipped with cotton wool.

4.4.1. Effect of vessel material in triclosan adsorption experiments

As TCS is a lipophilic compound the vials used for the adsorption experiments had to be tested. Two types of glass vials were tested, one with plastic lid and a second with metal lid, to determine whether the lid material would adsorb any TCS quantity and alter the final results. Apart from the lid material, two filtering materials were also tested, cotton wool packed in glass pipettes and Phenomenex HPLC filters, to check whether the cellulose in the cotton or the material in the filter would interfere and act as an adsorbent for TCS, altering the concentration of the final solution.

A solution of known TCS concentration ($7 \mu\text{g/mL}$) contained in either metal lid vials or plastic lid vials, was left shaking for set time periods. After shaking, the solution was analysed for its TCS content and the final TCS concentration was compared against the initial. The results are shown in **Figure 109** where it became apparent that the solution contained in the vials with the

plastic lid gave concentrations slightly lower than the initial one, showing that the plastic lid was able to adsorb a small quantity of TCS whereas the metallic lid showed no TCS concentration alterations after 30 minutes of contact time.

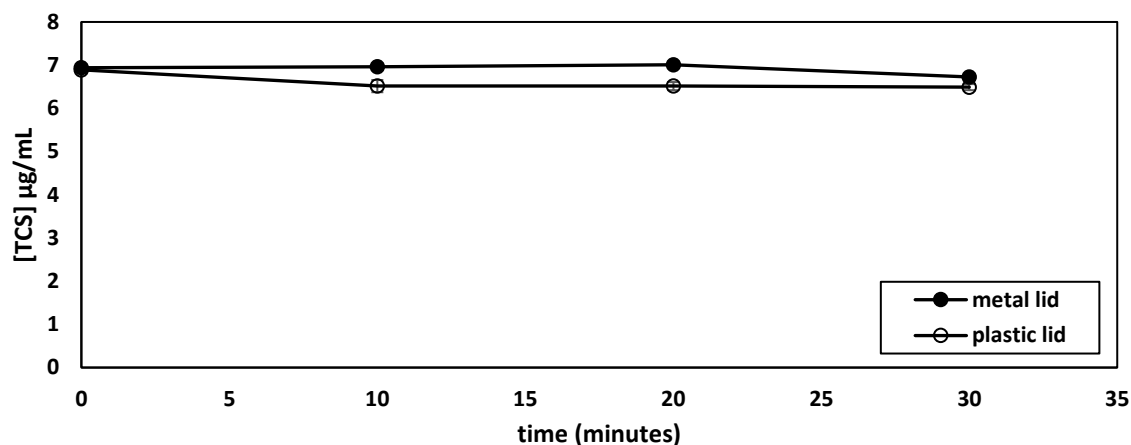


Figure 109: TCS concentration after different periods of time shaking inside glass vials with either metal lid (n=3) or plastic lids (n=3).

A similar test was conducted for the two filtering materials; a TCS solution of known concentration (5 µg/mL) was analysed for its TCS content before any treatment and after filtration either through a glass pipette packed with cotton wool or a Phenomenex HPLC filter attached to a syringe. The procedure was repeated three times for each filtering material and the final TCS concentrations were compared against the initial concentrations of the unfiltered solution. The results are shown in **Table 36**.

	no filtration	HPLC filter	cotton filter
	5.394	5.002	4.959
	5.394	5.525	5.133
	5.394	5.133	4.654
average	5.394	5.220	4.915

The filtration with the cotton wool packed in a glass pipette showed that some TCS might have been trapped onto the cellulose thus altering the final result and increasing the experimental error. The filtration with the Phenomenex filter resulted in a slightly decreased concentration with the difference being $\pm 0.26 \mu\text{g/mL}$ giving a smaller error than the previous material and so this was the filter used.

In conclusion, for the adsorption experiments to be as accurate as possible and in order to minimise the error, glass vials with metal lids were chosen and the filtration procedure was conducted with Phenomenex HPLC filters attached to syringes.

4.4.2. Triclosan adsorption kinetics at high concentrations

The influence of contact time in TCS adsorption was examined following the experimental procedure described in section 8.5.2, where glass vials containing 20 mg of SpECs and 5 mL of a TCS solution (6 mg/L) were left shaking in the orbital shaker for fixed sets of time (1 - 10 minutes). After filtration, the final solutions were analysed for their TCS content using an Agilent HPLC system and the TCS concentration was calculated using *Equation 30*.

Figure 110 presents the results of TCS adsorption by all the basic extraction types of SpECs together with raw spores. Raw spores exhibited a relatively poor adsorption performance which after the extraction procedures was altered completely. All three extracted SpECs exhibited an efficient and fast adsorption for TCS at high (6 mg/L) concentrations, achieving 90 to 100% removal in only two minutes of contact time. SpECs(1) presented the fastest adsorption of TCS reaching 100% removal in only five minutes.

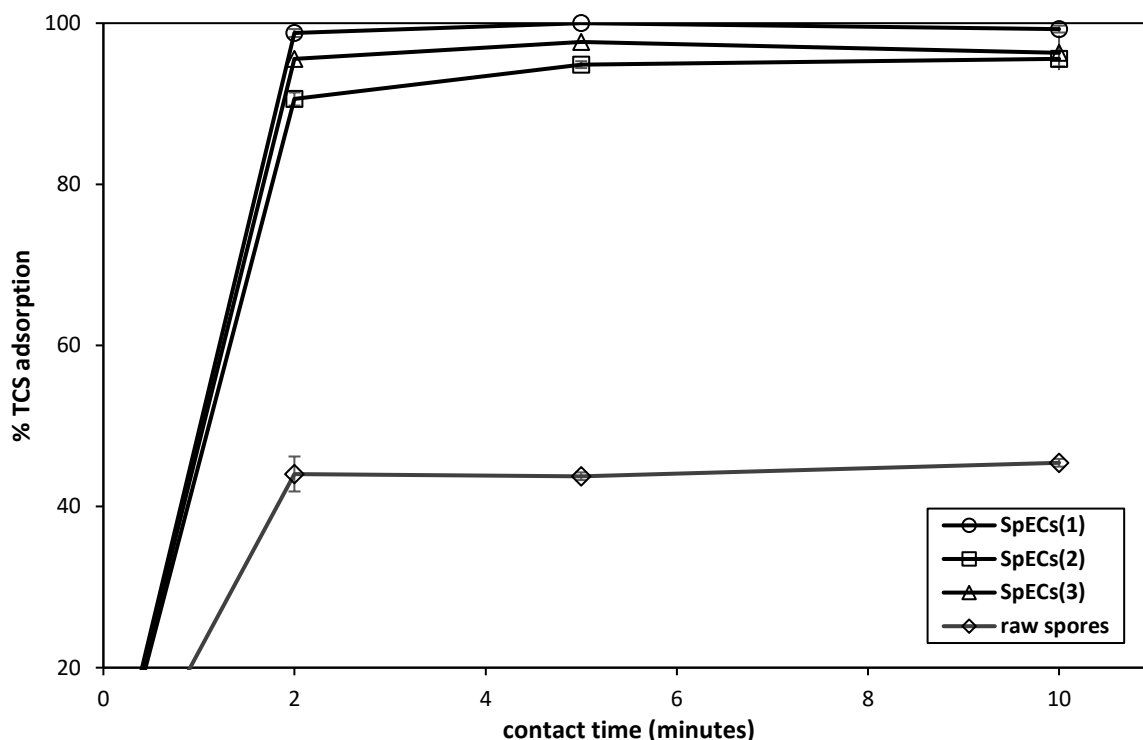


Figure 110: Effect of contact time on TCS adsorption by 5 g of raw spores or different SpECs; graph zoomed in the region of 20 - 100% of TCS removal (TCS dose: 6 mg/L, n=3).

A further investigation on the adsorption mechanisms of TCS on the different SpECs types, using the pseudo-first order, the pseudo-second order kinetic models and the intraparticle diffusion model was not possible. As described in the previous chapter, in order for these models to be applicable on the experimental data, the graph points taken into account have to be before reaching equilibrium conditions. All three SpECs types presented very efficient adsorption, reaching high TCS adsorption percentages in only two minutes of contact time and reaching equilibrium conditions really quickly. According to Simonin³⁰² it would be a mistake to use these models for the analysis of the experimental data obtained, unless data were obtained far before the equilibrium conditions, possibly at the contact point of 0.5 minute or even earlier.

4.4.3. Triclosan adsorption kinetics at low concentrations

The adsorption experiments were repeated for TCS with the only difference being the initial contaminant concentration (more details in experimental section 8.5.2). The lower concentration experiments were chosen to be more consistent with the literature values of environmentally relevant TCS concentrations detected in waters in different parts around the world.^{303–305} In this set of experiments, the C_0 was 2 $\mu\text{g/L}$, instead of 6 mg/L as used previously. The TCS detection was performed using an HPLC-MS/MS Shimadzu system and all analyses were performed using *Equation 31*.

The influence of contact time on TCS adsorption is presented in **Figure 111**. All three types of SpECs were investigated and were found to be more efficient for adsorbing TCS at this concentration compared with the higher concentrations. Approximately 97% of TCS removal was achieved in only one minute for SpECs(3), whereas SpECs(1) showed the fastest adsorption by removing all TCS quantity in only one minute of contact time. SpECs(2) presented the slowest adsorption of the three extractions, removing 92% of TCS during the first minute of contact time and reaching 97% removal at eight minutes.

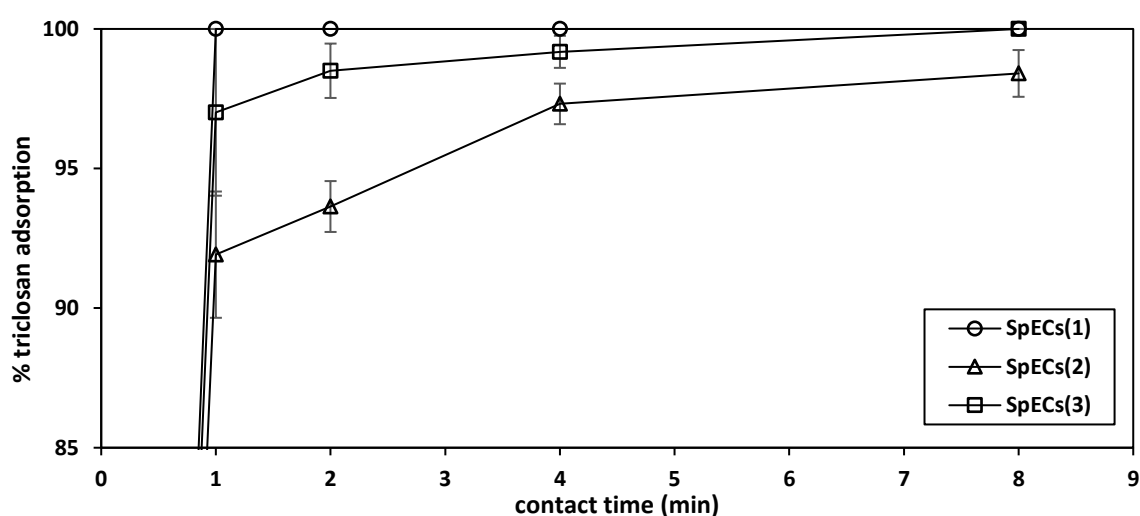


Figure 111: Effect of contact time on TCS adsorption by different SpECs, graph zoomed in the region of 85 - 100% of TCS adsorption (TCS dose: 2.3 $\mu\text{g/L}$, $n=3$).

The comparison of contact times influence between the two sets of concentrations can be seen in **Figure 112** where it is obvious that the different types of SpECs were slightly more efficient at lower initial TCS concentrations.

The three tested SpECs presented great efficiency for TCS adsorption with contact times for complete TCS removal in the scale of a few minutes. This can be attributed to the hydrophobic nature of the contaminant ($\log K_{ow} = 4.76$) leading to hydrophobic interactions with the SpECs surface (**Figure 113**).

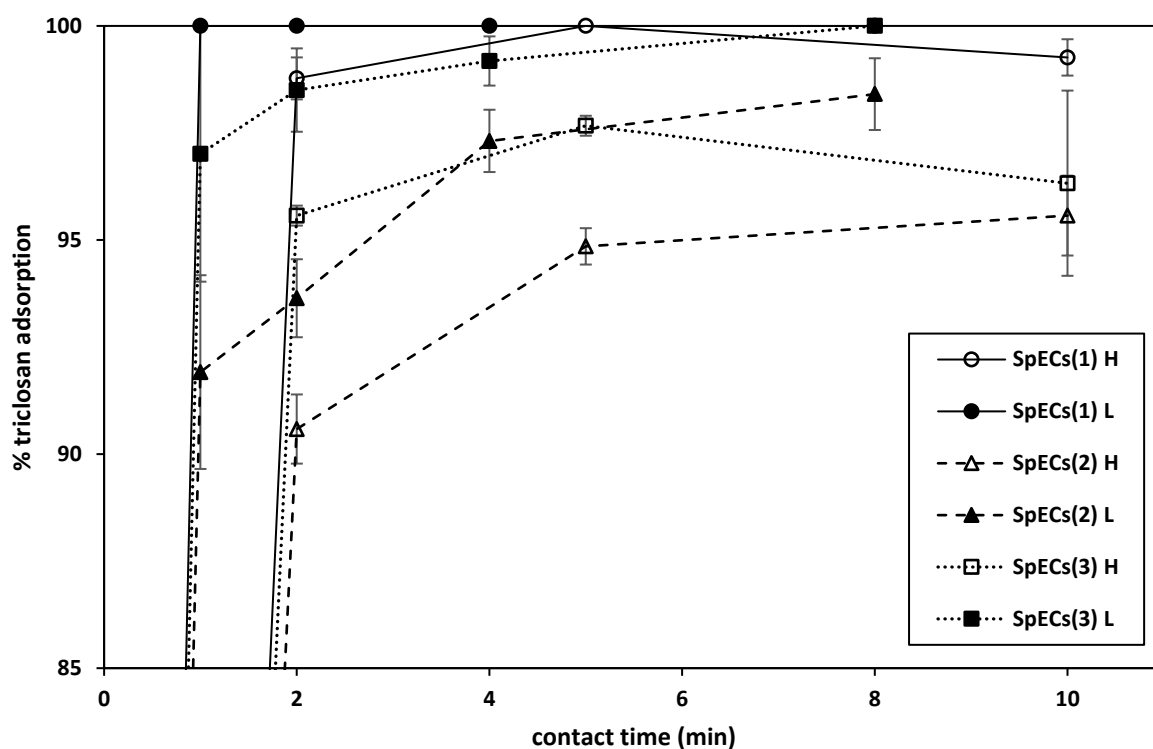


Figure 112: Effect of contact time and initial contaminant dose on TCS adsorption by SpECs, graph zoomed in the region of 85 - 100% TCS adsorption (TCS dose H: 6 mg/L, L: 2 μ g/L, n=3).

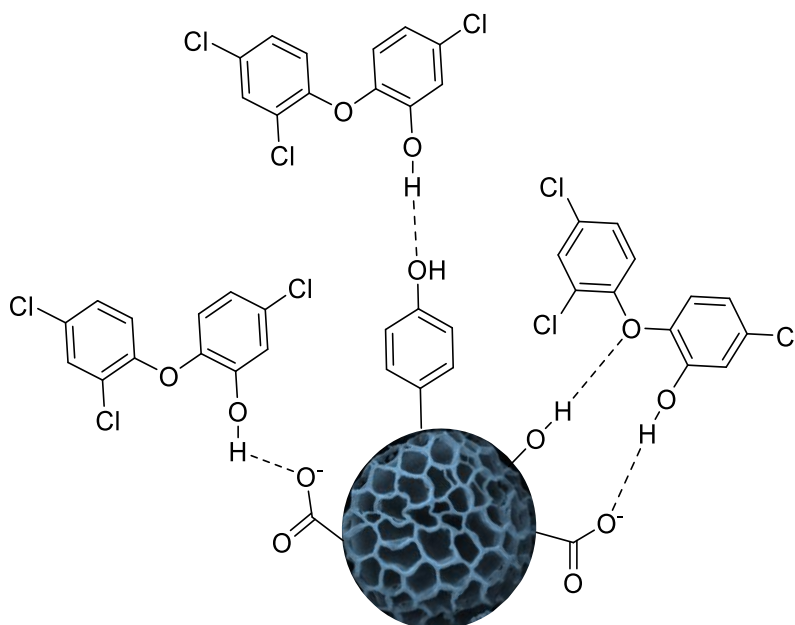


Figure 113: Schematic representation of possible adsorption forces between TCS and the functional groups on the surface of the different SpECs.

Another factor supporting the efficient adsorption of TCS by SpECs can be the molecule's size since there are reports showing that bigger molecules like TCS, present better adsorption rates compared to smaller molecules due to the time consuming diffusion process that small molecules need in order to reach into inner sites of the adsorbent's surface.³⁰⁶ The efficient TCS removal can also be attributed to the -OH group that the molecule contains, enhancing its adsorption. According to Chen *et al.*, molecules that contain more -OH groups compared to similar ones have higher adsorption affinity towards the adsorbents, possibly due to hydrogen bonding between their -OH groups and the material's oxygen containing groups, or due to the attractive interactions between the molecules that are already adsorbed and the ones that are still in the aqueous solution.^{307,308} Unfortunately, FT-IR analysis of the TCS loaded SpECs did not give any insight on the binding mechanisms between the contaminant and the adsorbent's surface.

4.4.4. Triclosan adsorption isotherms

In order to investigate the distribution of the adsorbed TCS molecules between the aqueous phase and the SpECs particles, the Langmuir and Freundlich models were used. As stated in the introduction, the Langmuir model describes a homogenous contaminant adsorption onto the surface of the adsorbent where each binding site of the surface can only be occupied by one molecule of pollutant. The linearized form of the equation is *Equation 33*:²⁵⁷

$$\frac{C_e}{Q_e} = \frac{C_e}{Q_m} + \frac{1}{K_L Q_m} \quad \text{Equation 33}$$

where C_e (mg/L) is the concentration of the adsorbate at equilibrium, Q_e (mg/g) is the amount of contaminant adsorbed per amount of adsorbent, K_L (L/mg) is the Langmuir adsorption equilibrium constant and Q_m (mg/g) is the maximum adsorption capacity of the material. Q_m indicates the amount of adsorbate needed for a complete monolayer and can be calculated from the slope of the line and K_L is a measure for the intensity of the adsorption process and can be calculated from the intercept.

On the other hand, Freundlich's model describes a multisite and reversible adsorption where the adsorbent's surface is heterogeneous, meaning that the bonding sites on the surface are of various energies and thus have affinity towards the contaminant. For this model, adsorption can happen in multilayers. The linearized form of the equation is *Equation 34*:²⁵⁸

$$\log Q_e = \log K_F + \frac{1}{n_F} \log C_e \quad \text{Equation 34}$$

where Q_e (mg/g) is the amount of adsorbate adsorbed per amount of adsorbent, C_e (mg/L) is the equilibrium concentration and K_F ($\text{mg}^{(1-1/n)}/\text{gL}^{-1/n}$) and n_F are Freundlich's constants. K_F is related to the material's adsorption capacity and can be calculated from the intercept of the line, where n_F is the heterogeneity factor of adsorption sites indicating the adsorption intensity and it can be calculated from the slope.

In this experiment, 5 mL of TCS solutions of different concentrations (0.5 - 50 $\mu\text{g}/\text{mL}$) interacted with 20 mg of the adsorbent for ten minutes of contact time at room temperature under orbital shaking. After filtration, the resulting solution was analysed for its TCS content and the final TCS concentration was compared to the initial concentration. The linear forms of the two models were plotted (**Figure 114** and **Figure 115**) and all the parameters for both Langmuir and Freundlich isotherms are presented in **Table 37**.

The low R^2 values of the Langmuir isotherms compared to the high ones obtained from the Freundlich model indicate that the best fitting for the adsorption of TCS by SpECs is the Freundlich isotherm model. Such a finding is in agreement with other materials found in the literature that were tested for TCS adsorption.^{38,301}

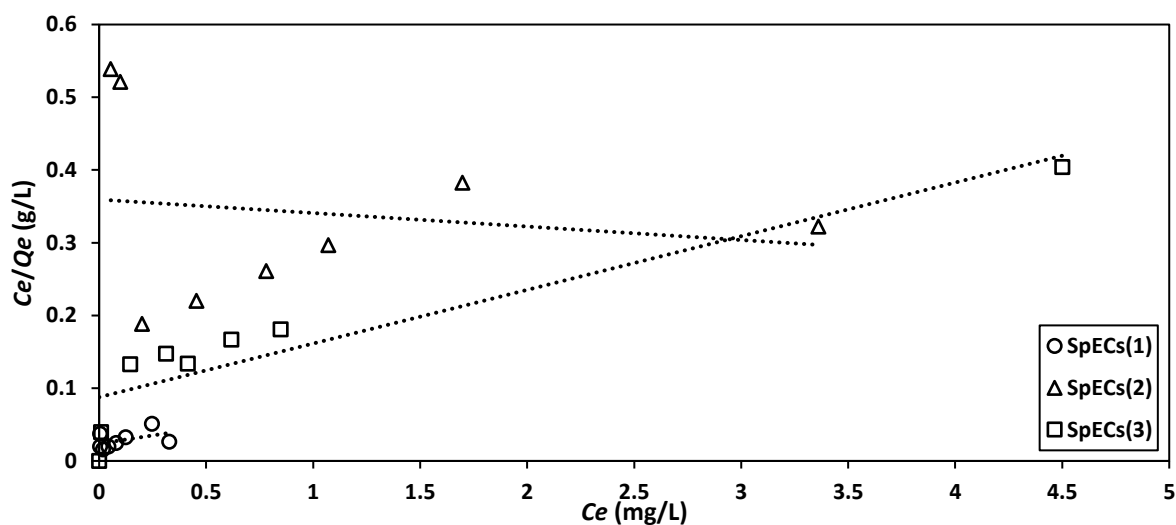


Figure 114: Langmuir linear adsorption isotherms for TCS uptake by different types of SpECs.

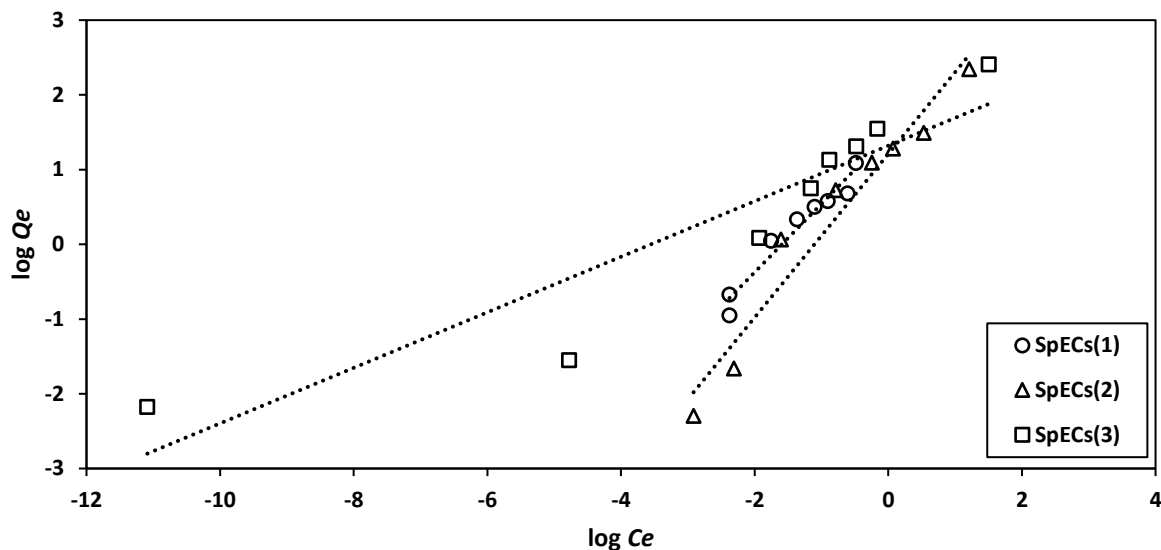


Figure 115: Freundlich linear adsorption isotherms for TCS uptake by different types of SpECs.

All tested SpECs gave results that were best fitted using the Freundlich model, showing that all three materials possess a heterogeneous surface with functional groups of different binding energies. As the Freundlich model is not suitable to predict the maximum adsorption capacity of the material, an indication of the adsorption capacity of the adsorbent can be the factor K_F . The greater the K_F value is, the more efficient the material is against the contaminant in target. In our case, the highest K_F value was given by SpECs(3) ($35.14 \text{ mg}^{(1-1/n)}/\text{gL}^{-1/n}$) indicating that this type of SpECs has a surface towards which the TCS molecules showed greater affinity. The $1/n_F$ value is another important factor that can provide useful information about the characteristics of the adsorption process. The highest $1/n_F$ value was presented by SpECs(2) and was higher than 1 (1.094) indicating the cooperative adsorption of TCS, possibly forming multi-layers on the surface of the material. SpECs(1) and SpECs(3) presented a $1/n_F$ value that was lower than one, a fact that implies that the adsorption of the TCS molecules is mainly happening through chemisorption.

Table 37: Adsorption isotherm parameters for the adsorption of TCS by different types of SpECs analysed with the Langmuir and Freundlich models.				
model parameters		type		
		SpECs(1)	SpECs(2)	SpECs(3)
Langmuir	Q_m (mg/g)	22.22	19.88	13.55
	K_L (L/mg)	1.891	0.134	0.842
	R^2	0.22	0.046	0.85
Freundlich	K_F (mg ^(1-1/n) /gL ^{-1/n})	25.67	16.18	35.14
	$1/n_F$	0.891	1.094	0.651
	R^2	0.935	0.951	0.99

Compared to values found in literature, SpECs(3) presented higher K_F values than sand,²⁸⁹ electrospun fibrous membranes²⁹⁴ and carbon nanotubes²⁵⁷ (7.4, 16.6 and 16 mg^(1-1/n)/gL^{-1/n} respectively) but not higher than sandy and silt loam,²⁸⁹ activated carbon and magnetic activated carbon²⁹⁵ (231, 344, 232 and 150 mg^(1-1/n)/gL^{-1/n} respectively).

4.4.5. Triclosan packed-bed studies

After the completion of small-scale experiments giving information on the characteristics of the adsorption process and the contact times needed for reaching equilibrium, the applicability of the material for contaminant adsorption for larger volumes had to be tested. Packed-bed experiments were conducted following the procedure described in section 8.9, where a glass column (30 cm × 2.5 cm) was tightly packed with a layer of 0.2 g SpECs(3) (0.4 cm high). The SpECs bed was covered with 2 g (0.4 cm high) low iron sand (Fisher Scientific) to put some extra weight on top of the SpECs and keep the particle bed tightly packed. Two different flow rates were tested (2 and 3 mL/min), as well as the regeneration and reusability of the material. A 10 mg/L TCS solution was passed through the SpECs layer under gravity until the complete saturation of the material. The flow rate was altered by adjusting the column's tap and the effluent was collected in fractions of 5 mL in the beginning and fractions of 25 - 10 mL later. All fractions were analysed for their TCS content with a HPLC system. The treated volume

was plotted against the recovered TCS concentration divided by the initial TCS concentration and the breakthrough curves were formed in Excel.

Since there exist reports in the literature about the TCS adsorption efficiency of sand,²⁸⁹ the low iron sand layer was checked individually for its TCS adsorption ability. A solution of known TCS concentration (10 mg/L) was passed through the sand bed and the initial and final concentration (C_f and C_o respectively) of TCS was measured and compared. The results presented in **Table 38** showed that the sand had no adsorption efficiency over TCS.

Table 38: TCS adsorption efficiency of 5 g of low iron sand (10 mg/L).			
fraction	volume (mL)	C_f (mg/L)	C_o (mg/L)
1	10	10.102	10.066
2	10	9.913	10.066
3	15	10.037	10.066
4	20	10.179	10.066
5	25	10.110	10.066
6	30	10.005	10.066
7	40	10.144	10.066
8	50	9.889	10.066
9	80	10.144	10.066

After the completion of the packed-bed experiment, all data obtained were analysed with the Yoon-Nelson model (*Equation 35*) in order to define variants such as the breakthrough point and the adsorption capacity of the material.⁸¹

$$C_t/C_0 = 1/[1 + \exp(K_{YN}\tau - K_{YN}t)] \quad \text{Equation 35}$$

where, C_t (mg/L) is the contaminant's concentration at time t (min), C_0 (mg/L) is the initial contaminant concentration, K_{YN} (min^{-1}) is the Yoon-Nelson rate constant and τ (min) is the

time required for 50% adsorbate breakthrough. K_{YN} and τ can be calculated from the linear form of the equation (Equation 36) by plotting $\ln(C_t/(C_0 - C_t))$ versus t .

$$\ln\left(\frac{C_t}{C_0 - C_t}\right) = K_{YN}(t - \tau) \quad \text{Equation 36}$$

The sorption capacity of the material q_0 (mg/g) can be calculated by using Equation 37:

$$q_0 = \frac{C_0 Q \tau}{m} \quad \text{Equation 37}$$

where Q is the flow rate (L/min) and m (g) is the mass of sorbent used in the column.

This calculated value (q_0) can then be compared to the experimental one ($q_{0,exp}$), defined by the Equation 38:

$$q_{0,exp} = \frac{m_{TCS\ ads}}{m_{SpECs}} \quad \text{Equation 38}$$

where $m_{TCS\ ads}$ (mg) is the adsorbed TCS mass and m_{SpECs} (g) is the mass of sorbent used in the column. $m_{TCS\ ads}$ was calculated using Equation 39.

$$m_{TCS\ tot} = m_{TCS\ el} - m_{TCS\ ads} \quad \text{Equation 39}$$

where $m_{TCS\ tot}$ is the total amount (g) of TCS that passed through the column and $m_{TCS\ el}$ is the amount (g) of TCS eluted. $m_{TCS\ tot}$ and $m_{TCS\ el}$ were calculated using *Equation 40* and *Equation 41*:

$$m_{TCS\ tot} = V_{tot} * C_0 \quad \text{Equation 40}$$

$$m_{TCS\ el} = C_{el} * V_{el} \quad \text{Equation 41}$$

where V_{tot} is the total volume of the contaminant solution that passed through the column, C_0 is the initial concentration of the contaminant, C_{el} is the concentration of the eluted solution after passing through the column and V_{el} is the volume of the eluted solution.

Figure 116 shows the breakthrough curves for TCS at two different flow rates (2 and 3 mL/min). It is obvious from the graph that a complete saturation of the material did not happen, meaning that the effluent concentration never reached the initial one. Even after treating 1.2 L of the TCS solution, the material kept adsorbing small quantities of TCS, indicating that there were still unoccupied sites left for binding, proving the good adsorption capacity of SpECs(3). The breakthrough point, where half of the initial concentration was able to pass through, occurred at around 400 mL for both flow rates, with the faster flow rate reaching it a bit earlier. This indicates that the material reaches its saturation point faster when applying a faster flow rate, even when the difference is of 1 mL/min faster.

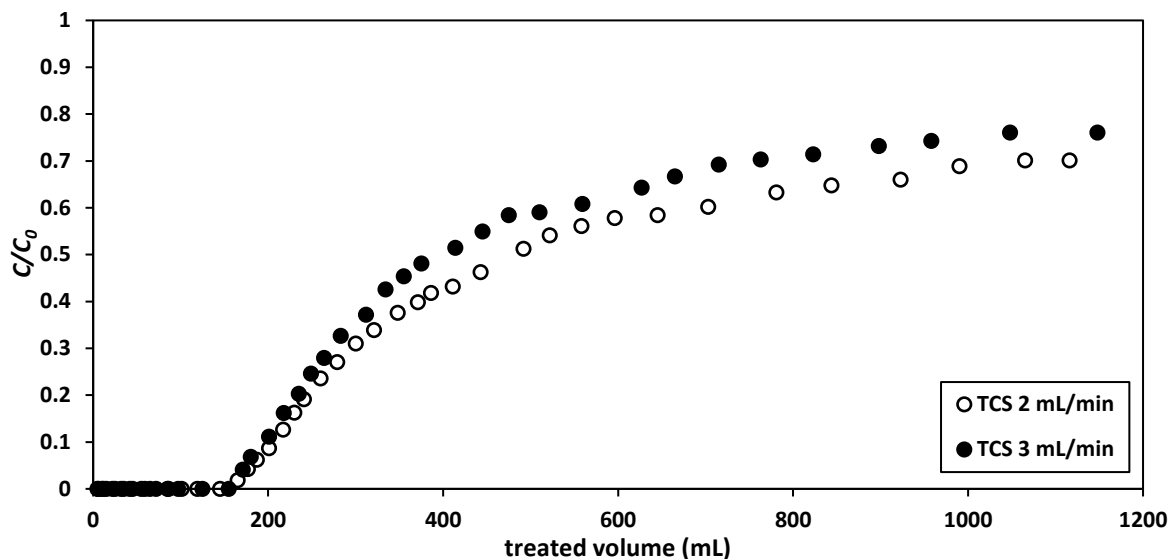


Figure 116: Breakthrough curves of 0.2 g SpECs(3) for TCS (10 mg/L) adsorption at two flow rates (2 and 3 mL/min).

The experimental data were analysed with the Yoon-Nelson model and the calculated values are summarised in **Table 39**. All values were in close agreement with the experimental ones, confirming that the Yoon-Nelson model is suitable for describing the adsorption of TCS by SpECs. The breakthrough point for the slower flow rate was at 242 minutes (~492 mL of treated volume) whereas for the faster flow rate it happened earlier, at 172 minutes (~415 mL of treated volume), showing that a faster flow rate is possibly not allowing good interaction between the contaminant molecules and the material. The adsorption capacity of the material was slightly affected by the change in flow rate, going from 35 mg/g for the slow flow rate, to 37 mg/g, suggesting that even a small difference can influence the material's efficiency.

For a flow rate of 3 mL/min, the TCS adsorption capacity of SpECs(3) was 37 mg/g, value that is much higher compared to kaolinite and montmorillonite (6.03 and 1.79 mg/mg respectively),³⁰⁹ but not as high as the values presented by carbon nanotubes, activated carbon, magnetic carbon and cellulose acetate fibres (558, 67, 171, 798 mg/g respectively).^{38,309-311}

Since the aforementioned experiments were not identical and presented differences in the

conditions (flow rate, pH, temperature, contaminant loading, material's mass), an accurate comparison cannot be made, unless all materials are tested under identical conditions. Furthermore, it is worth mentioning that the maximum reported annual water consumption of hospitals is ~660 million L²⁶³ and the reported TCS concentration in hospital effluents is 0.044 µg/L.²⁶¹ By combining the two values it can be concluded that in a year a hospital will only discharge 29 g of TCS. This would mean that a material with adsorption capacity values as high as the ones previously mentioned is not the required feature and is not as essential. The important factor for TCS adsorption used in a packed-bed setup would be the rate of adsorption since a high flow rate would be needed, of ~530 L/min, in order to treat the 660 million L of water for each hospital.

Table 39: Yoon-Nelson parameters and sorption capacities for the adsorption of TCS (10 mg/L) by 0.2 g SpECs(3) at two different flow rates.						
flow rate	K_{YN} (min ⁻¹)	τ (min)	τ_{exp} (min)	R^2	q_0 (mg/g)	$q_{0,exp}$ (mg/g)
2 mL/min	0.007	325.5	241.8	0.675	35.09	32.81
3 mL/min	0.009	239.8	171.7	0.651	37.15	33.54

In a theoretical scenario where a small water treatment setup would be built outside hospitals filtering their effluents, a cartridge containing 1 kg of SpECs(3) would be able to equivalently treat 477 million litres of contaminated water at a concentration of ~0.044 µg/L of TCS (TCS concentration in hospital effluents²⁶¹) before reaching the breakthrough point. It would therefore also be able to treat 2625 million litres of wastewater containing TCS at a concentration of 8 ng/L (reported wastewater value³¹²). The Massachusetts Water Resources Authority²⁶² reported annual water consumption of hospitals ranging from 15 million gallons (~68 million L) to 145 million gallons (~660 million L), of which approximately 42% is for sanitary purposes.²⁶³ This would mean that only one kilo of SpECs(3) would be enough for the annual requirements of each hospital. Combined with the information mentioned above that

within a year, a hospital will only discharge ~29 g of TCS, it can be concluded that SpECs is an excellent material for TCS adsorption for two basic reasons: it was proven to adsorb TCS at a very fast rate (total removal at only two minutes of contact time) as well as it presented an excellent efficiency under packed-bed conditions.

4.4.5.1. Regeneration and reusability of SpECs

After the completion of the packed-bed experiments, the packed SpECs were washed with milliQ water to check if the adsorbed TCS could be easily desorbed and subsequently contaminate clean water. The results in **Figure 117** show the region of the breakthrough curve and the region of the milliQ water washings after the completion of the breakthrough curve. It is evident that a small amount of TCS was able to desorb from the SpECs bed and contaminate the pure water passing through. The total quantity of TCS detected in the 1.3 L of water that passed through was 1.7 mg showing that the adsorption forces are not that strong, having as an effect the release of small quantities of TCS into pure water.

After the milliQ water washings, the packed SpECs were washed with absolute ethanol to remove all of the adsorbed TCS. The TCS recovery rate was checked as well as the material's reusability. The SpECs bed was washed with ethanol until the effluent contained no TCS quantity: in the 290 mL of ethanol that passed through, 3.5 mg of TCS were detected. Both water and ethanol combined together were able to recover around 85% of the trapped TCS with ethanol being a better regenerating agent since it removed the majority of the compound.

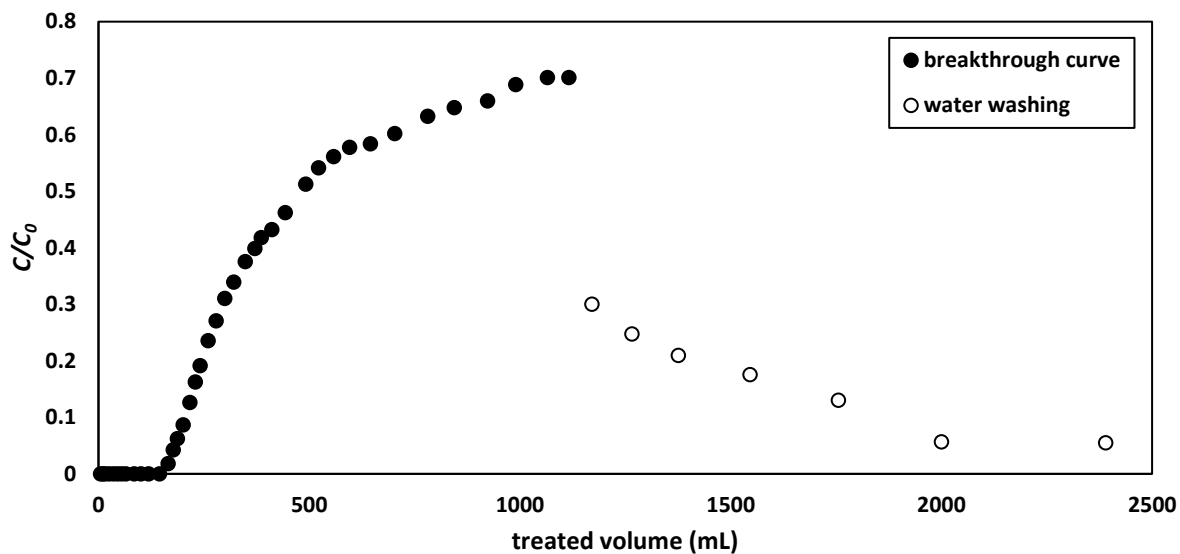


Figure 117: Packed SpECs(3) washed with milliQ water after the completion of the breakthrough curve against TCS.

The washed packed SpECs were reused for two more cycles in order to check and compare their adsorption performance and capacity between the three cycles. The experimental conditions were kept the same as before; the solution of TCS passed through the packed-bed aiming to the complete saturation of the material, the packed-bed was then washed with milliQ water and absolute ethanol until the complete removal of the contaminant and the material was reused for one more cycle.

Figure 118 shows the breakthrough curves for all the three cycles at the flow rate of 2 mL/min, whereas **Figure 119** presents the breakthrough curves for the flow rate of 3 mL/min. It is evident in both graphs that the material behaves similarly in all three cycles, with the third cycle being slightly more efficient than the previous two. This could be attributed to factors such as the particles being better packed after each cycle of use, the material being wetter with its active sites more available, or simply down to the experimental error.

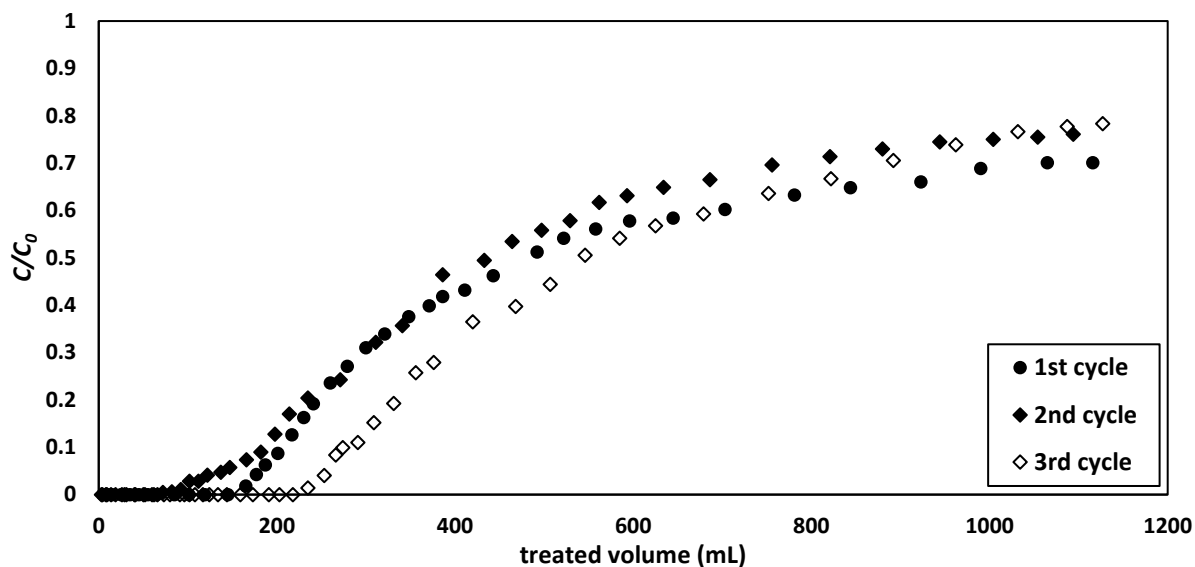


Figure 118: Breakthrough curves for TCS adsorption at a flow rate of 2 mL/min for three cycles of SpECs(3) reuse.

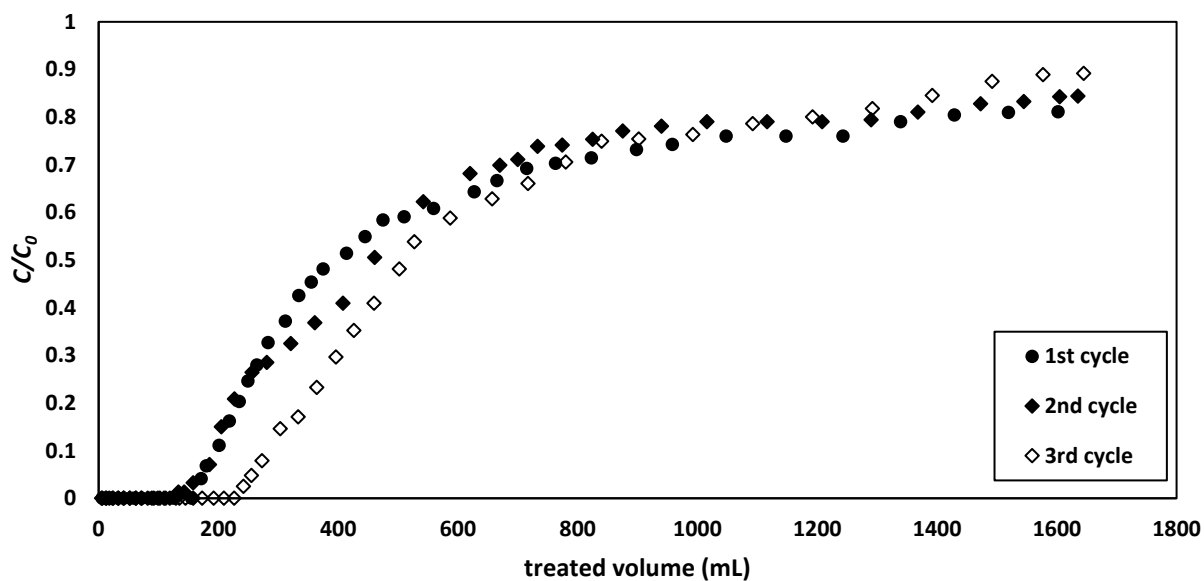


Figure 119: Breakthrough curves for TCS adsorption at a flow rate of 3 mL/min for three cycles of SpECs(3) reuse.

The data obtained for all cycles were analysed with the Yoon-Nelson model and the parameters are presented in **Table 40** together with the comparison to the first cycle. The breakthrough points for both flow rates did not present any significant variation between the three cycles, indicating that the material did not lose any of its adsorption efficiency and behaved the same

after it was regenerated with ethanol. The adsorption capacity on the other hand presented a rise cycle after cycle for both flow rates (**Figure 120**). The q_0 values started from 35 mg/g and reached 39.5 mg/g for the slow flow rate, whereas for the faster one q_0 was initially 37 mg/g and reached 40.7 mg/g in the third cycle. Such a finding is very surprising since it appears that the reuse of the material is increasing its adsorption capacity, possibly because the solvent passing through the bed is able to pack the particles tighter and tighter each time, or because the material is more wet and greater accessibility from the contaminant molecules. The increase in the R^2 values confirms that such a finding cannot be attributed to the experimental error.

Table 40: Yoon-Nelson parameters and sorption capacities for the adsorption of TCS (10 mg/L) by 0.2 g SpECs(3) at two different flow rates.

flow rate	K_{YN} (min^{-1})	τ (min)	τ_{exp} (min)	R^2	q_0 (mg/g)	$q_{0,exp}$ (mg/g)
2 mL/min	0.007	325.5	242	0.675	35.09	32.81
1st reuse	0.010	328.9	220	0.751	36.72	30.68
2nd reuse	0.009	353.3	271	0.789	39.45	33.46
3 mL/min	0.009	239.8	172	0.651	37.15	33.54
1st reuse	0.009	226.5	146	0.651	37.93	35.21
2nd reuse	0.009	256.4	171	0.768	40.65	36.19

In conclusion, SpECs(3) presented a very good adsorption behaviour for TCS when used under packed-bed conditions, proving that it is a very promising, efficient and reusable material. Its adsorption capacity and its low-cost production makes it a competitive candidate as a material for TCS adsorption and recovery, with absolute ethanol being a compatible regeneration reagent.

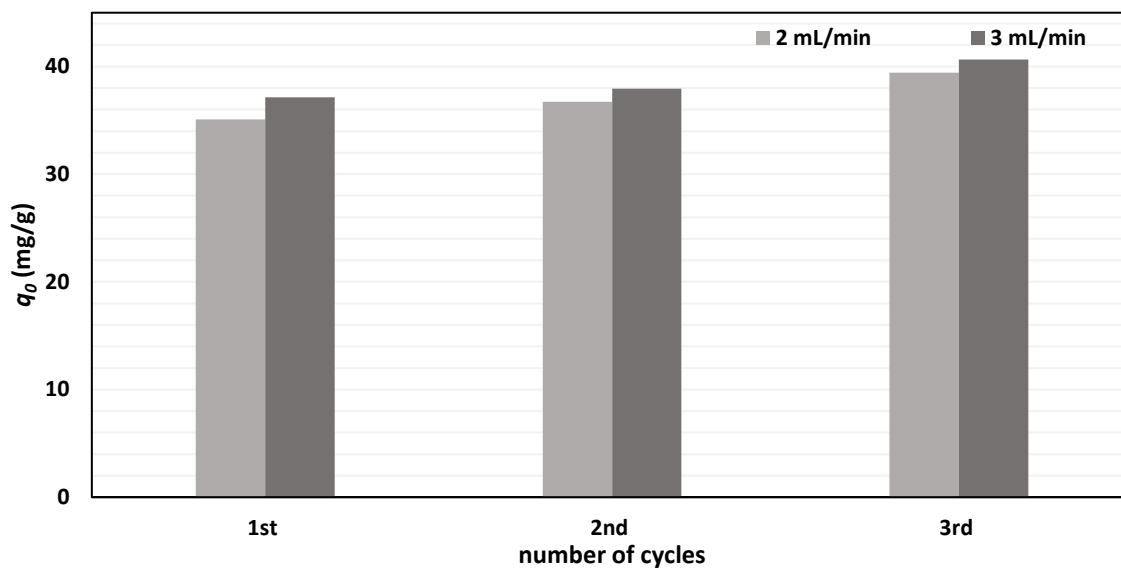


Figure 120: Comparison of the adsorption capacity of SpECs(3) between each cycle of reuse against TCS.

4.4.6. Adsorption of mixture of contaminants: diclofenac and triclosan

The experiments conducted so far involved solutions of only one contaminant. In real life situations contaminated water contains mixtures of different contaminants that would theoretically compete for the binding sites of the sorbent. For this reason, the same adsorption experiments were conducted, using a mixture of two contaminants, DCF and TCS.

The adsorption of a mixture of DCF and TCS in the same solution was examined, for the series of the standard SpECs types, 1, 2 and 3 and SpECs(2)APSH. The experimental procedure described in section 8.7.2 was followed, where 5 mL of the contaminant solution containing 6 µg/mL of each contaminant, were left under stirring together with 20 mg of SpECs for different periods of time, ranging from ten minutes to one hour. After filtration, the final solution was analysed for the content of both contaminants by HPLC.

Figure 121 shows the results obtained for SpECs(1) for the adsorption of mixed DCF and TCS. All TCS quantity was adsorbed after 10 minutes of contact time, while DCF adsorption appeared to be slower, with the adsorption being 70% after 10 minutes of contact time. It seems

that the adsorption of DCF happens much faster when in mixture rather than when it is individually present in the solution.

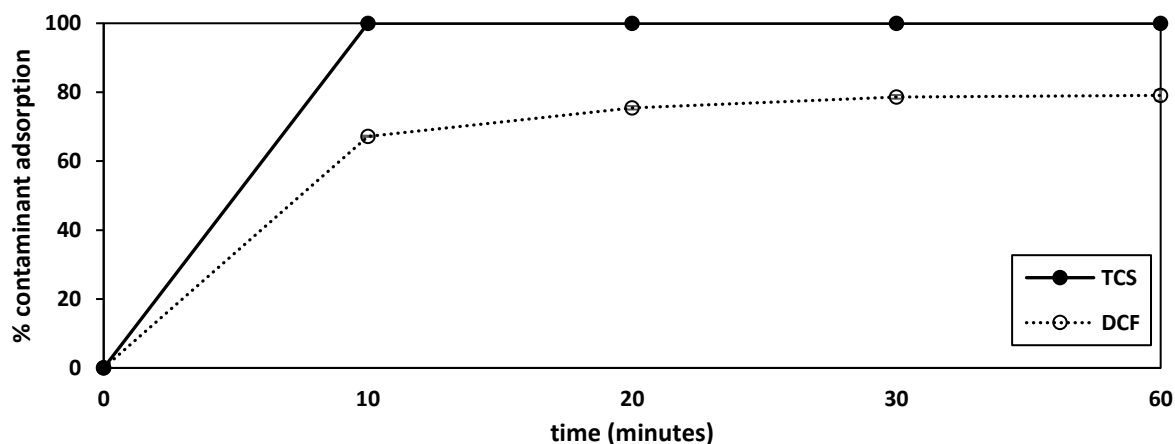


Figure 121: Effect of time on the adsorption of a mixture of DCF (6 mg/L) and TCS (6 mg/L) in water by SpECs(1) (n=3, total contaminant concentration 12 mg/L).

Figure 122 presents a comparison between the adsorption kinetic results obtained from the single contaminant experiments (chapters 3.4.3 and 4.4.2) and the current results concerning the adsorption from a mixture of contaminants. While the adsorption of TCS presented the same kinetics and was not affected by the presence of the DCF molecules, it seems that DCF gave higher adsorption percentages of a difference of 20% when in the mixed solution. Such a finding could be attributed to the TCS molecules being adsorbed first and creating a new monolayer on the surface of the SpECs, presenting new possible binding sites for the DCF molecules to be attached. Another explanation could be that the contaminant solution now contains more molecules and might be moving towards its saturation point, forcing the molecules to bind on the surface of the SpECs faster. Since none of the contaminants presented slower adsorption kinetics when in mixture compared to when alone, it can be suggested that DCF and TCS are competing for different active sites on the surface of this material.

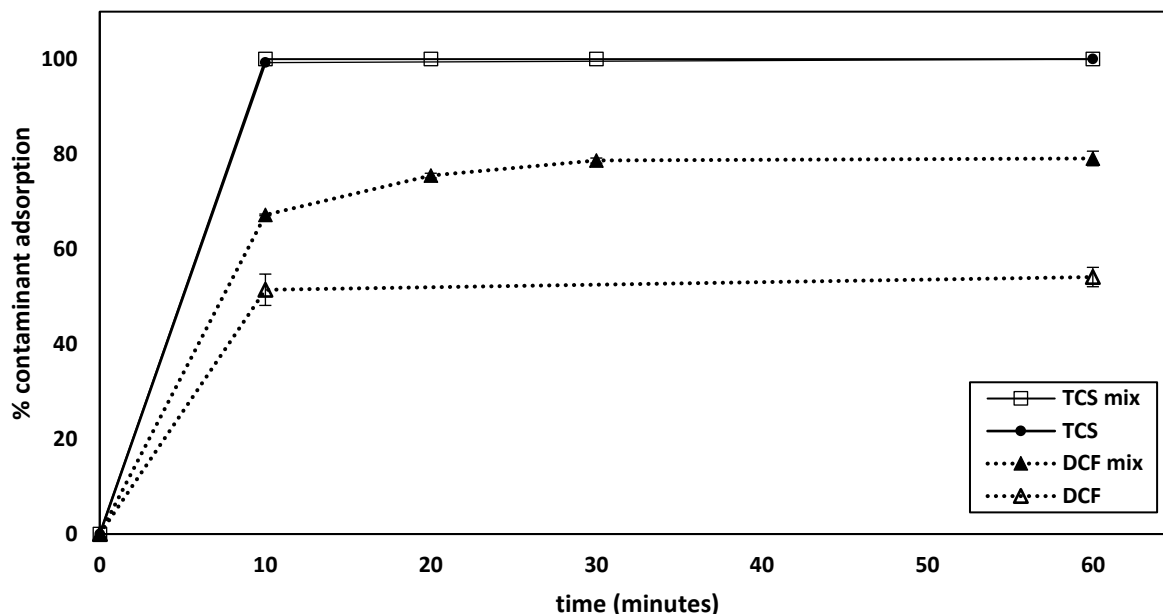


Figure 122: Comparison of the adsorption kinetics between single contaminant solution (either DCF or TCS alone, 6 $\mu\text{g}/\text{mL}$) and mixed contaminant solution (DCF and TCS together, 6 $\mu\text{g}/\text{mL}$ each, indicated by mix in the graph) by SpECs(1) (n=3).

The same experiment was conducted for SpECs(2) and similar results as SpECs(1) were obtained; TCS was completely adsorbed within 10 minutes of contact time and DCF presented a slower adsorption where only around 30% of the initial concentration was adsorbed within 30 minutes (**Figure 123**). Again, DCF presented a faster adsorption compared to the single contaminant experiment, but only for the first 30 minutes.

Figure 124 presents all the results together from the single contaminant experiments and the mixture, where a similar phenomenon as before is observed. While TCS adsorption followed the same kinetics as with the single contaminant experiments, the adsorption of DCF was more efficient in a mixture, with the results presenting a 15% increase in adsorption efficiency of DCF. An interesting fact is that after one hour of contact time, the adsorption percentages were equal, around 15%. It is possible that the TCS molecules were adsorbed first and created a new monolayer on the surface of SpECs(2), facilitating the binding of the DCF molecules as it was

also assumed for SpECs(1). After one hour though, the adsorption of DCF reached the same percentage either in mixture or on its own.

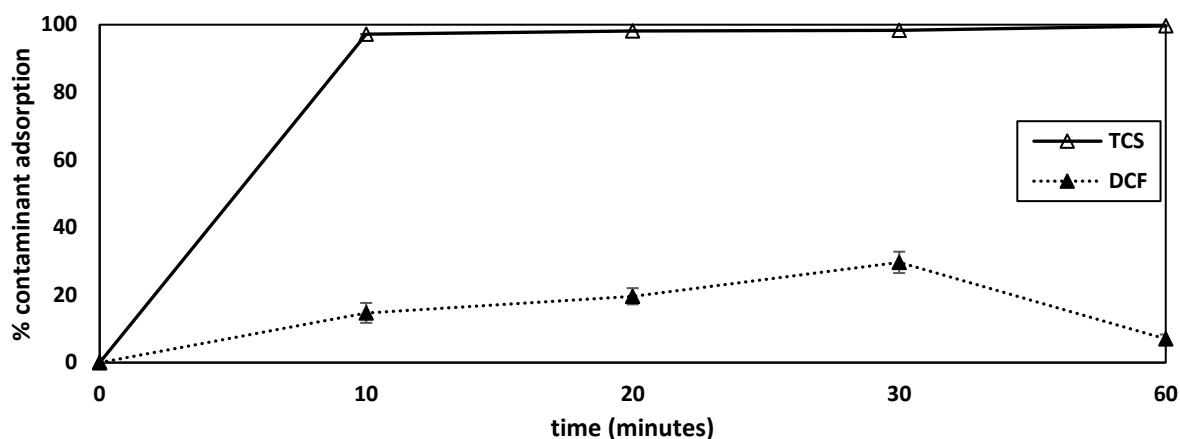


Figure 123: Effect of time on the adsorption of a mixture of DCF (6 mg/L) and TCS (6 mg/L) in water by SpECs(2) (n=3, total contaminant concentration 12 mg/L).

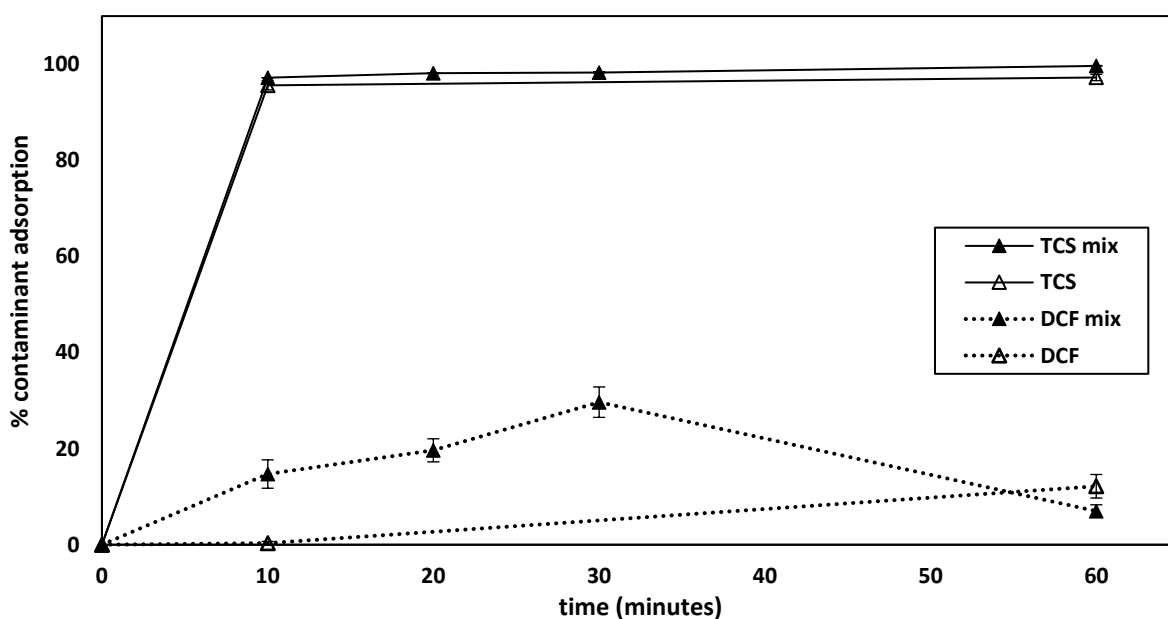


Figure 124: Comparison of the adsorption kinetics between single contaminant solution (either DCF or TCS alone, 6 $\mu\text{g}/\text{mL}$) and mixed contaminant solution (DCF and TCS together, 6 $\mu\text{g}/\text{mL}$ each, indicated by mix in the graph) by SpECs(2) (n=3).

The results obtained from the same experiments using SpECs(3) are presented in **Figure 125**, where it can be seen that the TCS adsorption followed the same efficient pattern as before, with its complete removal at 10 minutes of contact time. DCF adsorption was more effective compared to the previous material, SpECs(2), with around 70% removal after one hour of contact time. Interestingly, while for the previous two types of SpECs DCF adsorption was facilitated by the presence of TCS, for SpECs(3) it did not present any major differences.

The results for both the mixed contaminant and single contaminant adsorption by SpECs(3) are presented in **Figure 126**, where it is evident that the adsorption of TCS follows the same kinetics, either while being on its own or in a solution together with DCF. The adsorption of DCF was similar for both situations (single or mixed solution), presenting a small difference that can be easily attributed to experimental error, concluding that the adsorption of both contaminants was not affected by the presence of other molecules in the solution.

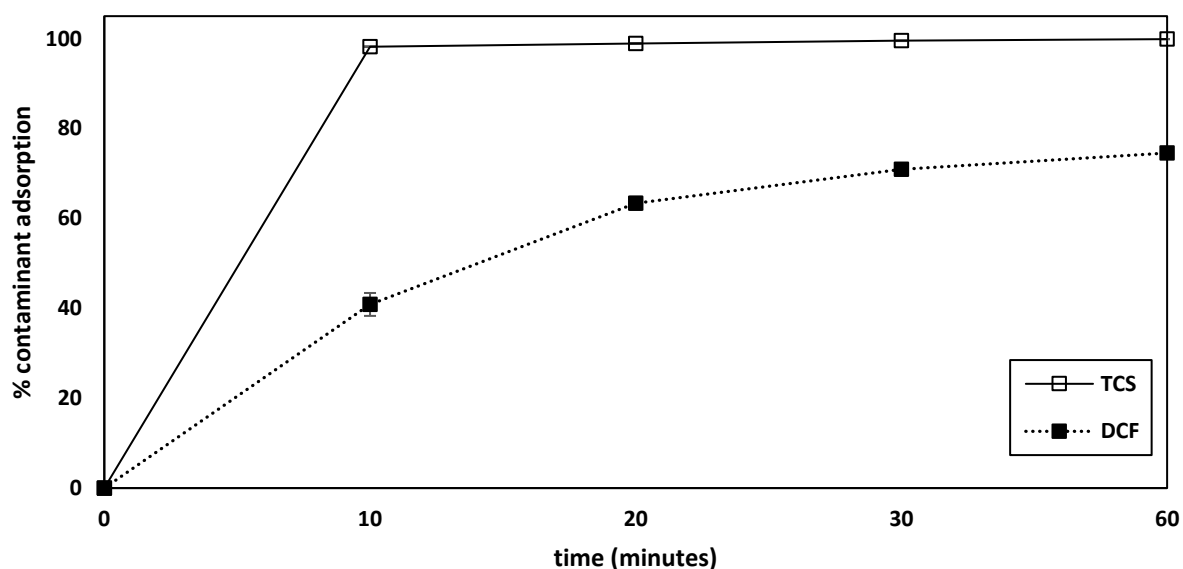


Figure 125: Effect of time on the adsorption of a mixture of DCF (6 mg/L) and TCS (6 mg/L) in water by SpECs(3) (n=3, total contaminant concentration 12 mg/L).

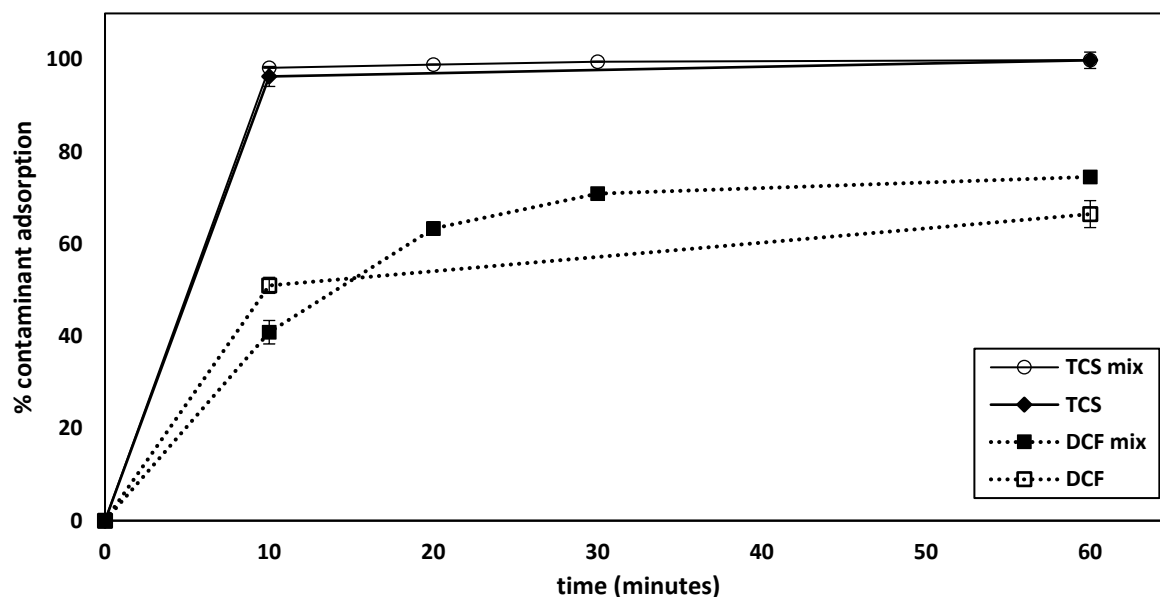


Figure 126: Comparison of the adsorption kinetics between single contaminant solution (either DCF or TCS alone, 6 $\mu\text{g}/\text{mL}$) and mixed contaminant solution (DCF and TCS together, 6 $\mu\text{g}/\text{mL}$ each, indicated by mix in the graph) by SpECs(3) ($n=3$).

The same experiment using SpECs(2)APSH presented similar results to the ones obtained from SpECs(3). Complete removal of TCS was achieved within 10 minutes of contact time, whereas DCF adsorption was slower, presenting 80% removal after one hour (**Figure 127**).

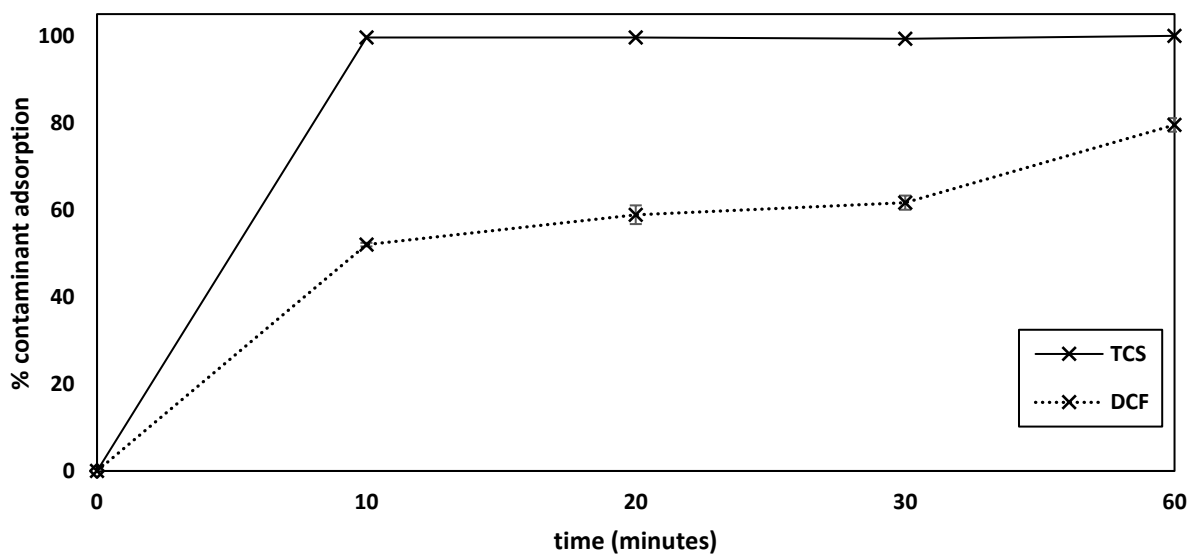


Figure 127: Effect of time on the adsorption of a mixture of DCF (6 mg/L) and TCS (6 mg/L) in water by SpECs(2)APSH ($n=3$, total contaminant concentration 12 mg/L).

Figure 128 presents the adsorption kinetics for the mixture of contaminants and the single contaminant experiments for SpECs(2)APSH. As with SpECs(3), the SpECs(2)APSH results are similar for both experiments, suggesting that the adsorption efficiency of the material is stable even when both molecules are present. A possible explanation for such a result could be that the contaminant molecules are binding on different active sites on the surface of the material and for this reason their adsorption is not affected when both of them are present in the same solution. Another explanation could be that the material has not reached its saturation point, having multiple sites unoccupied and available, leaving the adsorption of both contaminants unaffected by each other's presence. Furthermore, if the conclusions from SpECs(1) and SpECs(2) are correct, that TCS provides a new monolayer for TCS to bind, another possibility is that for SpECs(2)APSH as well, TCS might have been adsorbed really fast and then have provided an active site itself for DCF.

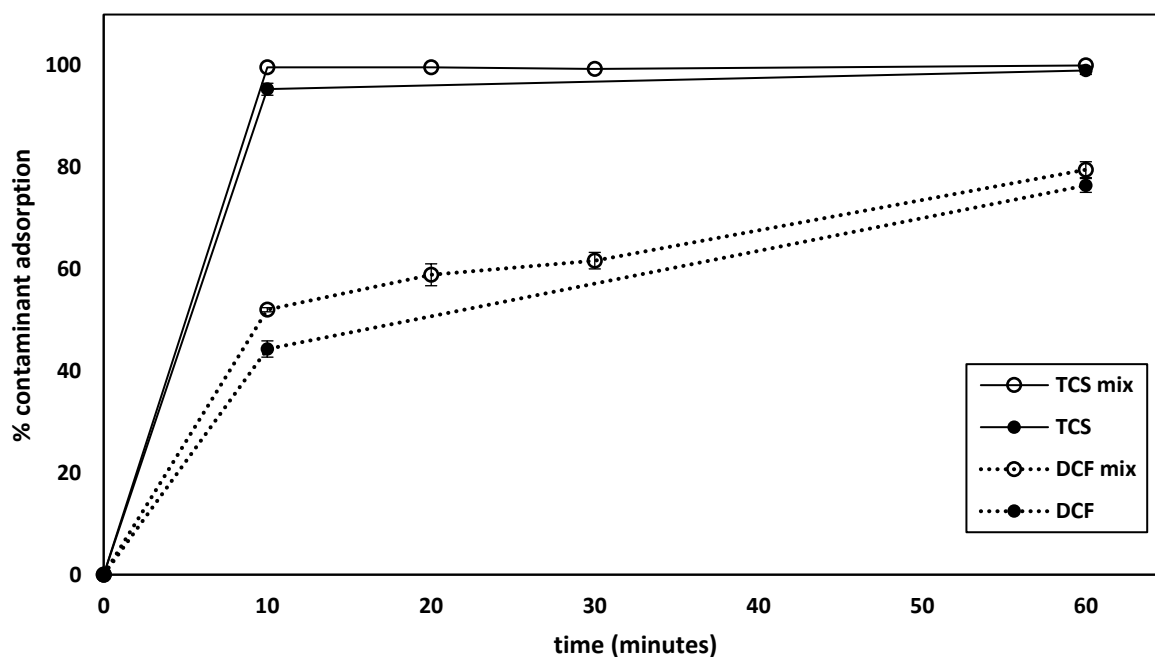


Figure 128: Comparison of the adsorption kinetics between single contaminant solution (either DCF or TCS alone, 6 $\mu\text{g}/\text{mL}$) and mixed contaminant solution (DCF and TCS together, 6 $\mu\text{g}/\text{mL}$ each, indicated by mix in the graph) by SpECs(2)APSH ($n=3$).

4.5. Conclusions

TCS is a broad-spectrum bactericide agent, present in many personal care products that has been proven toxic for aquatic organisms. It is environmentally persistent and can bioaccumulate, causing a major concern since it can be hazardous to the aquatic environment at concentrations as low as 0.3 mg/L. During conventional treatments it can convert into toxic by-products that are difficult to remove leading to their presence in the effluents of the WWTP. Furthermore, TCS has estrogenic and androgenic effects, it disrupts thyroid function, disturbs endobiotic and xenobiotic metabolism and can cause liver fibrosis and carcinogenesis.

The adsorption efficiency of SpECs for TCS was tested at two initial contaminant loadings; high (6 mg/L) and low - environmentally relevant³⁰³⁻³⁰⁵ (2 µg/L). All 3 types exhibited an efficient and fast adsorption for both concentrations by achieving 90 - 100% TCS removal in two minutes of contact time. SpECs(1) presented the fastest adsorption by removing all TCS quantity in only one minute of contact time.

Adsorption isotherm analysis showed that the Freundlich model is more suitable for describing the TCS adsorption on SpECs, indicating that all three materials possess a heterogeneous surface with functional groups of different binding energies. SpECs(3) presented the highest K_F value (35.14 mg^(1-1/n)/gL^{-1/n}) which compared to values found in literature, is higher than sand,²⁸⁹ electrospun fibrous membranes²⁹⁴ and carbon nanotubes²⁵⁷ (7.4, 16.6 and 16 mg^(1-1/n)/gL^{-1/n} respectively) but not higher than sandy and silt loam,²⁸⁹ activated carbon and magnetic activated carbon²⁹⁵ (231, 344, 232, 150 mg^(1-1/n)/gL^{-1/n} respectively). SpECs(3) also presented a lower than one $1/n_F$ value indicating that TCS adsorption is mainly happening through chemisorption.

Packed-bed studies were also performed, where breakthrough curves were formed and analysed with the Yoon-Nelson model. Two different flow rates were tested and showed that even a difference of 1 mL/min can affect the materials performance. For a flow rate of

3 mL/min, the adsorption capacity of SpECs(3) for TCS was 37 mg/g, value that is much higher compared to kaolinite and montmorillonite (6.03 and 1.79 mg/mg respectively),³⁰⁹ but not as high as the values presented by carbon nanotubes, activated carbon, magnetic carbon and cellulose acetate fibres (558, 67, 171, 798 mg/g respectively).^{38,309-311} As mentioned before, these materials might present higher capacities compared to SpECs but the important factor in TCS adsorption is the rate of adsorption, since the TCS content in hospital effluents is as low as 0.044 µg/L. It was calculated that 1 kg of SpECs(3) would be enough (in terms of capacity) to treat the annual discharge of one hospital, meaning that the adsorption capacity of the adsorbent does not have to be higher than the one presented by SpECs. For a packed-bed setup in hospital effluents, a high flow rate would be needed of ~530 L/min and SpECs are a great candidate having presented an excellent adsorption rate of complete TCS removal in two minutes of contact time.

The regeneration and reusability of SpECs(3) was also tested, where it was revealed that the reuse of the material cycle after cycle increased the material's adsorption capacity (from 35 to 39.5 mg/g and from 37 to 40.7 mg/g). Such a finding can be attributed to the better packing of the material as the solvent passes through, or to the better wetting of the material making its active sites more accessible for the contaminant molecules. Ethanol was proven to be an effective regenerative reagent for SpECs(3) as well as a good solvent for TCs recovery.

Additional experiments were conducted where adsorption from a mixture of contaminants was tested. It was proven that the adsorption efficiency of SpECs(3) and SpECs(2)APSH was not affected by the presence of TCS and DCF in the same solution, suggesting that the binding sites for each contaminant may be different or that the material's surface had enough binding sites for both contaminants and did not reach its saturation point. Another possibility could be that TCS was adsorbed very fast and was able to then provide new binding sites for TCS. SpECs(1) and SpECs(2) presented a different result, where DCF adsorption was proven to be

faster when in the same solution with TCS. Such a finding suggests that the TCS molecules create a first monolayer on the surface of the SpECs, forming new binding sites for DCF. Another explanation is that the contaminant solution might be saturated, forcing the molecules to bind on the surface of the SpECs quicker. Since none of the contaminants presented slower adsorption kinetics when in mixture compared to when alone, it was concluded that DCF and TCS are competing for different active sites on the surface of these two SpECs types.

In conclusion, SpECs(3) were proven to be a very effective material for TCS adsorption especially when tested for adsorbing TCS concentrations close to environmental ones and when used in a packed-bed system, configuration that is usually used in real world scenarios. The measured adsorption capacity of the material, its reusability, its low-cost production and its environmentally friendly sourcing makes it the ideal candidate for TCS adsorption and recovery.

5. Oestradiol

5.1. Introduction

Oestrogens are responsible for the growth, development, and the function of tissues in both female and male vertebrate reproductive systems, including the ovaries, the mammary gland, the uterus, the vagina, the prostate, the testis, and epididymis. In humans, they are mainly produced in the testes and ovaries, as well as the adrenals. They are important for maintaining the good health of the bones, the central nervous system and the cardiovascular system.³¹³

Oestrogenicity is the ability of a chemical to bind onto the oestrogen receptor affecting the balance of the endocrine system.³¹⁴ Since the human oestrogen receptor is approximately twice the size required for oestradiol (E2), there is space available for other molecules to bind, making the receptor non-specific to E2.³¹⁵ Even though oestrogen receptors of aquatic species are quite different to that of humans, their non-specificity is similar, meaning that endocrine disrupting compounds are able to cause serious problems.³¹⁶

Steroids are biologically active substances whose syntheses derive from cholesterol.³¹⁷ Their chemical structure consists of a tetracyclic network, formed of a phenolic ring, two cyclohexane rings and one cyclopentane, **Figure 129**.

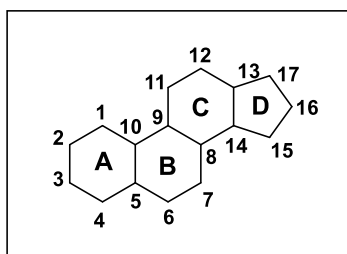


Figure 129: Steroidal chemical structure.

Different substitution patterns of the D ring at C17 and C16 position give different compounds with different chemical properties, **Figure 130**. Natural oestrogens share the same chemical structure and are part of a big family of compounds called steroidal hormones.³¹⁸

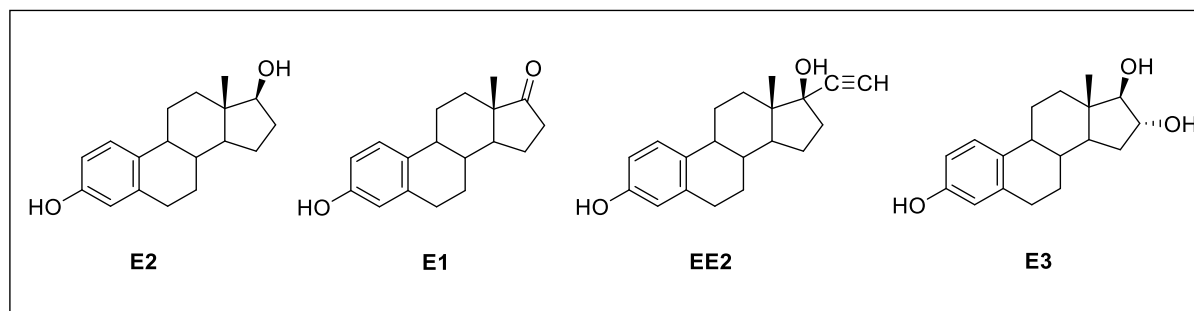


Figure 130: Chemical structures of the four oestrogens most found in the aquatic environment.

Pharmaceutical oestrogens are present in medicine prescribed for hormone replacement therapies³¹⁹ treating conditions like menopause³²⁰ and hypoestrogenism,³²¹ and are also present in contraception pills.³²² The active ingredients of these formulations usually include ethinyl-oestradiol (EE2), used in the contraceptive pill, 17β-oestradiol (E2), used for hormone therapy, and other esterified or conjugated oestrogens. The primary metabolites of these oestrogens are found in urine and faeces, and include compounds such as estrone (E1), E2, EE2 and estriol (E3) **Figure 130**.³²³

E2 derives from testosterone after the aromatisation of the ring A (**Figure 129**) using the p450 enzyme called aromatase or oestradiol synthase. It is the most active steroidal hormone and it has various effects on the developing brain since it expresses high levels of receptors for E2. It can have permanent effects on the brain including sex differentiation, prevention or promoting of apoptosis and synaptogenesis, or affect cellular physiology and morphometry of neurons.³²⁴ E2 is the active ingredient of many pharmaceuticals prescribed for problems associated with menopause and hypoestrogenism. It has a log *K_{ow}* of 3.94 and a solubility of 13 mg/L at 20 °C

which indicates its low volatility and its hydrophobic nature, increasing its potential to bind onto sediments, sludge and soil.³²⁵

Oestrogens in general, enter the aquatic environment mainly *via* the discharged domestic effluents, particularly from the most densely populated areas.³¹ The main source of E2 entering the environment is from human and animal faeces and urine, containing either the main compound or its glucuronide and / or sulfate conjugates **Figure 131**.³²⁶ Depending on the age of a person or an animal, the health status, the diet or whether they are pregnant, these compounds are excreted in different amounts, ending up in the environment either through sewage or animal waste disposal.^{327,328} Since oestrogenic compounds are hydrophobic, it is hard for the human body to excrete them. The body is able to inactivate and transform them into more soluble forms and discards them mainly through the kidneys. This metabolic transformation creates soluble conjugates that have no oestrogenic activity.³²⁹ Human urine usually contains the largest amount of oestrogens compared with faeces, with the glucuronide conjugate being the dominant form (85% in males, 65% in females) rather than the sulfate form (15% in males, 35% in females).³³⁰

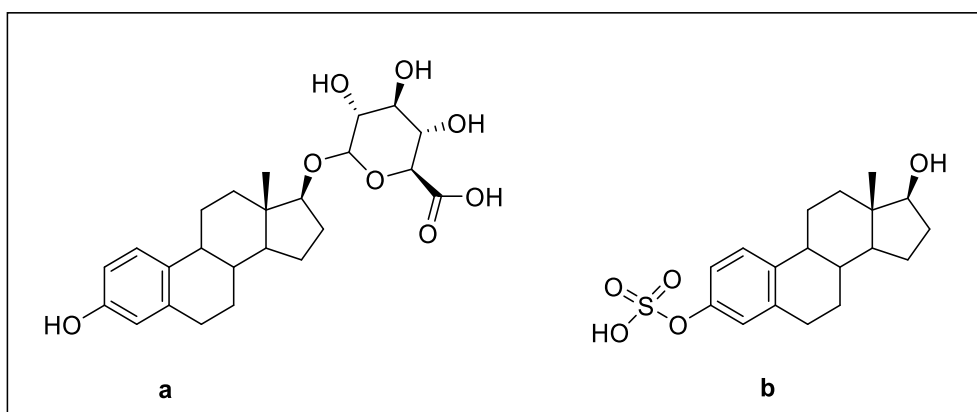


Figure 131: Chemical structures for E2 conjugates a) oestradiol glucuronide b) oestradiol sulfate.

As stated above, this conjugation of oestrogens increases their water solubility, making them more mobile in the environment compared to free hormones and for this reason they are considered pseudo-persistent, since they are introduced into the environment continuously, on a daily basis. For example, the average person excretes approximately 7.7 µg E2 per day.³³¹ Although these conjugates have lost their oestrogenic activity and are not active against oestrogen receptors, during the WWT they can be converted back into their active original structure by chemical or enzymatic procedures.³²⁶ In theory, there are eight different possible conjugates for E2 since it has two hydroxyl groups (possible positions) in its structure.³²⁹

In water, the most commonly found oestrogens are the natural ones, E1, E2 and E3 which are predominantly female hormones, and EE2 which is a synthetic one.³¹⁶ Between these four, EE2 has shown the highest oestrogenic potency, followed by E2.^{332,333} The main reason for E2 presence in the aquatic ecosystems is its incomplete removal during the process of wastewater treatment.^{31,334,335} Even at very low levels, E2 can provoke problems to non-target aquatic organisms. Concentrations as low as 1 ng/L are capable of making male fish synthesise and secrete a female-only egg yolk protein, called vitellogenin, developing intersex characteristics or failing to develop normal secondary characteristics leading to changes in their reproduction.^{316,317,336,337} In particular, a recent study of goldfish (*Carassius auratus*) revealed that exposure to E2 caused non-spawning and infertile males, leading to a significant decrease in their population.³³⁸ Another study on bluegill (*Lepomis macrochirus*) noted that exposure to 40 or 80 ng of E2 per litre had, as an effect, the morphological changes of the males causing again serious problems in reproduction and decline to their population.³³⁹ Apart from these direct effects, E2 is also suspected of bioaccumulation in the environment *via* the food chain.^{340,341} Compared with other compounds that are marked as endocrine disruptors, E1, E2 and EE2 have a higher endocrine potential that could provoke adverse effects within aquatic organisms.³¹

The concentrations of E2 in the environment are considered low, within the ng/L range, compared to the ones of traditional contaminants such as pesticides. In the UK, effluents from sewage treatment were analysed and E2 concentrations ranging from 1 - 50 ng/L were observed.³³³ In Germany, the concentration of E2 in similar effluents was found to be 3 ng/L whereas in Canada, 64 ng/L is the average value given.³³⁵ For river water, the concentrations tend to be lower, in the UK the range reported is between 0.4 and 4.3 ng/L³⁴² and in Italy it was found to be 0.04 - 1.5 ng/L.³⁴³ Sediment analysis for both upstream and downstream sites in the UK showed a range of 21.3 - 29.9 ng/kg.³⁴⁴

During conventional WWTPs, E2 can form other metabolites or return to its initial structure from the conjugate form. Under anoxic and aerobic conditions E2 will be oxidised to E1 and then further oxidised to unknown breakdown metabolites, ending up in the form of CO₂ and water.³⁴⁵ Under anaerobic conditions, E2 will be oxidised to E1 but no further oxidation will occur.^{31,345,346}

Research has shown that methods such as chlorination, sand filtration and reverse osmosis used in conventional water treatment plants are not very efficient nor specific in removing E2.¹⁹ Recent studies show that new methods are being explored for the removal of E2 like catalytic degradation, biodegradation, photo-catalytic degradation, advanced oxidation and adsorption with the latter being the one preferred because of its high efficiency and its environmentally friendly nature.³⁴⁷⁻³⁵²

Many sorbent materials have been developed and tested against E2 removal including granular or powdered activated carbon, ion exchange resins, bone char, single-walled or multi-walled carbon nanotubes, chitosan, chitin, natural sediments, polyamide membranes, molecularly imprinted polymers.^{16,352-360} The chemical composition and surface properties of the adsorbent together with its porosity, are factors that affect the effectiveness of the adsorption process, demanding more research into new promising materials.

5.2. Aims and Objectives

In this chapter, the adsorption of E2 by SpECs will be studied. As with the previous contaminants, all three different SpECs types will be examined in order to identify whether they are suitable for E2 adsorption, and which one is the most efficient. After examining the adsorption kinetics and spotting the most suitable SpECs type, the material's behaviour will be analysed using packed-bed studies.

5.3. Oestradiol detection and quantification

A stock solution of E2 was prepared in ethanol and further dilutions were made in milliQ water. The range of concentrations for the reference curve was decided to be from 0 to 10 $\mu\text{g/mL}$ since the solubility of the compound in water is reported to be low ($1.51 \pm 0.04 \text{ mg/L}$).³⁶¹ All standard solutions were prepared in triplicate and their analysis was performed with a UV-Vis spectrophotometer at 200 nm. Baseline calibration was performed using blank solutions of milliQ water, meaning that a concentration of 0 $\mu\text{g/mL}$ gave absorbance values of zero with no deviation from this value.

The reference curve is presented in **Figure 132** and *Equation 42* was used for the calculations of E2 concentrations (x) in all the experiments in this chapter with a LOD and a LOQ values at 0.02 $\mu\text{g/mL}$.

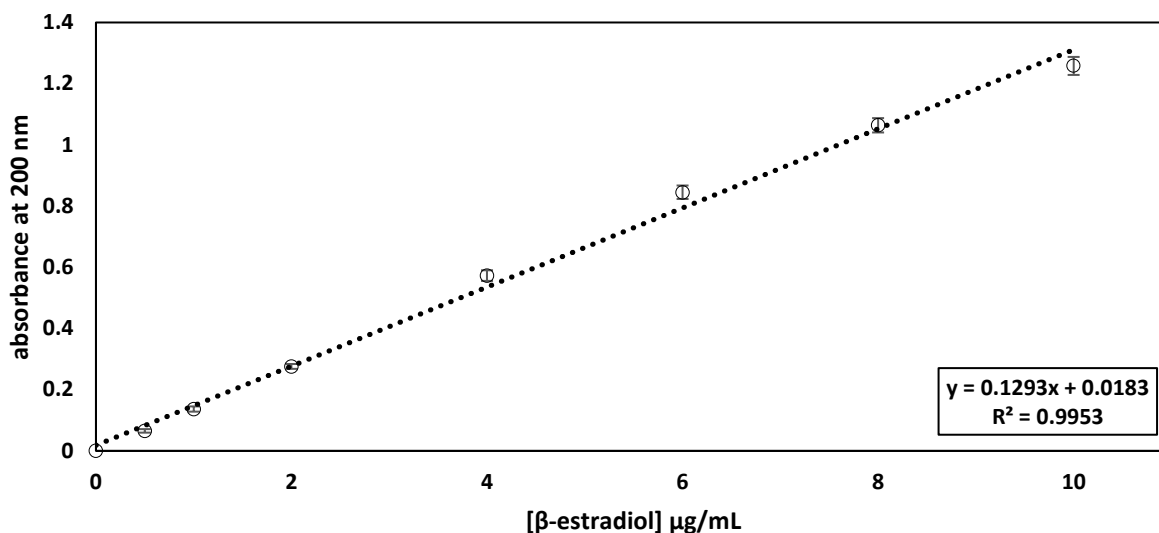


Figure 132: E2 reference curve in milliQ water, at 200 nm detection wavelength and at room temperature.

$$y = 0.1293x + 0.0183$$

Equation 42

Since the solubility of E2 is low, the stability of the standard solutions had to be tested. Vials containing the standard solutions were left at room temperature and their absorbance was measured at different time intervals, to verify whether the signal would stay stable over time. The results are presented in **Figure 133** where it is evident that for concentrations higher than 6 µg/mL the solutions are not stable, presenting an immediate decline in their signal.

Since the E2 concentration of 6 µg/mL was the highest limit, the same test was conducted for multiple preparations of a solution containing 6 µg/mL of E2, to ensure that its absorbance signal remains stable. **Figure 134** shows that the solution's absorbance signal remains stable within the error, even 22 hours after preparation, thus the concentration of 6 µg/mL was chosen for the adsorption kinetics experiments.

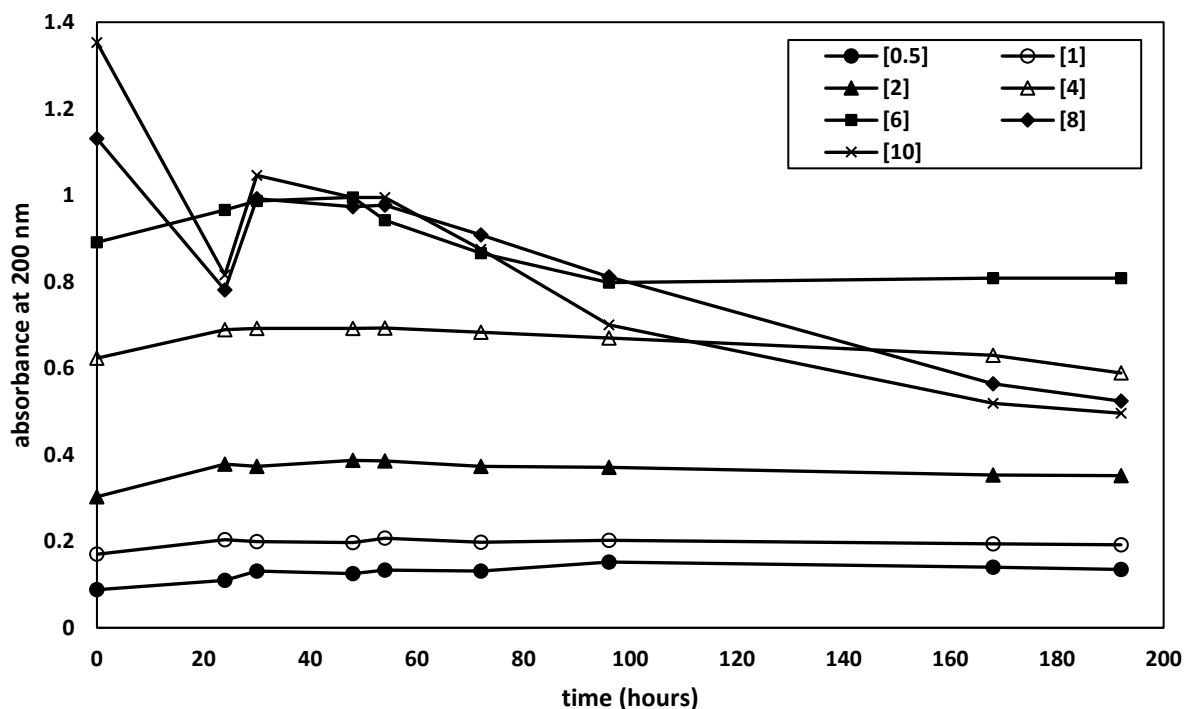


Figure 133: Absorbance of E2 standard solutions at different concentrations (0.5 - 10 $\mu\text{g/mL}$) and their stability after different time periods.

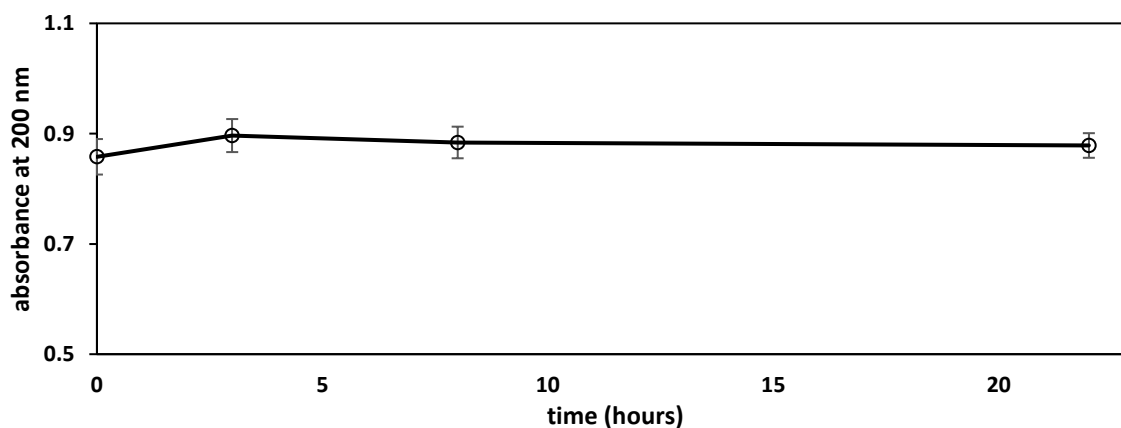


Figure 134: Absorbance of E2 solutions of 6 $\mu\text{g/mL}$ over 24 hours (n=4).

5.4. Oestradiol adsorption experiments

The E2 - SpECs adsorption experiments were conducted following the protocol described in the experimental section 8.6.3 (**Figure 135**), where a solution containing 6 $\mu\text{g/mL}$ E2 was left in contact with 20 mg of SpECs for different periods of time (1 - 10 hours). After filtration, the E2 concentration of the resulting solution was measured and compared to the initial

concentration. The E2 adsorption percentage was calculated using *Equation 43* and a plot against time was created in Excel.

$$\% E2 \text{ ads.} = \frac{(C_0 - C_{eq}) 100}{C_0} \quad \text{Equation 43}$$

where C_0 is the initial and C_{eq} is the final E2 concentration.

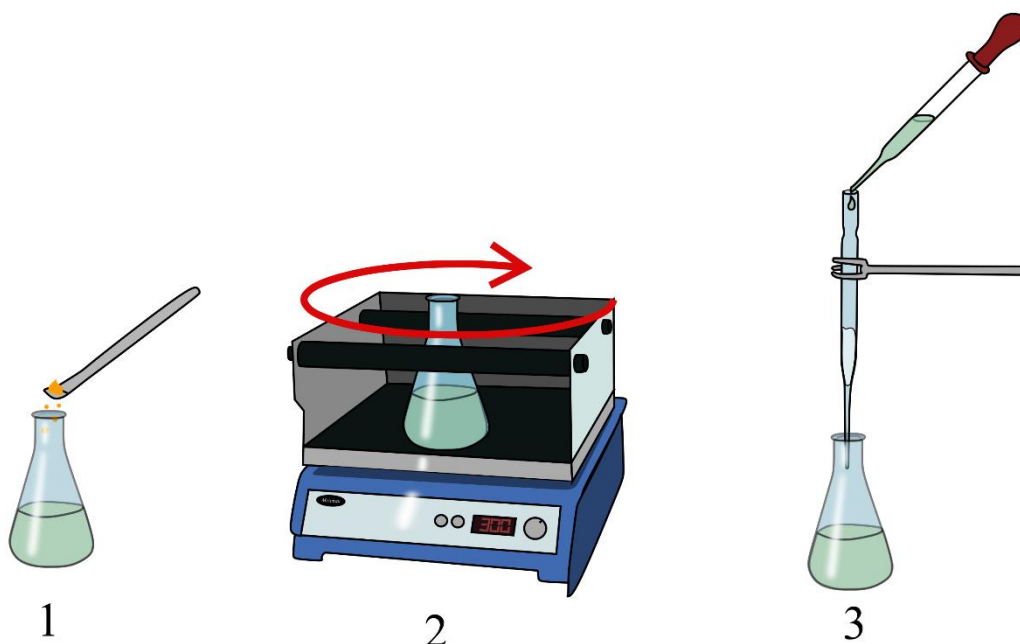


Figure 135: Experimental setup for the adsorption experiments describing the three-step procedure: 1) SpECs are added to the contaminant solution, 2) the suspension is shaken in the orbital shaking for a period of time, 3) the suspension is filtered through a pipette equipped with cotton wool.

5.4.1. Cotton interference in oestradiol adsorption experiments

Since E2 is a lipophilic compound, the filtration materials had to be tested in order to ensure that no E2 quantity would be adsorbed by either the cotton wool in the packed pipettes, or the membrane in the HPLC Phenomenex filters.

First, an E2 solution of known concentration (6 µg/mL) was analysed right after preparation. Then, the same solution was analysed after filtration, passed either through a glass pipette packed with cotton wool or a Phenomenex HPLC filter attached to a syringe. The procedure was repeated three times for each filtering material and the final solution's concentration was measured and compared to the concentration of the initial unfiltered solution. The results are shown in **Table 41**.

Table 41: Comparison of E2 absorbance signals before and after filtration.		
no filtration	HPLC filter	cotton wool filter
0.857	0.843	0.808
	0.864	0.794
	0.829	0.817

The filtration through cotton wool resulted in lower absorbance signals compared to the initial unfiltered one, meaning that some E2 quantity might have been trapped within the cellulose of the cotton wool thus altering the final result and increasing the experimental error. The filtration with the Phenomenex filter gave absorbance values similar to the initial ones making the procedure more accurate and so this was the filter that was chosen.

5.4.2. Oestradiol adsorption kinetics

The influence of contact time in E2 adsorption is presented in **Figure 136**. Raw spores showed a small efficiency by removing 20% of E2 in four hours of contact time. After the different extraction treatments, it is evident that the material gained some adsorption capacity over E2 by revealing the functional groups on its surface. All tested SpECs showed a good adsorption efficiency for E2, with the majority being able to remove ~80% in one hour of contact time. SpECs(1) presented the fastest adsorption, with 90% removal after only 15 minutes of contact time. SpECs(3) and their aminated form, SpECs(3)AM presented a similar behaviour after one

hour of contact time, but the aminated form presented much faster adsorption in the time window of 0 - 1 hour. In 30 minutes of contact time SpECs(3)AM were able to remove 80% of E2 whereas SpECs(3) only removed 65%.

As with the previous contaminants, in order to investigate the adsorption mechanisms of E2 on the different SpECs types, pseudo-first order and pseudo-second order kinetic models were applied to the experimental data, to further explore the potential rate controlling steps.

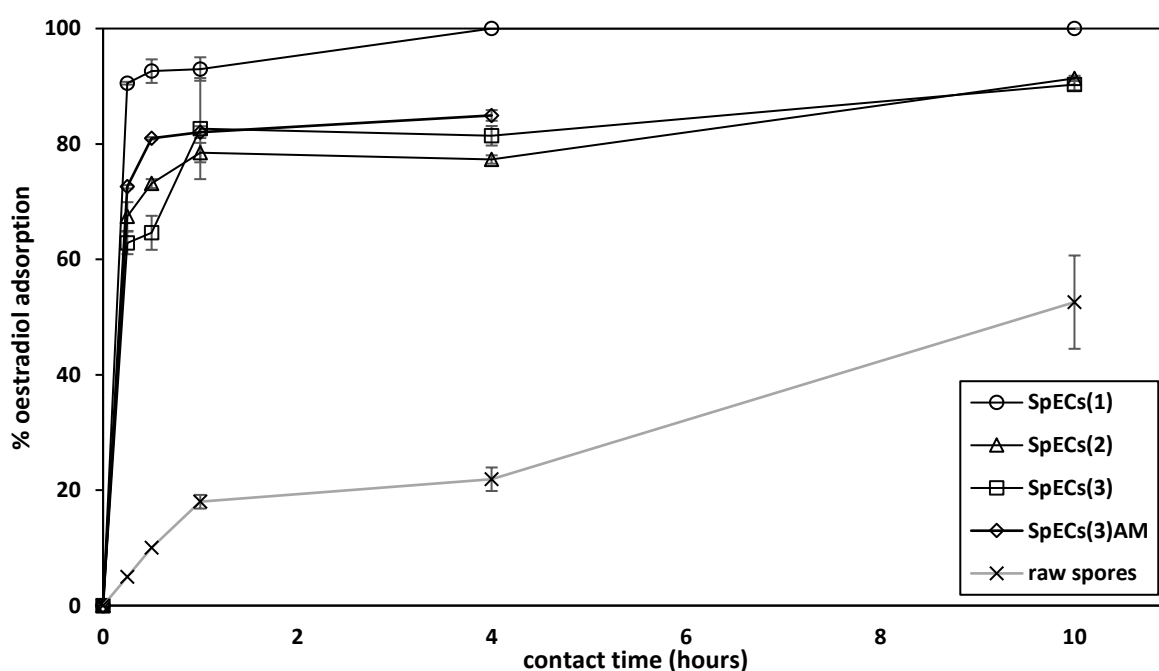


Figure 136: Effect of contact time on E2 adsorption, (E2 dose: 6 mg/L, n=3).

5.4.2.1. Pseudo-first order model

The pseudo-first order model or Lagergren's model⁷⁶ is generally applicable in the initial stage of the adsorption and is based on the assumption that the rate of adsorption is dependent on the concentration of the adsorbate. The linear form of the equation is expressed as follows (Equation 44):^{58,74}

$$\ln(q_e - q_t) = \ln q_e - k_1 t \quad \text{Equation 44}$$

where q_t (mg/g) is the amount of solute adsorbed per mass of adsorbent after a certain contact time t (min), q_e (mg/g) is the amount of solute adsorbed at equilibrium and k_1 (min^{-1}) is the pseudo-first order rate constant.

From the plot $\ln(q_e - q_t)$ versus t (**Figure 137**) the values of k_1 (slope) and $\ln q_e$ (intercept) were determined, from which the value of the maximum adsorption capacity $q_{e1,cal}$ was calculated. The experimental maximum adsorption capacity was calculated using *Equation 45*.

$$q_{e1,exp} = [E2] * \frac{V}{m_{SpECs}} \quad \text{Equation 45}$$

where $[E2]$ ($\mu\text{g/mL}$) is the concentration of E2 in the solution, V (mL) is the volume of the solution and m_{SpECs} (mg) is the mass of the SpECs used.

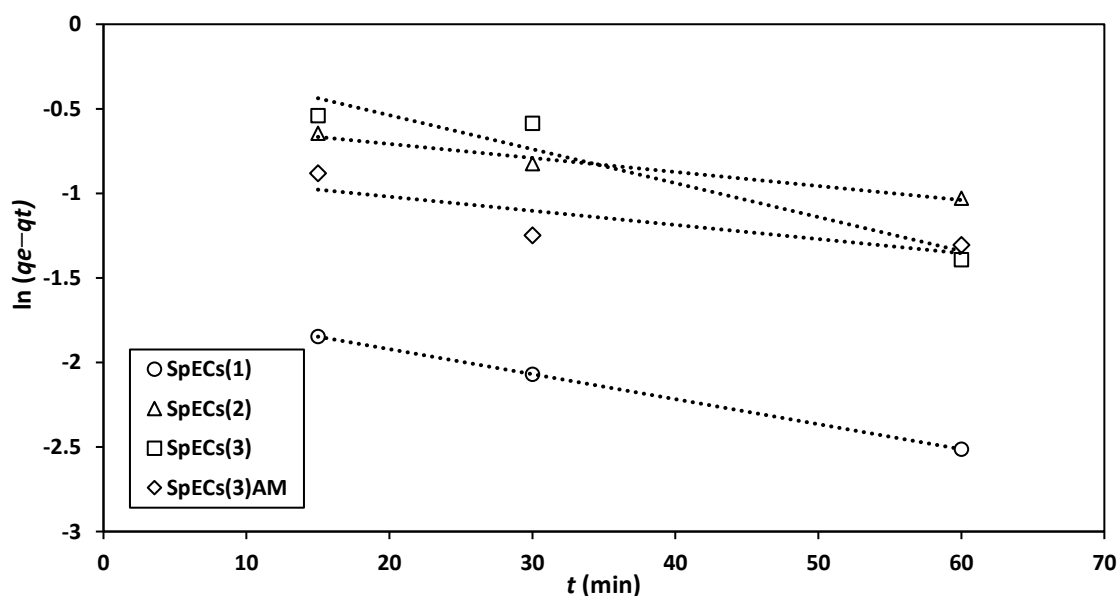


Figure 137: Kinetic investigation on the adsorption of E2 by different types of SpECs described by the pseudo-first order model.

All calculated values are summarised in **Table 42**, where it can be noticeable that for the majority of the tested SpECs the values of the correlation coefficient (R^2) are between 0.9 and 1 apart from the aminated form of SpECs(3). SpECs(3)AM presented a R^2 value of 0.693 indicating that the pseudo-first order model was not suitable for describing the adsorption of E2 on this material. SpECs(1) presented the highest R^2 value, 1, but the values of the experimental ($q_{e1,exp}$) and calculated ($q_{e1,cal}$) maximum adsorption capacity were not in agreement, 1.526 and 5.084 mg/g respectively, suggesting that the pseudo-first order model is not suitable for the description of E2 adsorption on SpECs(1). SpECs(2) presented a good R^2 value (0.987), with the experimental and calculated values of the maximum adsorption capacity being closer than SpECs(1) (1.544 and 1.719 mg/g respectively). SpECs(3) gave similar results, with the R^2 value being 0.921 and $q_{e1,exp}$ and $q_{e1,cal}$ 1.533 and 1.146 mg/g respectively. Analysis with the pseudo-second order model followed, in order to define which model was a better fit for the adsorption of E2 on the SpECs material.

5.4.2.2. Pseudo-second order model

The pseudo-second order model describes adsorption processes that involve chemisorption where the adsorption rate is dependent on the adsorption capacity of the adsorbent and not on the concentration of the contaminant in target. The model is expressed as (*Equation 46*):^{58,77}

$$\frac{1}{q_t} = \frac{t}{q_e} + \frac{1}{k_2 q_e^2} \quad \text{Equation 46}$$

where q_t (mg/g) is the amount of solute adsorbed per mass of adsorbent after a certain contact time t (min), q_e (mg/g) is the amount of solute adsorbed at equilibrium, while k_2 (g/mg min) is the pseudo-second order equilibrium rate constant. The slope and intercept derived from the

plots of t/q_t versus t (**Figure 138**) were used to calculate the values of the maximum adsorption capacity $q_{e2,cal}$ and the rate constant k_2 which are presented in **Table 42**.

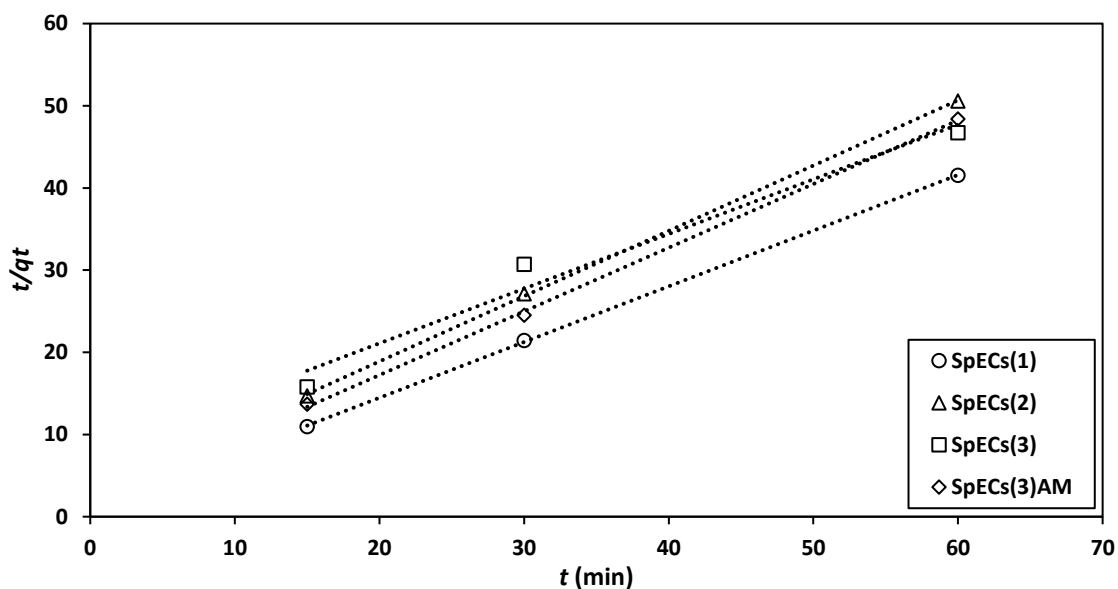


Figure 138: Kinetic investigations on the adsorption of E2 by different types of SpECs described by the pseudo-second order model.

Table 42: Kinetic parameters for E2 adsorption by different SpECs described by different models.				
model/ parameter	adsorbent			
	SpECs(1)	SpECs(2)	SpECs(3)	SpECs(3)AM
$q_{e,exp}$ (mg/g)	1.526	1.544	1.533	1.511
pseudo-first order				
$q_{e1,cal}$ (mg/g)	5.084	1.719	1.146	2.347
k_1	0.015	0.008	0.020	0.008
R^2	1	0.987	0.921	0.693
pseudo-second order				
$q_{e2,cal}$ (mg/g)	1.475	0.259	1.504	1.290
k_2	0.502	0.210	0.057	0.346
h (mg/g min)	1.092	0.332	0.128	0.576
R^2	0.999	0.999	0.971	0.999

The analysis using the pseudo-second order model gave higher R^2 values compared to the pseudo-first order model, with almost all SpECs giving R^2 values very close to unity. SpECs(1) and SpECs(2) gave the highest R^2 values, 0.999. With this model, SpECs(1) presented closer experimental and calculated maximum adsorption capacity values (1.475 and 1.526 mg/g respectively), concluding that this model is suitable to describe the E2 uptake by this material. Whereas SpECs(2) gave a high R^2 value, the difference between $q_{e1,exp}$ and $q_{e1,cal}$ was higher compared to the previous model, concluding that maybe the pseudo-first order model is better for the description of E2 adsorption on SpECs(2). It can also be concluded that the adsorption of E2 by SpECs(3) and SpECs(3)AM is described by the pseudo-second order model since both types presented higher R^2 values compared to the pseudo-first (0.971 and 0.999 respectively) combined with experimental and calculated maximum adsorption capacity values that were in close agreement. This confirms that for SpECs(1), SpECs(3) and SpECs(3)AM the adsorption process is controlled by chemisorption and that the reaction rate is dependent on the number of active sites on the surface of the material, meaning that the adsorption capacity of the sorbent controls the adsorption rate.

SpECs(3) and SpECs(1) were the materials that presented the highest maximum adsorption capacity values (1.50 and 1.48 mg/g respectively). Interestingly, the amination procedure on SpECs(3) did not add to the material's adsorption capacity with SpECs(3)AM presenting a capacity value of 1.29 mg/g.

The initial rate of sorption h (mg/g min) was also calculated using *Equation 47*:²⁵³

$$h = k_2 q_e^2 \quad \text{Equation 47}$$

The values of h (**Table 42**) showed a big variation with a range of 0.13 to 1.09 mg/g min for the different SpECs types tested. SpECs(3) presented the slowest adsorption rate, 0.13 mg/g min, which after their amination treatment was increased to 0.58 mg/g min confirming that the material became more efficient possibly by converting its active sites into more attractive ones for E2. SpECs(2) presented a value of 0.332 mg/g min whereas SpECs(1) presented the fastest rate, 1.09 mg/g min, which together with the high adsorption capacity values confirms that on the surface of SpECs(1) there are more available binding groups for E2 adsorption compared to the rest of the tested SpECs.

Research on testing the adsorption of E2 onto various materials such as graphene oxide nanosheets,³⁶² bone char,³⁵⁹ functionalised hydrochar³⁶³ or carbon nanotubes,^{351,358,364} revealed similar adsorption behaviours that follow the pseudo-second order kinetic model, suggesting that the mechanism of adsorption possibly involves chemical interactions with the material's surface, such as π - π interactions and hydrogen bonding (**Figure 139**).^{351,358,359,362-364}

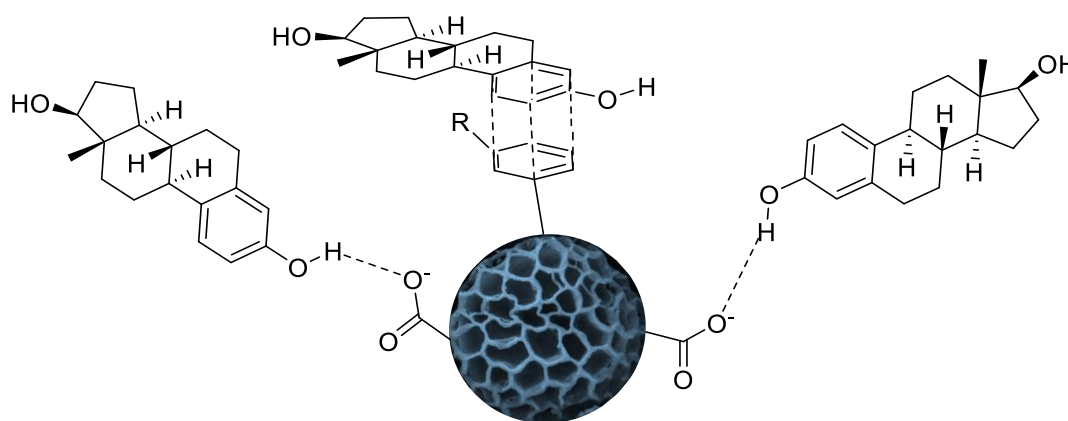


Figure 139: Schematic representation of the possible adsorption mechanisms happening between the SpECs surface and E2 molecules.

The different SpECs tested presented a relatively low maximum adsorption capacity (1.5 mg/g) compared to the values found in the literature for other materials; graphene oxide nanosheets presented a maximum adsorption capacity of 20.9 mg/g,³⁶² bone char 10.1 mg/g,³⁵⁹ functionalised hydrochar 47.4 mg/g³⁶³ and carbon nanotubes 18.9 mg/g.³⁴⁰ Since the parameters of the various experiments for the various materials were not identical (temperature, initial contaminant concentration, pH of solution, mass of sorbent), a conclusion cannot be made on whether SpECs were far less efficient in removing E2 from water.

5.4.2.3. Intraparticle diffusion model

In order to identify the diffusion mechanisms involved during the adsorption of E2, the data obtained were analysed with the intraparticle diffusion model. As defined previously, this model describes adsorption as a multi-step procedure, involving four diffusion steps: bulk diffusion, film diffusion, intraparticle diffusion and the adsorption of the contaminant molecules at the adsorbent's surface *via* ion exchange, chelation and/or complexation pathways.⁷⁴ Intraparticle diffusion can be quite a slow process, described by *Equation 48*:⁷⁸

$$q_t = k_i t^{0.5} + I \quad \text{Equation 48}$$

where q_t (mg/g) is the amount of solute adsorbed per mass of adsorbent at time t (min), k_i (mg/g min^{0.5}) is the rate constant for intraparticle diffusion model and I (mg/g) is the intercept which indicates the boundary layer thickness effect. A smaller I value indicates it is more likely that the kinetics are controlled only by intraparticle diffusion. The values of k_i and I can be obtained by the slope and intercept of the linear plot qt versus $t^{0.5}$ (**Figure 140**).

All the calculated parameters of the intraparticle diffusion model are presented in **Table 43**. It can be observed from the graph that the plots for SpECs(1) and SpECs(2) are linear whereas SpECs(3) and SpECs(3)AM presented multilinearity, meaning that the adsorption procedure involves more than one steps (a and b in the graph, **Figure 140**). The first linear part (a) corresponds to the migration of the E2 molecules from the solution to the surface of the SpECs through film diffusion whereas the second linear part (b) describes adsorption processes corresponding to intraparticle diffusion, possibly where the E2 molecules are gradually entering the pores of the SpECs.³⁶⁵ Since none of the lines passes through the origin it can be concluded that intraparticle diffusion is not the only rate controlling step of the adsorption of E2.

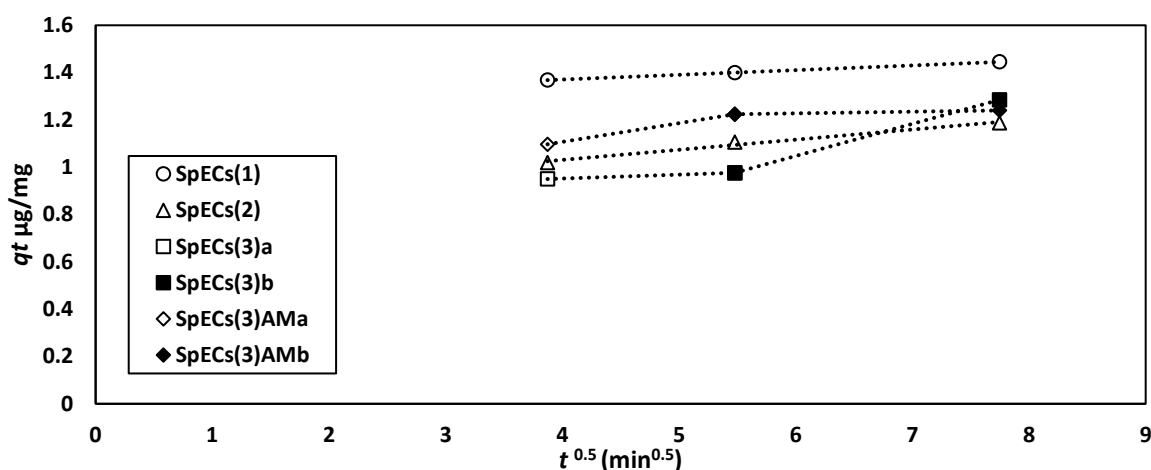


Figure 140: Intraparticle diffusion model for the adsorption of E2 onto different types of SpECs.

SpECs(3) presented a two-step diffusion process where the first step had a slower adsorption rate k_i compared to the second step (0.017 and 0.136 mg/g min^{0.5} respectively). On the contrary, the boundary layer effect presented a decrease in the second step; from 0.89 it went to 0.23. Both findings indicate that the E2 molecules are possibly forming a first layer on the surface

of SpECs(3) during the first step, which facilitates the further adsorption of the free E2 molecules and creates a second layer during the second step with the adsorption happening faster than before.

SpECs(3)AM also presented multilinearity with the first step having a faster adsorption rate than the second; 0.079 and 0.007 respectively. The increase in the I value from 0.79 to 1.19 indicated that the boundary layer effect increased during the second step, which together with the decrease in the k_i value proves that the boundary layer is affecting more the adsorption during the second step, thus slowing it down.

SpECs(1) presented the highest I value meaning that out of the four tested SpECs, it was the one with the greater effect of the boundary layer fact that was also confirmed by the low k_i value. SpECs(2) presented an average adsorption rate as well as an average boundary layer effect, 0.043 mg/g min^{0.5} and 0.86 respectively.

parameter	adsorbent					
	SpECs(1)	SpECs(2)	SpECs(3)		SpECs(3)AM	
			a	b	a	b
k_i (mg/g min ^{0.5})	0.020	0.043	0.017	0.136	0.079	0.007
I	1.29	0.86	0.89	0.23	0.79	1.19
R^2	1	0.987	1	1	1	1

5.4.3. Oestradiol adsorption isotherms

For the analysis of the distribution of the adsorbed E2 molecules between the aqueous phase and the SpECs particles during the equilibrium state, the Langmuir and Freundlich adsorption isotherm models were used.

As mentioned in the previous chapters, the Langmuir model describes the adsorption process as homogenous meaning that each active site on the surface of the SpECs can only be occupied

by one molecule of E2. For this analysis, the linear form of the model was used described by *Equation 49*:²⁵⁷

$$\frac{C_e}{Q_e} = \frac{C_e}{Q_m} + \frac{1}{K_L Q_m} \quad \text{Equation 49}$$

where C_e (mg/L) is the concentration of the adsorbate at equilibrium, Q_e (mg/g) is the amount of contaminant adsorbed per amount of adsorbent, K_L (L/mg) is the Langmuir adsorption equilibrium constant and Q_m (mg/g) is the maximum adsorption capacity of the material. Q_m indicates the amount of adsorbate needed for a complete monolayer and can be calculated from the slope of the line and K_L is a measure of the intensity of the adsorption process and can be calculated from the intercept.

Freundlich's model describes the adsorption process as multisite and reversible, assuming that the adsorbent's surface is heterogeneous, with active sites of various energies and thus affinity towards E2. The linearized form of the model is *Equation 50*:²⁵⁸

$$\log Q_e = \log K_F + \frac{1}{n_F} \log C_e \quad \text{Equation 50}$$

where Q_e (mg/g) is the amount of adsorbate adsorbed per amount of adsorbent, C_e (mg/L) is the equilibrium concentration and K_F ($\text{mg}^{(1-1/n)}/\text{gL}^{-1/n}$) and n_F are Freundlich's constants. K_F is related to the material's adsorption capacity and can be calculated from the intercept of the line, where n_F is the heterogeneity factor of adsorption sites indicating the adsorption intensity and it can be calculated from the slope.

The experimental procedure described in section 8.6.4 was followed, where 5 mL of E2 solutions of different concentrations (0.5 - 10 $\mu\text{g/mL}$) interacted with 20 mg of the different SpECs types for 10 minutes of contact time, at room temperature, under agitation. After filtration, the resulting solution was analysed for its E2 content and the linear forms of the two models were plotted in Excel (**Figure 141** and **Figure 142**).

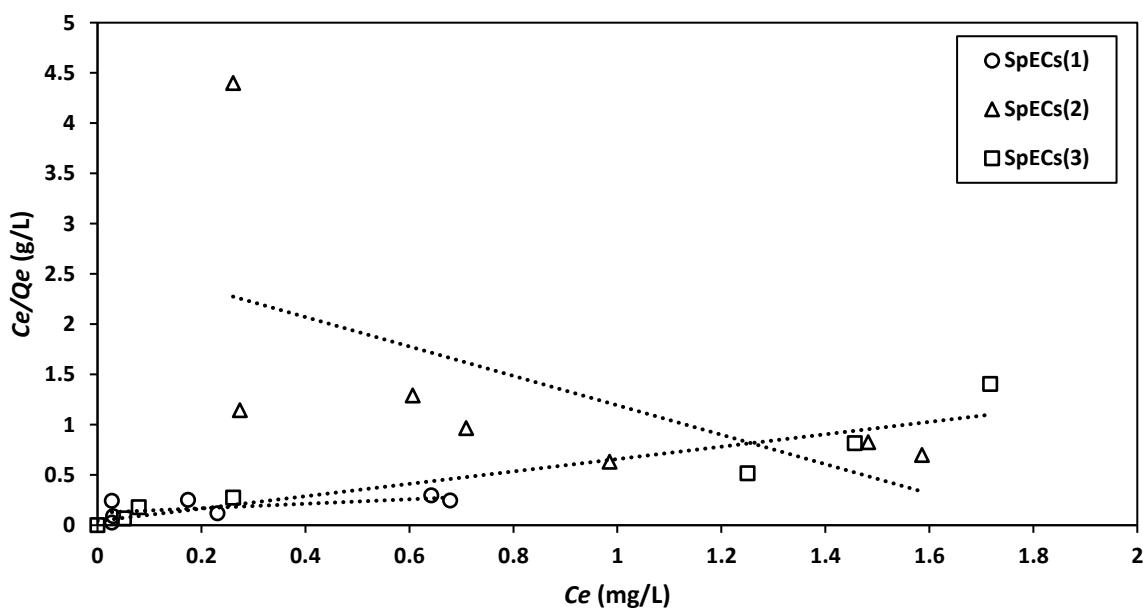


Figure 141: Langmuir linear adsorption isotherms for E2 uptake by different types of SpECs.

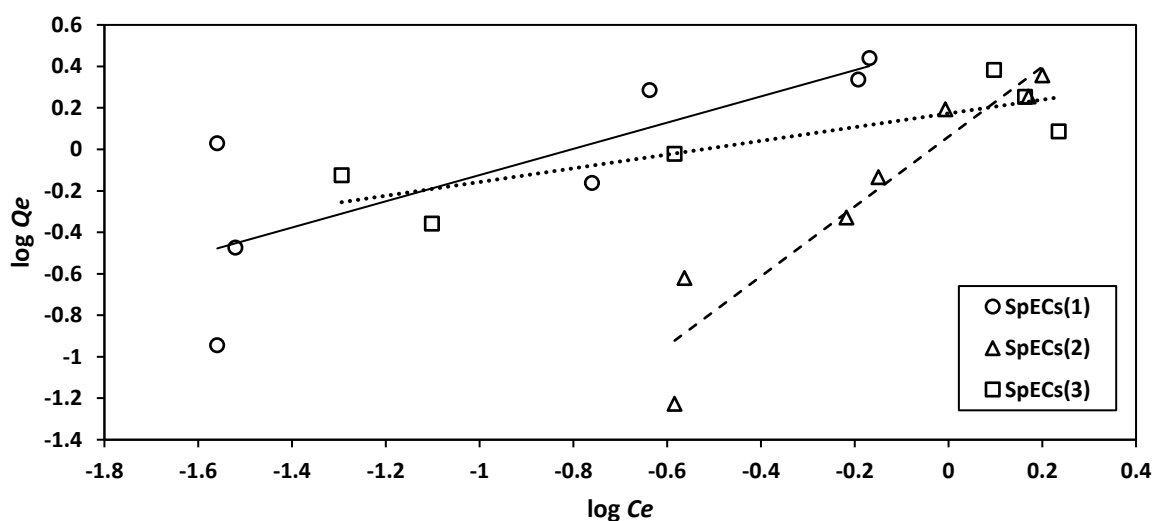


Figure 142: Freundlich linear adsorption isotherms for E2 uptake by different types of SpECs.

Q_e was calculated using Equation 51.

$$Q_e = \frac{(C_0 - C_e)V}{m} \quad \text{Equation 51}$$

where C_0 is the initial DCF concentration, V is the volume of the solution used and m is the mass of the adsorbent. Q_m was calculated from the slope of the Langmuir plot and K_L was calculated from the intercept. K_F was determined from the intercept of the Freundlich plot and n_F was calculated from the slope. All the parameters for both models (Langmuir and Freundlich) are presented in **Table 44**.

model	parameter	type		
		SpECs(1)	SpECs(2)	SpECs(3)
Langmuir	Q_m (mg/g)	4.480	0.683	1.620
	K_L (L/mg)	1.802	0.551	14.709
	R^2	0.391	0.345	0.860
Freundlich	K_F (mg ^(1-1/n) /gL ^{-1/n})	3.220	1.150	1.490
	$1/n_F$	0.632	1.680	0.331
	R^2	0.634	0.897	0.707

The Langmuir isotherms gave low R^2 values for SpECs(1) and SpECs(2) meaning that this model is not suitable to describe the adsorption procedure of E2 onto these two materials. The Freundlich model gave better R^2 values, not very close to unity, but higher than the Langmuir ones, indicating that the best fitting for the experimental data is the Freundlich isotherm model. For SpECs(3), the R^2 values were higher when the Langmuir model was applied but not far from each other, concluding that maybe for this type of SpECs, both models are able to describe

the adsorption of E2, result that is in agreement with other materials tested for E2 adsorption.^{359,363,364,366}

Since the Freundlich model presented a better fit for the experimental data, the heterogeneity of the SpECs surface can be confirmed, suggesting that the adsorption of the E2 molecules is reversible, by creating multilayers on the surface of the material. The Freundlich parameter $1/n$ is an indicator of the material's surface heterogeneity or the adsorption intensity. SpECs(1) and SpECs(3) gave values below 1, 0.632 and 0.331 respectively, which shows that the adsorption process is based on chemisorption. SpECs(3) presented a value closer to zero meaning that their surface is more heterogeneous compared to the other two types. The obtained value for SpECs(2) was above 1, indicating a cooperative adsorption of E2 onto its surface.

The K_F values for the different SpECs were relatively low compared to the values obtained for the other contaminants, triclosan and diclofenac, in the previous chapters. Their values showed a range between 1.15 and 3.22 $\text{mg}^{(1-1/n)}/\text{gL}^{-1/n}$, values much higher compared to bone char (0.35 $\text{mg}^{(1-1/n)}/\text{gL}^{-1/n}$) but much lower compared to other materials in the literature such as hydrochar,⁵⁰ molecularly imprinted particle embedded cryogels²⁹ or carbon nanotubes (16, 36 and 83 $\text{mg}^{(1-1/n)}/\text{gL}^{-1/n}$ respectively).^{43,57}

5.4.4. Oestradiol packed-bed studies

After the adsorption kinetics and isotherm investigation and after concluding that SpECs(1) is the most efficient type for E2 adsorption, the applicability of the material for contaminant adsorption on a bigger scale had to be tested. The procedure described in section 8.9 was followed, where a glass column (30 cm × 2.5 cm) was tightly packed with a layer of 0.2 g SpECs(1) (0.5 cm high) covered by a layer of 2 g low iron sand. A 6 mg/L solution of E2 passed through the SpECs(1) layer under gravity aiming to the complete saturation of the

material. Two different flow rates were tested (2 and 3 mL/min) by adjusting the column's tap. All data obtained were analysed with the Yoon-Nelson model (*Equation 52*), expressed as:⁸¹

$$C_t/C_0 = 1/[1 + \exp(K_{YN}\tau - K_{YN}t)] \quad \text{Equation 52}$$

where, C_t (mg/L) is the contaminant's concentration at time t (min), C_0 (mg/L) is the initial contaminant concentration, K_{YN} (min^{-1}) is the Yoon-Nelson rate constant and τ (min) is the time required for 50% adsorbate breakthrough. K_{YN} and τ can be calculated from the linear form of the equation (*Equation 53*) by plotting $\ln(C_t/(C_0 - C_t))$ versus t .

$$\ln\left(\frac{C_t}{C_0 - C_t}\right) = K_{YN}(t - \tau) \quad \text{Equation 53}$$

The sorption capacity of SpECs(1) q_0 (mg/g) was calculated by using *Equation 54*:

$$q_0 = \frac{C_0 Q \tau}{m} \quad \text{Equation 54}$$

where Q is the flow rate (L/min) and m (g) is the mass of the SpECs(1) used in the column.

This calculated value (q_0) can then be compared to the experimental one ($q_{0,exp}$), defined by

Equation 55:

$$q_{0,exp} = \frac{m_{E2\ ads}}{m_{SpECs}} \quad \text{Equation 55}$$

where $m_{E2\ ads}$ (mg) is the adsorbed E2 mass and m_{SpECs} (g) is the mass of the SpECs(1) used in the column. $m_{E2\ ads}$ was calculated using *Equation 56*.

$$m_{E2\ tot} = m_{E2\ el} - m_{E2\ ads} \quad \text{Equation 56}$$

where $m_{E2\ tot}$ is the total amount (g) of E2 that passed through the column and $m_{E2\ el}$ is the amount (g) of E2 eluted. $m_{E2\ tot}$ and $m_{E2\ el}$ (g) were calculated using *Equation 57* and *Equation 58*:

$$m_{E2\ tot} = V_{tot} * C_0 \quad \text{Equation 57}$$

$$m_{E2\ el} = C_{el} * V_{el} \quad \text{Equation 58}$$

where V_{tot} is the total volume of the contaminant solution that passed through the column, C_0 is the initial concentration of the contaminant, C_{el} is the concentration of the eluted solution and V_{el} is the volume of the eluted solution.

The SpECs(1) bed was covered with low iron sand (Fisher Scientific) to keep the particle bed tightly packed. The sand layer was checked individually for its E2 adsorption ability by passing through a solution of known E2 concentration (6 mg/L) and by comparing the initial and final concentration (C_f and C_0 respectively). The results presented in **Table 45** showed that the sand had no adsorption efficiency over E2.

Table 45: E2 adsorption efficiency of 5 g of low iron sand.			
fraction	volume (mL)	C_f (mg/L)	C_o (mg/L)
1	5	6.197	6.177
2	5	6.220	6.177
3	10	6.179	6.177
4	10	6.088	6.177
5	25	6.203	6.177
6	25	6.211	6.177
7	50	6.139	6.177

Initially, before the breakthrough point, while the effluent's E2 content was low, the effluent was collected in fractions of 5 mL. Later in the experiment, when the E2 concentration increased and was more stable, the fractions were collected in larger volumes (50 to 100 mL) and analysed with a UV-Vis spectrometer. The treated volume was plotted against the recovered E2 concentration divided by the initial E2 concentration and the breakthrough curves were formed in Excel.

Figure 143 shows the breakthrough curves for E2 at two different flow rates (2 and 3 mL/min) with the slower one presenting a slightly better performance. The graph shows that a complete saturation of the material did not happen until the end of the experiment at 2 L, indicating that even after treating 2 L of E2 solution, the SpECs surface still contained available active sites for the E2 molecules to bind with. The breakthrough point, where half of the initial concentration was able to pass through, occurred at around 1 L for both flow rates, indicating the good adsorption efficiency of the material.

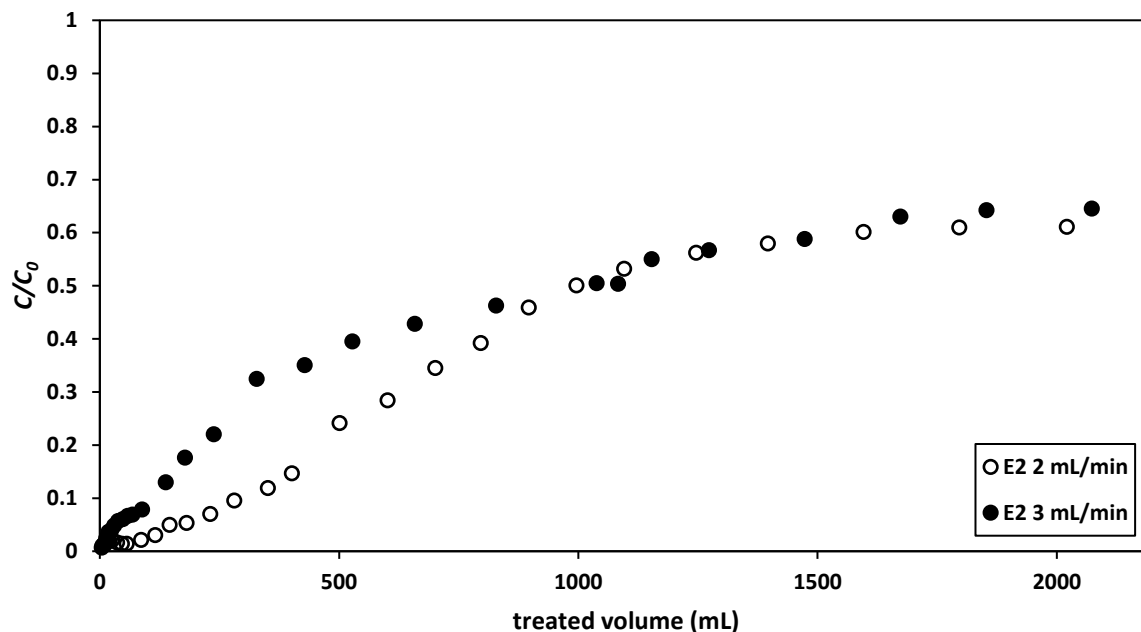


Figure 143: Breakthrough curves for 0.2 g packed SpECs(1) and E2 at 6 mg/L initial concentration (C_0) and at two different flow rates: 2 mL/min and 3 mL/min ($n=1$).

The Yoon-Nelson analysis (**Table 46**) showed that the adsorption capacities for both flow rates were close to the experimental ones, confirming the suitability of the model. Both flow rates presented a similar adsorption capacity, ~ 42 mg/g, indicating that a faster flow rate did not affect the material's efficiency, and similar breakthrough points at ~ 1 L of treated volume. Such a result would mean that in a larger scale and in terms of capacity, 1 kg of SpECs(1) would be able to equivalently treat 250 million litres of contaminated water at a concentration of ~ 0.12 $\mu\text{g/L}$ of E2 (mean value that was the reported concentration in hospital effluents²⁶¹) before reaching the breakthrough point. Such a quantity of SpECs(1) would therefore be able to treat 1200 million litres of wastewater at a concentration of 25 ng/L, an earlier stated mean concentration.³³³ The Massachusetts Water Resources Authority²⁶² reported annual water consumption of hospitals ranging from 15 million gallons (~ 68 million L) to 145 million gallons (~ 660 million L), of which approximately 42% is for sanitary purposes.²⁶³ This would

mean that the range of SpECs(1) required annually for treating these hospitals would be from ~1 - 3 kg, in terms of material capacity.

flow rate	K_{YN} (min^{-1})	τ (min)	τ_{exp} (min)	R^2	q_0 (mg/g)	$q_{0,exp}$ (mg/g)
2 mL/min	0.005	640.1	480	0.817	41.7	37.7
3 mL/min	0.006	437.6	330	0.747	42.5	38.6

5.4.4.1. Regeneration and reusability of SpECs

After the packed-bed study, the SpECs(1) bed was washed with approximately 150 mL of milliQ water in order to test if the adsorbed E2 molecules can migrate from the adsorbent back into solution and subsequently contaminate clean water. **Figure 144** shows the breakthrough curve obtained in the previous experiment, continuing into the region of the milliQ water washings, clearly indicating that the adsorbed molecules are strongly attached onto the surface of the SpECs(1) and are not able to pass through the water solution.

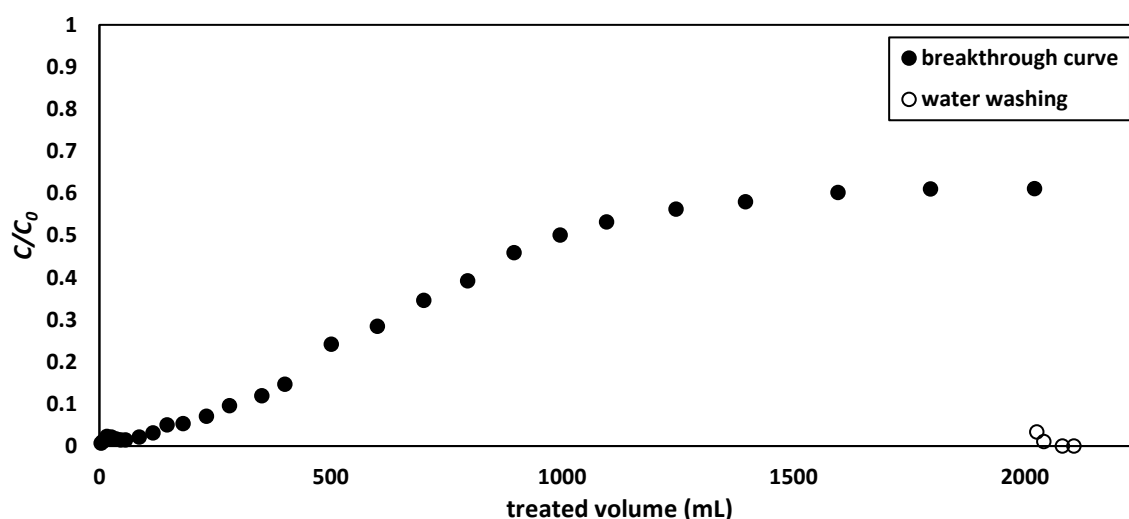


Figure 144: Packed SpECs(1) washed with milliQ water after the completion of the breakthrough curve for E2 adsorption.

Right after the milliQ water washings, the packed material was washed with absolute ethanol in order to remove all of the adsorbed E2 and test the reusability of the SpECs. The washed packed SpECs(1) were reused for two more cycles, under two different flow rates (2 and 3 mL/min), and their adsorption capacity was compared between the three cycles. **Figure 145** shows the breakthrough curves for all the three cycles at the flow rate of 2 mL/min, whereas **Figure 146** presents the breakthrough curves for the flow rate of 3 mL/min. It is evident from the graphs that in the slower flow rate the material behaved slightly differently in each cycle, with the first cycle being the most efficient, whereas for the faster flow rate the three cycles were similar.

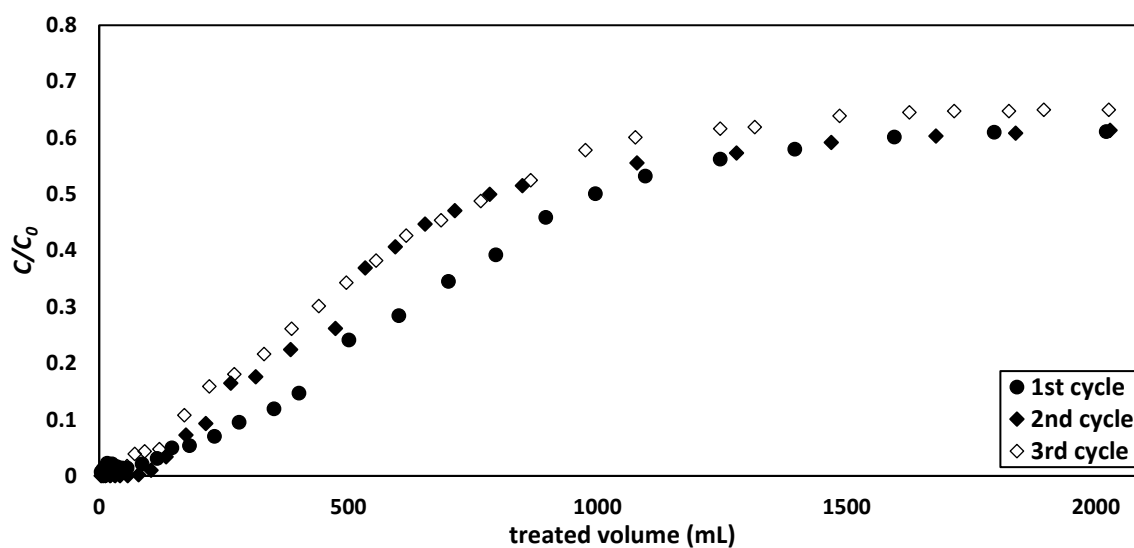


Figure 145: Breakthrough curves for 0.2 g packed SpECs(1) and E2 at 6 mg/L initial concentration (C_0) at a flow rate of 2 mL/min for three cycles of material reuse.

Analysis with the Yoon-Nelson model revealed that indeed for the slow flow rate, SpECs(1) were most efficient during the first cycle (**Table 47**). Their adsorption capacity presented its highest value during the first cycle of use, 41.4 mg/g, it decreased during the second cycle, 35.0 mg/g and finally reached 34.0 during the third cycle. The breakthrough point for this flow rate showed a variation as well, where during the first cycle it presented its highest value,

640 minutes (~800 mL of treated volume) that was later decreased to ~545 minutes (~780 mL of treated volume) for the two cycles of reuse.

On the contrary, the faster flow rate gave different results; during the first cycle of use, SpECs(1) presented a maximum adsorption capacity of 42.5 mg/g which increased at the second cycle, 50.5 mg/g and finally reached 39.8 mg/g for the last cycle. A similar pattern was observed for the breakthrough point where during the first cycle it presented a value of 438 minutes, during the second cycle it presented its highest value, 546 minutes and decreased again to a value close to the initial, 432 minutes. In terms of treated volume though, the breakthrough point remains consistent at ~1 L for the two first cycles and then is reduced to ~830 mL for the third cycle.

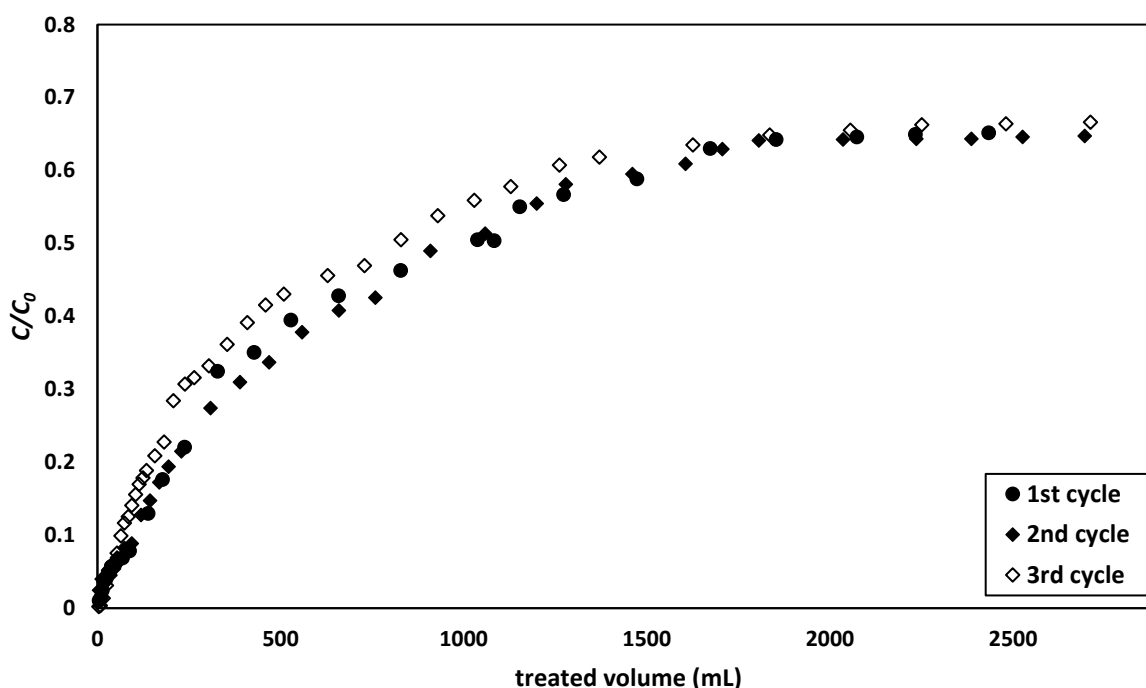


Figure 146: Breakthrough curves for 0.2 g packed SpECs(1) and E2 at 6 mg/L initial concentration (C_0) at a flow rate of 3 mL/min for three cycles of material reuse.

A comparison between the maximum adsorption capacities for each flow rate is presented in **Figure 147**, where it is evident that the two flow rates did not affect the material's adsorption capacity during the first cycle, but during the two following cycles a great variation can be observed. Taking into account the R^2 values obtained from the analysis with this model, initially being closer to unity but later on being much lower, it can be concluded that the two cycles of reuse do not present a good fitting to the model.

Table 47: Yoon-Nelson parameters and sorption capacities for the adsorption of E2 (6 mg/L) by 0.2 g SpECs(1) at two different flow rates.

flow rate	K_{YN} (min^{-1})	τ (min)	τ_{exp} (min)	R^2	q_0 (mg/g)	$q_{0,exp}$ (mg/g)
2 mL/min	0.005	640.1	480	0.817	41.37	37.7
1 st reuse	0.005	538.0	381	0.593	35.01	33.7
2 nd reuse	0.005	554.4	400	0.555	34.02	34.1
3 mL/min	0.006	437.6	330	0.747	42.51	38.6
1 st reuse	0.004	545.5	315	0.734	50.53	42.6
2 nd reuse	0.005	432.4	288	0.500	39.80	37.7

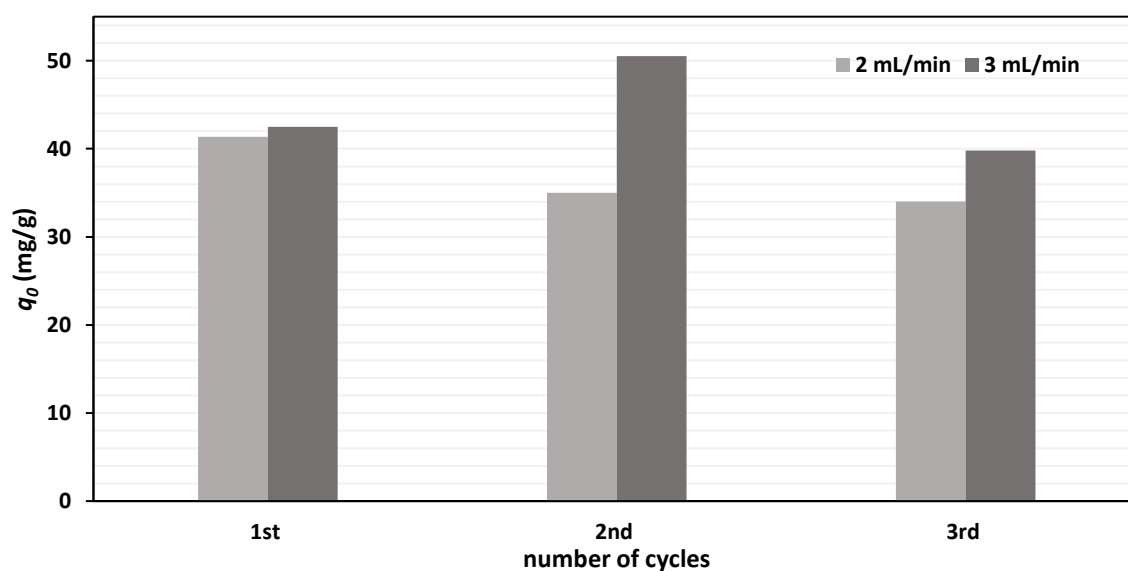


Figure 147: Comparison of the E2 adsorption capacity (q_0) of SpECs(1) between each cycle of reuse.

5.5. Conclusions

E2 is the active ingredient of many pharmaceuticals prescribed for problems associated with menopause and hypoestrogenism. It is the most active natural steroidal hormone and it can have permanent effects on the developing brain. The main source of E2 entering the environment is human and animal faeces and urine and the main reason for its presence in the aquatic ecosystems is its incomplete removal during the process of WWT. Even at very low levels of ng/L, E2 can provoke problems to non-target aquatic organisms such as making fish developing intersex characteristics or failing to develop normal secondary characteristics leading to changes in their reproduction.

The adsorption of E2 follows the pseudo-second order kinetics model for the majority of the tested SpECs, especially for SpECs(1), SpECs(3) and SpECs(3)AM. The adsorption process involves chemisorption and the adsorption capacity of the SpECs is what affects the adsorption rate. The maximum adsorption capacity was ~1.5 mg/g for the majority of the tested SpECs, a value relatively low compared to the literature on other materials,^{351,358,359,362-364} but as stated before, the experimental conditions were not identical to the ones used here, and a much higher value was achieved experimentally using the packed-bed studies (42.5 mg/g).

Analysis with the intraparticle diffusion model revealed that SpECs(1) and SpECs(2) involve only one diffusion step during the E2 adsorption whereas SpECs(3) and SpECs(3)AM involve a two-step diffusion process. For SpECs(3), it was concluded that the adsorption of E2 is happening in multilayers where during the first step of the diffusion process, E2 molecules are forming a first layer on its surface, which facilitates the further adsorption of the free E2 molecules and then creates a second layer during the second step.

The adsorption isotherm experiments indicated that the majority of SpECs presented a better fitting to the Freundlich model whereas for SpECs(3) it was concluded that both the Langmuir

and Freundlich models are able to describe the adsorption of E2, a result that is in agreement with other materials tested for E2 adsorption.^{359,363,364,366} The heterogeneity of the SpECs surface was confirmed, with SpECs(3) being the most heterogeneous compared to the other two types, suggesting that the adsorption of the E2 molecules is reversible, by creating multilayers on the surface of the material. The K_F values obtained for the adsorption of E2 by the tested SpECs were relatively low (1.15 and 3.22 $\text{mg}^{(1-1/n)}/\text{gL}^{-1/n}$) compared to the values obtained for the other contaminants, TCS and DCF but much higher compared to bone char (0.35 $\text{mg}^{(1-1/n)}/\text{gL}^{-1/n}$). Other materials in the literature showed higher K_F values such as hydrochar,⁵⁰ molecularly imprinted particle embedded cryogels²⁹ or carbon nanotubes (16, 36 and 83 $\text{mg}^{(1-1/n)}/\text{gL}^{-1/n}$ respectively) but with differences in the experimental procedures.^{43,57}

SpECs(1) were tested under a packed-bed setup where a flow rate of 3 mL/min presented a maximum adsorption capacity of 42.5 mg/g with a breakthrough point at 440 minutes. The material was efficiently regenerated with pure ethanol and used for two more cycles, where it presented a variation in its maximum adsorption capacity; 50.5 mg/g for the second cycle and 39.8 mg/g for the last cycle, confirming its reusability potential.

All different types of SpECs tested exhibited a good level of adsorption capacity for E2 but had far longer contact times for complete contaminant removal, on the scale of hours rather than minutes. This was much slower adsorption rates when compared to the previously examined compounds, DCF and TCS. It has been shown that the material capacity for adsorption for all the contaminants is far beyond what would be required for water concentrations found in hospital effluent or surface waters. However, it was determined that the rate of effluent from a hospital would be approximately (55 - 530 L/min), which clearly displays the need for a fast rate of adsorption being of far higher importance than maximum capacity. SpECs(1) showed the best efficiency, achieving 90% E2 removal in 15 minutes and complete E2 removal in four hours. Clearly, this would not meet the requirements for treating

such a fast-flowing body of water and maybe a different treatment setup, more suitable for the material's potential, would be better for this type of adsorbent.

6. Phosphates

6.1. Introduction

No life, even microbial life, is possible without phosphorus. Phosphorus is a rather scarce element in the biosphere but an essential one since it participates in vital functions such as replication and transcription of RNA and DNA, metabolism and contribution to cell structure.^{367,368} Both DNA and RNA depend on phosphates since they are formed by mononucleotide units that are linked through phosphodiester bonds. Phosphates are also responsible for the energy that all living organisms require. This energy comes from a breaking down reaction of adenosine triphosphate to adenosine diphosphate; when the phosphate bond breaks, energy is released.^{369,370} In cells, phosphates are also present in the form of phospholipids, which are the major components of the cell membranes.^{371,372}

Phosphorus can be found on earth in both the trivalent negative and the pentavalent positive states, but the form that is most commonly found is the orthophosphate ion (PO_4^{3-}) which composes minerals belonging to the apatite group.^{372,373} In water, phosphorus may be present in different forms of soluble phosphates, H_3PO_4 , H_2PO_4^- , HPO_4^{2-} and PO_4^{3-} , depending on the pH.³⁷⁴ Other species of phosphorus existing in waters are organic phosphates and polyphosphates, mainly deriving from detergents, with both forms being able to gradually hydrolyse to orthophosphates.

Even though phosphorus is essential for living cells, high levels of phosphate in surface water of rivers, lakes and seas can cause eutrophication. Eutrophication is mainly caused by over-enrichment with phosphate, affecting rivers, lakes and coastal oceans mainly by influencing the algal or the phytoplankton growth. Such an issue can lead to a series of other problems such as depletion of the dissolved oxygen, damage and loss of coral reefs and plant beds,

depopulating of aquatic species leading to reduction of the water quality and accelerating water scarcity.^{375–378} According to Awual *et al.* (2011), in order to prevent eutrophication the levels of phosphates present in water should be less than 50 µg/L, whereas Yao *et al.* (2011) and Kilpima *et al.* (2014) report that a concentration higher than 20 µg/L is enough to trigger the problem of eutrophication.^{379–381}

Phosphates can end up in water through agricultural routes as well as urban activities such as industrial and domestic wastewaters. Excess use of fertilisers and excess produce of manure leads to a phosphorus surplus which accumulates in soil and can be easily transported to the aquatic environment *via* treated sewage effluents or fertiliser spreading and dissolution in rain water.³⁷⁸ Wastewater deriving from domestic use involves water from washings, bathing, cleaning sewage or septic systems.³⁸² Industrial wastewater that contains high loading of phosphorus usually involves effluents from mining industries, metallurgy, pharmaceutical, pigment, meat processing, petrochemical and textile industries.^{383–385} The different sources of phosphates in the environment are presented in **Table 48** together with the loading they provide.

Table 48: The different sources and concentrations of phosphates in the aquatic environment. ³⁸⁶		
wastewater source	concentration	reference
domestic	3 - 10 mg/L	Hilbrandt <i>et al.</i> ³⁸⁷
general sources	200 mg/L	Rajmohan <i>et al.</i> ³⁸⁸
fertilizer industry	1000 mg/L	Rajmohan <i>et al.</i> ³⁸⁸

Phosphates deriving from fertilisers lead to harmful cyanobacterial blooms (blue green algae) responsible for the production of a variety of compounds that can affect the taste and odour of water but are also responsible for producing cyanotoxins, which are extremely toxic.^{389–391} *Microcystis aeruginosa* is a very toxic and harmful algae thriving in eutrophic environments,

impacting the appearance and smell of waters.³⁹² Microcystins are a group of toxins that are the main metabolites of harmful algae, they are of high concern due to their ubiquity and high toxicity and they can accumulate in the aquatic environment leading to a decrease in aquatic diversity.^{391,393} There is also a direct risk to human populations as microcystins can enter the food chain through irrigation and drinking water, hence affecting human health.³⁹⁴

There is a growing interest in the development of new technologies to tackle phosphate removal from wastewaters, with three method categories being the most popular: chemical, physical and biological.^{386,395,396} Chemical and physical processes include methods such as reverse osmosis, ion exchange, electrocoagulation, electrodialysis, precipitation, filtration, addition of a variety of metallic salts.^{380,397,398} The main drawback for technologies involving chemical procedures is the amount of sludge produced from phosphorus precipitation which can then lead to further pollution.³⁸⁰ The need for further treatment, the high cost of these procedures and the low removal efficiency make them not the ideal candidate for phosphorus removal. Physical treatments for phosphorus can be extremely expensive with examples being reverse osmosis and electrodialysis. The biological methods mainly involve anaerobic-oxic and extended anaerobic sludge contact processes.^{382,399} These biological procedures involve costly treatments with sensitive operation parameters making the method's efficiency unstable.⁴⁰⁰ Adsorption procedures may be preferable since they promise the potential of both low cost and high efficiency but also they provide the advantage of no sludge formation.^{105,401-404}

6.2. Aims and Objectives

The aims in this chapter are to investigate the adsorption efficiency of the different SpECs types for phosphates and examine the effect that deposition of iron salts or oxides on the surface of the material will have on their adsorption efficiency. Different iron loading methods will be

tested to determine the optimal percentage of iron loading to induce maximum adsorption efficiency for phosphates.

6.3. Phosphates detection and quantification

6.3.1. Phosphates colorimetric detection

In order to detect the total phosphate content in the experimental samples of this chapter, several methods were tested, either involving reactions with malachite green or molybdenum blue. After many trials, a colorimetric protocol described in ‘Standard Methods for the Examination of Water and Wastewater’⁴⁰⁵ was followed based on the well-known molybdenum blue reaction, with all the details described in section 8.8.1.

6.3.1.1. The molybdenum blue reaction

The molybdenum blue reaction is a widely recognised procedure used in the detection of orthophosphates (including other labile phosphorus species) with the use of spectrophotometry.^{406,407} The reaction was first mentioned by Scheele back in 1783 but it is mainly attributed to Berzelius who was the first to synthesise $\text{Mo}_5\text{O}_{14}\cdot n\text{H}_2\text{O}$ in 1826.⁴⁰⁸ In 1934, Keggin revealed the structures of several 12-heteropoly acids (containing a hetero-atom) and the suggested ion was named after him, Keggin ion $[\text{XM}_{12}\text{O}_{40}]^{n-}$ (**Figure 148**).^{409,410}

The molybdenum blue reaction is a two-step procedure in which the Keggin ion is formed around the analyte giving a structure that is called 12-phosphomolybdic or molybdophosphoric acid (12-MPA). This acid, also called heteropoly acid, is then reduced to form a product that is of very deep blue colour called phosphomolybdenum blue.⁴⁰⁷ The two steps of the molybdenum blue reaction are the following:

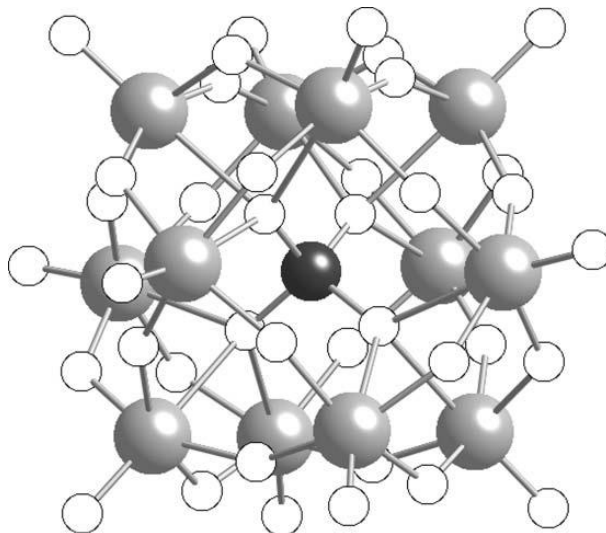


Figure 148: Structure of the Keggin ion $[\text{XM}_{12}\text{O}_{40}]^{n-}$.^{410,411}

For the experiments described in this chapter, a solution of mixed reagents was prepared, containing a mixture of molybdenum and antimony in an acidic environment. The reductant chosen was ascorbic acid which in combination with Sb(III) can reduce 12-MPA in about ten minutes without heating, generating a product that can remain stable for hours.⁴¹²⁻⁴¹⁴ After the addition of 1 mL of the mixed reagent into 4 mL of the phosphate sample, the solution was left to develop its deep blue colour (**Figure 149**). The optimal time for this colour development was measured to be 21 minutes, meaning that the colour was stabilised and no difference in its absorbance was observed after that moment on.

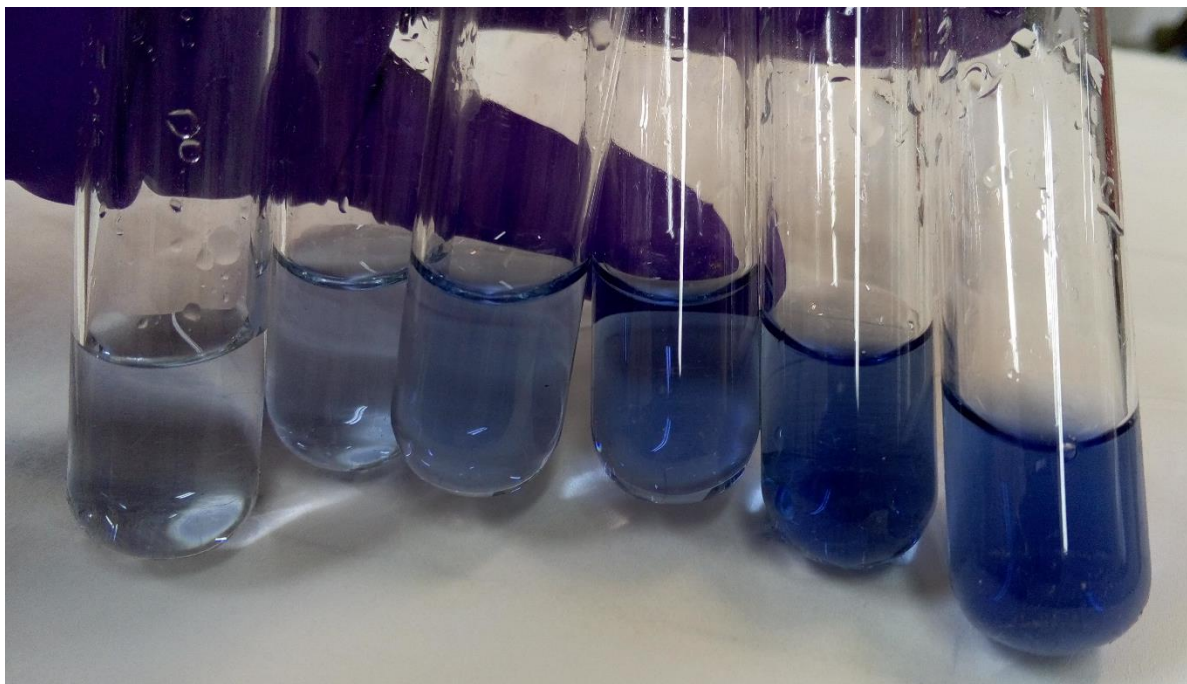


Figure 149: Samples containing different concentrations of phosphates (L to R: 0.5, 1, 2, 4, 6 and 8 mg/L) and the blue colour developed after 21 minutes of addition of the mixed reagent.

6.3.1.2. Phosphates colorimetric quantification

A stock solution of potassium phosphate in milliQ water was prepared which was further diluted to give a range of concentrations from 0 to 10 $\mu\text{g/mL}$. All the solutions for the standard points were prepared in triplicate and their analysis was conducted with a UV-Vis spectrophotometer in the IR region, at 890 nm. Baseline calibration was performed using blank solutions of milliQ water together with the mixed reagent (chromophore reagent), meaning that a concentration of 0 $\mu\text{g/mL}$ gave absorbance values of zero with no deviation from this value. A reference curve was created by plotting the mean values of the absorbance of the different solutions *versus* the concentration of potassium phosphate.

The reference curve is presented in **Figure 150** and *Equation 59* was used for the calculations of phosphate concentrations (x) in all the experiments in this chapter, with LOD and LOQ values at 0.004 $\mu\text{g/mL}$.

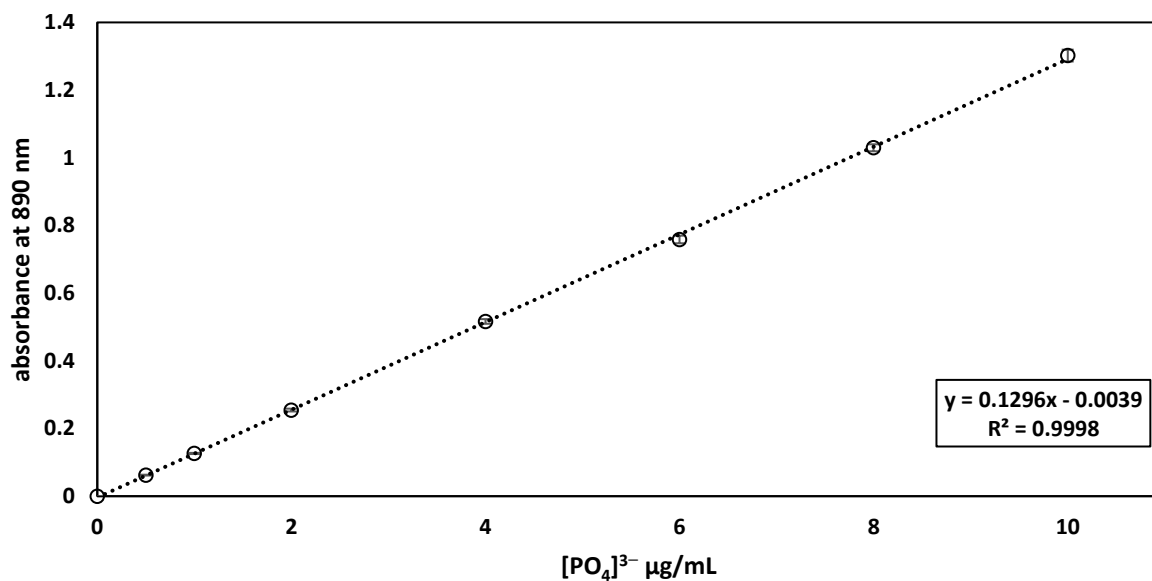


Figure 150: $[\text{PO}_4]^{3-}$ reference curve at the concentration region of 0 - 10 $\mu\text{g/mL}$ at 890 nm detection wavelength (LOD = LOQ = 0.004 $\mu\text{g/mL}$, $n=3$).

$$y = 0.1296x - 0.0039$$

Equation 59

6.4. Phosphates adsorption experiments

The phosphates adsorption experiments were conducted in accordance with the protocol described in section 8.8.3. Briefly, a solution of known phosphates concentration (6 $\mu\text{g/mL}$, 5 mL) was left in contact with the different extraction types of SpECs (20 mg) for different periods of time (30 - 90 minutes). After filtration, 4 mL of the resulting solution was added to 1 mL of the mixed reagent (see section 8.8.1 for more information) and after the colour development, the absorbance of the final solution was measured. A comparison against the initial phosphates concentration results in the phosphates adsorption percentage which was calculated with *Equation 60*:

$$\% \text{ phosphates ads.} = [(C_0 - C_{eq})100]/C_0 \quad \text{Equation 60}$$

where C_0 is the initial and C_{eq} is the final $[\text{PO}_4]^{3-}$ concentration.

In order to investigate the adsorption mechanisms taking place during the phosphates uptake and the potential rate controlling steps, all experimental data were analysed with the pseudo-first order and pseudo-second order kinetic models.

The pseudo-first order model, or Lagergren's model,⁷⁶ describes adsorption that occurs through diffusion through the interface, assuming that adsorption is dependent on the adsorption capacity of the adsorbent. The linear form of the equation is expressed as *Equation 61*.^{58,74}

$$\ln(q_e - q_t) = \ln q_e - k_1 t \quad \text{Equation 61}$$

where q_t (mg/g) is the amount of solute adsorbed per mass of adsorbent after a certain contact time t (min), q_e (mg/g) is the amount of solute adsorbed at equilibrium and k_1 (min^{-1}) is the pseudo-first order rate constant.

From the plot $\ln(q_e - q_t)$ versus t the values of k_1 (slope) and $\ln q_e$ (intercept) can be determined, from which the value of the maximum adsorption capacity $q_{e1,cal}$ is calculated.

The experimental maximum adsorption capacity was calculated using *Equation 62*.

$$q_{e1,exp} = [\text{phosphates}] * \frac{V}{m_{SpECs}} \quad \text{Equation 62}$$

where $[\text{phosphates}]$ ($\mu\text{g/mL}$) is the concentration of phosphates in the solution, V (mL) is the volume of the solution and m_{SpECs} (mg) is the mass of the SpECs used.

The pseudo-second order model describes adsorption processes that involve chemisorption and assumes that the rate of adsorption is dependent on the adsorption capacity of the adsorbent and not the concentration of the adsorbate. It is expressed as (Equation 63):⁷⁷

$$\frac{1}{q_t} = \frac{t}{q_e} + \frac{1}{k_2 q_e^2} \quad \text{Equation 63}$$

where q_t (mg/g) is the amount of solute adsorbed per mass of adsorbent after a certain contact time t (min), q_e (mg/g) is the amount of solute adsorbed at equilibrium, while k_2 (g/mg min) is the pseudo-second order equilibrium rate constant. The slope and intercept derived from the plots of t/q_t versus t give the values of the maximum adsorption capacity $q_{e2,cal}$ and the rate constant k_2 .

6.4.1. Cotton interference in phosphates adsorption experiments

As with the previous contaminants, cotton wool was tested for its adsorption efficiency against phosphates and whether its use for the pipette microfiltration would affect the final phosphates concentration. A phosphates solution of known concentration (6 $\mu\text{g/mL}$) was prepared and divided into six portions of 4 mL. The absorbance of three portions was measured directly after preparation (and after the colour development procedure) without any filtration whereas the absorbance of the rest was measured after filtration through cotton wool followed by the colour development. The results are presented in **Table 49**, showing that the cotton wool did not present any adsorption properties against phosphates, making it a good material for filtration.

Table 49: Comparison of phosphates absorbance signals before and after filtration.	
no filtration	after cotton wool filtration
0.732	0.735
0.752	0.749
0.748	0.754

6.4.2. Phosphates adsorption onto unmodified SpECs

The influence of contact time on phosphates adsorption was tested for SpECs(1-3) and is presented in **Figure 151**. All three SpECs types showed little to no adsorption efficiency for phosphates, with only SpECs(3) presenting a low adsorption of 5% phosphate removal after 90 minutes of contact time.

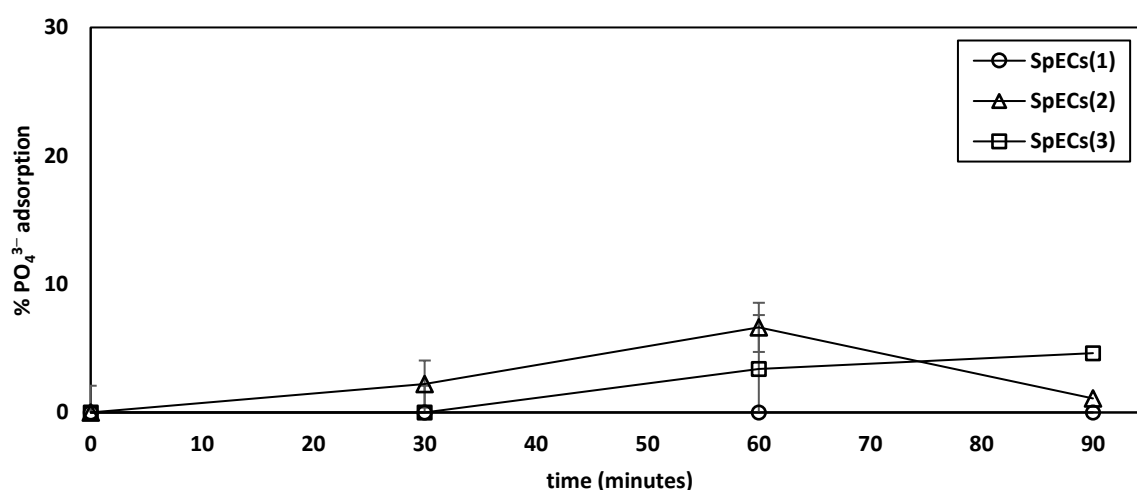


Figure 151: Effect of contact time on phosphates adsorption by different SpECs types, graph zoomed in the region of 0 - 30% of phosphates removal (PO_4^{3-} dose: 6 mg/L, $n=3$).

6.4.3. Phosphates adsorption onto Fe loaded SpECs

Since all three types of SpECs exhibited no adsorption efficiency for phosphates, the SpECs were then loaded with iron to give a surface which is highly positively charged. As the contaminant is negatively charged, the positive surface would attract the negative contaminant molecules by electrostatic interactions and increase the material's efficiency (**Figure 152**).

Several different methods were tested for iron loading onto SpECs with regards to the solvent used, which are described in section 8.2.5.

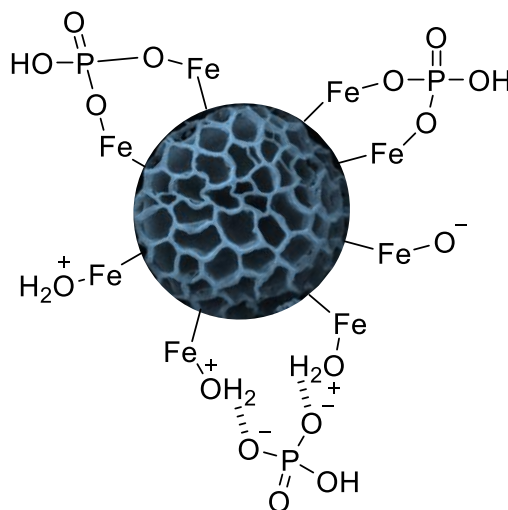


Figure 152: Schematic representation of the possible adsorption mechanisms happening between the iron loaded SpECs surface and phosphates.

6.4.3.1. Phosphates adsorption onto Fe/water loaded SpECs

The iron salts ($\text{FeCl}_3 \cdot 6\text{H}_2\text{O}$ and $\text{FeCl}_2 \cdot 4\text{H}_2\text{O}$) were dissolved in water following the procedure described in section 8.2.5.1, and SpECs(1), SpECs(2) or SpECs(3) were added into the solution and left under stirring overnight. After filtration, washing and drying under air flow, the material was ready for use. The elemental analysis of the final products, together with the ICP-OES analysis for iron loading are presented in **Table 50**.

From the ICP-OES results (**Table 50**), it is evident that after the treatment of SpECs with Fe salts, the material was successfully loaded with a small percentage of iron crystals. SpECs(2) exhibited the strongest affinity for Fe loading, 2.9%, whereas SpECs(3) presented the lowest Fe loading, 0.6%.

Table 50: Results obtained from elemental analysis for CHN and ICP-OES for Fe for SpECs and Fe loaded SpECs in water.				
sample	%C	%H	%N	%Fe
SpECs(1)	58.65	7.24	0.12	0.00
M9SpECs(1)	58.78	7.47	0.00	1.67
SpECs(2)	59.00	8.89	0.56	0.00
M11SpECs(2)	51.94	7.68	0.91	2.93
SpECs(3)	60.10	7.57	0.17	0.00
M10SpECs(3)	60.66	6.74	0.15	0.63

6.4.3.1.1. Effect of contact time on phosphates adsorption onto Fe/water loaded SpECs

After iron loading, all different Fe loaded SpECs were tested for their phosphate adsorption efficiency and the results are presented in **Figure 153**. Compared with untreated SpECs (**Figure 151**) it is evident that the iron-loaded material's phosphate adsorption efficiency is improved. Fe-SpECs(1) [M9SpECs(1)] exhibited the highest efficiency with 50% phosphates removal in half an hour of contact time and 70% removal after 90 minutes of contact time.

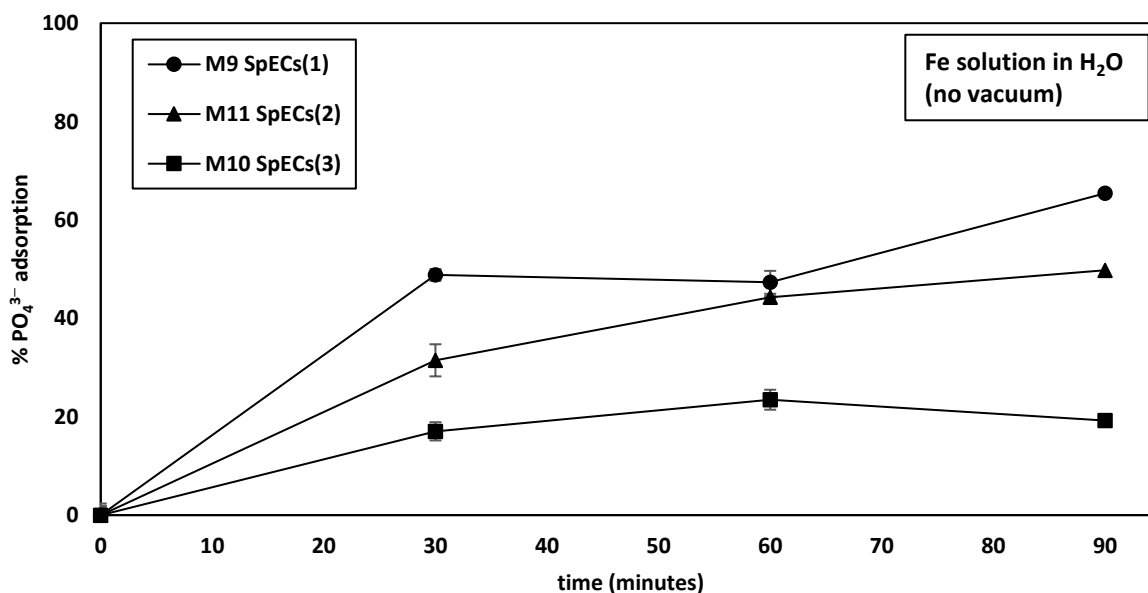


Figure 153: Effect of contact time on phosphates adsorption by Fe loaded SpECs in water without vacuum (PO_4^{3-} dose: 6 mg/L, n=3).

The same iron loading procedure was followed as previously described in section 8.2.5.2, but this time the Fe loading was conducted under vacuum overnight, in order to test whether the loading percentage would be higher and whether this would affect the phosphate adsorption properties of the SpECs. After filtration, washing and drying under air flow, the material was analysed with elemental analysis and ICP-OES analysis for iron loading and the results are presented in **Table 51**.

sample	%C	%H	%N	%Fe
SpECs(1)	58.65	7.24	0.12	0.00
M20SpECs(1)	55.50	7.01	0.17	3.33
SpECs(2)	59.00	8.89	0.56	0.00
M21SpECs(2)	53.19	7.42	1.11	3.38
SpECs(3)	60.10	7.57	0.17	0.00
M22SpECs(3)	60.06	7.60	0.11	1.77

From the ICP-OES results (**Table 51**), it is evident that after the treatment of SpECs with Fe salts under vacuum, the material was successfully loaded to a higher percentage of iron compared to the procedure without vacuum. SpECs(1) and SpECs(2) (M20 and M21) exhibited similar iron loadings of around 3.35% whereas without vacuum the percentage for SpECs(1) was almost half (1.7%) and for SpECs(2) was quite close, around 3%. For SpECs(3), this technique increased the iron loading from 0.6% without vacuum to 1.8% with the use of vacuum.

Since the data obtained displayed that a higher Fe loading was achieved under vacuum, it was decided that the iron loading procedure should be conducted under vacuum. The resulting Fe-loaded SpECs were tested for their adsorption efficiency against phosphates and the results are presented in **Figure 154**.

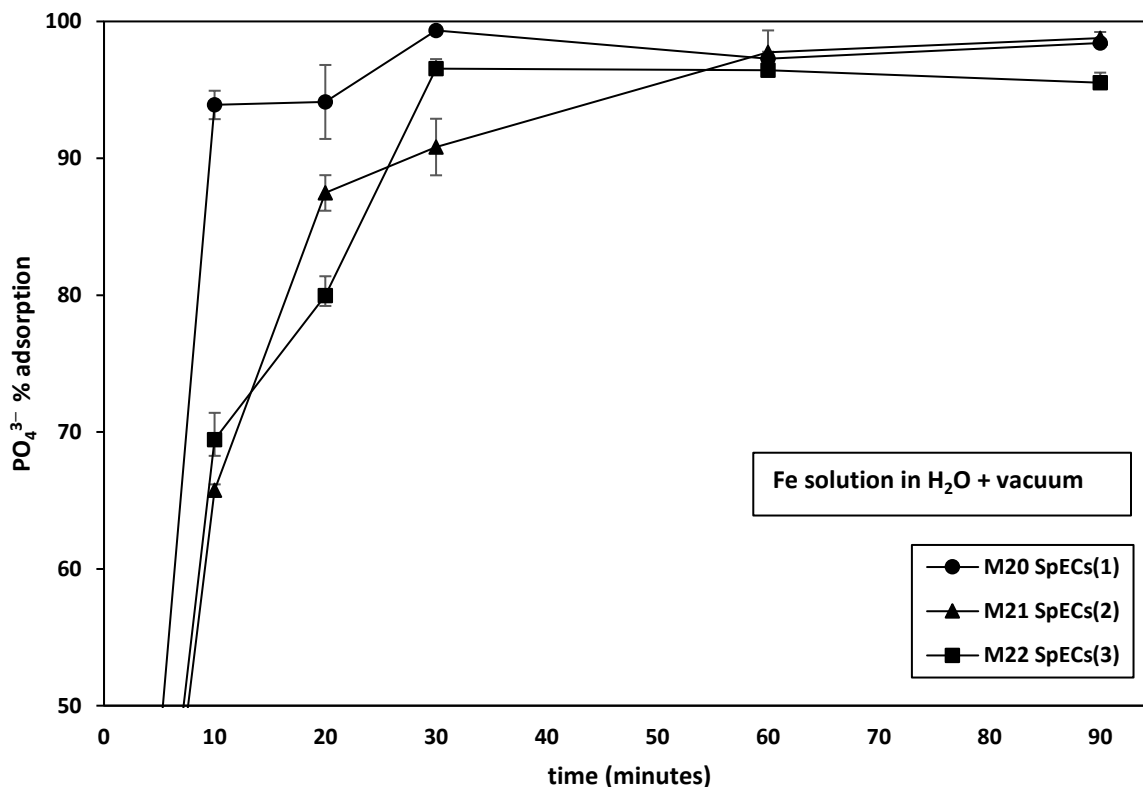


Figure 154: Effect of contact time on phosphates adsorption by Fe loaded SpECs in water under vacuum, graph zoomed in the region of 50 - 100% of phosphates removal (PO_4^{3-} dose: 6 mg/L, $n=3$).

The treatment of SpECs with iron salts in an aqueous medium under vacuum exhibited that Fe loading of their surface was higher compared to the same treatment without vacuum and that this increase in the iron loading enhanced their adsorption properties against phosphates (**Figure 154**). Iron loaded SpECs(1) (M20SpECs(1)) presented doubling in Fe-loading percentage and better adsorption efficiency: after 30 minutes of contact time they were able to remove the total quantity of the phosphates present in the solution whereas before, the percentage achieved was around 50%. A similar result was obtained for iron loaded SpECs(3) as well, where Fe loading under vacuum was doubled compared to without vacuum and their adsorption efficiency increased from 15% to 95% for a 30 minute contact time [M10SpECs(3) and M22SpECs(3) respectively]. Despite the fact that iron loaded SpECs(2) gave a similar iron

loading for both techniques used [M11SpECs(2) and M21SpECs(2)], their adsorption efficiency against phosphates was much higher when the iron loading was performed under vacuum, suggesting that a loading of a specific Fe salt might be predominant with this technique, making the material more attractive to the phosphate ions. Or perhaps that rather than having a thick layer of iron on the surface of the material, the vacuum may have induced a more homogenous spread of the iron throughout the walls and the inside of the shell, fact that was confirmed by SEM (see chapter 2 for more information). This would then present a higher surface area of Fe oxide crystals than if they were lumped together only on the outside, which in turn should promote a higher efficacy of adsorption, like what was observed. Another likely effect of the vacuum would be a more rapid crystallisation of the iron crystals, which would result in a larger number of smaller crystals (from a rapid, forced saturation point) which again would increase the surface area. As stated in chapter 2.7.4, according to the SEM images, it can be concluded that iron prefers to localise on the inside of the wall on SpECs(1) and SpECs(2) which is not the case for SpECs(3). Maybe this is a possible explanation why the vacuum procedure gave a better loading for SpECs(1) and SpECs(2) but not for SpECs(3).

Analysis of the experimental data using the pseudo-first and pseudo-second order model (**Table 52**) revealed that the adsorption of phosphates is better described by the pseudo-second order model for all three types, since the R^2 values are close to unity and the experimental maximum loading capacity is in agreement with the calculated one. This means that phosphates bind on the material through processes mainly involving chemisorption and that the adsorption rate depends on the adsorption capacity of the sorbent. Iron loaded SpECs(1) and SpECs(2) presented a similar maximum loading capacity of ~1.65 mg/g whereas SpECs(3) presented a higher one, 2.09 mg/g.

Table 52: Kinetic parameters for phosphates adsorption by Fe/water loaded SpECs (under vacuum) described by different models.

type	parameter		type	parameter		type	parameter	
SpECs(1)M20	$q_{e,exp}$ (mg/g)	1.58	SpECs(2)M21	$q_{e,exp}$ (mg/g)	1.60	SpECs(3)M22	$q_{e,exp}$ (mg/g)	1.54
	pseudo-first			pseudo-first			pseudo-first	
	$q_{e1,cal}$ (mg/g)	1.39		$q_{e1,cal}$ (mg/g)	1.27		$q_{e1,cal}$ (mg/g)	3.16
	k_1	0.15		k_1	0.04		k_1	0.14
	R^2	0.754		R^2	0.775		R^2	0.837
	pseudo-second			pseudo-second			pseudo-second	
	$q_{e2,cal}$ (mg/g)	1.69		$q_{e2,cal}$ (mg/g)	1.62		$q_{e2,cal}$ (mg/g)	2.09
	k_2	0.21		k_2	0.12		k_2	0.04
	h (mg/g min)	0.59		h (mg/g min)	0.30		h (mg/g min)	0.17
	R^2	0.987		R^2	0.988		R^2	0.923

6.4.3.2. Phosphates adsorption onto Fe/acetone loaded SpECs

Iron loading of SpECs in water under vacuum resulted in SpECs with good adsorption behaviour against phosphates. It was now decided to test the same loading procedure in a more volatile solvent, acetone, to check whether the rate of solvent evaporation would affect the iron crystal formation and furthermore the SpECs surface area and their phosphate adsorption capacity. The same experiment was conducted as previously with the only difference being the dissolution of iron salts ($\text{FeCl}_3 \cdot 6\text{H}_2\text{O}$ and $\text{FeCl}_2 \cdot 4\text{H}_2\text{O}$) in acetone. The procedure described in section 8.2.5.3 was followed, and the resulting Fe-loaded SpECs were analysed with elemental analysis and ICP-OES analysis for their iron content. The results are presented in **Table 53**.

Iron loading of SpECs(1) and SpECs(3) in acetone under vacuum gave the highest iron content compared to the previous procedures. Iron loaded SpECs(1) [M18SpECs(1)] presented a 11.6% w/w Fe content with this method, whereas previously they were only loaded with ~3.4%. Iron loaded SpECs(3) [M19SpECs(3)] presented 8.4% iron loading whereas the previous method in water had only achieved a 1.8% Fe loading. For SpECs(2), the iron loading in acetone produced a material [M17SpECs(2)] with much higher Fe content compared to the iron loading in water, 10% and 3% respectively.

Table 53: Results obtained from elemental analysis for CHN and ICP-OES for Fe for SpECs and Fe loaded SpECs in acetone under vacuum.				
sample	%C	%H	%N	%Fe
SpECs(1)	58.65	7.24	0.12	0.00
M18SpECs(1)	46.96	6.16	0.15	11.57
SpECs(2)	59.00	8.89	0.56	0.00
M17SpECs(2)	44.40	6.77	0.92	9.91
SpECs(3)	60.10	7.57	0.17	0.00
M19SpECs(3)	51.11	6.23	0.00	8.36

6.4.3.2.1. Effect of contact time on phosphates adsorption onto Fe/acetone loaded SpECs

Treatment of SpECs with iron salts dissolved in acetone gave the highest iron loading percentage compared to the previous methods used, and also resulted in SpECs types that exhibited the highest adsorption efficiency for phosphates (**Figure 155**). All three types of loaded SpECs achieved great adsorption percentages in the first 10 minutes of contact time.

Iron loaded SpECs(1) [M18SpECs(1)] removed 94% of the total contaminant quantity in 10 minutes and reached 99% adsorption in 30 minutes of contact time. The loaded SpECs(3) [M19SpECs(3)] showed a great efficiency by removing 97% of the total phosphates within 10 minutes of contact time. Iron loaded SpECs(2) [M17SpECs(2)] showed an improvement in their adsorption efficiency by removing 98% of the total phosphate content in 20 minutes of contact time.

Iron loading of SpECs in acetone under vacuum resulted in a material containing the highest Fe loading percentages compared to water loading, also exhibiting the greatest adsorption affinity towards phosphates. Such a finding could possibly be attributed to the rate of the solvent evaporation; acetone evaporates faster than water, leading to the formation of smaller iron crystals and furthermore to a material with higher surface area. Under vacuum, a higher iron loading was achieved, possibly meaning that acetone achieved a better penetration through

the SpECs pores, since it has lower surface tension than water and it might have been able to get into areas inside the SpECs that water could not possibly reach.

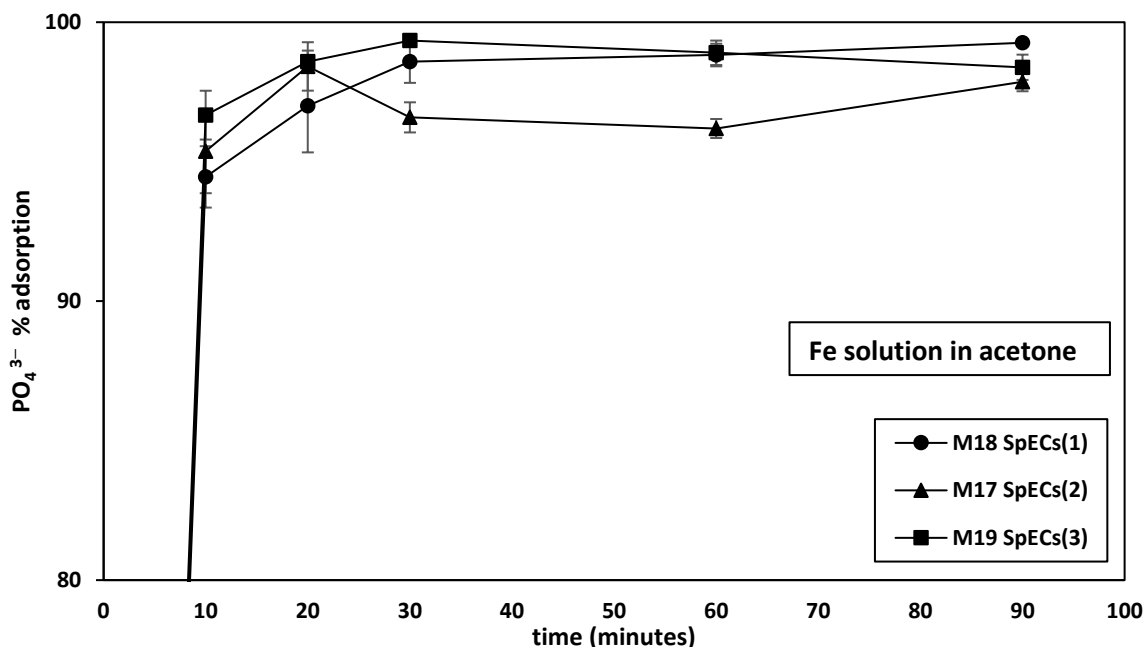


Figure 155: Effect of contact time on phosphates adsorption by Fe loaded SpECs in acetone under vacuum, graph zoomed in the region of 80 - 100% of phosphates removal (PO_4^{3-} dose: 6 mg/L, $n=3$).

Analysis of the experimental data using the pseudo-first and pseudo-second order model (Table 54) revealed that the adsorption of phosphates is described by the pseudo-second order model for all three types, since the R^2 values are close to unity and the experimental maximum loading capacities are in agreement with the calculated ones. This result indicates that the process of phosphate adsorption is mainly happening through chemisorption on the material's surface with the adsorbate's adsorption capacity affecting the rate of adsorption. All three types presented a similar maximum loading capacity of ~ 1.65 mg/g similar to the values obtained from the water/Fe loaded SpECs. This batch of tested SpECs presented a variation in their initial sorption rates, with SpECs(1) and SpECs(2) having a value ~ 0.9 mg/g min whereas SpECs(3) presented a much higher value of 3.7 mg/g min.

Table 54: Kinetic parameters for phosphates adsorption by Fe/acetone loaded SpECs (under vacuum) described by different models.

type	parameter		type	parameter		type	parameter	
SpECs(1)M18	$q_{e,exp}$ (mg/g)	1.60	SpECs(2)M17	$q_{e,exp}$ (mg/g)	1.57	SpECs(3)M19	$q_{e,exp}$ (mg/g)	1.58
	pseudo-first			pseudo-first			pseudo-first	
	$q_{e1,cal}$ (mg/g)	1.31		$q_{e1,cal}$ (mg/g)	1.68		$q_{e1,cal}$ (mg/g)	8.05
	k_1	0.13		k_1	0.10		k_1	0.08
	R^2	0.837		R^2	0.861		R^2	1
	pseudo-second			pseudo-second			pseudo-second	
	$q_{e2,cal}$ (mg/g)	1.67		$q_{e2,cal}$ (mg/g)	1.64		$q_{e2,cal}$ (mg/g)	1.61
	k_2	1.34		k_2	0.32		k_2	1.42
	h (mg/g min)	0.94		h (mg/g min)	0.85		h (mg/g min)	3.7
	R^2	0.997		R^2	0.997		R^2	1

6.4.4. Comparisons between the adsorption performances

SpECs loaded in the different mediums under vacuum presented good adsorption properties against phosphates with the acetone ones presenting the fastest adsorption reaching 95 - 100 % phosphates removal in 30 minutes. Both batches presented adsorption kinetics that were best described by the pseudo-second order model and the comparison of their maximum adsorption capacities is presented in **Table 55**.

Table 55: Adsorption capacities of the different Fe loaded SpECs against phosphates.

	adsorbent / $q_{e2,cal}$ (mg/g)		
medium for Fe loading	SpECs(1)	SpECs(2)	SpECs(3)
water	1.69	1.62	2.09
acetone	1.67	1.64	1.61

The Fe loaded SpECs presented similar values of adsorption capacity against phosphates in the range of 1.7 - 2.1 mg/g (**Table 55**). Iron loading in water under vacuum produced a material presenting the highest adsorption capacity (2.1 mg/g) according to the pseudo-second model, whereas iron loading in acetone under vacuum produced SpECs with a faster phosphate adsorption rate compared to the water loaded ones (**Figure 156**).

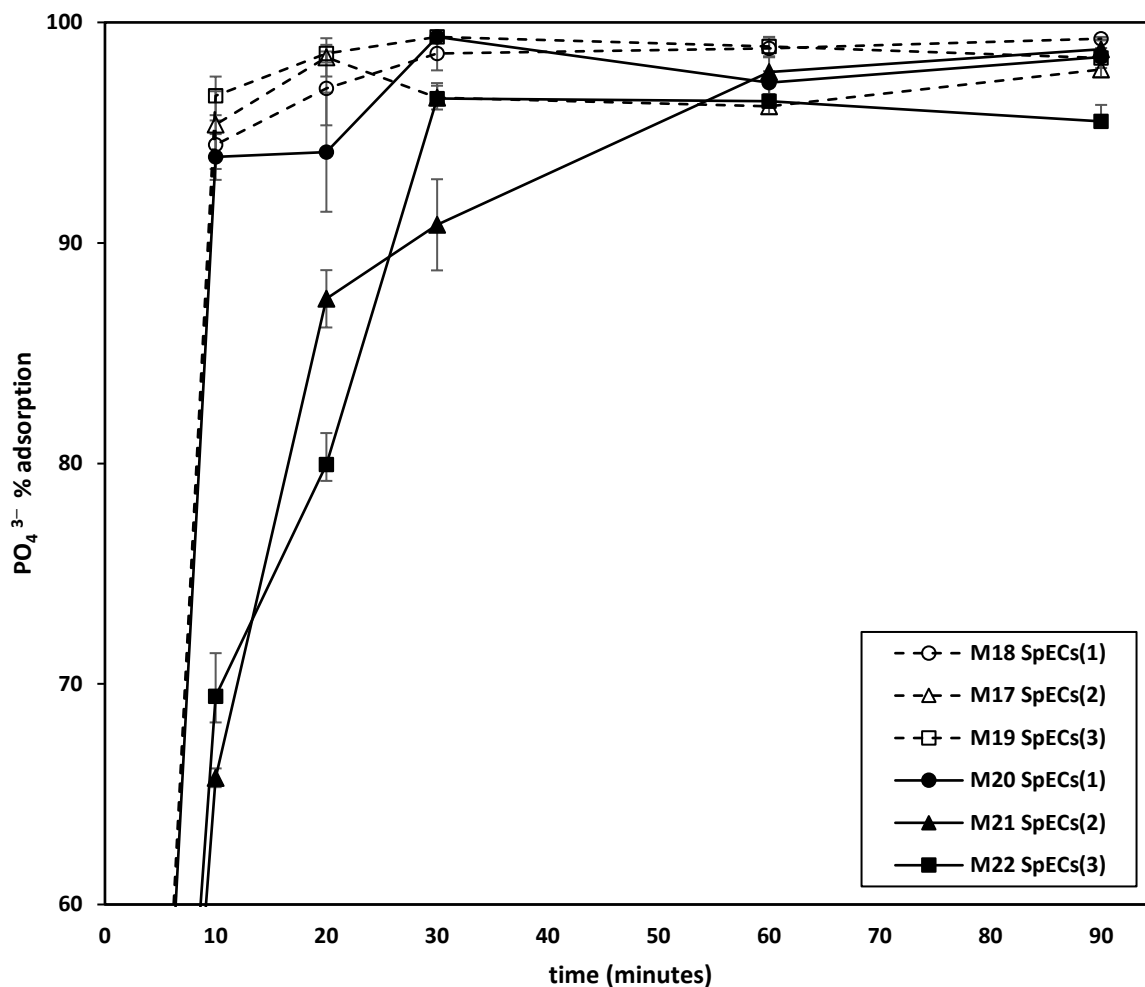


Figure 156: Comparison of the phosphates adsorption performance of iron loaded SpECs in water and acetone, graph zoomed-in the region of 60 - 100% phosphates adsorption. M17-M19 SpECs are loaded in acetone. M20-M22 SpECs are loaded in water, both procedures were performed under vacuum (n=3).

6.5. Conclusions

Even though phosphorus is essential for all living cells, high levels of phosphate in water can cause a variety of problems such as eutrophication, depletion of the dissolved oxygen, damage and loss of coral reefs and plant beds, depopulating of aquatic species leading to reduction of the water quality and acceleration of water scarcity. Phosphates can end up in water through agricultural routes as well as urban activities such as industrial and domestic wastewaters, leading to a phosphorus surplus which accumulates in soil and can be easily transported to the

aquatic environment. There is a growing interest in the development of new technologies to tackle phosphate removal from wastewaters with adsorption procedures being the most promising ones since they offer both low cost and high efficiency but also no sludge formation. SpECs extracted by the three standard methods discussed in this thesis, were tested for their phosphate adsorption affinity and were found inefficient. Thus, their surface was further modified by treatment with iron chlorides. Two different solvents were tested for the iron loading; water and acetone, after concluding that the application of vacuum was beneficial for increasing the loading levels. Both treatments resulted in materials loaded with different Fe percentages, with acetone resulting in the highest loading for all three types of SpECs. The successful iron loading was confirmed with elemental analysis and SEM imaging and the resulting iron loaded SpECs were tested for their phosphate affinity.

The fastest adsorption was achieved by Fe-SpECs(3) prepared in acetone, which removed almost 100% of the initial phosphate concentration (6 mg/L) in 30 minutes of contact time. All kinetic results were analysed with the pseudo-first and pseudo-second order models where it was concluded that the adsorption of phosphates on iron loaded SpECs is best described by the pseudo-second order kinetic model. Such a finding means that for this experimental setup, the adsorption of phosphates is mainly happening through chemisorption and that the most important parameter affecting the adsorption is the adsorption capacity of the material. The tested SpECs presented similar adsorption capacities, with the water/Fe loaded SpECs(3) presenting the highest, 2.1 mg/g.

7. Conclusions

SpECs derived from *Lycopodium clavatum* were tested for their adsorption efficiency against four contaminants, diclofenac, triclosan, oestradiol and phosphates. Under the different experimental setups, the tested SpECs presented different maximum adsorption capacities for either adsorption from a solution described by several kinetic models, or adsorption through a packed-bed.

For DCF, the most efficient SpECs type was the aminated form of SpECs(3) [SpECs(3)AM], presenting both the highest maximum adsorption capacity together with the fastest adsorption rate. After one minute of contact time, 0.2 g SpECs(3)AM were able to adsorb 100% of the DCF quantity (6 mg/L), presenting the highest adsorption rate (0.318 mg/g min) meaning that out of all tested SpECs, SpECs(3)AM is possibly the one with the most available active sites for DCF to bind. Under packed-bed studies, SpECs(3)AM presented a maximum adsorption capacity value of 27.4 mg/g with a breakthrough point at ~480 mL of treated volume. Such results would mean that on a larger scale and before reaching the breakthrough point, 1 kg of the aminated SpECs(3) would be able to equivalently treat 320,000 litres of contaminated water at a concentration of ~0.07 mg/L of DCF (an averaged DCF concentration from a range of hospital effluents²⁶¹). In terms of capacity, it would mean that the range of aminated SpECs(3) required annually for treating these hospitals would be from ~90 - 860 kg (range of effluent per year of hospitals of Massachusetts).^{262,263}

For TCS, all three SpECs types exhibited an efficient and fast adsorption by achieving 90 - 100% TCS removal in only two minutes of contact time. SpECs(3) was the most efficient type, presenting a K_F value of 35.14 mg^(1-1/n)/gL^{-1/n} for adsorption from a solution or a maximum adsorption capacity of 37 mg/g under packed-bed setup. Since the TCS content in hospital

effluents is as low as $0.044 \mu\text{g/L}$,²⁶¹ the important factor for TCS adsorption under a packed-bed setup would be the rate of adsorption of the adsorbent, as a high flow rate of $\sim 55 - 530 \text{ L/min}$ would be needed. In terms of capacity, it was calculated that 1 kg of SpECs(3) would be enough to treat the annual discharge of one hospital ($\sim 1.2 - 12 \text{ g TCS}$ in $\sim 28,000,000 - 277,000,000 \text{ L}$). They also presented an excellent adsorption rate of complete TCS removal in two minutes of contact time.

Experiments on the adsorption of DCF and TCS from the same solution suggested that the active sites on the surface of the SpECs may be different for each contaminant since none of the contaminants presented slower adsorption kinetics when in mixture compared to when alone. SpECs(1) and SpECs(2) presented a faster DCF adsorption when in the same solution with TCS, suggesting that maybe the TCS molecules initially create a monolayer on the surface of the SpECs, possibly forming new binding sites for DCF.

For E2, the maximum adsorption capacity for adsorption at equilibrium conditions was $\sim 1.5 \text{ mg/g}$ for the majority of the tested SpECs, whereas packed-bed studies revealed that SpECs(1) was the most efficient type, presenting a maximum adsorption capacity of 42.5 mg/g . Such a result would mean that in a larger scale and in terms of capacity, 1 - 3 kg of SpECs(1) would be able to equivalently treat the annual discharge of one hospital containing $\sim 0.12 \mu\text{g/L}$ of E2 (reported E2 concentration in hospital effluents²⁶¹). Whereas SpECs exhibited a good level of adsorption capacity for E2, they presented much slower adsorption rates when compared to the previously examined compounds, DCF and TCS. Even though the material's adsorption capacity is far beyond what would be required for treating hospital effluent or surface waters, it was calculated that the rate of effluent discharge would be $\sim 55 - 530 \text{ L/min}$,^{262,263} which clearly displays the need for a fast adsorption rate being of far higher importance than the material's maximum adsorption capacity. It was concluded that SpECs

would not meet the requirements for treating such a fast-flowing body of water and maybe a different water treatment setup would be more ideal.

Experiments on phosphates adsorption only involved adsorption from a solution and revealed that all iron loaded SpECs presented similar adsorption capacities, with the water/Fe loaded SpECs(3) presenting the highest, 2.1 mg/g. The fastest adsorption was achieved by the acetone/Fe SpECs(3), which removed almost 100% of the initial phosphates concentration (6 mg/L) in 30 minutes of contact time.

As stated in the introduction, the most efficient approach to tackle the emerging contaminant problem would be the immediate treatment of the sources of these contaminants, before reaching the environment and being further dilute or mixed with other contaminants. A major source of releasing pharmaceuticals in the aquatic environment are hospitals and a scenario of a small water treatment setup containing SpECs cartridges filtering their effluents does not sound unreasonable after the results obtained from this research. Whereas other materials existing in recent publications presented higher adsorption capacity values, it was pointed out that the differences in the experimental conditions make the direct comparisons with SpECs very hard to judge. Furthermore, even though a high adsorption capacity value is a feature highly needed, other factors are of more importance for the make of a successful adsorbent such as the rate of adsorption, the reusability of the material, the production procedure being low-cost, fast and environmentally friendly.

SpECs presented adsorption capacity values far beyond what would be required for treating hospital effluent or surface waters and very good adsorption rates, especially for DCF and TCS. SpECs(3) and their aminated form, SpECs(3)AM were proven to be the best candidates for contaminant adsorption, with SpECs(3) ticking all the boxes for a successful adsorbent; apart from their excellent adsorption behaviour, their production is fast and low-cost, they are

environmentally friendly since they derive from plant spores and the chemicals used are not harsh to the environment and they also presented good reusability.

Future work should include more experiments on the aminated SpECs, identifying the exact conditions that affect their performance and giving them an expiry date on their adsorption properties. Packed-bed studies using the aminated form should be further investigated as well as an exhaustive study of a more efficient regenerating agent. Contaminant adsorption research should include experiments on mixed systems that would include more than two contaminants in different concentrations, also including ions and elements present in real water and wastewater samples. Different pH values should be tested, variations in temperature and initial contaminant dose, closer to real water samples conditions and properties.

Most important of all, future work should include packed-bed studies that are conducted under more realistic conditions:

- bigger SpECs bed volumes, closer to the values calculated for treating hospital effluents,
- variation of flow rates closer to the range of (50 - 500 L/min) needed for hospital effluents treatment and
- spiked real water samples with lower contaminant concentrations closer to the ones reported in the literature.

In conclusion, SpECs were proven to be an effective adsorbent material for some of the tested contaminants, presenting very promising results and good adsorption behaviour. Their use in WWTPs would be beneficial when included in adsorption procedures, offering a low-cost and environmentally friendly approach to tackling the problem of emerging contaminants.

8. Experimental

8.1. SpECs extraction

Raw *Lycopodium clavatum* was purchased from Sporomex Ltd (Hull, UK). NaOH 98%, NaHCO₃ 99%, KOH 86%, NaOCl 14%, H₂SO₄ 98% and HCl 37% were purchased from Fisher Scientific (Loughborough, UK). Na₂CO₃ was purchased from Prime Chemicals (Rotherham, UK). Acetone and absolute ethanol were purchased from VWR chemicals (Lutterworth, UK). Ammonium persulfate 98% and *tert*-butyl hydroperoxide 70% were purchased from Acros Organics (Geel, Belgium). Diclofenac sodium salt was purchased from Sigma-Aldrich (Dorset, UK).

8.1.1. SpECs(1) KOH hydrolysis - H₃PO₄ treatment

L.clavatum raw spores (50 g) were stirred in acetone (225 mL) under reflux at 60 °C for 4 hours. The suspension was then left to cool down, was filtered through a grade 2 porosity sinter and washed with acetone until the solvent was colourless. The defatted spores were treated with KOH 6% (250 mL) under reflux at 80 °C for 6 hours. The suspension was filtered and retreated with a fresh KOH 6% solution for another 6 hours. The extract was filtered and washed with deionised water until neutral pH and the cleaned spores were treated with H₃PO₄ (350 mL) under reflux at 85 °C for 5 days. The solution was left to cool down and after reaching room temperature it was filtered and carefully washed with deionised water until the washed off solution became neutral (pH 6 - 7). The clean solid was washed with absolute ethanol and left to dry under vacuum overnight. Mass of final product: 19 g.

8.1.2. SpECs(2) NaOH hydrolysis

L. clavatum raw spores (500 g) were stirred in NaOH 6% (2.5 L) under reflux at 80 °C overnight. The cooled suspension was filtered with porosity grade 2 filter and the solid was meticulously washed with deionised water until the washed off solution became neutral (pH 6 - 7). The clean solid was washed with absolute ethanol and left to dry under vacuum overnight. Mass of final product: 200 g.

8.1.3. SpECs(3)HCl hydrolysis

L. clavatum raw spores (500 g) were stirred in HCl 9 M (2 L) under reflux at 100 °C for 2 hours. The cooled suspension was filtered with porosity grade 2 filter and the solid was washed several times with deionised water until the washed off solution became neutral (pH 6 - 7). The extract was washed with absolute ethanol and left to dry under vacuum overnight. Mass of final product: 245 g.

8.1.3.1. Drying conditions of SpECs(3)

A quantity of the extracted SpECs(3) was further dried in a desiccator under vacuum for five days. Another quantity was dried in the oven at 100 °C for three days.

8.2. SpECs surface modification

8.2.1. SpECsBL - Bleach (NaOCl) treatment

SpECs (2 g) were treated with 25 mL NaOCl (Fischer Scientific 14% Cl availability) under stirring for one hour at room temperature. The modified exines were filtered and washed with hot deionised water, followed by washings with HCl 2 M. The resulting product was washed

with deionised water until the washed off solution was of neutral pH. A final washing with absolute ethanol followed and the modified SpECs were left to dry under vacuum overnight.

8.2.2. SpECs(2)HCl - HCl treatment

2 g of the base extracted exines, SpECs(2), were treated with 50 mL HCl 9 M under stirring at room temperature for three hours. The resulting exines were filtered and washed with deionized water until the washed off solution was of neutral pH. A final washing with absolute ethanol followed and the modified SpECs were left to dry under vacuum overnight.

8.2.3. SpECsAPS - Ammonium Persulfate treatment

8.2.3.1. APS 1 M treatment at room temperature - SpECsAPSR1

The different extractions of SpECs (1 g) were treated with 20 mL APS 1 M diluted in H₂SO₄ 1 M (4.56 g APS in 20 mL sulfuric acid 1 M - 1.68 mL H₂SO₄ in a 30 mL volumetric flask filled with distilled water) for three hours at room temperature. The modified SpECs were filtered and washed with distilled water until the washed off solution was neutral (pH 6 - 7). A final washing with absolute ethanol followed and the modified SpECs were left to dry under vacuum overnight. The resulting exines were named SpECs APSR1.

8.2.3.2. APS treatment at 90 °C - SpECsAPSH

The different extractions of SpECs (12 g) were treated with 250 mL APS 1 M diluted in H₂SO₄ 1 M (57 g APS in 250 mL sulfuric acid 1 M - 14 mL H₂SO₄ in a 250 mL volumetric flask filled with distilled water) for three hours under reflux at 90 °C. The modified SpECs were filtered and washed with distilled water until the washed off solution was neutral (pH 6 - 7). A final washing with absolute ethanol followed and the modified SpECs were left to dry under vacuum

overnight. The resulting exines were named SpECs APSH1. Following the same procedure, different concentrations of APS were tested, in the range of 0.5 - 2 M.

8.2.4. *Tert*-butyl-hydroperoxide treatment - SpECsTBHP

The different extractions of SpECs (2 g) were treated with 50 mL TBHP (no dilution) for 3 hours at room temperature. The modified exines were filtered and washed with distilled water until the washed off solution was coming out neutral (pH 6 - 7). A final washing with absolute ethanol followed and the modified SpECs were left to dry under vacuum overnight. The resulting SpECs were named SpECsTBHP.

8.2.5. Iron loading onto SpECs

8.2.5.1. Iron loading onto SpECs in water

15.5 g $\text{FeCl}_3 \cdot 6\text{H}_2\text{O}$ (0.057 mol) were dissolved into 20 mL milliQ water. 23.25 g $\text{FeCl}_2 \cdot 4\text{H}_2\text{O}$ (0.117 mol) were dissolved in 27 mL milliQ water and the two iron solutions were united under stirring in a water bath at 30 °C until the complete dissolution of the Fe salts. At 20 mL of the Fe salt solution, 1 g of extracted SpECs was added at room temperature and the mixture was left stirring overnight. The following day, the mixture of SpECs and Fe salts was filtered and washed with milliQ water until the rinsate was clear and free from iron salts. The resulting SpECs were washed with absolute ethanol and left to dry in the vacuum pump.

8.2.5.2. Iron loading onto SpECs in water under vacuum

4.5 g $\text{FeCl}_3 \cdot 6\text{H}_2\text{O}$ (0.017 mol) were dissolved into 10 mL milliQ water. 6.8 g $\text{FeCl}_2 \cdot 4\text{H}_2\text{O}$ (0.034 mol) were dissolved in 10 mL of milliQ water and the two iron solutions were united under stirring in a water bath at 30 °C until complete dissolution of the Fe salts. At 20 mL of

the Fe salt solution 1 g of extracted SpECs was added at room temperature and the mixture was left stirring under vacuum until complete evaporation of the solvent (two nights). The dried mixture was filtered and washed with milliQ water until the rinsate was clear and free from iron salts. The resulting SpECs were washed with absolute ethanol and left to dry in the vacuum pump.

8.2.5.3. Iron loading in acetone

4.8 g $\text{FeCl}_3 \cdot 6\text{H}_2\text{O}$ (0.018 mol) were dissolved into 10 mL acetone. 7.3 g $\text{FeCl}_2 \cdot 4\text{H}_2\text{O}$ (0.037 mol) were dissolved in 10 mL acetone and the two iron solutions were united. 5 mL milliQ water were added and the mixture was left stirring in a water bath at 30 °C until the complete dissolution of the Fe salts. 1 g of extracted SpECs was added at room temperature and the mixture was left stirring under vacuum until complete evaporation of the solvent (one night). Filtering and washings with acetone and milliQ water followed until the rinsate was clear and clean from iron salts. The resulting iron loaded SpECs were washed with ethanol and dried in the vacuum pump.

8.2.5.4. Magnetic SpECs

Following the protocol described in the literature,¹⁶⁰ 13.32 g $\text{FeCl}_3 \cdot 6\text{H}_2\text{O}$ were dissolved into 20 mL milliQ water followed by the addition of 19.88 g $\text{FeCl}_2 \cdot 4\text{H}_2\text{O}$ diluted in 20 mL milliQ water. 5 mL HCl 5 M and 5 mL absolute ethanol were added and the mixture was left under stirring in a water bath at 30 °C until the complete dissolution of the Fe salts. 2 g of extracted SpECs were added at room temperature and were left stirring for 2 hours. The mixture of SpECs and Fe salts was then filtered and washed with milliQ water until the rinsate was clear. The loaded SpECs were transferred to a flask containing 30 mL 1 M ammonia solution and left

stirring for 1 hour. The resulting SpECs were filtered, washed with milliQ water and oven dried at 40 °C.

8.2.6. Aminated SpECs

Different extractions of SpECs (3 g) were added into a solution of 1,6-hexanediamine (7.1 g) in toluene (30 mL) and heated at 120 °C in a Dean Stark apparatus for 24 hours. The suspension was allowed to cool down and was filtered through a grade 2 porosity sinter. The resulting SpECs were washed successively with toluene (100 mL), HCl 2M (150 ml), NaOH 2 M (150 mL), milliQ water until the pH of the effluent was neutral (400 mL), methanol (150 mL) and dichloromethane (150 mL). The aminated SpECs were left to dry under vacuum overnight. Mass of final product 2.7 g.

8.3. SpECs analysis

8.3.1. Boehm titration

The different extractions of SpECs (0.3 g) were treated with 20 mL of three different base salts (NaOH, NaHCO₃, Na₂CO₃) 0.1 M for 24 hours under agitation at the orbital shaker. The suspensions were filtered through grade 2 porosity sinters and washed with milli-Q water until the rinsate was coming off neutral. The solid was washed with absolute ethanol and left to dry under vacuum overnight. The loaded SpECs were analysed with ICP-OES for their sodium loading.

8.3.2. IR analysis

SpECs were analysed by FT-IR spectroscopy, using a Thermo Scientific Nicolet iS5 spectrometer, equipped with a iD1 Transmission chamber. All disks were created using a

Specac manual press and were compressed at 1 ton. A highly accurate balance was used (5 decimal places), where 1 mg of SpECs was weighed and mixed with 130 mg of KBr (Alfa Aesar). All spectra were normalised using second derivative methodology and finally normalised between 0 and 1 using CH₂ peaks (~2875 cm⁻¹). All measurements were repeated in triplicate and then normalisation was performed, leading to identical overlays.

8.4. Diclofenac experiments

All diclofenac experiments were carried out using an orbital shaker (model PSU-10i Grant-bio). For the concentration range 0.5 to 10 µg/mL, all analyses were conducted with a 6705 UV/Vis Spectrophotometer JENWAY Single cell holder having as a reference blank milliQ water. For the lower concentrations ranging from 0.06 ng/mL to 10 µg/mL all analyses were conducted using a Shimadzu HPLC-ESI-MS/MS equipped with a Shimadzu Shim-Pack GISS-HP 3 µm C18 column (100 x 3 mm) and coupled with a Shimadzu triple quadrupole tandem mass spectrometer. The solvents used were LC-MS grade water (VRW chemicals) spiked with 0.1% formic acid and LC-MS grade acetonitrile (VRW chemicals). The oven temperature was set at 40 °C. The details of the analysis method are below:

flow: 0.6 mL/min injection volume: 5 µL

gradient: 0-3 min 70% H₂O-30% MeCN

3-4 min 0% H₂O-100% MeCN

4-4.2 min 70% H₂O-30% MeCN

8.4.1. Diclofenac reference curve

For the higher DCF concentrations experiments, a stock solution of diclofenac sodium salt 0.99 M was prepared, where DCF (31.6 mg) was diluted in milliQ water (100 mL). This stock

solution was further diluted to a series of eight standard solutions with concentrations ranging from 0.5 to 10 $\mu\text{g/mL}$. The absorbance of the standard solutions was measured against a blank (milliQ water) at 275 nm. The procedure was repeated three times (both stock solution preparations and analyses). A reference curve was created in Excel by plotting the mean values of the absorbance *versus* the concentration of DCF.

For the lower DCF concentrations experiments, a stock solution of diclofenac sodium salt 2.2 M was prepared, where DCF (70 mg) was diluted in milliQ water (100 mL). This stock solution was further diluted to a series of seven standard solutions with concentrations ranging from 0.06 ng/mL to 10 $\mu\text{g/mL}$. The standards were analysed with the HPLC-MS/MS system and the procedure was repeated three times (both stock solution preparations and analyses). A reference curve was created in Excel by plotting the mean values of the peak area of the chromatograms *versus* the concentration of DCF.

8.4.2. Diclofenac adsorption kinetics

SpECs (20 mg) were placed in vials containing 5 mL of DCF 6 $\mu\text{g/mL}$ (0.019 mM for the high DCF concentration experiments) or 3 ng/mL (0.009 μM for the low DCF concentration experiments) and were agitated using an orbital shaker at a speed of 340 rpm, for different periods of time ranging from 1 to 73 hours. A blank sample was also included containing SpECs (20 mg) and milliQ water (5 mL). The experiment was conducted in triplicates for each duration. For the high concentration, the suspensions were filtered with Pasteur pipettes stuffed with cotton wool, after ensuring that the cotton does not interfere with the initial DCF concentration. The absorbance of each filtered solution was measured at 275 nm against a blank (milliQ water). For the low concentration, the suspension was filtered using a Phenomenex HPLC filter and the effluent was analysed using the HPLC-MS/MS system. The DCF concentration of the final solutions was calculated using the reference curves.

8.4.3. Diclofenac adsorption isotherms

A stock solution of diclofenac sodium salt was prepared, where DCF (31.6 mg) was diluted in milliQ water (100 mL). This stock solution was further diluted to a series of 14 standard solutions with concentrations ranging from 0.5 to 25 $\mu\text{g/mL}$. 5 mL of each standard solution were placed in vials containing SpECs (20 mg) and were agitated at 340 rpm for 24 hours. The experiment was repeated three times for each concentration. The suspensions were filtered with Pasteur pipettes stuffed with cotton wool. The absorbance of each filtered solution was measured at 275 nm against a blank (milliQ water). The DCF concentration of the final solution was determined by using the reference curve. The adsorption isotherms were created by plotting the amount of DCF (μg) adsorbed per mass of SpECs (mg) *versus* the final concentration of the solution ($\mu\text{g/mL}$).

8.4.4. SpECs wettability and diclofenac adsorption

SpECs (20 mg) were placed in closed vials containing 3 mL milliQ water and left to soak for 17 days. After this period, 2 mL of diclofenac solution (15 $\mu\text{g/mL}$) was added in each vial, and the mixtures were agitated at 340 rpm for different periods of time. The suspensions were filtered with Pasteur pipettes stuffed with cotton wool. The absorbance of each filtered solution was measured at 275 nm against a blank (milliQ water). The DCF concentration of the final solution was determined by using the reference curve.

8.5. Triclosan experiments

All triclosan experiments were carried out using an orbital shaker (model PSU-10i Grant-bio). For the concentration range 0.5 to 10 $\mu\text{g/mL}$, all analyses were conducted with an Agilent HPLC system equipped with an autosampler and a Phenomenex Gemini 5 μm C18 column

(110Å, 150 x 4.60 mm). The solvents used were HPLC grade acetonitrile (Honeywell) and milliQ water. The oven temperature was set at 30 °C and the retention time was ~15:20. The data acquisition and analysis were conducted with the Laura software. The details of the analysis method are below:

flow: 1 mL/min injection volume: 20 µL

gradient: 0-10 min 80:20 H₂O:MeCN

10-20 min 100% MeCN

20-22 min 80:20 H₂O:MeCN

For the lower concentrations ranging from 0.06 ng/mL to 10 µg/mL all analyses were conducted using a Shimadzu HPLC-ESI-MS/MS at the negative mode equipped with a Shimadzu Shim-Pack GISS-HP 3 µm C18 column (100 x 3 mm) and coupled with a Shimadzu triple quadrupole tandem mass spectrometer. The solvents used were LC-MS grade water (VRW chemicals) spiked with 0.1% formic acid (VRW chemicals) and LC-MS grade acetonitrile (VRW chemicals). The oven temperature was set at 40 °C and the retention time was ~3:30. The data acquisition and analysis were conducted with the LabSolutions software.

The details of the analysis method are below:

flow: 0.6 mL/min injection volume: 5 µL

gradient: 0 - 0.1 min 100% H₂O

0.1 - 3.0 min 70:30 H₂O:MeCN

3.0 - 4.2 min 100% MeCN

4.2 - 6.0 min 70:30 H₂O:MeCN

8.5.1. Triclosan reference curve

For the higher triclosan concentrations experiments, a stock solution of TCS 0.32 mM was prepared, where TCS (4.6 mg) was diluted in absolute ethanol (50 mL). This stock solution was further diluted in milliQ water to a series of eight standard solutions with concentrations ranging from 0.5 to 14 $\mu\text{g/mL}$. Each solution was analysed in triplicate using the HPLC system at two detection wavelengths, 220 nm and 280 nm. Two reference curves were created in Excel, one for each wavelength, by plotting the mean values of the peak area of the chromatograms *versus* the concentration of TCS.

For the lower TCS concentrations experiments, a stock solution of TCS 1.2 M was prepared, where TCS (34.4 mg) was diluted in absolute ethanol (50 mL). This stock solution was further diluted to a series of seven standard solutions with concentrations ranging from 0.06 ng/mL to 10 $\mu\text{g/mL}$. The standards were analysed with the HPLC-MS/MS system and the procedure was repeated three times (both stock solution preparations and analyses). A reference curve was created in Excel by plotting the peak area of the chromatograms *versus* the concentration of TCS.

8.5.2. Triclosan adsorption kinetics

SpECs (20 mg) were placed in vials containing 5 mL of TCS 6 $\mu\text{g/mL}$ (0.021 mM for the high TCS concentration experiments) or 2 ng/mL (0.01 μM for the low TCS concentration experiments) and were agitated using an orbital shaker at a speed of 340 rpm, for different periods of time ranging from 1 to 4 hours and 2 to 10 minutes. A blank sample was also included containing SpECs (20 mg) and milliQ water (5 mL). The experiment was performed in triplicates for each duration. The suspensions were filtered using Phenomenex HPLC filters after testing that they are safe and do not absorb any quantity of TCS. Each filtered solution was analysed with either the HPLC system for the higher concentrations or the HPLC-MS/MS

system for the lower concentrations. The TCS content of the final solutions was calculated using the reference curves.

8.5.3. Triclosan adsorption isotherms

A stock solution of triclosan was prepared, where TCS (3.7 mg) was diluted in absolute ethanol (50 mL). This stock solution was further diluted in milliQ water to a series of 11 standard solutions with concentrations ranging from 0.5 to 55 $\mu\text{g/mL}$. 5 mL of each standard solution were placed in vials containing SpECs (20 mg) and were agitated at 340 rpm for 10 minutes. The experiment was repeated three times for each concentration. The suspensions were filtered through Phenomenex HPLC filters and analysed in the HPLC system. The TCS concentration of the final solution was calculated by using the reference curve. The adsorption isotherms were created by plotting the amount of TCS (μg) adsorbed per mass of SpECs (mg) *versus* the final TCS concentration of the solution ($\mu\text{g/mL}$).

8.6. Oestradiol experiments

All E2 experiments were carried out using an orbital shaker (model PSU-10i Grant-bio). All analyses were conducted with a 6705 UV/Vis Spectrophotometer JENWAY Single cell holder, using milliQ water as the blank standard.

8.6.1. Oestradiol solution stability

A stock solution of E2 2.3 mM was prepared, where E2 (31 mg) was diluted in absolute ethanol (50 mL). This stock solution was further diluted in milliQ water to a series of seven standard solutions with concentrations ranging from 0.5 to 10 $\mu\text{g/mL}$. The absorbance of the standard solutions was measured against a blank (milliQ water) at 200 nm right after their preparation.

In order to check the stability of each solution, a measurement of their absorbance was taken at different time intervals starting from 24 hours after their preparation and ending after 180 hours. The solutions were stored at room temperature. A plot of their absorbance values *versus* time was created in Excel.

8.6.2. Oestradiol reference curve

A stock solution of E2 2.3 mM was prepared, where E2 (31 mg) was diluted in absolute ethanol (50 mL). This stock solution was further diluted in milliQ water to a series of seven standard solutions with concentrations ranging from 0.5 to 10 µg/mL. The absorbance of the standard solutions was measured against a blank (milliQ water) at 200 nm. The procedure was repeated three times. A reference curve was created in Excel by plotting the mean values of the absorbance *versus* the concentration of E2.

8.6.3. Oestradiol adsorption kinetics

SpECs (20 mg) were placed in vials containing 5 mL of E2 6 µg/mL (0.021 mM) and were agitated using an orbital shaker at a speed of 340 rpm, for different periods of time ranging from 1 to 48 hours. A blank sample was also included containing SpECs (20 mg) in milliQ water (5 mL). The experiment was performed in triplicates for each duration. The suspensions were filtered through Phenomenex HPLC filters after ensuring that the filters do not absorb any E2 quantity. The absorbance of each filtered solution was measured at 200 nm against a blank (milliQ water). The E2 concentration of the final solution was calculated using the reference curve equation.

8.6.4. Oestradiol Adsorption Isotherms

A stock solution of E2 2.3 mM was prepared, where E2 (31 mg) was diluted in absolute ethanol (50 mL). This stock solution was further diluted in milliQ water to a series of seven standard solutions with concentrations ranging from 0.5 to 10 µg/mL. 5 mL of each standard solution were placed in vials containing SpECs (20 mg) and were agitated at 340 rpm for 24 hours. The experiment was repeated three times for each concentration. The suspensions were filtered through Pasteur pipettes stuffed with cotton wool. The absorbance of each filtered solution was measured at 200 nm against a blank (milliQ water). The E2 concentration of the final solution was calculated by using the reference curve. The adsorption isotherms were created by plotting the amount of E2 (µg) adsorbed per mass of SpECs (mg) *versus* the final concentration of E2 in the solution (µg/mL).

8.7. Mixed contaminants experiment

The mixed contaminants experiment was carried out using an orbital shaker (model PSU-10i Grant-bio). All analyses were conducted with an Agilent HPLC system equipped with an autosampler and a Phenomenex Gemini 5 µm, C18 column (110 Å, 150 x 4.60 mm). The oven temperature was set at 30 °C. The details of the analysis method are below:

flow: 1 mL/min injection 20 µL

gradient: 0-10 min 100% H₂O-MeCN 80:20

10-20 min 100% MeCN

20-22 min 100% H₂O-MeCN 80:20

8.7.1. Mixed contaminant reference curve

TCS and DCF stock solutions were prepared, where 0.05 g of DCF were diluted in 50 mL milliQ water (1 mg/mL) and 0.03 g of TCS were diluted in 50 mL pure ethanol (0.6 mg/mL). A stock solution was prepared in milliQ water, containing both contaminants with an individual concentration of 10 µg/mL. Standard solutions were prepared by further diluting the mixed stock solution for a range of individual concentrations of 0.5 to 10 µg/mL.

The standard solutions were analysed with the HPLC Agilent system, at two different wavelengths 220 and 280 nm. Plots of the peak area against the concentration of each contaminant were created with Excel and individual reference curves were obtained with individual equations.

8.7.2. Mixed contaminants adsorption experiments

A solution containing 6 µg/mL of DCF and 6 µg/mL of TCS was prepared and labelled mixed DCF/TCS. SpECs (20 mg) were placed in vials containing 5 mL of mixed DCF/TCS and were agitated using an orbital shaker at a speed of 340 rpm, for different periods of time ranging from 10 to 60 minutes. A blank sample was also included containing SpECs (20 mg) in milliQ water (5 mL). The experiment was performed in triplicates for each duration. The suspensions were filtered through Phenomenex HPLC filters and the filtrate was analysed in the HPLC system. The DCF and TCS concentrations were calculated using their reference curves.

8.8. Phosphates experiments

All phosphate experiments were carried out using an orbital shaker (model PSU-10i Grant-bio). All analyses were carried out using a 6705 UV/Vis Spectrophotometer JENWAY Single cell holder, with milliQ water as the reference blank.

8.8.1. Phosphates detection method

For the detection of phosphates in aqueous solutions, the protocol described in the literature was followed.⁴⁰⁵

Mixed reagent preparation: In a 25 mL volumetric flask, 1 g $(\text{NH}_4)_6\text{Mo}_7\text{O}_{24}$ and 0.07 g $\text{K}(\text{SbO})\text{C}_4\text{H}_4\text{O}_6$ were added and shaken with milliQ water until complete dissolution. 7.2 mL of the Mo/Sb solution were transferred to a clean and dry vial and 24 mL H_2SO_4 5 N were added under gentle stirring. When the solution turned clear from cloudy, 14.4 mL of 0.1 M ascorbic acid (0.44 g in 25 mL milliQ water) was added and the solution was gently shaken again.

In 4 mL water sample, 1 mL of the mixed reagent was added and after vortex stirring, the sample was set aside for 21 minutes to develop its colour. The absorbance was then measured at 890 nm against a blank sample (4 mL milliQ water + 1 mL mixed reagent).

8.8.2. Phosphates reference curve

A stock solution of potassium phosphate 0.078 M was prepared, where potassium phosphate (0.53 g) was diluted in milliQ water (50 mL). This stock solution was further diluted to a series of seven standard solutions with concentrations ranging from 0.5 to 10 $\mu\text{g}/\text{mL}$. After reacting with the mixed reagent, the absorbance of the standard solutions was measured against a blank (milliQ water + mixed reagent) at 890 nm. The procedure was repeated three times. A reference curve was created in Excel by plotting the mean values of the absorbance *versus* the concentration of potassium phosphate.

8.8.3. Phosphates adsorption kinetics

SpECs (20 mg) were placed in vials containing 5 mL of phosphates 6 µg/mL (0.044 M) and were agitated using an orbital shaker at a speed of 340 rpm, for different periods of time ranging from 30 to 90 minutes. A blank sample was also included containing SpECs (20 mg) and milliQ water (5 mL). The experiment was performed in triplicates for each duration. The suspensions were filtered with Pasteur pipettes stuffed with cotton wool after ensuring that the cotton does not absorb any quantity of phosphates. After reacting with the mixed reagent, the absorbance of each filtered solution was measured at 890 nm against a blank (milliQ water + mixed reagent). The phosphates concentration of the final solution was calculated using the reference curve equation.

8.9. Packed-bed studies

8.9.1. Column preparation

Different masses of SpECs were placed in a glass column of 30 cm high and 2.5 cm diameter and 250 mL total volume equipped with a sinter filter. SpECs were tightly packed using ethanol and compressed air followed by the addition of 2 g of low iron sand (Fisher scientific) as a second layer on top of the SpECs layer. The packed-bed was washed several times with milliQ water to wash off any impurities and to remove any air bubbles trapped between the layers and the particles. The height of the packed SpECs and sand layer was noted down individually.

8.9.2. Packed-bed experiments

A contaminant solution (DCF, TCS or E2) of known concentration was passed through the SpECs and sand layer under gravity at different flow rates. The flow rate was adjusted using the column's tap and a timer. Initially, the effluent was collected in small portions (5 mL) and

was analysed for its contaminant content. Later, when the contaminant concentration was more stable, the collected portions were bigger (20 - 50 mL). The experiment kept going until the complete saturation of the SpECs, where the effluent's contaminant content was equal to the initial contaminant concentration. The ratio of the effluent's concentration to initial concentration (C/C_0) was calculated for each portion and the plot of C/C_0 versus treated volume was created in Excel.

Different initial contaminant concentrations were tested, as well as different SpECs masses and flow rates.

9. References

- 1 S. Álvarez, R. S. Ribeiro, H. T. Gomes, J. L. Sotelo and J. García, *Chem. Eng. Res. Des.*, 2015, **95**, 229–238.
- 2 A. S. Mestre, J. Pires, J. M. F. Nogueira, J. B. Parra, A. P. Carvalho and C. O. Ania, *Bioresour. Technol.*, 2009, **100**, 1720–1726.
- 3 A. Nikolaou, S. Meric and D. Fatta, *Anal. Bioanal. Chem.*, 2007, **387**, 1225–1234.
- 4 D. Tiwari, C. Lalhriatpuia and S. Lee, *J. Ind. Eng. Chem.*, 2015, **30**, 167–173.
- 5 J. P. Bound and N. Voulvoulis, *Environ. Health Perspect.*, 2005, **113**, 1705–1711.
- 6 S. L. Atkin, S. Barrier, Z. Cui, P. D. I. Fletcher, G. MacKenzie, V. Panel, V. Sol and X. Zhang, *J. Photochem. Photobiol. B Biol.*, 2011, **102**, 209–217.
- 7 Y. Zhang, S. Geißen and C. Gal, *Chemosphere*, 2008, **73**, 1151–1161.
- 8 T. A. Ternes, *Wat. Res.*, 1998, **32**, 3245–3260.
- 9 A. S. Mestre and A. P. Carvalho, *Molecules*, 2019, **24**, 1–40.
- 10 J. O’Neill, *Antimicrobial Resistance : Tackling a crisis for the health and wealth of nations*, 2014.
- 11 K. Ikehata, N. J. Naghashkar and M. G. El-Din, *Sci. Eng.*, 2006, **28**, 353–414.
- 12 L. Joseph, J. Heo, Y. Park, J. R. V Flora and Y. Yoon, *Desalination*, 2011, **281**, 68–74.
- 13 C. P. Silva, M. Otero and V. Esteves, *Environ. Pollut.*, 2012, **165**, 38–58.
- 14 R. Lopez-Fernandez, F. V. F. Tavares, M. Gómez, R. Irusta and P. Le-Clech, *Desalin. Water Treat.*, 2013, **51**, 2336–2342.
- 15 P. Fernández-Alvarez, M. Le Noir and B. Guieysse, *J. Hazard. Mater.*, 2009, **163**, 1107–1112.
- 16 M. Le Noir, A. Lepeuple, B. Guieysse and B. Mattiasson, *Water Res.*, 2007, **41**, 2825–2831.
- 17 R. H. Kaufman, E. Adam, E. E. Hatch, K. Noller, A. L. Herbst, J. R. Palmer and R. N. Hoover, *Obstet. Gynecol.*, 2000, **96**, 483–489.
- 18 R. J. Golden, K. L. Noller, L. Titus-Ernstoff, R. H. Kaufman, R. Mittendorf, R. Stillman and E. A. Reese, *Crit. Rev. Toxicol.*, 1998, **28**, 109–227.
- 19 I. Koc, G. Baydemir, E. Bayram, H. Yavuz and A. Denizli, *J. Hazard. Mater.*, 2011, **192**, 1819–1826.
- 20 C. Kuo, S. Yang, P. Kuo and C. Hung, *Kaohsiung J. Med. Sci.*, 2012, **28**, S37–S42.
- 21 W. G. Foster, M. S. Neal and E. V Younglai, *Int. Congr. Ser.*, 2004, **1266**, 126–132.
- 22 G. P. Daston, J. W. Gooch, W. J. Breslin, D. L. Shuey, A. I. Nikiforov, T. A. Fico and J. W. Goruch, *Reprod. Toxicol.*, 1997, **11**, 465–481.

- 23 J. A. McLachlan, E. Simpson and M. Martin, *Best Pract. Res.*, 2006, **20**, 63–75.
- 24 F. Maranghi and A. Mantovani, *Reprod. Toxicol.*, 2012, **33**, 290–296.
- 25 S. A. Ahmed, *Toxicology*, 2000, **150**, 191–206.
- 26 A. Casanova-Nakayama, M. Wenger, R. Burki, E. Eppler and A. Krasnov, *Mar. Pollut. Bull.*, 2011, **63**, 412–416.
- 27 M. Ogiue-Ikeda, N. Tanabe, H. Mukai and Y. Hojo, *Brain Res. Rev.*, 2008, **57**, 363–375.
- 28 K. M. Frick, S. M. Fernandez and L. L. Harburger, *Biochim. Biophys. Acta*, 2010, **1800**, 1045–1055.
- 29 T. H. Hutchinson, *Toxicol. Lett.*, 2002, **131**, 75–81.
- 30 K. Bay, C. Asklund and A. Andersson, *Best Pract. Res. Clin. Endocrinol. Metab.*, 2006, **20**, 77–90.
- 31 T. A. Ternes, M. Stumpf, J. Mueller, K. Haberer and R. Wilken, *Sci. Total Environ.*, 1999, **225**, 81–90.
- 32 E. Benfenati, D. Barcelo, I. Johnson, S. Galassi and K. Levsen, *Trends Anal. Chem.*, 2003, **22**, 757–765.
- 33 M. Petrovic, S. Gonzalez and D. Barcelo, *Trends Anal. Chem.*, 2003, **22**, 685–696.
- 34 C. E. Purdom, P. A. Hardiman, V. V. J. Bye, N. C. Eno, C. R. Tyler and J. P. Sumpter, *Chem. Ecol.*, 1994, **8**, 275–285.
- 35 H. H. Tabak, R. N. Bloomhuff and R. L. Bunch, *Dev. Ind. Microbiol.*
- 36 M. S. Pollock, M. G. Dube and R. Schryer, *Environ. Toxicol. Chem.*, 2010, **29**, 952–965.
- 37 Y. S. Wee, Z. A. Aris, F. Yusoff and S. M. Praveena, *Chemosphere*, 2021, **264**, 128488.
- 38 H. Cho, H. Huang and K. Schwab, *Langmuir*, 2011, **27**, 12960–12967.
- 39 T. N. and F. R. BKH Consulting Engineers, *EUROPEAN COMMISSION DG ENV Towards the establishment of a priority list of substances for further evaluation of their role in endocrine disruption*, Delft, Zeist, The Netherlands, 2000.
- 40 R. N. Carvalho, L. Ceriani, A. Ippolito and T. Lettieri, *Development of the first Watch List under the Environmental Quality Standards Directive water policy*, 2015.
- 41 P. L. Yap, J. Nine, K. Hassan, T. T. Tung, D. N. H. Tran and D. Losic, *Adv. Funct. Mater.*, 2021, **31**, 1–25.
- 42 N. B. Singh, G. Nagpal, R. Agrawal and Rachna, *Environ. Technol. Innov.*, 2018, **11**, 187–240.
- 43 S. Bolisetty, M. Peydayesh and R. Mezzenga, *Chem. Soc. Rev.*, 2019, **48**, 463–487.
- 44 M. Martz, *Pharm. Eng.*, 2012, **32**, 48–62.
- 45 M. M. Huber, S. Canonica, G. Park and U. Von Gunten, *Environ. Sci. Technol.*, 2003,

- 37, 1016–1024.
- 46 T. Ternes, M. Meisenheimer, D. Mcdowell and F. Sacher, *Environ. Sci. Technol.*, 2002, **36**, 3855–3863.
- 47 C. Hartig, M. Ernst and M. Jekel, *Water Res.*, 2001, **35**, 3998–4003.
- 48 S. A. Snyder, P. Westerhoff, Y. Yoon and D. Sedlak, *Environ. Eng. Sci.*, 2003, **20**, 449–469.
- 49 R. Broseus, S. Vincent, K. Aboufaldl, A. Daneshvar, S. Sauve, B. Barbeau and M. Prevost, *Water Res.*, 2009, **43**, 4707–4717.
- 50 Q. Sui, J. Huang, S. Deng, G. Yu and Q. Fan, *Water Res.*, 2010, **44**, 417–426.
- 51 M. Grassi, G. Kaykioglu, V. Balgiorino and G. Lofrano, in *Removal of emerging contaminants from water and wastewater by adsorption process*, ed. G. Lofrano, Springer, Netherlands, 2012, pp. 15–37.
- 52 H. Yu, E. Nie, J. Xu, S. Yan, W. J. Cooper and W. Song, *Water Res.*, 2013, **47**, 1909–1918.
- 53 M. M. Huber, S. Korhonen, T. A. Ternes and U. Von Gunten, 2005, **39**, 3607–3617.
- 54 T. A. Larsen, J. Lienert, A. Joss and H. Siegrist, *J. Biotechnol.*, 2004, **113**, 295–304.
- 55 P. W. Seo, B. N. Bhadra, I. Ahmed, N. A. Khan and S. H. Jhung, *Sci. Rep.*, 2016, **6**, 1–10.
- 56 L. Wang, C. Shi, L. Wang, L. Pan, X. Zhang and J. J. Zou, *Nanoscale*, 2020, **12**, 4790–4815.
- 57 S. D. Faust and O. M. Aly, *Adsorption processes for water treatment*, Butterworth Publishers, Stoneham, 1986.
- 58 T. R. Sahoo and B. Prelot, in *Nanomaterials for the Detection and Removal of Wastewater Pollutants*, eds. B. Bonelli, F. S. Freyria, I. Rosetti and R. Sethi, Elsevier Inc., 2020, pp. 161–122.
- 59 R. J. Hunter, *Introduction to modern colloid science*, Oxford University Press, Oxford, 1993.
- 60 F. Rouquerol, J. Rouquerol and K. Sing, *Adsorption by powders and porous solids*, Academic Press, San Diego, 1999.
- 61 G. Limousin, J. P. Gaudet, L. Charlet, S. Szenknect, V. Barthes and M. Krimissa, *Appl. Geochemistry*, 2007, **22**, 249–275.
- 62 E. Bulut, M. Ozacar and I. A. Sengil, *Microporous Mesoporous Mater.*, 2008, **115**, 234–46.
- 63 K. Y. Foo and B. H. Hameed, *Chem. Eng. J.*, 2010, **156**, 2–10.
- 64 K. V. Kumar and S. Sivanesan, *Dye. Pigm.*, 2007, **72**, 130–133.
- 65 C. H. Giles, D. Smith and A. Huitson, *J. Colloid Interface Sci.*, 1974, **47**, 755–765.
- 66 C. Hinz, *Geoderma*, 2001, **99**, 225–243.

- 67 B. Zohra, K. Aicha, S. Fatima, B. Nourredine and D. Zoubir, *Chem. Eng. J.*, 2008, **136**, 295–305.
- 68 A. S. Bhatt, P. L. Sakaria, M. Vasudevan, R. R. Pawar, N. Sudheesh, H. C. Bajaj and H. M. Mody, *RSC Adv.*, 2012, **2**, 8663–8671.
- 69 S. J. Allen, G. Mckay and J. F. Porter, *J. Colloid Interface Sci.*, 2004, **280**, 322–333.
- 70 H. Chen and J. Zhao, *Adsorption*, 2009, **15**, 381–389.
- 71 K. Fytianos, E. Voudrias and E. Kokkalis, *Chemosphere*, 2000, **40**, 3–6.
- 72 I. A. W. Tan, A. L. Ahmad and B. H. Hameed, *J. Hazard. Mater.*, 2008, **154**, 337–346.
- 73 B. Crittenden and W. J. Thomas, *Adsorption Technology and Design*, Butterworth-Heinemann, London, 1st edn., 1998.
- 74 B. K. Nandi, A. Goswami and M. K. Purkait, *J. Hazard. Mater.*, 2009, **161**, 387–395.
- 75 E. Worch, *Adsorption Technology in Water Treatment, Fundamentals, Processes and Modeling*, De Gruyter, Berlin/Boston, 2012.
- 76 S. Lagergren, *K. Sven. Vetenskapsakademiens Handl.*, 1989, **24**, 1–39.
- 77 B. Noroozi, G. A. Sorial, H. Bahrami and M. Arami, *J. Hazard. Mater. B*, 2007, **139**, 167–174.
- 78 W. J. Weber and J. C. Morris, *J. Sanit. Eng. Div. Am. Soc. Civ. Eng.*, 1963, **89**, 31–60.
- 79 E. Rosales, J. Meijide, M. Pazos and M. A. Sanroman, *Bioresour. Technol.*, 2017, **246**, 176–192.
- 80 D. M. Ruthven, *Principles of adsorption and adsorption processes*, John Wiley & Sons, New York, 1984.
- 81 Y. K. Recepoglu, N. Kabay, I. Y. Ipek, M. Arda, M. Yüksel, K. Yoshizuka and S. Nishihama, *Desalination*, 2018, **437**, 1–6.
- 82 A. Derylo-Marczewska and A. W. Marczewski, *Appl. Surf. Sci.*, 2002, **196**, 264–272.
- 83 T. L. Jones-Lepp and R. Stevens, *Anal. Bioanal. Chem.*, 2007, **387**, 1173–1183.
- 84 G. S. Dhillon, S. Kaur, R. Pulicharla and S. K. Brar, *Int. J. Environ. Res. Public Health*, 2015, **12**, 5657–5684.
- 85 E. Commission, *Pollutants in urban wastewater and sewage sludge*, 2001.
- 86 L. R. Radovic, I. F. Silva, J. I. Ume and J. A. Menbndez, *Carbon N. Y.*, 1997, **35**, 1339–1348.
- 87 G. L. Dotto and G. Mckay, *J. Environ. Chem. Eng.*, 2020, **8**, 103988.
- 88 S. Wong, N. Ngadi, I. M. Inuwa and O. Hassan, *J. Clean. Prod.*, 2018, **175**, 361–375.
- 89 G. Selvaraju and N. K. Abu Bakar, *J. Clean. Prod.*, 2017, **141**, 989–999.
- 90 H. N. Tran, S. J. You and H. P. Chao, *J. Environ. Manag.*, 2017, **188**, 322–336.
- 91 E. K. Putra, R. Pranowo, J. Sunarso, N. Indraswati and S. Ismadji, *Water Res.*, 2009, **43**, 2419–2430.

- 92 M. B. Ahmed, J. L. Zhou, H. H. Ngo and W. Guo, *Sci. Total Environ.*, 2015, **532**, 112–126.
- 93 S. Babel and T. Kurniawan, *J. Hazard. Mater.*, 2003, **97**, 219–243.
- 94 G. Crini, *Bioresour. Technol.*, 2006, **97**, 1061–1085.
- 95 J. R. Andrade, M. F. Oliveira, M. G. C. Silva and M. G. A. Vieira, *Ind. Eng. Chem. Res.*, 2018, **57**, 3103–3127.
- 96 M. F. Brigatti, E. Galan and B. K. Theng, *Elsevier*, 2006, **1**, 19–86.
- 97 D. S. Tong, C. H. Zhou, Y. Lu, H. Yu, G. F. Zhang and W. H. Yu, *Appl. Clay Sci.*, 2010, **50**, 427–431.
- 98 Z. J. Lin, J. Lu, M. Hong and R. Cao, *Chem. Soc. Rev.*, 2014, **16**, 1–29.
- 99 P. Kumar, V. Bansal, K. H. Kim and E. E. Kwon, *J. Ind. Eng. Chem.*, 2018, **62**, 130–145.
- 100 H. Furukawa, K. E. Cordova, M. O’Keeffe and O. M. Yaghi, *Science (80-.)*, 2013, **341**, 974.
- 101 M. R. Azhar, H. R. Abid, H. Sun, V. Periasamy, M. O. Tade and S. Wang, *J. Colloid Interface Sci.*, 2016, **478**, 344–352.
- 102 Y. Pi, X. Li, Q. Xia, J. Wu, Y. Li, J. Xiao and Z. Li, *Chem. Eng. J.*, 2018, **337**, 351–371.
- 103 J. Lehmann and S. Joseph, *Biochar for environmental management: Science, Technology and Implementation*, Earthscan, London, 2nd edn., 2015.
- 104 S. Meyer, B. Glaser and P. Quicker, *Environ. Sci. Technol.*, 2011, **45**, 9473–9483.
- 105 A. Bhatnagar and M. Sillanpää, *Chem. Eng. J.*, 2011, **168**, 493–504.
- 106 S. De Gisi, G. Lofrano, M. Grassi and M. Notarnicola, *SUSMAT*, 2016, **9**, 10–40.
- 107 G. Crini and P. M. Badot, *Sorption Processes and Pollution: Conventional and Non-conventional Sorbents for Pollutant Removal from Wastewaters*, Presses Universitaires de Franche-Comté, 2011.
- 108 M. Antunes, V. I. Esteves, R. Guegan, J. S. Crespo, A. N. Fernandes and M. Giovanela, *Chem. Eng. J.*, 2012, **192**, 114–121.
- 109 E. Contreras, L. Sepulveda and C. Palma, *Int. J. Chem. Eng.*, 2012, **2012**, 1–9.
- 110 C. Gerente, V. K. C. Lee, P. L. Cloirec and G. McKay, *Crit. Rev. Environ. Sci. Technol.*, 2007, **37**, 41–127.
- 111 M. Sener, B. Kayan, S. Akay, B. Gozmen and D. Kalderis, *Desalin. Water Treat.*, 2016, **57**, 28294–28312.
- 112 A. M. Hassan, W. A. Wan Ibrahim, M. B. Bakar, M. M. Sanagi, Z. A. Sutirman, H. R. Nodeh and M. M. A., *J. Environ. Manage.*, 2020, **253**, 1–11.
- 113 A. Çimen, A. Bilgiç, A. N. Kursunlu, I. H. Gübbük and H. I. Uçan, *Desalin. Water Treat.*, 2014, **52**, 4837–4847.

- 114 I. Sargin and G. Arslan, *Desalin. Water Treat.*, 2016, **57**, 10664–10676.
- 115 N. F. Ahmad, M. A. Kamboh, H. R. Nodeh, S. N. Binti Abd Halim and S. Mohamad, *Environ. Sci. Pollut. Res.*, 2017, **24**, 21846–21858.
- 116 A. Markus, A. O. Gbadamosi, A. S. Yusuff, A. Agi and J. Oseh, *Environ. Sci. Pollut. Res.*, 2018, **25**, 35130–35142.
- 117 S. F. F. S. Yaacob, M. A. Kamboh, W. A. Wan Ibrahim and S. Mohamad, *R. Soc. Open Sci.*, 2018, **5**, 1–14.
- 118 K. Chandrasekaram, Y. Alias, S. F. Fathullah, S. V Lee, N. Haron, M. Raoov, N. Zakaria and S. Mohamad, *Mater. Today Commun.*, 2021, **28**, 1–14.
- 119 M. A. Kamboh, S. S. Arain, A. H. Jatoi, B. Sherino, T. S. Algarni, W. A. Al-Onazi, A. M. Al-Mohaimed and S. Rezanja, *Environ. Res.*, 2021, **201**, 1–9.
- 120 C. E. Agashe S.N., *Pollen and Spores: Applications with Special Emphasis on Aerobiology and Allergy*, CRC PRESS, 2009.
- 121 H. Tutar, E. Yilmaz, E. Pehlivan and M. Yilmaz, *Int. J. Biol. Macromol.*, 2009, **45**, 315–320.
- 122 K. E. Espelie, F. A. Loewus, R. J. Pugmire, W. R. Woolfenden, B. G. Baldi and P. H. Given, *Phytochemistry*, 1989, **28**, 751–753.
- 123 T. Fan, M. G. Potroz, E. Tan, M. S. Ibrahim, E. Miyako and N. Cho, *Sci. Total Environ.*, 2019, **9**, 1–13.
- 124 E. Katifori, S. Alben, E. Cerda, D. R. Nelson and J. Dumais, *Proc. Natl. Acad. Sci.*, 2010, **107**, 7635–7639.
- 125 A. Diego-Taboada, L. Maillet, J. H. Banoub, M. Lorch, A. S. Rigby, A. N. Boa, S. L. Atkin and G. Mackenzie, *J. Mater. Chem. B*, 2013, **1**, 707–713.
- 126 S. J. Archibald, S. L. Atkin, W. Bras, A. Diego-Taboada, G. Mackenzie, J. F. W. Mosselmans, S. Nikitenko, P. D. Quinn, F. Thomas and N. A. Young, *J. Mater. Chem. B*, 2014, **2**, 945–959.
- 127 F. Schulte, J. Lingott, U. Panne and J. Kneipp, *Anal. Chem.*, 2008, **80**, 9551–9556.
- 128 A. K. F. Dyab and K. U. Sadek, *RSC Adv.*, 2018, **8**, 23241–23251.
- 129 S. Barrier, A. Diego-Taboada, M. J. Thomasson, L. Madden, J. C. Pointon, J. D. Wadhawan, S. T. Beckett, L. Atkin and G. Mackenzie, *J. Mater. Chem.*, 2011, **21**, 975–981.
- 130 J. Brooks and G. Shaw, *Grana*, 1978, **17**, 91–97.
- 131 B. P. Binks, A. N. Boa and M. A. Kibble, *Soft Matter*, 2011, **7**, 4017–4024.
- 132 P. F. Van Bergen, P. Blokker, M. . Collinson, S. Damste and J. W. De Leeuw, *The Evolution of Plant Physiology. From wholes plants to ecosystems*, Elsevier Academic Press, London, 2004.
- 133 M. Hesse, H. Halbritter, R. Zetter, M. Weber, R. Buchner, A. Frosch-Radivo and S. Ulrich, *Pollen terminology. An illustrated handbook*, Springer, New York, 2009.

- 134 F. Zetzsche and K. Huggler, *Justus Liebigs Ann. Chem.*, 1928, **461**, 89.
- 135 F. Zetzsche and O. Kalin, *Helv. Chim. Acta*, 1931, **14**, 517–519.
- 136 E. Domínguez, J. A. Mercado, M. A. Quesada and A. Heredia, *Sex. Plant Reprod.*, 1999, **12**, 171–178.
- 137 W. T. Fraser, A. C. Scott, A. E. S. Forbes, I. J. Glasspool, R. E. Plotnick, F. Kenig and B. H. Lomax, *New Phytol.*, 2012, **196**, 397–401.
- 138 M. J. Thomasson, D. J. Baldwin, A. Diego-Taboada, S. L. Atkin, G. Mackenzie and J. D. Wadhawan, *Electrochem. Commun.*, 2010, **12**, 1428–1431.
- 139 P. Blokker, P. Boelen, R. Broekman and J. Rozema, *Plant Ecol.*, 2006, **182**, 197–207.
- 140 G. Mackenzie, A. N. Boa, A. Diego-Taboada, S. L. Atkin and T. Sathyapalan, *Front. Mater.*, 2015, **2**, 1–5.
- 141 A. Meuter-Gerhards, S. Riegert and R. Wiermann, *J. Plant Physiol.*, 1999, **154**, 431–436.
- 142 W. S. Meuter-Gerhards A, Schwerdtfegera C, Steuernagelb S, Wilmesmeier S, *Verlag der Zeitschrift für Naturforschung.*, 1995, **50c**, 487–492.
- 143 S. Gubatz and R. Wiermann, *Zeitschrift für Naturforsch. - Sect. C J. Biosci.*, 1993, **48**, 10–15.
- 144 A. Boom, Amsterdam: Universiteit van Amsterdam, 2004.
- 145 F. Li, P. Phyto, J. Jacobowitz, M. Hong and J. Weng, *Nat. Plants*, 2019, **5**, 41–46.
- 146 A. Mikhael, J. Banoub, K. Jurcic, C. Schneider, D. Karr, G. L. Fisher, T. D. Fridgen, A. Diego-Taboada, P. E. Georghiou, G. Mackenzie and J. Banoub, *Rapid Commun. Mass Spectrom.*, 2020, **34**, 1–22.
- 147 A. Diego-Taboada, P. Cousson, E. Raynaud, Y. Huang, M. Lorch, B. P. Binks, Y. Queneau, A. N. Boa, S. L. Atkin, S. T. Beckett and G. MacKenzie, *J. Mater. Chem.*, 2012, **22**, 9767–9773.
- 148 J. R. Thio, K. K. Clark and A. A. Keller, *J. Hazard. Mater.*, 2011, **194**, 53–61.
- 149 V. N. Paunov, G. Mackenzie and S. D. Stoyanov, *J. Mater. Chem.*, 2007, **7**, 609–612.
- 150 D. Hussain, M. Najam-ul-Haq, S. Majeed, S. G. Musharraf, Q. Lu, X. He and Y.-Q. Feng, *Anal. Bioanal. Chem.*, 2019, **411**, 3373–3382.
- 151 N. Unlu and M. Ersoz, *J. Hazard. Mater.*, 2006, **136**, 272–280.
- 152 S. Barrier, University of Hull, 2008.
- 153 R. C. Mundargi, M. G. Potroz, J. H. Park, J. Seo, E. L. Tan, J. H. Lee and N. J. Cho, *Sci. Rep.*, 2016, **6**, 1–14.
- 154 W. T. Fraser, J. S. Watson, M. A. Sephton, B. H. Lomax, G. Harrington, W. D. Gosling and S. Self, *Rev. Palaeobot. Palynol.*, 2014, **201**, 41–46.
- 155 W. Montgomery, C. Potiszil, J. S. Watson and M. A. Sephton, *Macromol. Chem. Phys.*, 2016, **217**, 2494–2500.

- 156 M. Ucan, A. Gurten and A. Ayar, *Colloids Surfaces A Physicochem. Eng. Asp.*, 2003, **219**, 193–199.
- 157 A. Ayar and B. Mercimek, *Process Biochem.*, 2006, **41**, 1553–1559.
- 158 E. Pehlivan, M. Ersoz, M. Pehlivan, S. Yildiz and H. J. Duncan, *J. Colloid Interface Sci.*, 1995, **170**, 320–325.
- 159 G. Shaw, M. Sykes, R. W. Humble, G. Mackenzie, D. Marsden and E. Pehlivan, *React. Polym. Ion Exch. Sorbents*, 1988, **9**, 211–217.
- 160 M. S. Abd Wahib, A. W. Wan Ibrahim, M. Marsin Sanagi, M. Afzal Kamboh and A. S. Abdul Keyon, *J. Chromatogr. A*, 2018, **1532**, 50–57.
- 161 A. Diego-Taboada, L. Maillet, J. H. Banoub, M. Lorch, A. S. Rigby, A. N. Boa, L. Atkin and G. Mackenzie, *J. Mater. Chem. B*, 2013, **1**, 707–713.
- 162 Z. Deng, Y. Pei, S. Wang, B. Zhou, X. Hou, J. Li, B. Li and H. Liang, *J. Agric. Food Chem.*, 2020, **68**, 13990–14000.
- 163 A. Wakil, G. Mackenzie, A. Diego-Taboada, J. G. Bell and S. L. Atkin, *Lipids*, 2010, **45**, 645–649.
- 164 K. Stamatopoulos, V. Kafourou, H. Batchelor and S. J. Konteles, *Small*, 2021, **17**, 1–12.
- 165 J. Uddin, P. Gonzalez-Cruz, J. Warzywoda and H. S. Gill, *Adv. Ther.*, 2020, **3**, 1–14.
- 166 F. E. Atalay, A. Bingol, H. Kaya, H. H. Bas and A. A. Culum, *ACS Omega*, 2020, **5**, 20417–20427.
- 167 R. Adamson, S. Gregson and G. Shaw, *Int. J. Pept. Protein Res.*, 1983, **22**, 560–564.
- 168 M. Keleş, *Synth. React. Inorganic, Met. Nano-Metal Chem.*, 2013, **43**, 575–579.
- 169 A. F. F. S. Yaacob, N. S. A. Razak, T. T. Aun, S. K. M. Rozi, A. K. M. Jamil and S. Mohamad, *Ind. Crop. Prod.*, 2018, **124**, 442–448.
- 170 P. E. Jardine, F. A. J. Abernethy, B. H. Lomax, W. D. Gosling and W. T. Fraser, *Rev. Palaeobot. Palynol.*, 2017, **238**, 1–6.
- 171 M. Bağcıoğlu, B. Zimmermann and A. Kohler, *PLoS One*, 2015, **10**, 1–19.
- 172 B. Zimmermann, *Appl. Spectrosc.*, 2010, **64**, 1364–1373.
- 173 B. Zimmermann, M. Bağcıoğlu, C. Sandt and A. Kohler, *Planta*, 2015, **242**, 1237–1250.
- 174 A. Lutzke, K. J. Morey, J. I. Medford and M. J. Kipper, *Phytochemistry*, 2020, **170**, 1–15.
- 175 B. Zimmermann and A. Kohler, *PLoS One*, 2014, **9**, 1–12.
- 176 E. G. Palacios, G. Juárez-López and A. J. Monhemius, *Hydrometallurgy*, 2004, **72**, 139–148.
- 177 H. O. Dessey, in *Acid Derivatives Volume 2*, ed. S. Patai, John Wiley & Sons Ltd., 1st edn., 1992, pp. 271–303.

- 178 W. T. Fraser, M. A. Sephton, J. S. Watson, S. Self, B. H. Lomax, D. I. James, C. H. Wellman, T. V. Callaghan and D. J. Beerling, *Polar Res.*, 2011, **30**, 1–6.
- 179 J. S. Watson, M. A. Sephton, S. V. Sephton, S. Self, W. T. Fraser, B. H. Lomax, I. Gilmour, C. H. Wellman and D. J. Beerling, *Photochem. Photobiol. Sci.*, 2007, **6**, 689–694.
- 180 B. G. Pummer, H. Bauer, J. Bernardi, B. Chazallon, S. Facq, B. Lendl, K. Whitmore and H. Grothe, *J. Raman Spectrosc.*, 2013, **44**, 1654–1658.
- 181 S. Wilmesm eier, R. Wiermann and S. Steuernagel, *Zeitschrift fur Naturforsch. - Sect. C J. Biosci.*, 1993, **48**, 697–701.
- 182 P. D. A. Pudney, K. J. Mutch and S. Zhu, *Phys. Chem. Chem. Phys.*, 2009, **11**, 5010–5018.
- 183 K. V. Berezin and V. V. Nechaev, *J. Appl. Spectrosc.*, 2005, **72**, 164–171.
- 184 S. Krimm and C. Y. Liang, *J. Appl. Phys.*, 1958, **29**, 1407–1411.
- 185 R. Świsłocka, M. Kowczyk-Sadowy, M. Kalinowska and W. Lewandowski, *Spectroscopy*, 2012, **27**, 35–48.
- 186 H. W. Li, H. L. Strauss and R. G. Snyder, *J. Phys. Chem. A*, 2004, **108**, 6629–6642.
- 187 K. M. Mena Aguilar, Y. Amano and M. Machida, *J. Environ. Chem. Eng.*, 2016, **4**, 4644–4652.
- 188 B. Piskin and M. Turkun, *J. Endod.*, 1995, **21**, 253–255.
- 189 S. P. De Souza, J. Bassut, H. V. Marquez, I. I. Junior, L. S. M. Miranda, Y. Huang, G. Mackenzie, A. N. Boa and R. O. M. A. De Souza, *Catal. Sci. Technol.*, 2015, **5**, 3130–3136.
- 190 S. Barrier, A. Lobbert, A. J. Boasman, A. N. Boa, M. Lorch and L. Atkin, *Green Chem.*, 2010, **12**, 234–240.
- 191 H. P. Boehm, *Carbon N. Y.*, 1994, **32**, 759–769.
- 192 R. Homlok, E. Takács and L. Wojnárovits, *Chemosphere*, 2011, **85**, 603–608.
- 193 D. B. França, P. Trigueiro, E. C. S. Filho, M. G. Fonseca and M. Jaber, *Chemosphere*, 2020, **242**, 1–15.
- 194 N. Vieno and M. Sillanpää, *Environ. Int.*, 2014, **69**, 28–39.
- 195 K. A. K. Musa and L. A. Eriksson, *Phys. Chem. Chem. Phys.*, 2009, **11**, 4601–4610.
- 196 P. M. Peltzer, R. C. Lajmanovich, C. Martinuzzi, A. M. Attademo, L. M. Curi and M. T. Sandoval, *Sci. Total Environ.*, 2019, **683**, 624–637.
- 197 B. Hoeger, K. Bernd, D. R. Dietrich and B. Hitzfeld, *Aquat. Toxicol.*, 2005, **75**, 53–64.
- 198 U. Sarkar, K. C. Ravindra, E. Large, C. L. Young, D. Rivera-Burgos, J. Yu, M. Cirit, D. J. Hughes, J. S. Wishnok, D. A. Lauffenburger, L. G. Griffith and S. R. Tannenbaum, *Drug Metab. Dispos.*, 2017, **45**, 855–866.
- 199 M. Bernardo, S. Rodrigues, N. Lapa, I. Matos, F. Lemos, M. K. S. Batista, A. P. Carvalho and I. Fonseca, *Int. J. Environ. Sci. Technol.*, 2016, **13**, 1989–2000.

- 200 L. Charuaud, E. Jardé, A. Jaffrézic, M. Liotaud, Q. Goyat, F. Mercier and B. Le, *Sci. Total Environ.*, 2019, **664**, 605–615.
- 201 S. Fekadu, E. Alemayehu, R. Dewil and B. Van Der Bruggen, *Sci. Total Environ.*, 2019, **654**, 324–337.
- 202 M. Williams, R. S. Kookana, A. Mehta, S. K. Yadav, B. L. Tailor and B. Maheshwari, *Sci. Total Environ.*, 2019, **647**, 1256–1265.
- 203 M. Petrovic, S. Sabater and A. Elosegi, in *Emerging contaminants in river ecosystems Occurrence and effects under multiple stress conditions*, ed. D. Barcelo, Springer, Cham, 2016, pp. 219–220.
- 204 J. Näslund, N. Asker, J. Fick, D. G. J. Larsson and L. Norrgren, *Aquat. Toxicol.*, 2020, **227**, 1–13.
- 205 L. Arpin-Pont, M. J. Martinez Bueno, E. Gomez and H. Fenet, *Environ. Sci. Pollut. Res.*, 2016, **23**, 4978–4991.
- 206 S. Gaw, K. V Thomas and T. H. Hutchinson, *Philos. Trans. R. Soc. B*, 2014, **369**, 1–11.
- 207 M. C. V. M. Starling, C. C. Amorim and M. M. D. Leão, *J. Hazard. Mater.*, 2019, **372**, 17–36.
- 208 A. M. Ali, H. T. Ronning, W. Alarif, R. Kallenborn and S. S. Al-Lihaibi, *Chemosphere*, 2017, **175**, 505–513.
- 209 S. Gonzalez-Alonso, M. L. Merino, S. Esteban, M. L. de Alda, D. Barcelo, J. J. Duran, J. Lopez-Martinez, J. Acena, S. Perez, N. Mastroianni, A. Silva, M. Catala and Y. Valcarcel, *Environ. Pollut.*, 2017, **229**, 241–254.
- 210 J. Lee, K. Ji, Y. Lim, P. Kim and K. Choi, *Ecotoxicol. Environ. Saf.*, 2011, **74**, 1216–1225.
- 211 A. C. Mehinto, E. M. Hill and C. R. Tyler, *Environ. Sci. Technol.*, 2010, **44**, 2176–2182.
- 212 J. Chae, M. Seon, Y. Hwang, B. Min, S. Kim, H. Lee and M. Park, *Chemosphere*, 2015, **120**, 52–58.
- 213 J. D. Cardoso-Vera, H. Islas-Flores, N. Juan-Reyes and S. G. Medina, in *Nonsteroidal Anti-Inflammatory Drugs (NSAIDs): Common Uses, Risks and Effectiveness*, ed. D. Flores, Nova Science Publishers Inc., 2017, pp. 51–87.
- 214 V. Prakash, D. J. Pain, A. A. Cunningham, P. F. Donald, N. Prakash and A. Verma, *Biol. Conserv.*, 2003, **109**, 381–390.
- 215 J. L. Oaks, M. Gilbert, M. Z. Virani, R. T. Watson, C. U. Meteyer, B. A. Rideout, H. L. Shivaprasad, S. Ahmed, M. Jamshed, I. Chaudhry, M. Arshad, S. Mahmood, A. Ali and A. A. Khan, *Nature*, 2004, **427**, 630–633.
- 216 R. Yasmee, L. Asif and S. Djeflal, *Pakistan J. Zool.*, 2021, **51**, 1–9.
- 217 V. Naidoo, K. Wolter, R. Cuthbert and N. Duncan, *Regul. Toxicol. Pharmacol.*, 2009, **53**, 205–208.
- 218 S. Joachim, R. Beaudouin, G. Daniele, A. Geffard, A. Bado-Nilles, C. Tebby, O.

- Palluel, O. Dedourge-Geffard, M. Fieu, M. Bonnard, M. Palos-Ladeiro, C. Turi, V. David, P. Baudoin, A. James, S. Andres and J. M. Porcher, *Ecotoxicol. Environ. Saf.*, 2021, **211**, 1–15.
- 219 E. T. Thomas and G. C. Richards, *BMJ Evidence-Based Med.*, 2021, **26**, 196–199.
- 220 D. O. Flynn, J. Lawler, A. Yusuf, A. Parle-Mcdermott, D. Harold, M. Cloughlin and L. Holland, *Anal. Methods*, 2021, **13**, 575–594.
- 221 S. Tavazzi, B. Paracchini, G. Suurkuusk, G. Mariani, R. Loos, M. Ricci and B. M. Gawlik, *Water Framework Directive Watch List Method Analysis of diclofenac in water*, 2014.
- 222 H. Fenet, L. Arpin-Pont, A. Vanhoutte-Brunier, D. Munaron, A. Fiandrino, M. M. Bueno, C. Boillot, C. Casellas, O. Mathieu and E. Gomez, *Environ. Int.*, 2014, **68**, 177–184.
- 223 A. Pal, K. Y. Gin, A. Y. Lin and M. Reinhard, *Sci. Total Environ.*, 2010, **408**, 6062–6069.
- 224 T. A. Ternes, N. Herrmann, M. Bonerz, T. Knacker, H. Siegrist and A. Joss, *Water Res.*, 2004, **38**, 4075–4084.
- 225 K. Kimura, H. Hara and Y. Watanabe, *Environ. Sci. Technol.*, 2007, **41**, 3708–3714.
- 226 B. Quintana, S. Weiss and T. Reemtsma, *Water Res.*, 2005, **39**, 2654–2664.
- 227 E. S. Rigobello, A. Di Bernardo Dantas, L. Di Bernardo and E. M. Vieira, *Chemosphere*, 2013, **92**, 184–191.
- 228 G. Luongo, M. Guida, A. Siciliano, G. Libralato, L. Saviano, A. Amoresano, L. Previtera, G. Di and A. Zarrelli, *J. Pharm. Biomed. Anal.*, 2021, **194**, 1–9.
- 229 J. Rivera-Utrilla, M. Sánchez-Polo, M. Á. Ferro-García and G. Prados-Joya, *Chemosphere*, 2013, **93**, 1268–1287.
- 230 L. F. Delgado, P. Charles, K. Glucina and C. Morlay, *Sci. Total Environ.*, 2012, **435–436**, 509–525.
- 231 A. Karami, R. Sabouni and M. Ghommem, *J. Mol. Liq.*, 2020, **305**, 1–9.
- 232 C. B. Godiya, S. Kumar and Y. Xiao, *J. Hazard. Mater.*, 2020, **393**, 1–12.
- 233 M. Cuccarese, S. Brutti, A. De Bonis, R. Teghil, I. M. Mancini, S. Masi and D. Caniani, *Sci. Rep.*, 2021, **11**, 1–15.
- 234 J. Y. Song, B. N. Bhadra and S. H. Jung, *Microporous Mesoporous Mater.*, 2017, **243**, 221–228.
- 235 F. M. Rodríguez-Zamarripa, I. Trejo-Carrizalez and E. Cervantes-González, *Int. J. Environ. Sci. Technol.*, , DOI:10.1007/s13762-021-03214-4.
- 236 V. Beri, K. Yaah, M. Zbair, S. Botelho and D. O. Satu, *Nanotechnol. Environ. Eng.*, 2021, **6**, 1–12.
- 237 L. Wu, C. Du, J. He, Z. Yang and H. Li, *J. Hazard. Mater.*, 2020, **384**, 1–10.
- 238 S. Zhuang, R. Chen, Y. Liu and J. Wang, *J. Hazard. Mater.*, 2020, **385**, 1–8.

- 239 T. Shahnaz, V. V. Priyan, S. Pandian and S. Narayanasamy, *Environ. Pollut.*, 2021, **268**, 1–14.
- 240 L. Bi, Z. Chen, L. Li, J. Kang, S. Zhao, B. Wang, P. Yan, Y. Li, X. Zhang and J. Shen, *J. Hazard. Mater.*, 2021, **407**, 1–12.
- 241 B. Czech, M. Konczak, M. Rakowska and P. Oleszczuk, *J. Clean. Prod.*, 2021, **288**, 1–11.
- 242 Y. Lv, Z. Liang, Y. Li, Y. Chen, K. Liu, G. Yang, Y. Liu, C. Lin, X. Ye, Y. Shi and M. Liu, *Environ. Res.*, 2021, **194**, 1–12.
- 243 S. Bratos, *J. Chem. Phys.*, 1975, **63**, 3499–3509.
- 244 Y. Marechal, *J. Chem. Phys.*, 1967, **48**, 3697–3705.
- 245 B. Athokpam, S. G. Ramesh and R. H. Mckenzie, *Chem. Phys.*, 2017, **488–489**, 43–54.
- 246 E. Arunan, G. R. Desiraju, R. A. Klein, J. Sadlej, S. Scheiner, I. Alkorta, D. C. Clary, R. H. Crabtree, J. J. Dannenberg, P. Hobza, H. G. Kjaergaard, A. C. Legon, B. Mennucci and D. J. Nesbitt, *Pure Appl. Chem.*, 2011, **83**, 1619–1636.
- 247 J. Simonin, *Chem. Eng. J.*, 2016, **300**, 254–263.
- 248 L. Huang, N. Mao, Q. Yan, D. Zhang and Q. Shuai, *ACS Appl. Nano Mater.*, 2020, **3**, 319–326.
- 249 J. M. N. Santos, C. R. Pereira, E. L. Foletto and G. L. Dotto, *Int. J. Biol. Macromol.*, 2019, **131**, 301–308.
- 250 S. Zhang, Y. Dong, Z. Yang, W. Yang, J. Wu and C. Dong, *Chem. Eng. J.*, 2016, **304**, 325–334.
- 251 S. Álvarez-Torrellas, M. Munoz, J. Gläsel, Z. M. de Pedro, C. M. Domínguez, J. García, B. J. M. Etzold and J. A. Casas, *Chem. Eng. J.*, 2018, **347**, 595–606.
- 252 K. A. Lin, H. Yang and W. Lee, *RSC Adv.*, 2015, **5**, 81330–81340.
- 253 Y. S. Ho, D. A. J. Wase and C. F. Forster, *Environ. Technol.*, 1996, **17**, 71–77.
- 254 M. A. Al-Ghouti, M. A. M. Kraishah, M. N. M. Ahmad and S. Allen, *J. Hazard. Mater.*, 2009, **165**, 589–598.
- 255 D. Kumar and J. P. Gaur, *Bioresour. Technol.*, 2011, **102**, 633–640.
- 256 T. C. Nguyen, P. Loganathan, T. V. Nguyen, S. Vigneswaraan, J. Kandasamy and R. Naidu, *Chem. Eng. J.*, 2015, **270**, 393–404.
- 257 Y. S. Ho and G. McKay, *Chem. Eng. J.*, 1998, **70**, 115–124.
- 258 M. K. Purkait, D. S. Gusain, S. DasGupta and S. De, *Sep. Sci. Technol.*, 2005, **39**, 2419–2440.
- 259 H. J. An, B. N. Bhadra, N. A. Khan and S. H. Jung, *Chem. Eng. J.*, 2018, **343**, 447–454.
- 260 A. G. N. Wamba, S. K. Ndi, E. C. Lima, J. G. Kayem, P. S. Thue, T. M. H. Costa, A. B. Quevedo, E. V. Benvenutti and F. M. Machado, *J. Taiwan Inst. Chem. Eng.*, 2019, **102**, 321–329.

- 261 F. Orias and Y. Perrodin, *Sci. Total Environ.*, 2013, **455**, 250–276.
- 262 Massachusetts Water Resources Authority, Water Efficiency for Hospitals
Massachusetts Water Resources Authority,
<https://www.mwra.com/comsupport/ici/hospitals.htm>.
- 263 Massachusetts Water Resources Authority, Water Use Case Study: Norwood Hospital
Massachusetts Water Resources Authority,
<https://www.mwra.com/04water/html/bullet1.htm>.
- 264 V. Karzi, M. N. Tzatzarakis, E. Vakonaki, T. Alegakis, I. Katsikantami, S. Sifakis, A. Rizos and A. M. Tsatsakis, *J. Appl. Toxicol.*, 2018, **38**, 1144–1152.
- 265 H. Li, W. Zhang, Z. Zhang and X. Zhang, *Sci. Total Environ.*, 2017, **580**, 1318–1326.
- 266 T. Geens, H. Neels and A. Covaci, *Chemosphere*, 2012, **87**, 796–802.
- 267 M. Adolfsson-Erici, M. Pettersson, J. Parkkonen and J. Sturve, *Chemosphere*, 2002, **46**, 1485–1489.
- 268 D. G. Lee, *Environ. Eng. Res.*, 2015, **20**, 111–120.
- 269 K. C. Ahn, B. Zhao, J. Chen, G. Cherednichenko, E. Sanmarti, M. S. Denison, B. Lasley, I. N. Pessah, D. Kültz, D. P. Y. Chang, S. J. Gee and B. D. Hammock, *Environ. Health Perspect.*, 2008, **116**, 1203–1210.
- 270 J. A. Arnot, S. Pawlowski and S. Champ, *Sci. Total Environ.*, 2018, **618**, 1506–1518.
- 271 G. Shanmugam, K. Ramasamy, K. K. Selvaraj, S. Sampath and B. R. Ramaswamy, *Environ. Forensics*, 2014, **15**, 207–212.
- 272 M. A. Coogan, R. E. Edziyie, T. W. La Point and B. J. Venables, *Chemosphere*, 2007, **67**, 1911–1918.
- 273 X. Bai and K. Acharya, *J. Hazard. Mater.*, 2016, **315**, 70–75.
- 274 M. Yueh and R. H. Tukey, *Annu. Rev. Pharmacol. Toxicol.*, 2016, **56**, 251–272.
- 275 S. M. Castro, A. B. Araújo, R. F. P. Nogueira and S. Guerini, *Appl. Surf. Sci.*, 2017, **403**, 519–524.
- 276 M. Ricart, H. Guasch, M. Alberch, D. Barceló, C. Bonnineau, A. Geiszinger, J. Ferrer, F. Ricciardi, A. M. Romaní, S. Morin, L. Proia, L. Sala, D. Sureda and S. Sabater, *Aquat. Toxicol.*, 2010, **100**, 346–353.
- 277 M. Coogan and T. La Point, *Environ. Toxicol. Chem.*, 2008, **27**, 1788–1793.
- 278 C. J. Houtman, A. Brouwer and M. H. Lamoree, *Environ. Sci. Technol.*, 2004, **38**, 6415–6423.
- 279 P. A. Fair, H. Lee, J. Adams, C. Darling, G. Pacepavicius, M. Alae, G. D. Bossart, N. Henry and D. Muir, *Environ. Pollut.*, 2009, **157**, 2248–2254.
- 280 B. A. Wilson, V. H. Smith, F. DeNoyelles and C. K. Larive, *Environ. Sci. Technol.*, 2003, **37**, 1713–1719.
- 281 R. Oliveira, I. Domingues, G. Koppe and A. Soares, *Environ. Sci. Pollut. Res. Int.*, 2009, **16**, 679–688.

- 282 T. Stoker, E. Gibson and L. Zorrilla, *Toxicol. Sci.*, 2010, **117**, 45–53.
- 283 E. Jung, B. An, K. Choi and E. Jeung, *Toxicol. Lett.*, 2012, **208**, 142–148.
- 284 C. M. Foran, E. R. Bennett and W. H. Benson, *Mar. Environ. Res.*, 2000, **50**, 153–156.
- 285 V. Kumar, A. Chakraborty, M. Raj and P. Roy, *Reprod. Toxicol.*, 2009, **27**, 177–185.
- 286 K. M. Crofton, K. B. Paul, M. J. Devito and J. M. Hedge, *Environ. Toxicol. Pharmacol.*, 2007, **24**, 194–197.
- 287 K. B. Paul, J. T. Thompson, S. O. Simmons, J. P. Vanden and K. M. Crofton, *Toxicol. Vitro.*, 2013, **27**, 2049–2060.
- 288 L. M. Zorrilla, E. K. Gibson, S. C. Jeffay, K. M. Crofton, W. R. Setzer, R. L. Cooper and T. E. Stoker, *Toxicol. Sci.*, 2009, **107**, 56–64.
- 289 C. C. Helbing, G. Van Aggelen and N. Veldhoen, *Toxicol. Sci.*, 2011, **119**, 417–418.
- 290 D. C. McAvoy, B. Schatowitz, M. Jacob, A. Hauk and W. Eckhoff, *Environ. Toxicol. Chem.*, 2002, **21**, 1323–1329.
- 291 M. Balmer, T. Poiger, C. Droz, K. Romanin, P. Bergovist, M. Muller and H. Buster, *Environ. Sci. Technol.*, 2004, **38**, 390–395.
- 292 E. M. Fiss, K. L. Rule and P. J. Vikesland, *Environ. Sci. Technol.*, 2007, **41**, 2387–2394.
- 293 A. Kanetoshi, E. Katsura, H. Ogawa, T. Ohyama, H. Kaneshima and T. Miura, *Arch. Environ. Contam. Toxicol.*, 1992, **23**, 91–98.
- 294 J. Buth, M. Grandbois, P. Vikesland, K. McNeill and W. Arnold, *Environ. Toxicol. Chem.*, 2009, **28**, 2555–2563.
- 295 D. E. Latch, J. L. Packer, W. A. Arnold and K. McNeill, *J. Photochem. Photobiol. A Chem.*, 2003, **158**, 63–66.
- 296 D. Latch, J. Packer, B. Stender, J. VanOverbeke, W. Arnold and K. McNeill, *Environ. Toxicol. Chem.*, 2005, **24**, 517–525.
- 297 R. U. Halden and D. H. Paull, *Environ. Sci. Technol.*, 2005, **39**, 1420–1426.
- 298 K. Styszko, K. Nosek, M. Motak and K. Bester, *Comptes rendus - Chim.*, 2015, **18**, 1134–1142.
- 299 R. Xu, Y. Si, X. Wu, F. Li and B. Zhang, *Chem. Eng. J.*, 2014, **255**, 63–70.
- 300 C. Wu, A. L. Spongberg and J. Witter, *J. Agric. Food Chem.*, 2009, **57**, 4900–4905.
- 301 A. Karnjanapiboonwong, A. N. Morse, J. D. Maul and T. A. Anderson, *J. Soils Sediments*, 2010, **10**, 1300–1307.
- 302 J. Simonin, *Chem. Eng. J.*, 2016, **300**, 254–263.
- 303 M. S. Praveena, M. S. N. Shaifuddin, S. Sukiman, M. F. A. Nasir, Z. Hanafi, N. Kamarudin, T. T. H. Ismail and Z. A. Aris, *Sci. Total Environ.*, 2018, **642**, 230–240.
- 304 J. Wu, P. N. Lam, D. Martens, A. Kettrup and Z. Cai, *Talanta*, 2007, **72**, 1650–1654.
- 305 L. W. B. Olaniyan, N. Mkwetshana and A. I. Okoh, *Springer Plus*, 2016, **5**, 1–17.

- 306 I. I. Fasfous, E. S. Radwan and J. N. Dawoud, *Appl. Surf. Sci.*, 2010, **256**, 7246–7252.
- 307 W. E. I. Chen, L. I. N. Duan and D. Zhu, *Environ. Sci. Technol.*, 2007, **41**, 8295–8300.
- 308 W. E. I. Chen, L. I. N. Duan, L. Wang and D. Zhu, *Environ. Sci. Technol.*, 2008, **42**, 6862–6868.
- 309 S. K. Behera, S. Oh and H. Park, *J. Hazard. Mater.*, 2010, **179**, 684–691.
- 310 X. Zhu, Y. Liu, G. Luo, F. Qian, S. Zhang and J. Chen, *Environ. Sci. Technol.*, 2014, **48**, 5840–5848.
- 311 G. Zhang, M. Sun, Y. Liu, H. Liu, J. Qu and J. Li, *Langmuir*, 2015, **31**, 1820–1827.
- 312 G. Zheng, B. Yu, Y. Wang, C. Ma and T. Chen, *Environ. Int.*, 2020, **134**, 1–9.
- 313 K. Shimada, K. Mitamura and T. Higashi, *J. Chromatogr. A*, 2001, **935**, 141–172.
- 314 E. J. Routledge and J. P. Sumpter, *J. Biol. Chem.*
- 315 A. M. Brzozowski, A. C. W. Pike, Z. Dauter, R. Hubbard, T. Bonn, O. Engstrom, L. Ohman, G. L. Greene, J.-A. Gustafsson and M. Carlquist, *Nature*, 1997, **389**, 753–758.
- 316 L. Racz and R. K. Goel, *J. Environ. Monit.*, 2010, **12**, 58–70.
- 317 G. Ying, R. S. Kookana and Y. Ru, *Environ. Int.*, 2002, **28**, 545–551.
- 318 G. Hall and T. J. Phillips, *J. Am. Acad. Dermatol.*, 2005, **53**, 555–568.
- 319 R. K. Ross, A. Paganini-Hill, P. C. Wan and M. C. Pike, *J. Natl. Cancer Inst.*, 2000, **92**, 328–332.
- 320 S. A. Samaan and M. H. Crawford, *JACC*, 1995, **26**, 1403–1410.
- 321 L. A. Da Silva Lara, B. U. Useche, R. A. Ferriani, M. R. Rosana, M. F. Silva De Sá, M. M. Sabino De Freitas, J. C. Rosa E Silva and A. C. Japur De Sá Rosa, *J. Sex. Med.*, 2009, **6**, 30–39.
- 322 L. P. Shulman, *Am. J. Obstet. Gynecol.*, 2011, **205**, S9–S13.
- 323 J. P. Laurenson, R. A. Bloom, S. Page and N. Sadrieh, *Am. Assoc. Pharm. Sci.*, 2014, **16**, 299–310.
- 324 M. M. McCarthy, *Physiol. Rev.*, 2008, **88**, 91–134.
- 325 K. M. Lai, K. L. Johnson, M. D. Scrimshaw and J. N. Lester, *Environ. Sci. Technol.*, 2000, **34**, 3890–3894.
- 326 X. Bai, F. X. M. Casey, H. Hakk, T. M. Desutter, P. G. Oduor and E. Khan, *Chemosphere*, 2015, **119**, 1322–1328.
- 327 W. Zheng, S. R. Yates and S. A. Bradford, *Environ. Sci. Technol.*, 2008, **42**, 530–535.
- 328 T. A. Hanselman, D. A. Graetz and A. C. Wilkie, *Environ. Sci. Technol.*, 2003, **37**, 5471–5478.
- 329 H. R. Andersen, J. Kjølholt, M. Hansen, F. Stuer-Lauridsen, T. D. Blicher, F. Ingerslev and B. Halling-Sørensen, *Degradation of Estrogens in Sewage Treatment Processes*, Denmark, 2004.

- 330 T. Matsuda, S. Matsui, H. Takigami, J. Adachi and O. Shiypu, in *EcoSan*, Nanning, China, 2002, p. 2002.
- 331 P. D. Anderson, C. Johnson, D. Pfeiffer, D. J. Caldwell, R. Hannah, F. Mastrocco, J. P. Sumpter and R. J. Williams, *Environ. Toxicol. Chem.*, 2012, **31**, 1407–1415.
- 332 D. G. J. Larsson, E. M. Adolfsson, J. Parkkonen, M. Pettersson, A. H. Berg, P. E. Olsson and L. Forlin, *Aquat. Toxicol.*, 1999, **45**, 91–97.
- 333 K. L. Thorpe, R. I. Cummings, T. H. Hutchinson, M. Scholze, G. Brighty, J. P. Sumpter and C. R. Tyler, *Environ. Sci. Technol.*, 2003, **37**, 1142–1149.
- 334 D. M. Leech, M. T. Snyder and R. G. Wetzel, *Sci. Total Environ.*, 2008, **407**, 2087–2092.
- 335 H. M. Kuch and K. Ballschmiter, *Environ. Sci. Technol.*, 2001, **35**, 3201–3206.
- 336 P. D. Hansen, H. Dizer and B. Hock, *Trac. Trend. Anal. Chem.*, 1998, **17**, 448–451.
- 337 C. D. Metcalfe, T. L. Metcalfe and Y. Kiparissis, *Environ. Toxicol. Chem.*, 2001, **20**, 297–308.
- 338 M. Kobayashi, M. Kijima, Y. Matsuzuka, Y. Hayakawa, E. Iwata and T. Kimura, *Fish. Sci.*, 2021, **87**, 93–104.
- 339 N. P. Karki, R. E. Colombo, K. F. Gaines and A. Maia, *Environ. Sci. Pollut. Res.*, 2021, **28**, 6450–6458.
- 340 R. L. Gomes, H. H. Deacon, K. M. Lai, J. W. Birkett, M. D. Scrimshaw and J. N. Lester, *Environ. Toxicol. Chem.*, 2004, **23**, 105–108.
- 341 A. Takahashi, T. Higashitani, Y. Yakou, M. Saitou, H. Tamamoto and H. Tanaka, *Water Sci. Technol.*, 2003, **47**, 71–76.
- 342 R. J. Williams, A. C. Johnson, J. J. L. Smith and R. Kanda, *Environ. Sci. Technol.*, 2003, **37**, 1744–1750.
- 343 C. Baronti, R. Curini, G. D’Ascenzo, A. Di-Corsia, A. Gentili and R. Sameri, *Environ. Sci. Technol.*, 2000, **34**, 5059–5066.
- 344 M. Peck, R. W. Gibson, A. Kortenkamp and E. M. Hill, *Environ. Toxicol. Chem.*, 2004, **23**, 945–952.
- 345 M. D. Jürgens, K. I. E. Holthaus, A. C. Johnson, J. J. L. Smith, M. Hetheridge and R. J. Williams, *Environ. Toxicol. Chem.*, 2002, **21**, 480–488.
- 346 A. Joss, H. Andersen, T. Ternes, P. R. Richle and H. Siegrist, *Environ. Sci. Technol.*, 2004, **38**, 3047–3055.
- 347 P. M. Bradley and J. H. Writer, *J. Am. Water Assoc.*, 2014, **50**, 334–342.
- 348 W. Zhang, Y. Li, Q. Wang, C. Wang, P. Wang and K. Mao, *Environ. Sci. Pollut. Res.*, 2013, **20**, 1431–1440.
- 349 C. L. Hu, W. F. Wang and Y. H. Hsieh, *Chem. React. Eng.*, 2015, **48**, 458–462.
- 350 C. Qin, D. Troya, C. Shang, S. Hildreth, R. Helm and K. Xia, *Environ. Sci. Technol.*, 2015, **49**, 956–964.

- 351 F. Wang, W. Sun, W. Pan and N. Xu, *Chem. Eng. J.*, 2015, **274**, 17–29.
- 352 Y. Yoon, P. Westerhoff, S. A. Snyder and M. Esparza, *Water Res.*, 2003, **37**, 3530–3537.
- 353 M. L. Mashtare, B. Khan and L. S. Lee, *Chemosphere*, 2011, **82**, 847–852.
- 354 E. A. McCallum, H. Hyung, A. T. Do, C. Huang and J. Kim, *J. Memb. Sci.*, 2008, **319**, 38–43.
- 355 Y. Zhang and J. L. Zhou, *Water Res.*, 2005, **39**, 3991–4003.
- 356 J. L. Sangster, H. Oke, Y. Zhang and S. L. Bartelt-Hunt, *J. Hazard. Mater.*, 2015, **299**, 112–121.
- 357 W. Sun and K. Zhou, *Chem. Eng. J.*, 2014, **258**, 185–193.
- 358 Q. Zaib, I. A. Khan, N. B. Salch, R. V Flora, Y.-G. Park and Y. Yoon, *Water Air Soil Pollut*, 2012, **223**, 3281–3293.
- 359 S. Patel, J. Han and W. Gao, *J. Environ. Chem. Eng.*, 2015, **3**, 1562–1569.
- 360 Z. Niavarani, D. Breite, A. Prager, B. Abel and A. Schulze, *Membranes (Basel)*, 2021, **11**, 99.
- 361 A. Shareef, M. J. Angove, J. D. Wells and B. B. Johnson, *J. Chem. Eng. Data*, 2006, **51**, 879–881.
- 362 L. Jiang, Y. Liu, G. Zeng, F. Xiao and X. Hu, *Chem. Eng. J.*, 2016, **284**, 93–102.
- 363 Q. Ning, Y. Liu, S. Liu, L. Jiang, G. Zeng, Z. Zeng, X. Wang, J. Li and Z. Kare, *RSC Adv.*, 2017, **7**, 37122–37129.
- 364 W. Shi, S. Li, B. Chen, C. Wang and W. Sun, *Chem. Eng. J.*, 2017, **326**, 1134–1144.
- 365 F. Wu, R. Tseng and R. Juang, *Chem. Eng. J.*, 2009, **153**, 1–8.
- 366 L. Jiang, Y. Liu, G. Zeng, S. Liu, X. Hu, L. Zhou, X. Tan, N. Liu, M. Li and J. Wen, *Chem. Eng. J.*, 2018, **339**, 296–302.
- 367 R. W. Fairbridge, in *The Encyclopedia of Geochemistry and Environmental Sciences*, Van Nostrand Reinhold, New York, 1972, pp. 74–82.
- 368 M. A. Pasek, J. M. Sampson and Z. Atlas, *PNAS*, 2014, **111**, 15468–15473.
- 369 V. Smil, *Annu. Rev. Energy Environ.*, 2000, **25**, 53–88.
- 370 E. S. Deevey, *Sci. Am.*, 1970, **223**, 148–158.
- 371 F. H. Westheimer, *Science (80-)*, 1987, **235**, 1173–1178.
- 372 C. Fernandez-Garcia, A. J. Coggins and M. W. Powner, *Life*, 2017, **7**, 31.
- 373 E. Macia, M. V. Hernandez and J. Oro, *Orig. Life Evol. Biosph.*, 1997, **27**, 459–480.
- 374 J. Hem, *Study and interpretation of the chemical characteristics of natural water*, Alexandria, 1992.
- 375 C. Warwick, A. Guerreiro and A. Soares, *Biosens. Bioelectron.*, 2013, **41**, 1–11.
- 376 K. G. Sellner, G. J. Doucette and G. J. Kirkpatrick, *J. Ind. Microbiol. Biotechnol.*,

- 2003, **30**, 383–406.
- 377 L. Fang, W. Zeng, L. Xu and L. Z. Huang, *Chem. Eng. J.*, 2020, **388**, 124198.
- 378 S. R. Carpenter, N. F. Caraco, D. L. Correll, R. W. Howarth, A. N. Sharpley and V. H. Smith, *Ecol. Appl.*, 1998, **8**, 559–568.
- 379 M. R. Awual, A. Jyo, T. Ihara, N. Seko, M. Tamada and K. T. Lim, *Water Res.*, 2011, **45**, 4592–4600.
- 380 Y. Yao, B. Gao, M. Inyang, A. R. Zimmerman, X. Cao, P. Pullammanappallil and L. Yang, *J. Hazard. Mater.*, 2011, **190**, 501–507.
- 381 S. Kilpimaa, H. Runtti, T. Kangas, U. Lassi and T. Kuokkanen, *Chem. Eng. Res. Des.*, 2014, **92**, 1923–1933.
- 382 E. Nassef, *Eng. Sci. Technol. Int. J.*, 2012, **2**, 409–413.
- 383 L. Delgadillo-Marquez, F. Lopes, B. Taidi and D. Pareau, *Biotechnol. Rep.*, 2016, **11**, 18–26.
- 384 R. J. Haynes, *Crit. Rev. Environ. Sci. Technol.*, 2015, **45**, 1041–1103.
- 385 K. Wu, Y. Li, T. Liu, Q. Huang, S. Yang, W. Wang and P. Jin, *Appl. Surf. Sci.*, 2019, **478**, 539–551.
- 386 K. Velusamy, S. Periyasamy, P. S. Kumar, D. V Nguyen Vo, J. Sindhu, D. Sneka and B. Subhasini, *Environ. Chem. Lett.*, 2021, **19**, 3165–3180.
- 387 I. Hilbrandt, H. Shemer, A. S. Ruhl, R. Semiat and M. Jekel, *Sep. Purif. Technol.*, 2019, **221**, 23–28.
- 388 K. S. Rajmohan, M. Gopinath and R. Chetty, *J. Environ. Biol.*, 2016, **37**, 1519–1528.
- 389 J. Huisman and F. D. Hulot, in *Aquatic Ecology series*, eds. J. Huisman, H. C. P. Matthijs and P. M. Visser, Springer, 2005, pp. 143–176.
- 390 G. Fan, L. Hong, J. Luo, Y. You, J. Zhang, P. Hua, B. Du, J. Zhan, R. Ning and M. Bao, *Chem. Eng. J.*, 2020, **392**, 123767.
- 391 V. K. Sharma, T. M. Triantis, M. G. Antoniou, X. He, M. Pelaez, C. Han, W. Song, K. E. O. Shea, A. A. De, T. Kaloudis, A. Hiskia and D. D. Dionysiou, *Sep. Purif. Technol.*, 2012, **91**, 3–17.
- 392 X. Wang, J. Zhao, J. Song, J. Wang, R. Ma and J. Ma, *Chem. Eng. J.*, 2017, **320**, 253–263.
- 393 R. Dai, P. Wang, P. Jia, Y. Zhang, X. Chu and Y. Wang, *World J. Microbiol. Biotechnol.*, 2016, **32**, 1–7.
- 394 H. Li and G. Pan, *Environ. Sci. Technol.*, 2015, **49**, 6249–6256.
- 395 D. Wang, G. Yang, X. Li, W. Zheng, Y. Wu and Q. Yang, *Biotechnol. Bioeng.*, 2012, **109**, 2798–2807.
- 396 R. Li, J. J. Wang, B. Zhou, Z. Zhang and S. Liu, *J. Clean. Prod.*, 2017, **147**, 96–107.
- 397 M. Chiban, A. Soudani, F. Sinan, S. Tahrouch and M. Persin, *Clean Soil, Air, Water*, 2011, **39**, 376–383.

- 398 D. Sun, X. Hong, K. Wu, K. S. Hui, Y. Du and K. N. Hui, *Water Res.*, 2020, **169**, 115239.
- 399 J. L. Barnard, P. Dunlap and N. Steichen, *Water Environ. Res.*, 2017, **89**, 2043–2054.
- 400 J. Sun, Q. Yang, D. Wang, S. Wang, F. Chen, Y. Zhong, K. Yi, F. Yao, C. Jiang, S. Li, X. Li and G. Zeng, *Chem. Eng. J.*, 2017, **313**, 415–423.
- 401 P. Loganathan, S. Vigneswaran and J. Kandasamy, *Crit. Rev. Environ. Sci. Technol.*, 2014, **44**, 847–907.
- 402 L. Kong, Y. Tian, Z. Pang, X. Huang, M. Li, R. Yang, N. Li, J. Zhang and W. Zuo, *Chem. Eng. J.*, 2019, **371**, 893–902.
- 403 G. W. Kajjumba, E. Yildirim, S. Aydin, S. Emik, T. Agun, F. Osra and J. Wasswa, *J. Environ. Manag.*, 2019, **247**, 356–362.
- 404 H. Qiao, L. Mei, G. Chen, H. Liu, C. Peng, F. Ke, R. Hou, X. Wan and H. Cai, *Appl. Surf. Sci.*, 2019, **483**, 114–122.
- 405 L. Clesceri, A. Greenberg and A. Eaton, in *Standard Methods for the Examination of Water and Wastewater*, ed. M. A. H. Franson, American Public Health Association, Washington, 20th edn., 1999, pp. 252–254.
- 406 P. J. Worsfold, L. J. Gimbert, U. Mankasingh, O. Ndukaku, G. Hanrahan, P. C. F. C. Gardolinski, P. M. Haygarth, B. L. Turner, M. J. Keith-Roach and I. D. McKelvie, *Talanta*, 2005, **66**, 273–293.
- 407 I. D. McKelvie, D. M. W. Peat and P. J. Worsfold, *Anal. Proc. Incl. Anal. Commun.*, 1995, **32**, 437–445.
- 408 A. Muller and C. Serain, *Acc. Chem. Res.*, 2000, **33**, 2–10.
- 409 J. F. Keggin, *Proc. R. Soc. Lond. Ser. A*, 1934, **144**, 75–100.
- 410 C. G. Bochet, T. Draper, B. Bocquet, T. Pope and A. F. Williams, *Dalt. Trans.*, 2009, **26**, 5127–5131.
- 411 G. M. Brown, M. R. Noe-Spirlet, W. R. Busing and H. A. Levy, *Acta Cryst.*, 1977, **B33**, 1038–1046.
- 412 L. Drummond and W. Maher, *Anal. Chim. Acta*, 1995, **302**, 69–74.
- 413 J. Murphy and J. P. Riley, *Anal. Chim. Acta*, 1962, **27**, 31–36.
- 414 A. Sjosten and S. Blomqvist, *Water Res.*, 1997, **31**, 1818–1823.